THE BIOMECHANICS OF SKELETAL MUSCLE VENTRICLES

Thesis submitted in accordance with the requirements of the

University of Liverpool

for the degree of

Doctor in Philosophy

by

Martin M. N. KWENDE

September 1995

MAXIM'S MAXIMS

Don't accept the status quo

Question everyone and everybody

Stand up for what you believe to be right

Try as hard as you can

Don't give up until you've won

When you work get a result, don't waste time

Work as a team

Be proud of results

Give credit, don't plagiarise

Teach and pass on knowledge

Don't voluntarily miscommunicate or lie

Take direction enthusiastically.

Learning without thought is labour lost; thought without learning is perilous.

Confucius.

Abstract

Cardiac assistance from an autograft of suitably conditioned skeletal muscle is now emerging as a potential alternative to transplantation for treatment of patients in end-stage heart failure. Under long-term electrical stimulation, skeletal muscle is rendered sufficiently fatigue-resistant to sustain cardiac levels of work. This thesis is based on an approach in which circulatory assistance will be provided by a skeletal muscle ventricle (SMV) fashioned from the patient's latissimus dorsi (LD) muscle. The aims are to determine efficient geometrical configurations of SMVs and to develop optimal stimulation patterns (OSPs) for the muscles that will control the force profile, minimise muscle fatigue and increase pacemaker lifetime.

Firstly, software was developed to afford computer control of a servomotor transducer for the measurement of muscle mechanical properties. Studies of the effects of chronic electrical stimulation on muscle mechanical properties were thus carried out. The software was extended to load rabbit tibialis anterior (TA) muscles with the complex loads that they would experience in an SMV wall, and to measure their functional response.

Secondly, a numerical model of an SMV was developed from muscle mechanical characteristics. These were fitted to mathematical relationships so that they were defined by equations with known constants. The equations were then incorporated into software that calculated the function of the muscle as though it was formed into a cylindrical pumping chamber. Predictions using TA properties agreed well with the complex load measurements. Sheep LDs were used to form pumping chambers that were connected to a mock circulation, and their performance compared with the mathematical predictions. The observed differences could be associated with the surgical formation of the ventricles, suggesting that this area needs particular attention. The best ejection fractions (EF) were predicted for a small ventricle, which generated higher pressures, whereas stroke volume (SV) peaked at a larger SMV size. The model thus suggests a design compromise: to achieve adequate EFs so as to reduce the risk of thromboembolism, SMVs should be made at sizes with sub-optimal SVs. This model could be extended to predict hydraulic performance in complete pumping cycles - it will then be a useful guide to the surgeon in the construction of functional SMVs.

Lastly, three approaches were used to determine stimulation patterns that optimize force-time integral in isometric contractions of rabbit TA muscles. OSPs for fast muscles consist of an initial high-frequency portion followed by impulses at a lower frequency. For muscles stimulated chronically at a low constant frequency, the initial high-frequency portion has no benefit. Thus, OSPs have potential for clinical use, but their value will depend strongly on the activation characteristics of the stimulated muscle.

Acknowledgements

I am most indebted to my supervisors, Dr. Jonathan C. Jarvis and Prof. Stanley Salmons, for their constant support and encouragement. Their supervision was second to none, as they were always available whenever I needed help. I benefited academically as well as socially from them. I am ever so grateful. God bless!

I wish to thank the Wellcome Trust for the very generous support I enjoyed while I carried out this work. I held a Wellcome Prize Studentship for 4 years under a special Mathematical Biology scheme. This provided an extra year of sponsorship to allow me improve my knowledge of biology. The Trust also sponsored annual conferences at which I developed my communication skills. The Wellcome Trust's support has therefore allowed me to transfer into the biomedical field, for which I am most thankful.

I also wish to thank the following:

Prof. J.R. Jones, Head of the Electrical Engineering and Electronics Department, who initiated my liaison with Prof. S. Salmons and Dr. J.C. Jarvis. Also, I thank Dr. D.W. Shimmin, who was always in the background in case of any problems with the electronics.

Everyone in Prof. Salmons' laboratory - it was truly a family scenario. I thank Miss H. Sutherland, especially, who helped me with a lot of the experimental work - she was always so patient. Many thanks also to A. Hall, Dr. H. Degens, Mrs. M. Hastings (Shelly), S.J. Gilroy, A. Craven, Dr. T. Mokrusch, and all the others in the laboratory. They were always there at the most difficult moments.

Drs. A. Shortland and R.A. Black of the Clinical Engineering Department, who were involved in the sheep work. Many thanks.

All the great friends that I made in and around Liverpool for my long 7 years in the city, especially A.M. Boyo, C. Nche, C.S. Ngwa, E.E. Kwame, J.B. Fodje, C. Yakum, J.G. Davies and H.P. Vu. They all contributed to my success in various ways, and I thank them.

My family, most of whom have been far away in body but have been with me in spirit throughout my struggles. Their constant moral support has been invaluable.

Everyone else I have not mentioned who helped in any way at all.

God Almighty, above all. When my 'get up and go' had got up and gone, He got me up. I thank Him for all the strength and wisdom he has given me throughout the years. I pray that his kindness continues to guide me through the future.

Mukah Kwende

September 1995

Dedication

To my mother, Mary Anyo, and to my grandmother, Abbott Fritong.

Table of contents

List of Abbreviations

ACE	angiotensin-converting enzyme
ADC, A/D	analog-to-digital
ADP	adenosine diphosphate
ATP	adenosine triphosphate
CABG	coronary artery bypass grafting
CC	contractile component
CCSS	computer-controlled servo system
CHF	congestive heart failure
CI, CO	cardiac index, cardiac output
CPK	creatine phosphokinase
CPU	central processing unit
Cr	creatine
CRO	cathode ray oscilloscope
CT	contraction time
DAC, D/A	digital-to-analog
EDL	extensor digitorium longus
EDV	end-diastolic volume
EF	ejection fraction
FES	functional electrical stimulation
F-F	force-frequency
F-L	force-length
F-V	force-velocity
FTI	force-time integral
FTIpP	force-time integral per pulse
IABP	intra-aortic balloon pump
IDE	integrated development environment
IM	intramuscular
IPI	interpulse interval
I/O	input/output
LAVD	left ventricular assist device
LC	light chain

LD	latissimus dorsi
LSLV	large single-layered ventricle
LV	left ventricle
LVEDP	left ventricular end-diastolic pressure
MHC	myosin heavy chain
MLC	myosin light chain
NAD	nicotinamide-adenine dinucleotide
NADH	reduced nicotinamide-adenine dinucleotide
OSP	optimal stimulation pattern
PCr	phosphocreatine
PDP	peak developed pressure
PEC	parallel elastic component
PVC	polyvinyl chloride
RNA, mRNA	ribonucleic acid, messenger RNA
ROM	range of movement
R/Th	radius/thickness ratio
RT	relaxation time
SDLV	small double-layered ventricle
SDS PAGE	sodium dodecyl sulfate polyacrylamide gel electrophoresis
SEC	series elastic component
SMV	skeletal muscle ventricles
SMVT	skeletal muscle tube ventricle
SSLV	small single-layered ventricle
SV	stroke volume
TA	tibialis anterior
TAH	total artificial heart
TW:TET	twitch to tetanus ratio
V/M	volume/mass ratio

List of Symbols

α, β, μ, A, B, C	constants
$\overline{\sigma}$	mean wall stress
a, b	Hill's constants
A	amplitude
F	flow, force
f	frequency
H	height
K	ratio of circumference to TA length
L, l	length
Lo	optimal length
N	number of cycles
ω	angular velocity
P	pressure
π	Pi
Po	peak isometric force
q, r, s	constants
R	radius
R_{in}, R_i	internal radius
R_{io}	nominal radius
R_{new}	new inner radius
R_o	outer radius
σ	stress
θ	phase angle
t	time
T	period of oscillation
V	velocity
Vopt	optimum velocity of contraction
Vmax	maximum velocity of contraction
W	wall thickness
Wc	cylindrical wall thickness

Wnew	new cylindrical wall thickness
X, Xarea, Ao	cross-sectional area
Xlin	linear cross-sectional area
Xcyl	cylindrical cross-sectional area

1. General Introduction

1.1. Introduction

Circulatory assistance derived from an autograft of suitably conditioned skeletal muscle is now emerging as a potential alternative to transplant surgery for treating patients in end-stage heart failure. The power available for cardiac assistance in this way is harnessed most efficiently by configuring the skeletal muscle as an independent auxiliary pouch-shaped or tube-shaped ventricle (Pochettino *et al.* 1991; Salmons & Jarvis 1992). As illustrated in Figure 1.1, this is achieved by wrapping the muscle around a suitable mandrel; the mandrel is subsequently removed, leaving a skeletal muscle ventricle (SMV) or a skeletal muscle tube ventricle (SMVT) that can be connected to the circulation and stimulated to function as a synchronous or counterpulsatory assist (Acker *et al.* 1986; Mannion *et al.* 1986; Anderson *et al.* 1988, 1991; Pochettino *et al.* 1991).

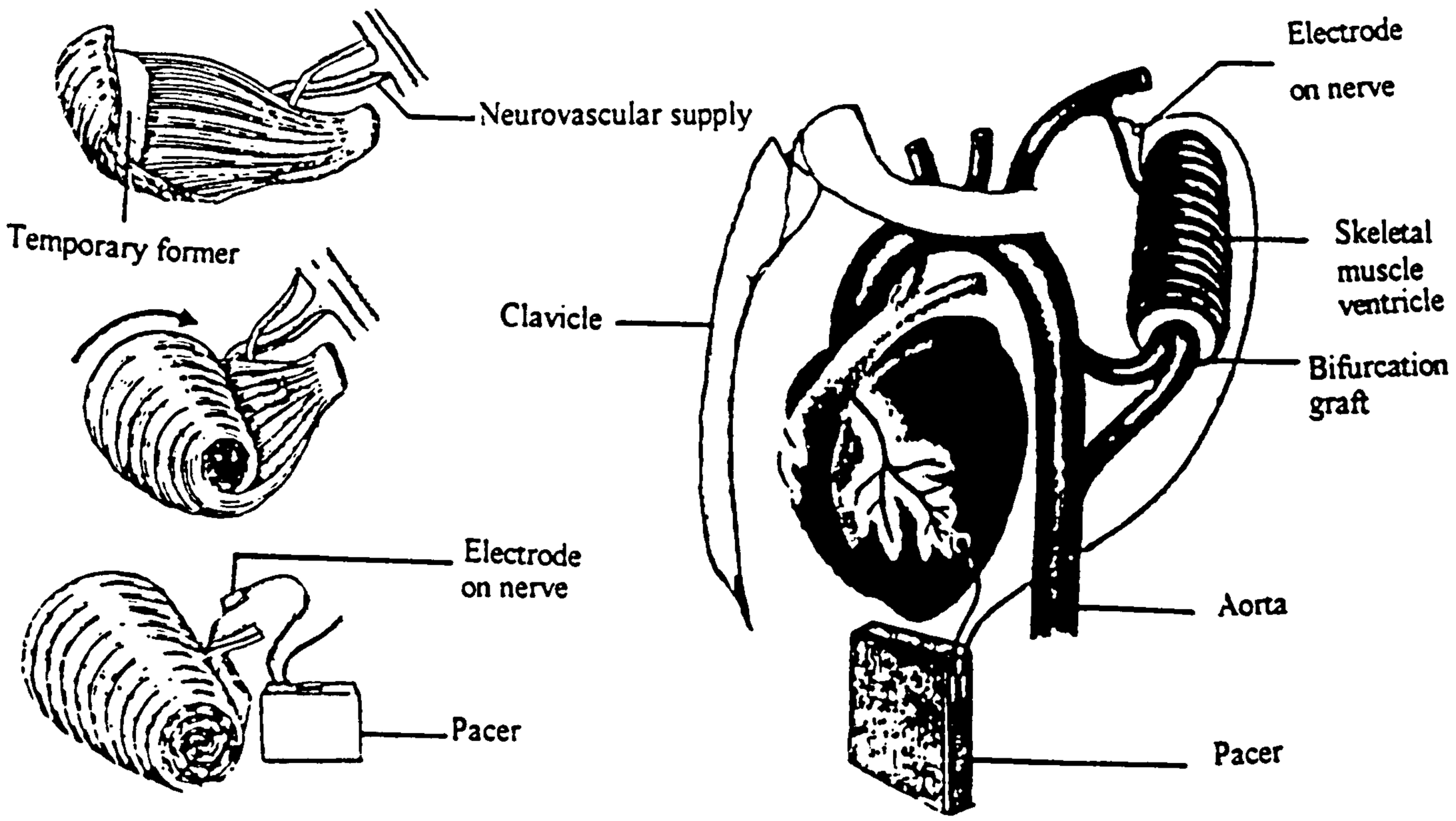

Figure 1.1. *Construction of an SMV from the latissimus dorsi muscle and its connection to the circulation. Diagrams after L.W. Stephenson.*

This thesis is part of a major project to establish a new surgical treatment for terminal cardiac failure in which an auxiliary ventricle fashioned from the patient's latissimus dorsi

(LD) muscle will provide heart assistance. Hence, this work addresses some of the important considerations necessary to design an efficient skeletal muscle pump. These include economical stimulation protocols for transformation and activation of the grafted muscle, and configurations of ventricles that would allow the most power to be harnessed from the muscle. A well-designed pump, based on a systematic optimization procedure that employs detailed knowledge of skeletal muscle properties, may provide useful information that could be applied to other forms of skeletal muscle assist. More importantly, efficiently designed SMVs will offer an alternative solution to the problem of congestive heart failure.

1.2. Congestive heart failure - the problem

Heart disease is a major cause of death and morbidity in the western world. In the United States, approximately 2 million Americans suffer from congestive heart failure (CHF) and over 400,000 new cases are diagnosed every year (Furberg & Yusuf 1985). Of these, it has been estimated that between 17,000 and 35,000 people each year have CHF sufficiently bad to warrant transplantation, while only about 400 to 1,100 viable donor hearts (10% of the estimated need) become available (Evans *et al.* 1986).

Chronic heart failure, which results from coronary and valvular heart diseases and hypertension (Ho *et al.* 1993; Pfeffer *et al.* 1993; Gaasch *et al.* 1994), is a clinical problem characterised by left ventricular systolic and diastolic dysfunction, impaired quality of life, and a markedly shortened life expectancy (Cohn 1988). Left ventricular dysfunction results from a remodelling of the ventricle with reactive hypertrophy, loss of diastolic recoil, and continual dilatation (McKay *et al.* 1986; Preffer & Preffer 1987; Pfeffer *et al.* 1993; Gaasch 1994). This leads to insufficient cardiac output to meet the metabolic needs of the body. Consequently, end-stage heart failure patients have a low exercise tolerance and restricted function, and most of these patients die prematurely: the overall 1-year and 5-year survival rates are 57% and 25% in men and 64% and 38% in women, respectively (Ho *et al.* 1993). Survival rates in patients with new-onset heart

failure after acute myocardial infarction are even worse, with only a minority staying alive at 5 years (Norris *et al.* 1970). Since human life span has increased on average over time with improved economic conditions (Minsky 1994), and as the prevalence of CHF increases with age, the magnitude of the problem is on the increase (Smith 1985). This unfortunate trend has necessitated the search for alternative means of cardiac assist.

1.3. Alternative methods of cardiac assist

Despite technological advances in medicine and surgery, there are limited options for patients with end-stage heart disease. These patients have been managed with a combination of drug therapy and surgical intervention.

1.3.1. Medical therapy

Medical or pharmacological therapy as an option for circulatory assist of CHF patients has a very modest impact on survival; however, survival can be improved with knowledge gained from large clinical trials. Options of medical therapy include drugs that unload the myocardium by reducing systemic vascular resistance thereby improving hemodynamics, exercise tolerance, and consequently quality of life (Cohn 1988). In addition to the standard medical regimens of diuretics and digitalis, other drugs may be used including vasodilators and inotropic medication such as milrinone and amrinone (Furberg & Yusuf 1985; Tommaso 1986; Cohn 1988). The 5-year survival rate is reported to be between 64-68% (Pryor *et al.* 1987; Bounous *et al.* 1988), but could be even lower than 50% in patients with severe ventricular dysfunction (Alderman *et al.* 1983; Bounous *et al.* 1988).

As reviewed by Orie (1991), medical therapy has led to an improvement of symptoms and exercise tolerance of end-stage heart disease patients, but the drugs have had limited clinical trials. However, there have been, and there are on-going, extensive clinical trials of medical therapy for congestive heart failure as is evident from recent reviews (Magovern *et al.* 1993; Pfeffer *et al.* 1993; Swedberg 1993; Gaasch 1994). Several studies conclude that chronic therapy with angiotensin-converting enzyme (ACE)

inhibitors, which may reduce ventricular filling pressures and attenuate cardiac dilatation, offers the best choice of medical therapy.

However, one of the major problems with the use of pharmacotherapy is in diagnosis of CHF, as some patients may show significant systolic dysfunction - ejection fractions less than 40% - but be asymptomatic of heart failure (Pfeffer *et al.* 1993; Gaasch 1994). Thus, proper diagnosis and therefore appropriate treatment, as suggested by Gaasch (1994), should prolong survival. Furthermore, the effects of most of these drugs on survival remain controversial or even detrimental (Tommaso 1986; Cody 1988; Swedberg 1993). In spite of optimal pharmacological therapy, mortality remains high in CHF. Hence, the therapeutic application of medical therapy to heart assist is limited.

1.3.2. Heart transplantation

Heart transplantation is the most successful option so far for patients in terminal heart failure, and has led to a revolution in the management of end-stage heart disease patients (Griffith *et al.* 1986; Magovern *et al.* 1993). Cardiac transplantation now has 5- and 10-year survival rates of 66% and 52%, respectively, as stated in the official report of The Registry of the International Society for Heart and Lung Transplantation (1993). Just over half a decade earlier, the five-year survival rate was reported to be 55% (Schroeder & Hunt 1987). Thus the technique continues to be improved upon.

Nevertheless, cardiac tranplantation is plagued by a number of problems so that less than 1% of CHF patients benefit from it (Franciosca *et al.* 1983; Shaver 1988). The limited scope of applicability is mainly due to the shortage of donor hearts (Evans *et al.* 1986) that is further decreased by the relatively strict criteria applied in recipient selection (Schroeder & Hunt 1987). Hence, a large number of patients die while waiting for a donor heart. Although artificial devices are sometimes used as a "bridge" to transplant (Pennington *et al.* 1983), this may be problematic in the long run if more donor hearts were unavailable.

In addition, cardiac transplantation is expensive to the individual in terms of an altered lifestyle, the necessity for close proximity to a transplant hospital, and an extensive immunosuppressive drug therapy to prevent tissue rejection by the recipient. Anti-rejection drugs, such as cyclosporine, prednisone, steroids and azathioprine (Griffith *et al.* 1986; Uretsky *et al.* 1987; Magovern *et al.* 1993), often have serious side effects. Immunosuppressants, while helping the patient to survive on the one hand, may lead to premature death on the other. This is manifested as a constantly high incidence of accelerated coronary artery disease – a narrowing of the coronary arteries that supply the myocardium – reported to involve as many as 50% of all transplanted hearts by 5 years post-transplant (Griepp *et al.* 1977; Uretsky *et al.* 1987). Other problems include opportunistic infection and hypertension (Schroeder & Hunt 1987; Magovern *et al.* 1993).

Furthermore, surgeons are usually faced with the ethical dilemma of deciding who gets the limited hearts available. Should an available heart be given to the one who is first on the list, or should it be given to the younger person who may have more fruitful years following the transplant operation?

Despite its potential success, cardiac transplantation is relatively limited in its scope of applicability primarily because of the shortage of donor hearts. It is hoped that with more publicity and an increase in awareness, more hearts would become available. However, there is an upper limit to the number of hearts that could ever be made available for transplantation.

1.3.3. Cardiac xenotransplantation

Xenotransplantation, the transplantation of organs between species, offers a potential solution to the problem of lack of donor organs. The first cardiac xenotransplantation was carried out in a baby about two decades ago (Bailey *et al.* 1985). The major problem with xenografting, as cited in the American Medical Association's Council on Scientific

Affairs report (1985), is one of rejection (Pierson *et al.* 1994). Also, there is an ethical stigma to contend with (Caplan 1985).

White and Wallwork (1993) used molecular biology techniques to genetically engineer transgenic pigs that could potentially overcome rejection of their organs by humans. Despite a primate model (McManus *et al.* 1991) and state-of-the-art immunosuppression, heart xenografts have been unsuccessful (Hastillo & Hess 1993). Thus, cardiac xenotransplantation remains a conceptual alternative whilst the immunological problems of rejection persist.

1.3.4. Coronary artery bypass grafting

Coronary artery bypass grafting (CABG) is one of the surgical techniques commonly used on patients with extensive peripheral vascular disease, angina, and coronary heart disease (Spencer *et al.* 1971; Liao *et al.* 1992). CABG has been administered to a large number of patients with reasonable success (Alderman *et al.* 1983; Pryor *et al.* 1987; Bounous *et al.* 1988; Magovern *et al.* 1993): 3- and 5-year survival rates of 86% and 80%, respectively, have been achieved (Bounous *et al.* 1987). Such high survival values seen in recent years can be attributable, at least in part, to overall improvements in the surgical technique (Pryor *et al.* 1987).

In all patients, CABG led to improved left ventricular function, measured as an enhanced ventricular ejection fraction (Magovern *et al.* 1993). Paradoxically, the benefits of CABG are better for patients with worse left ventricular dysfunction (Alderman *et al.* 1983; Bounous *et al.* 1988); but the operative mortality rate in such patients is greater.

The improved symptomatic benefit following CABG may, nevertheless, be limited to a small group of patients, as such benefit has been shown in patients suffering primarily from angina and not in those with mainly heart failure (Alderman *et al.* 1983). Also, the problem of restenosis may be as high as 50%. Moreover, it is still not clear exactly what

the patient selection criteria are (Bounous *et al.* 1988; Magovern *et al.* 1993). Further work is thus needed to outline such criteria.

1.3.5. Mechanical devices

Mechanical assist devices and the total artificial heart (TAH) have been used successfully as a bridge to transplantation (Pennington *et al.* 1983; Hill 1988; Miller *et al.* 1990), providing temporary support of a failing heart until a donor heart becomes available. Such devices comprise the hemopump (Merhige *et al.* 1989), the intra-aortic balloon pump (IABP, Gewirtz *et al.* 1982; Fuchs *et al.* 1983; Kantrowitz *et al.* 1992), and several TAHs, which include the Baylor (Shiono *et al.* 1992; Orime *et al.* 1994) and the Jarvik versions (DeVries *et al.* 1984; Griffith *et al.* 1986).

1.3.5.1. The hemopump

The hemopump is an axial flow blood pump (Reul 1990; Butler *et al.* 1992) introduced by means of an intra-ventricular implantation into the aorta. It provides cardiac augmentation (Loisance 1990) by unloading the left ventricle (van Ommen 1990). This device has been in wide clinical use in Europe and the USA (Loisance 1990; Butler *et al.* 1992).

1.3.5.2. The intra-aortic balloon pump

The IABP has been used to relieve myocardial ischemia in patients with unstable angina pectoris by reducing the oxygen consumption of the myocardium (Gewirtz *et al.* 1982; Williams *et al.* 1982; MacDonald *et al.* 1987). However, controversy still abounds as to whether the IABP can actually increase coronary perfusion (Fuchs *et al.* 1983; MacDonald *et al.* 1987). Therefore, newer experimental approaches have involved combining the IABP with other modalities, resulting in better performance (Imanishi *et al.* 1989; Nanas *et al.* 1990). However, in a comparison of the hemopump with the IABP, van Ommen (1990) stated that both approaches lead to severe aortic and peripheral

vascular diseases. Because of the numerous requirements of a mechanical circulatory support system - flow performance, physiological compatibility, durability, reliability, size, and cost - these devices are continuously being improved.

1.3.5.3. The total artificial heart

Following the first clinical use of the TAH (DeVries *et al*, 1984), it has been employed successfully as a bridge to transplantation (Griffith *et al.* 1986; Hill 1988; El Oakley & Jarvis 1994). Much effort has been expended in developing TAHs that satisfy the requirements, stated above, of a circulatory support system (Imachi *et al.* 1991; Snyder *et al.* 1991; Shiono *et al.* 1992; Orime *et al.* 1994). However, the persistence of the associated problems of infective and thromboembolic complications (Griffith *et al.* 1988) has limited TAHs to mainly short-term use.

By and large, there are several problems associated with mechanical assist devices. In addition to infective and thromboembolic complications, mechanical assist devices are usually bulky, require an external power source, and the costs could be prohibitively high (Salmons & Salmons 1992). Thus the long-term efficacy of these devices is questionable.

1.3.6. Skeletal muscle assists

The adaptive transformation of skeletal muscle that follows increased use or chronic electrical stimulation (Salmons & Henriksson 1981; Pette & Vrbová 1985; Salmons 1971, 1980, 1987; Salmons & Stephenson 1989; Salmons & Jarvis 1991), through which the muscle can acquire a markedly increased resistance to fatigue (Salmons & Sréter 1976; Armenti *et al.* 1985; Mannion *et al* 1986; Jarvis *et al.* 1991a, b, 1994; Mayne *et al.* 1994), has revitalised interest in the possibility of diverting skeletal muscle from its normal function to perform in a cardiac assist role. There are two main approaches of harnessing skeletal muscle power for cardiac assistance, reviewed by Salmons and Jarvis (1992). These are summarized in Figure 1.2.

1.3.6.1. Category one assists

These assists preserve the natural endothelial lining of the patient's cardiovascular system. Firstly, there is cardiomyoplasty (Fig. 1.2A) in which intermittent compression is produced by skeletal muscle wrapped around the patient's left ventricle (Carpentier & Chachques 1985; Magovern 1985; Chagas *et al.* 1989; Hagege *et al.* 1990). Secondly, there is aortomyoplasty (Fig. 1.2B) which involves either directly wrapping the ascending (Chachques *et al.* 1990) or descending (Cummings *et al.* 1990; Pattison *et al.* 1991) aorta, or indirectly arranging for the muscle to inflate a cuff (Fig. 1.2C) placed around the vessel (Kochamba *et al.* 1988).

1.3.6.2. Category two assists

These assists, on the other hand, include an independent structure connected to the circulation so that an artificial surface is placed in contact with the blood. Skeletal muscle may be used to power a mechanical artificial heart or ventricular assist device through a mechanical (Fig. 1.2F), hydraulic (Fig. 1.2G), or electrical link (Fig. 1.2H) (Frey *et al.* 1986; Ugolini 1986). Alternatively, an auxiliary pouch-shaped or tube-shaped ventricle can be formed by wrapping skeletal muscle around a suitable mandrel, as explained in Section 1.1, resulting in an SMV (Fig. 1.2D) or an SMVT (Fig. 1.2E) that can be connected to the circulation as a synchronous or counterpulsatory assist (Acker *et al.* 1986; Anderson *et al.* 1991; Pochettino *et al.* 1991). Coronary blood flow that supplies oxygen to the myocardium occurs during diastole when the heart is filling up with blood. Synchronous assists, which function during cardiac systole (the pumping cycle of the heart), are primarily aimed at increasing ventricular stroke volume (Grandjean *et al.* 1991). Counterpulsatory assists, on the other hand, function during diastole and so may promote myocyte recovery by increasing coronary blood flow and thus oxygen supply to the myocardium while also reducing cardiac workload: such assists are therefore geared towards long-term cardiac support.

Figure 1.2. *A highly schematic representation of the approaches considered for biomechanical cardiac assist: (A) cardiomyoplasty, (B) aortomyoplasty, (C) compression of aorta by a cuff, (D) skeletal muscle ventricle, (E) skeletal muscle tube ventricle, (F) left ventricular assist device (LVAD) energised mechanically, (G) LVAD energised hydraulically, (H) LVAD energised electrically.* ***Diagrams reproduced from Salmons and Jarvis (1992).***

1.3.6.3. Advantages of skeletal muscle heart assist

The surgical use of skeletal muscle in cardiac assistance has some distinct advantages, which have been summarised by Salmons (1990). Firstly, skeletal muscle is fuelled by high-energy phosphate compounds, which it synthesizes from oxygen and nutrients brought to it via the circulation, thus eliminating the need for an external power source. Secondly, skeletal muscle is more efficient than any man-made actuator, requiring only a few electrical impulses to release large amounts of energy from the muscle. Although it may generate unwanted heat, this is probably less than the heat produced by man-made machines, and, in any event, the heat is easily dissipated by blood. Thirdly, the use of the patient's own muscle avoids the problems of donor shortage and rejection, which remain the major drawbacks of the otherwise successful heart transplant. Conceivably, skeletal muscle assists should be available at a fraction of the cost of alternative therapies. Finally, surgeons are relieved of the ethical dilemma of deciding who gets the limited donor hearts.

1.4. Earlier attempts of skeletal muscle cardiac assist

The idea of using skeletal muscle for cardiac surgery has been around for more than half a century, as reviewed by Thomas and Stephenson (1994). In 1931, De Jesus used the pectoralis muscle to repair a penetrating cardiac injury in a young man. Two years later, Leriche and Fontaine reinforced an infarcted canine myocardium by grafting a pectoralis major muscle to its surface. The graft was still viable after a few months, and was well incorporated into the surrounding myocardial tissue. Beck showed in 1935 that such grafts could even develop collateral blood vessels that helped to maintain their viability. In the early sixties, Petrovsky reported on the use of diaphragmatic pedicle grafts in the treatment of left ventricular aneurysms with good results. Thus, the contractile properties of skeletal muscles could be exploited for diverse purposes.

Kantrowitz and McKinnon were the first to exploit the contractile properties of skeletal muscle in a cardiac assist role (Kantrowitz & McKinnon 1959; Kantrowitz 1960). They wrapped canine left hemidiaphragm around the heart and stimulated the graft via the phrenic nerve. On stimulation of the graft in diastole, they observed a short-lived diastolic pressure augmentation. It was evident that muscle fatigue was a major obstacle to the use of skeletal muscles for long-term heart assistance (Nakamura & Glenn 1964; Kusaba *et al.* 1973; Spotnitz *et al.* 1974; Dewar *et al.* 1984). Skeletal muscle heart assist was therefore abandoned.

1.5. Resurgence of interest in skeletal muscle cardiac assist

In the late 1960s, it was discovered that long-term, low-frequency electrical stimulation caused transformation of fast to slow muscle. By the mid 1970s, it was established that transformation also led to the muscle becoming relatively free of fatigue and thereby providing a biological continuous source of power from the muscle mass of the body for heart assist. These discoveries, reviewed by Magovern (1991), were the culmination of work that had begun much earlier.

1.5.1. Muscle fibre types

More than three centuries ago, Stephano Lorenzini (1678) first commented on the different types of muscle in animals and referred to them as red and white muscles. About two centuries later, Ranvier (1873) observed a physiological difference, relating the red fibres to slow and the white fibres to fast contractions. By 1919, Bullard was able to show that most skeletal muscles consist of light, dark, and intermediate fibres. Working on human muscles in 1962, Engel favoured a two-fibre type system based on the myofibrillar ATPase, type I having a low and type II a high ATPase activity. These works led Schiaffano *et al.* (1970) to conclude that the variable structural pattern of muscular fibres is related to two distinct physiologic parameters: speed of contraction and fatigue resistance. Today, biochemical, histochemical techniques, and physiological

measurements, are used to classify muscle fibres. This classification is summarised in Table 1. The differences stated in this table are very broad; for example, not all species show the differences in fibre diameter.

Table 1.1. *Properties of skeletal muscle fibre types.* **Adapted from "Calcium in Muscle Contraction" by Rüegg, J.C. (1992).**

Fibre type	IIB	IIA	I
Colour	White	Red	Red
Contraction	Fast twitch	Fast twitch	Slow twitch
Fatigue resistance	Low	Medium	High
Metabolism	Glycolytic	Glycolytic and oxidative	Oxidative
Lactic dehydrogenase	High	Medium or high	Low
Succinic dehydrogenase	Low	Medium	High
Fibre diameter	large	intermediate	small
Z-line thickness	narrow	intermediate	wide
Glycogen content	high	intermediate	low
Capillaries	few	many	many
Myoglobin content	low	high	high

1.5.2. Energy for muscle contraction

Force generation by skeletal muscle, by cross-bridge formation and dissociation, and the active Ca^{++} ion transport systems involved in the relaxation phase, demand energy, which is generated ultimately through aerobic and anaerobic respiration. During contraction, energy is released by the hydrolysis of adenosine triphosphate (ATP) to adenosine diphosphate (ADP) and inorganic phosphate (Pi):

$$ATP \xrightarrow[\text{actomyosin ATPase}]{} ADP + P_i \qquad (1.1)$$

However, the used ATP is rapidly restored by the rephosphorylation of ADP using phosphocreatine (PCr) in a reversible reaction in the presence of the enzyme creatine phosphokinase (CPK):

$$ADP + PCr \xleftrightarrow{CPK} ATP + Cr \qquad (1.2)$$

One of the end products of this reaction is creatine (Cr). The effective energy production reaction, therefore, is the hydrolysis of PCr. At the end of contraction, however, the used PCr must be restored in a recovery process. This uses the produced Cr and generates heat (recovery heat) in a complex set of chemical reactions which also use oxygen, glycogen, and fatty acids from foodstuffs. The resulting end products of these reactions which take place in the mitochondria are PCr, ready for the next contraction, and water and carbon dioxide (CO_2), which are eliminated as waste.

The complex series of metabolic reactions which produce ATP for muscle contraction by rephosphorylation of ADP is represented by the glycolytic pathway, which comprises aerobic and anaerobic glycolysis. The Embden-Meyerhof pathway (McMahon 1984), which is common to both aerobic and anaerobic metabolism, is a sequence of reactions that use glucose, derived from stored glycogen, to produce pyruvic acid. Nicotinamide-adenine dinucleotide (NAD) carries hydrogen as NADH to the final stage, the cytochrome chain. Aerobic metabolism, however, has an extra pathway called the tricarboxylic acid cycle (TCA cycle or Krebs cycle) in which pyruvic acid and fatty acids from foodstuffs enter a circuit of reactions. CO_2 leaves this circuit as a waste product. The rephosphorylation of ADP takes place in the cytochrome chain in which molecular oxygen combines with electrons brought in by NADH and protons to form water.

Because the ATP concentration in resting muscle fibre is limited (about 0.1 μM, Rüegg 1992), the metabolic pathways above, which are controlled by various metabolic enzymes and are different for fast and slow muscle fibres, generate ATP during muscle

contraction. Slow fibres get their energy largely from aerobic oxidation, particularly of fats and fatty acids. These fibres therefore contain abundant mitochondria and are served by numerous capillaries, which maintain the necessary supply of nutrients and oxygen. The oxygen is transported by the many myoglobin molecules (Wittenberg & Wittenberg 1989). On the other hand, fast muscle fibres obtain their energy for contraction mainly from anaerobic glycolysis, and are supplied with few mitochondria and a much less extensive capillary network. Furthermore, fast fibres have a high glycogen content required for glycolysis. Because ATP hydrolysis in fast fibres takes place in the absence of oxygen, whose limited rate of supply may limit the rate of energy supply and thus retard contraction speed in slow fibres, fast fibre contractions result in rapid and high force development. However, such powerful contractions are usually accompanied by a build-up of lactic acid, the hallmark of muscle fatigue. Thus, fast fibres normally have long quiescent periods between contractions during which glycogen and other reserves are replenished.

1.5.3. Mechanical properties of skeletal muscles

Whole anatomical skeletal muscle consists of regularly arranged contractile cells (muscle fibres), a meshwork of elastic connective tissue and the elastic tendons that attach the muscle to bone. These various components interact to impart to the muscle complex mechanical properties.

1.5.3.1. The sarcomere

The contractile muscle organelle, the myofibril, runs from one end of the muscle fibre to the other and is subdivided by partitions, called the Z-discs, which run right across the myofibril; the segment between two Z-discs is called the sarcomere. The sarcomere is the contractile unit of muscle and composes mainly of two contractile protein filaments, actin and myosin. The actin (thin) and myosin (thick) filaments are arranged in an interdigitated fashion as shown in Figure 1.3.

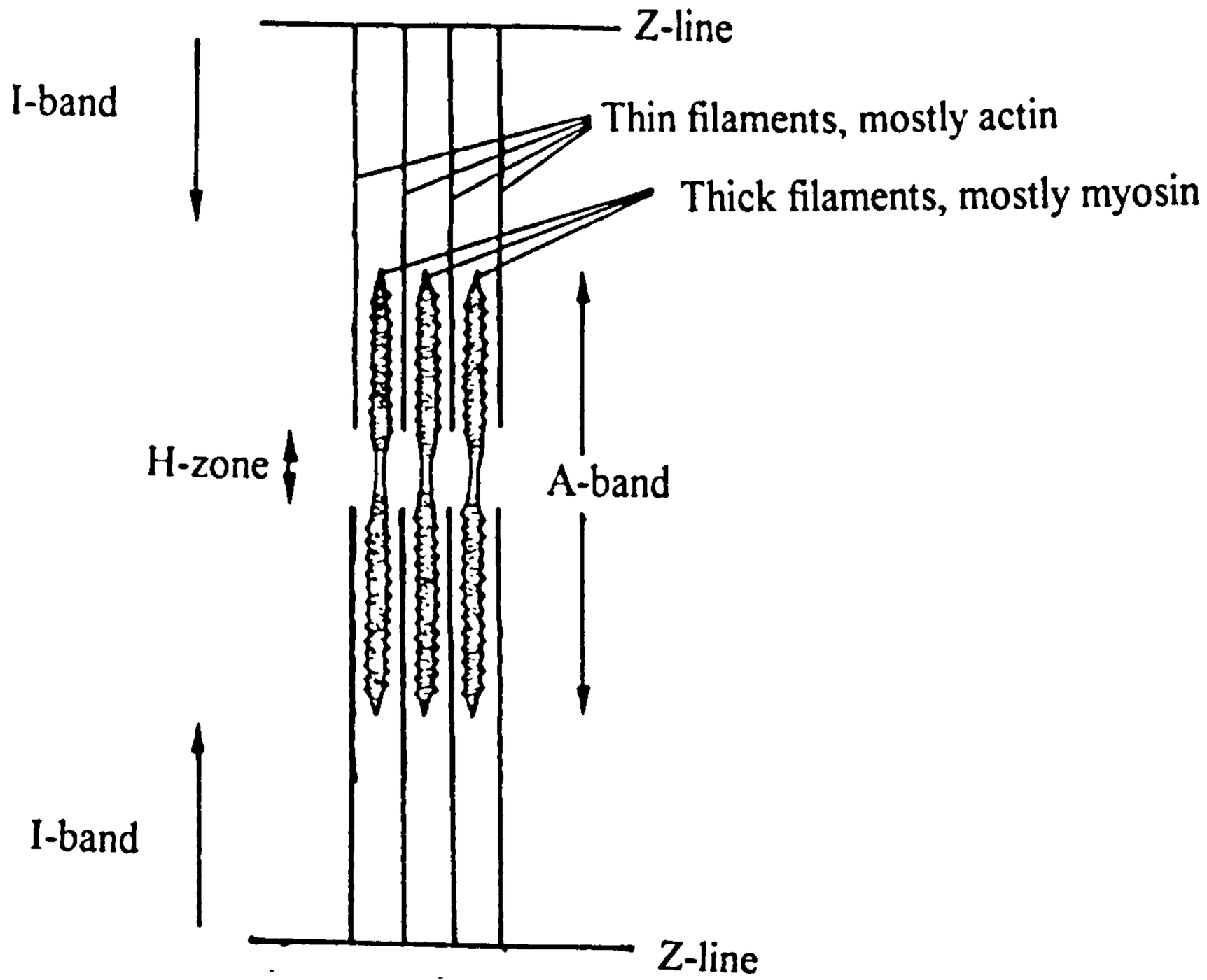

***Figure 1.3**. The sarcomere, showing the interdigital arrangement of the thick and thin filaments. Diagram adapted from Wilkie, D.R. (1976).*

The entire length of the thick filaments is called the A-band. The actin and myosin filaments overlap in the centre of the sarcomere, over most of the A-band, to form an anisotropic region, which is birefringent and thus has a high refractive index. In the middle of the A-band is a less electro-dense region, the H-zone, consisting only of myosin filaments. The rest of the sarcomere consists of actin filaments only, and is called the I-band or isotropic region. Except for the pseudo-H-zone, there are projections sticking out of the sides of the myosin filaments called cross-bridges (Huxley 1960; Haselgrove & Reedy 1978), which are important in force production in muscle (Huxley & Simmons 1971).

The sarcomere also contains functional and structural proteins. Tropomysin and the three troponins (TnC, TnT and TnI) are functional constituents of the thin filaments; tropomyosin blocks myosin binding sites until caused to move by Ca^{++} binding to troponin C. There are several structural proteins, including titin, which links the myosin

filaments to the Z line, nebulin, α-actinin, desmin, spectrin and dystrophin (Jones & Round 1990).

1.5.3.2. Muscle force generation

Force generation by muscle is believed to result from the movement of the cross-bridges, enabling the thick and thin filaments to slide over one another in the overlap region (Huxley & Hanson 1954; Huxley & Niedergerke 1954; Huxley 1957); this is the sliding filament theory of muscle contraction. The movement of the cross-bridges requires energy which is obtained from the hydrolysis of ATP (see above). The rate and extent of force generation depends on several parameters which include the nature of the activation, the nature of the myosin heavy chain, the overlap of the filaments or muscle length, and the temperature.

1.5.3.3. The force-frequency relationship

The response to activating a muscle with a single stimulus, called a twitch, is a single transient rise in tension; the time from the start of the transient to peak force is called the twitch contraction time (CT), and the time from this peak force to half its value is the half-relaxation time (0.5RT). The time course of the twitch response is dependent on both the muscle temperature (Ranatunga 1982; Faulkner *et al.* 1990) and the strength of the stimulus. If the stimulus passes a threshold value, the response increases monotonically as more and more muscle fibres are recruited until all the fibres are activated. At this point, an increase in stimulus intensity results in no further increase in force response; this stimulus level is called maximal stimulation, and is predominantly used for experimental purposes in order to produce repeatable responses from the whole muscle.

Summation of the force response occurs when a second stimulus is added before the response to the first has completely decayed. When stimuli are repeated regularly at a sufficiently high frequency, a smooth tetanus results, with force maintained at a high level

until the stimulus ceases. However, the high force level may start to drop before the end of the stimulus due to muscle fatigue. Muscle force output therefore increases with increasing frequency of stimulation, but levels out shortly after the tetanic fusion frequency and may even drop slightly at very high frequencies, the latter response due to a phenomenon defined as the sag property of muscle (Burke *et al.* 1976).

1.5.3.4. Mechanical components in muscle

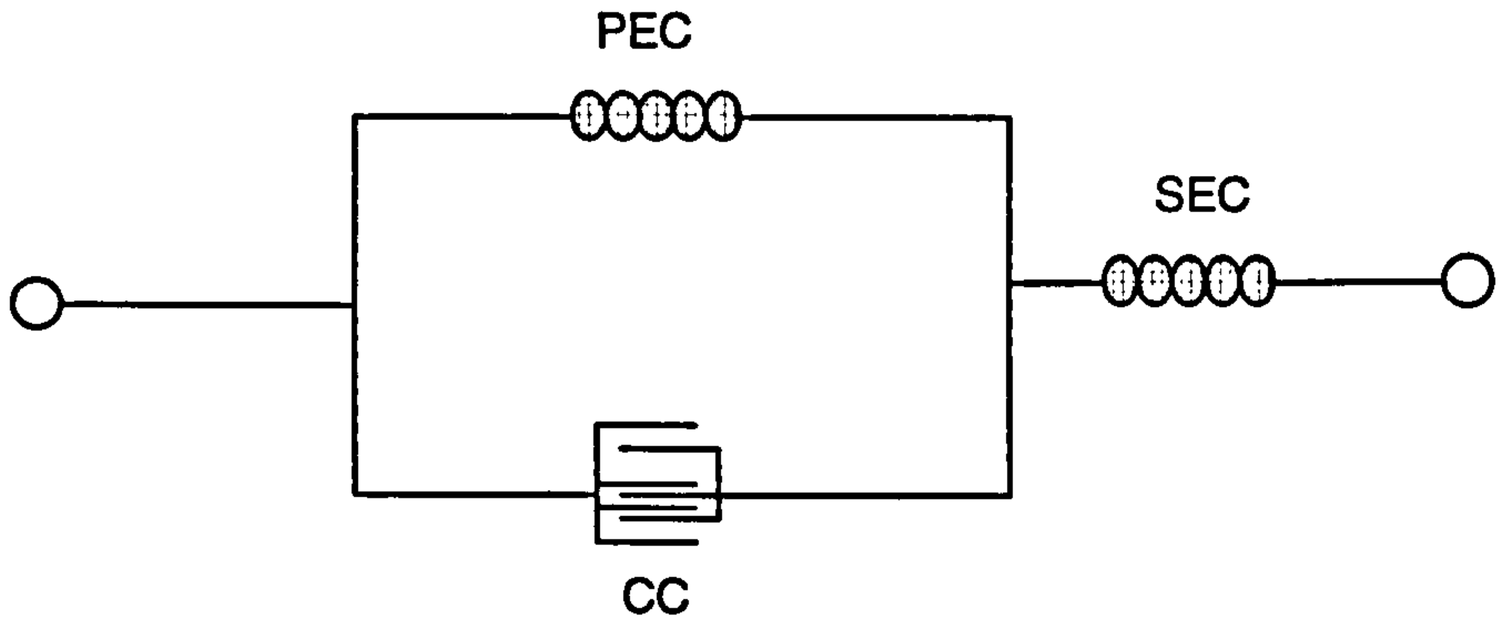

Figure 1.4. *Gross features of whole muscle mechanics. The three-component model for muscle described by A.V. Hill. CC = contractile component; PEC = parallel elastic component; SEC = series elastic component.*

Figure 1.4 shows the mechanical components in muscle. The contractile component (CC) is in parallel with the connective tissue, which is represented as a parallel elastic component (PEC). The tendons contribute a series elastic component (SEC). Thus, skeletal muscle can be regarded mechanically as a three-component system (Hill 1938).

1.5.3.5. The force-length relationship

Muscle can be viewed as having two states, the resting and the active states (Hill 1938). Resting muscle possesses a 'pseudo-elasticity' that is responsible for the increasing stiffness of the passive force-length curve. This resting non-linear elasticity is due primarily to the meshwork of connective tissue and to titin, which become tensed at high extension, thereby adding their spring stiffness in parallel (PEC). The elastic tendons that attach the muscle to bone add a series component to the output. When a muscle is stimulated at increasing lengths the CC develops tension, which increases from zero to a

peak value and then falls back to zero in a bell shape. Thus, there is a length of muscle at which the force production is maximal; this is the optimal length, Lo.

Fung (1967) showed that many collagenous tissues, including tendon and resting skeletal muscle, obey a similar exponential relationship between stress and strain. This idea was applied to the passive force-length curve of papillary heart muscle of a rabbit (Pinto & Fung 1973) to obtain the following relationship:

$$\sigma = \mu \exp\left(\alpha \frac{L}{L_o}\right) - \beta \qquad (1.3)$$

where σ is the stress in the cross-section of the muscle of rest length Lo, stretched to a new length L; α, β and μ are constants. This equation can be rearranged to give the force (F), as stress is the force per unit area, so that

$$F = A \exp\left(B \frac{L}{L_o}\right) - C \qquad (1.4)$$

where A, B and C are constants. The above equation can thus be used to fit the passive force-length curve of muscle.

1.5.3.6. The force-velocity relationship

Using heat measurements, Hill (1938) showed that a supramaximally stimulated shortening muscle liberated energy both as heat and external work. The shortening heat was independent of muscle load, but inversely proportional to the rate of energy liberation. In a shortening muscle, the external work is the product of the shortening and the load, which is therefore inversely related to the rate of energy liberation. Hence, the force exerted by shortening muscle is smaller the faster the shortening until at a certain speed it exerts no force at all. This behaviour is also partly explained by the inertia of the load: the greater the load, the greater the inertia that has to be overcome, resulting in slower muscle contraction for larger loads.

Following the experimental measurements of the force-velocity curve by Fenn and Marsh (1935), which showed a non-linear relationship, Hill (1938) proposed an empirical relation between force and velocity: the force is related to the velocity in a hyperbolic manner such that

$$(P+a)(V+b)=b(Po+a) \tag{1.5}$$

where Po is the isometric tension (a force against which the muscle neither shortens nor lengthens), V is the velocity, P is the force, and a and b are constants; Po, a, and b are called the dynamic constants of muscle. Equation (1.5) can be rearranged to give the velocity as

$$V = b\,\frac{(Po-P)}{(P+a)} \tag{1.6}$$

The Hill equation is found to describe nearly all muscle types including cardiac, smooth, skeletal and even contracting actomyosin threads (McMahon 1984).

Because of the nature of the force-velocity curve, the mechanical power output, which is the product of the force and the velocity (P×V), reaches a maximum when the force on the muscle and the maximum speed of contraction are between one-quarter and one-third of their maximal values. Therefore, muscle can function most efficiently if such loads are presented to it.

Fenn (1923) had proposed that a biochemical reaction controlled the rate of energy release and thus the mechanical properties of muscle. The force-velocity curve is therefore an expression of the fact that force production in a muscle is linked to the rate of energy production. Consequently, the force-velocity relationship is a functionally fundamental property of muscle.

1.5.4. Adaptive transformation of skeletal muscle

Long-term electrical stimulation of muscle results in changes in its physiological, morphological, and biochemical properties. These changes can also result, though to a lesser extent, from exercise. Since terminally differentiated skeletal muscle is able to further differentiate, it is said to show plasticity of behaviour, as explained below. The overall beneficial effect of chronic electrical stimulation of muscle is an increase in fatigue resistance.

1.5.4.1. History of the development of skeletal muscle plasticity

The solution to the problem of skeletal muscle fatigue, which had thwarted previous attempts at using skeletal muscle for circulatory assist, dates back to the work of Buller *et al.* (1960a, b). Cross-innervation of the motoneurones to fast and slow muscles of the cat hindlimb resulted in the fast muscles becoming slower and the slow muscles becoming faster. These observations were interpreted as due to chemical 'trophic' substances transported by the motor nerves, the fast nerve thus exerting a quickening influence and the slow nerve a slowing influence on the muscles. The implication was that fibre type composition in fully developed muscle could be altered, introducing the important concept of muscle plasticity. Dubowitz (1967) observed that cross-innervation of mammalian skeletal muscle had a dramatic influence on its histochemical and physiological properties, but he could not demonstrate any significant difference in the ATPase activities of the slow and fast muscles. However, pronounced but incomplete biochemical changes following cross-innervation were observed by Sréter *et al.* (1975).

Salmons & Vrbová (1969) discovered that muscles of the fast-twitch, fatiguable type subjected to a chronic increase in aggregate activity by indirect electrical stimulation underwent complete fibre type transformation: the transformed fibres acquired all the physiological attributes of a slow-twitch, fatigue-resistant muscle (see Table 1.1). Following this discovery, Salmons and Sréter (1976) provided evidence to suggest that

the changes associated with cross-innervation may reflect a capacity of skeletal muscle to respond adaptively to different functional requirements. They showed the influence of impulse activity on skeletal muscle type transformation by using long-term electrical stimulation both to reproduce and to oppose the effects of cross-innervation. Fast to slow fibre transformation is also effected by chronic phasic high-frequency stimulation (Sréter *et al.* 1982; Hudlická *et al.* 1982; Kernell *et al.* 1987a, b), provided the aggregate number of pulses delivered to the muscle matches that of a low-frequency chronic stimulation regime. Also, prolonged endurance training in humans and other animals leads to similar changes, although to a lesser extent (Gollnick & King 1969; Andersen & Henriksson 1977; Jansson *et al.* 1978; Green *et al.* 1984; Pette 1986). Thus, fast-twitch, fatiguable muscle fibres stimulated chronically with electrical impulses could acquire all the physiological, biochemical and morphological attributes of slow-twitch, fatigue-resistant fibres.

1.5.4.2. Effects of chronic electrical stimulation of muscle

There are comprehensive reviews of the effects of chronic electrical stimulation on the properties of skeletal muscle (Salmons & Henriksson 1981; Pette 1984; Salmons 1990). The physiological and morphological changes that take place following long-term electrical stimulation will be explained here at some length. However, the associated biochemical changes will be presented only briefly.

1.5.4.2.1. Physiological changes

These include alterations in mechanical properties, blood flow and oxygen consumption. The end result is a muscle that can utilize oxygen more efficiently and is fatigue-resistant.

1.5.4.2.1.1. Mechanical properties

In terms of the mechanical behaviour of the muscle, the overall response to long-term stimulation is a reduction in contractile speed (Salmons & Vrbová 1969; Al-Amood *et al.*

1973; Pette *et al.* 1973), manifested as a marked prolongation of the contraction and relaxation phases of the isometric twitch, a higher twitch:tetanus ratio and a lower fusion frequency for tetanic stimulation (Salmons & Sréter 1976). There is also a marked increase in fatigue resistance (Salmons & Sréter 1967; Hudlická *et al.* 1977; Armenti *et al.* 1985; Mannion *et al* 1986; Jarvis *et al.* 1991a, b, 1994; Mayne *et al.* 1994).

1.5.4.2.1.2. Blood flow and oxygen consumption

Hudlická *et al.* (1977) observed little effect of chronic low-frequency stimulation on resting blood flow, O_2 or glucose consumption. Glycogen content increased constantly and was observable after only a couple of days. In a short period of vigorous isometric contractions, however, they observed a markedly greater blood flow in the chronically stimulated muscles compared to the unstimulated controls. This contrasted with blood flow observations by Mannion *et al.* (1989), who showed that blood flow in chronically stimulated muscles during a fatigue test was significantly lower than that in unconditioned control muscles. They further showed that blood flow in the former were less affected by collateral blood vessel ligation. However, both sets of investigators established that the chronically stimulated muscles were less susceptible to fatigue (Hudlická *et al.* 1977; Mannion *et al.* 1989). This, coupled with the limited effect of collateral vessel ligation on blood flow, is advantageous to the use of chronically stimulated muscles for cardiac assist.

1.5.4.2.2. Changes in fibre type and muscle bulk

Walker (1982) showed the normal fibre type distribution in rabbit TA to be 58% type IIB, 38% type IIA and 4% type I. At the molecular level, long-term electrical stimulation of this muscle for up to six weeks results in transformation from IIB to IIA to I, i.e. conversion of fast glycolytic to fast oxidative to slow fibres (Sréter et al. 1974; Pette *et al.* 1976; Kernell *et al.* 1987a; Staron & Pette 1987; Hudlická & Price 1990).

Muscle wet weight in low-frequency stimulated muscles decreases to about 50% of the contralateral controls after 6 weeks of stimulation (Pette *et al.* 1976; Salmons & Henriksson 1981; Eisenberg and Salmons 1984; Jarvis *et al.* 1991b). Such a decrease has been shown to result from a reduction in the cross-sectional area of individual fibres, with the total number of fibres remaining the same (Pette *et al.* 1976; Salmons & Henriksson 1981). Muscle mass can, however, be maintained with other stimulation patterns (Ferguson *et al.* 1989; Jarvis *et al.* 1991b), and gain in mass may even occur following high-frequency burst stimulation (Kernell *et al.* 1987a).

1.5.4.2.3. Morphological changes

Structural changes occur as part of transformation towards a slower, oxidative fibre type. These include changes in the capillaries, myofibrillar structure and organelles important in muscle contraction. However, the functional significance of some of these changes, such as changes in the size of the Z-band, are not certain. Overall, these changes are believed to result in muscles better able to contract for long periods of time.

1.5.4.2.3.1. Capillaries

Four weeks of low-frequency stimulation results in a doubling of the capillary density (number of capillaries per mm^2) in various muscles (Brown *et al.* 1976; Myrhage & Hudlická 1978; Hudlická *et al.* 1982, 1987; Hudlická & Tyler 1984; Hudlická & Price 1990). Increased numbers of capillaries facilitate blood flow (Hudlická *et al.* 1977), and may be elicited by factors associated with elevated blood flow such as shear stress or wall tension (Hudlická *et al.* 1984). The consequence is a muscle with an adequate blood supply to support aerobic respiration, and thus an increased fatigue resistance to sustained activity.

1.5.4.2.3.2. Myofibrillar structure

At the ultrastructural level, fast-to-slow fibre type transformation following long-term electrical stimulation results in thicker Z discs. They thus become similar to those seen in slow muscles (Salmons *et al.* 1978; Eisenberg & Salmons 1981).

1.5.4.2.3.3. Organelles

The volume density of mitochondria in stimulated muscles increases (Eisenberg & Salmons 1981; Reichmann *et al.* 1985; Hoppeler *et al.* 1987), while fractional volumes of T-tubules, terminal cisternae, and sarcoplasmic reticulum (SR) decrease, reaching typical levels of slow muscle after only two weeks of stimulation (Eisenberg & Salmons 1981). The Golgi apparatus enlarges and the amount of rough endoplasmic reticulum increases: these changes would be consistent with an increased rate of protein synthesis. Functional changes affecting Ca^{++} transport by the SR are also observed (Sréter *et al.* 1974; Salmons & Sréter 1976; Salmons 1981, Heilmann *et al.* 1981) - see below.

1.5.4.2.4. Biochemical changes

Biochemical changes accompanying fast-to-slow transformation are both qualitative and quantitative. On the whole, there are increases in protein levels, indicative of protein synthesis (McGurk & Salmons 1982; Pette 1984; Salmons *et al.* 1987); however, the total amount of protein may be lower due to the more than 50% mass reduction. Also, there are elevations of levels of enzymes for oxidative metabolic pathways and a decrease in those for glycolytic pathways (high-energy phosphate metabolism and glucose/glycogen metabolism). These changes were reviewed by Pette (1984), and may be regarded as a "white to red" metabolic transformation.

1.5.4.2.4.1. Sarcoplasmic reticulum

Concomitant with decreases in fractional volumes of SR are decreases both in the initial rate and in the maximum capacity of Ca^{2+} uptake by the SR (Salmons & Sréter 1976;

Heilmann & Pette 1979; Heilmann *et al.* 1981; Mabuchi *et al.* 1982). There are also decreases in calsequestrin (Wiehrer & Pette 1983), the main Ca^{2+}-binding protein within the SR, and parvalbumin (Klug *et al.* 1983a, b), a major Ca^{2+}-binding protein in the cytosol, especially in fast-twitch fibres (Celio & Heizmann 1982). These reductions result in a lowered capacity of Ca^{2+}-binding. Further changes include the lowering of the amount and activity of the Ca^{2+}-pumping ATPase (Ramirez & Pette 1974; Salmons & Sréter 1976; Heilmann & Pette 1979; Heilmann *et al* 1981; Klug *et al.* 1983b; Wiehrer & Pette 1983) and its phosphorylated intermediate (Heilmann & Pette 1979). The overall effect is a longer-lasting Ca^{2+} transient in the cytosol following excitation, resulting in an increase in the twitch:tetanus ratio, the time to peak contraction and the half-relaxation time of chronically stimulated muscle.

1.5.4.2.4.2. Structural proteins

The interaction between actin and myosin, the two major structural proteins of muscle, results in muscle contraction and thus force production. Actin comprises several isoforms but only one of these is present in normal mammalian skeletal muscle, the other forms being found in cardiac muscle and non-muscle tissues. Myosin is a hexameric molecule composed of two heavy chains (MHC), which are alpha helical rods with a large globular head region, and four light chains (LC), which are associated non-covalently with the head region. Sodium dodecyl sulfate polyacrylamide gel electrophoresis (SDS PAGE) has been predominantly used (Giometti 1981; Mabuchi *et al.* 1982; Bar & Pette 1988) to show that both fast and slow isomyosins contain several types of light chain (LCF and LCS) and heavy chain (MHC1 and MHC2) (Pette & Vrbová 1985; Buckingham 1985).

Chronic electrical stimulation results in changes in myosin isoforms. Sréter *et al.* (1975) first showed that N^{τ}-methylhistidine, an amino acid only present in fast MHC, decreased with stimulation. Cessation of stimulation, however, led to its recovery back to normal levels (Sréter *et al.* 1973; 1975). Stimulation also results in the complete replacement of

the fast LC by the slow isoforms (Salmons & Sréter 1976; Seedorf *et al.* 1983; Brown *et al.* 1983). Although myosin isoforms are characteristic of different muscle types, there is a co-existence of isoforms in individual fibres during transformation (Pette & Scnez 1977; Rubinstein *et al.* 1978). This, together with the fact that no neonatal heavy chain was detectable during transformation (Brown *et al.* 1983), is evidence of the direct transition between adult myosin isoforms during transformation.

1.5.4.2.4.3. Protein levels and nucleic acids

The changes in phenotypic expression evoked by chronic stimulation may result from both qualitative and quantitative alterations of transcriptional activity. During electrical stimulation, total RNA content initially trebles but then settles at a two-fold higher level than control muscle (McGurk & Salmons 1982; Heilig & Pette 1983; Joplin *et al.* 1987). This level is similar to that of normal slow-twitch muscle, such as *m. soleus* (Heilig & Pette 1983; Pluskal & Sréter 1983). As indicated above, the levels of some proteins rise while others fall during stimulation. DNA levels double during the first 3 weeks of electrical stimulation (McGurk & Salmons 1982; Pette 1984; Salmons 1987; Joplin *et al.* 1988). The levels of mRNA encoding certain genes were shown to be concurrent with the changes observed in the genes (Williams *et al.* 1986, 1987; Brownson *et al.* 1988).

Chronic stimulation also leads to qualitative alterations in gene expression (Heilig & Pette 1983; Pluskal & Sréter 1983; Heilig *et al.* 1984). In vitro studies by Brownson *et al.* (1988) showed the co-expression of fast- and slow-type myosin light chains due to the presence of the respective mRNA species in stimulated muscles. Such qualitative change in transcriptional activity was confirmed *in vivo* by Pluskal and Sréter (1983). Therefore, chronic electrical stimulation is associated with phenotypic modulation by specific switching on and off of gene expression, bringing about the transition from fast to slow fibres.

1.5.4.2.5. Summary

The changes in the myosin isoforms result in less rapid cycling of the propulsive cross-bridges that form between thick and thin filaments to effect a contraction (Rüegg, 1987). Consequently, the muscle can develop substantial forces at much lower activation frequencies with a reduced energy cost (Crow and Kushmerick 1982). In effect, ATP production can match ATP utilization in continuous working conditions (Clark *et al.* 1988).

In conclusion, the stimulated muscle develops an increased capacity for oxidative phosphorylation as well as acquiring more favourable bioenergetics of contraction through changes in calcium kinetics and myosin isoforms. Such muscles therefore show more efficient coupling between the development and maintenance of force and the consumption of oxygen (Acker *et al.* 1987c).

1.5.4.3. Effects of cessation of stimulation

Transformed muscle fibres revert to their natural fast state following cessation of chronic stimulation or detraining, despite a different time course (Eisenberg *et al.* 1984; Brown *et al.* 1985, 1989; Salmons 1990; Kernell & Eerbeek 1991). Mechanical properties, such as twitch speed and maximum tetanic force recover within 4 weeks of the cessation of stimulation. Fatigue resistance also reverts over a prolonged time-course to that of a fast-twitch muscle (Brown et al. 1989), though it stays slightly enhanced (Kernell & Eerbeek 1991). At an ultrastructural level, the T-system increases to levels typical of fast-twitch muscle by 4 weeks, with full recovery by 12 weeks, and the wide Z-bands decrease to a thickness characteristic of fast-twitch fibres in the same time period (Eisenberg *et al.* 1984). The mitochondrial volume remains stable. The recovery of the muscle characteristics is further evidence of an adaptive nature of skeletal muscle (Salmons 1971, 1980; Salmons & Henriksson 1981; Salmons & Stephenson 1989) whereby sustained levels of use favour differentiation of properties at the slow, fatigue-resistant end of the

spectrum, while absence of such activity results in oppositely directed differentiation to a native fast state.

1.5.4.4. Adverse effects of transformation

Although long-term electrical stimulation of muscle results in the much desired fatigue resistance, there are accompanying changes that are detrimental to the use of the muscle for heart assist. First, muscle conditioning reduces the maximum power available from the muscle (Salmons & Jarvis 1990a, 1990b, 1991) and thus the power available for assistance. Secondly, transformation results in slowing of the relaxation and contraction of the muscle (Salmons & Vrbová 1967, 1969). In an application such as cardiomyoplasty, in which muscle is wrapped around the heart, a muscle contracting and relaxing slowly will be unable to follow the myocardial wall movements precisely. The consequence is incomplete reinforcement during systole and the possibility that filling may be restricted during diastole. Slowness is also detrimental in other forms of skeletal muscle cardiac assist, for it reduces power-generating capacity substantially and poses analogous difficulties of synchronization with the cardiac cycle (Salmons & Jarvis 1992). Thirdly, muscle transformation results in loss of muscle mass, which is critical in the provision of adequate long-term power (Geddes & Badylak 1991) for cardiac assistance. Nonetheless, the power available from such muscle is still sufficient to be exploited in heart assist (Salmons & Jarvis 1990).

1.6. The power capability of skeletal muscle

Analog computer modelling studies, short-term acute animal studies, and chronic animal studies have shown that skeletal muscle has the potential to carry out adequate work to be harnessed either for circulatory assist or for other prostheses, as reviewed by Badylak (1991). With respect to ventricular assist devices, the term "work" refers to the movement of a given volume of fluid of known weight against a known resistance or pressure head; thus work is the product of volume and a pressure head, or for a vessel of

given cross-sectional area simply a force multiplied by a displacement, and is measured in joules (J) or newton-metres (Nm). In the left ventricle, for example, the work done in ejecting a given volume of blood can be calculated if the end-diastolic pressure (preload) and the arterial pressure (afterload) are known. Power, on the other hand, is the rate of doing work, i.e. work done per second, and is measured in watts (Js^{-1}).

Geddes *et al.* (1990, 1991) have developed empirical equations that allow calculation of input and output power from a skeletal muscle arranged to function as a cardiac assist. The output power (W) is evaluated as

$$\text{Output power} = 23.5 \times 10^{-4} (P_m - PDP)F \qquad (1.7)$$

where P_m is mean arterial pressure (mmHg) and PDP is the pouch diastolic pressure (mmHg); F is the pouch output flow (litres/min). The input power (W) is calculated as 20.1 times the oxygen consumed by the muscle (ml/s), which is equal to the product of the capillary blood flow and the A-VO_2 (arteriovenous oxygen) difference across the muscle. Bard (1956) reported that basal O_2 consumption of skeletal muscle is about 0.156 ml O_2/min per 100 gm of muscle; the O_2 consumption rises to 12 ml/min per 100 gm with maximum exercise. Using equation (1.7), and assuming the above values of oxygen consumption, the output and input powers of a skeletal muscle providing heart assist, and thus its efficiency (the ratio between the output and input powers), can be calculated.

Geddes *et al.* (1990, 1991) computed the output power of a typical 350 gm heart at rest at about 3.5 W/kg (equivalent to 1.23 W) from an input power calculated as 9.799 W; this represents an efficiency of approximately 12%, a typical value for a chemical engine. Geddes *et al.* (1992) also showed that linearly contracting canine latissimus dorsi, gastrocnemius and triceps arranged to compress a pouch could attain linear efficiencies of up to 27.3%. It was concluded that skeletal muscle could produce 10-15 mW per gram

power (Geddes *et al.* 1990, 1991), more than three-fold the power output of a resting heart.

Despite this apparently high instantaneous power output of skeletal muscle compared to cardiac muscle, the ability of the former to produce sustainable power is limited. Moreover, the efficiency of energy conversion of the skeletal muscle may be lowered if the fluid pressure against which it functions increases its intramural pressure thereby reducing blood flow to the capillaries, and hence its input power. Therefore, there must be enough skeletal muscle mass to provide energy in W/kg compatible with continuous work for an indefinite period. The above power levels must therefore be interpreted with caution.

An electrical model of the circulation with an interposed SMV, and computer models of an SMV (Babbs *et al.* 1984, Voytik *et al.* 1990), have predicted a 10 W/kg power output by skeletal muscle. If a 10% efficiency is assumed, this leads to a 1.0 W/kg power generation. Also, constructed SMVs have shown sustained power outputs of 1.1 mW/g (Geddes *et al.* 1990, 1991). Considering the 3.5 mW/g power output of a resting heart, a skeletal muscle output of 1.1 mW/g is equivalent to 31% of the power required by a healthy heart for normal cardiac output.

Furthermore, Acker *et al.* (1986, 1987b, c) demonstrated that SMVs constructed from canine LDs could produce between 30% and 50% of the stroke work of the left ventricle after several weeks of continuous pumping. Chronic animal studies by Salmons and Jarvis (1990) showed that even though the maximum power output of stimulated muscle is greatly decreased, enough is retained to meet the specifications of a circulatory assist device; however, such a device must be carefully designed to ensure that the muscle exerts force against a suitably matched load at all times. Fatigue tests from this work also suggested that the maximum power output levels of stimulated muscles could be maintained indefinitely without decrement. Therefore, electrically stimulated autologous

skeletal muscle offers a potential power source for cardiac assistance with the capability of assuming up to 50% of the natural heart's workload, provided the muscle is appropriately loaded.

1.7. The latissimus dorsi flap

Latissimus dorsi (Mathes & Nahai 1982; McCraw & Arnold 1986) is the muscle of choice for cardiac assist. It is a large, powerful muscle whose blood and nerve supplies enter it at the upper end, allowing relative freedom of mobilisation of the whole muscle (Olivari 1976). Because the LD is non-essential, loss of function resulting from its removal is limited (Laitung & Peck 1979). Its flat shape allows easy manipulation into a pouch, and its naturally superficial position in the body facilitates dissection of its attachments.

The LD has approximately the same mass as the left ventricle (Mannion *et al.* 1986); it should, theoretically, be possible for the LD to support fully the circulation.

Other muscles, such as rectus abdominis (Spotnitz 1974), could also provide adequate power for cardiac assist. However, the LD has the advantage of proximity to the heart and surgeons are familiar with it from previous use in plastic surgery (Zancolli & Mitre 1973; Hester & Bostwick, III 1982). The LD in the human is between 11-13 mm thick (Chachques *et al.* 1986) and about 260 mm long (Stanaway 1990; Sola *et al.* 1991), allowing the construction of ventricles of up to 33 mm in radius or cardiomyoplasty wraps around hypertrophied hearts of similar radii.

The first step in the use of the LD for cardiac assist is its surgical mobilization. In the operative procedure, the bulk of the LD is isolated (Heckler & White 1991) at its distal end but remains intact at the neurovascular pedicle, which enters the muscle along the tendon of insertion. Mobilization of the muscle is associated with loss of alternate blood capillaries, ischemia, and a change in length, which, together, result in a muscle that functions less efficiently and is less powerful.

1.8. Cardiomyoplasty procedure

Cardiomyoplasty, introduced in 1985 by Carpentier and Chachques working in Paris, is the first clinical application of skeletal muscle circulatory assist. From very cautious beginnings, the technique is now being assessed in countries all over the world, including Russia, Canada, Latin America, Europe and the United States, for the treatment of patients with severe heart failure (Carpentier & Chachques 1991; Magovern *et al.* 1993; Chiu *et al.* 1993). By 1993, more than 200 patients had undergone the technique (Hooper & Salmons 1993), and the numbers are growing steadily (it is probably more than 500 at present).

The surgical procedures of clinical cardiomyoplasty were described previously (Chachques *et al.* 1989) and experimental research has employed similar methods (Hulme 1986; Chachques *et al.* 1986). The procedure may be described briefly as follows. After isolation of the LD, a section of the third rib is removed and the muscle delivered into the thoracic cavity. The mobilized muscle is then securely wrapped around the heart; if the muscle length is insufficient to enclose the heart, a patch of pericardium is sometimes used to complete the wrap. A vascular delay period of two to three weeks (Mannion *et al.* 1989) is then allowed in which the distal part of the muscle recovers from the loss of its blood supply. During this time also, adhesions develop between the muscle graft and the ventricular wall. At the end of the vascular delay period, graded muscle stimulation is then initiated to effect transformation of the muscle graft (Carpentier & Chachques 1991; Chachques *et al.* 1989, 1991). Subsequently, the muscle graft is stimulated to contract in synchrony with the heart using a programmable, implantable muscle stimulator triggered by the R-wave of the electrocardiogram.

The results of cardiomyoplasty are encouraging. Despite an appreciable overall early mortality of more than 20% (Grandjean *et al.* 1991), partly reflecting inexperience with both the method and the selection of suitable patients, improvements have been reported

in the symptoms of heart failure in the majority of patients (Hagege *et al.* 1990; Moreira *et al.* 1990; Grandjean *et al.* 1991).

However, the muscle graft in cardiomyoplasty is not believed to contribute very actively to the contraction of the myocardium (Salmons & Jarvis 1990a, 1991a), but may serve merely as a passive reinforcement that resists further cardiac dilatation. Certainly the reinforcing action would diminish systolic wall stress, thus reducing myocardial oxygen consumption and enhancing contractility (Lee *et al.* 1991). Nevertheless, the contractile power available from the muscle may not be exploited adequately in this configuration for cardiac assist. This is due to the limited control the surgeon has over the configuration: only the fibre direction can be altered, as the size is dictated by that of the heart around which the LD is wrapped. Furthermore, when pericardium is used to complete the wrap in a highly hypertrophied heart, the cardiomyoplasty is bound to function suboptimally. Moreover, as patients have to wait for up to two weeks during the post-operative delay period for revascularization of the ischemic distal portion of the LD, the approach is only suitable for a few patients who have adequate residual left ventricular function to survive this waiting period. Hence, cardiomyoplasty is limited to a selected class of patients.

1.9. Skeletal muscle ventricles

In this alternative to cardiac assist, the latissimus dorsi muscle is configured as an auxiliary pumping chamber for circulatory support (Figure 1.1). A purpose-designed electrode is placed around the thoracodorsal nerve and connected to a fully implantable nerve stimulator (Pochettino *et al.* 1991). After the post-operative delay period, the temporary former (usually a Teflon mandrel) is removed and the SMV is connected to the circulation or to a mock circulation device for testing, via a bifurcation or trouser graft (Figure 1.1).

Despite the numerous studies that have shown the potential efficiency of SMVs for circulatory assistance, the approach remains largely empirical because several parameters

need further study for optimization. There are comprehensive reviews of the experience with SMVs (Badylak 1991; Pochettino *et al.* 1991; Hooper & Salmons 1994). Of particular significance was the work of Acker *et al.* (1986, 1987b, c) who showed in mock circulation studies that SMVs constructed from canine LDs were able to generate 'heartlike' work for several weeks. Mannion *et al.* (1987) subsequently showed that such ventricles functioned successfully when pumping directly into the circulation. Most of these studies have, however, concentrated on demonstrating the long-term applicability of SMVs. It is therefore not yet clear what the optimum loading conditions of the ventricles should be, or what parameters will best describe adequate performance. An important question to resolve is 'How well would skeletal muscle ventricles function under physiological conditions?' It is thus important to characterize the SMV as a circulatory assist device by studying its ventricular mechanics.

1.9.1. Measurement of ventricular performance

Several properties are used to characterize a ventricular pump. The most commonly used hemodynamic measures of the heart as a pump include cardiac output or index (CO or CI), left ventricular end-diastolic pressure (LVEDP), systolic ejection fraction (Cohn *et al.* 1974; Fox 1993), and left ventricular radius to wall thickness ratio (Gaasch 1979). CI is the product of stroke volume (the volume ejected in one heartbeat) and heart rate, and is influenced by the autonomic nervous system and the Frank-Starling effect. The Frank-Starling law is an intrinsic property of the heart muscle and states that an increase in end-diastolic volume (EDV) within the physiological range results in an increased contraction strength and, consequently, an increased stroke volume. LVEDP may be indicative of the EDV and the ventricular wall stiffness, which, together, influence the overall degree of coronary blood flow: a very high LVEDP leads to increased intramuscular pressure and hence a reduced coronary blood flow (Van Leeuwen & Spoor 1992). The EDV, the amount of blood in the ventricles pre-contraction, presents a workload to the ventricles prior to contraction; as work is the product of volume and pressure, the pressure

associated with the EDV is referred to as preload. The systolic ejection fraction, the ratio of the stroke volume to the EDV, may reflect the contractile state of the myocardium and so is an important parameter of ventricular function. The pressure presented to the left ventricle as it pumps into the aorta, and thus into the peripheral circulation, is called afterload. Stroke work, another important hemodynamic measure, is the product of the stroke volume and the difference between the LVEDP and the afterload.

As reviewed by Hunter *et al.* (1979), mechanical parameters such as elasticity and resistance are also used to characterize the left ventricle. Elasticity reflects the degree to which changes in volume will alter ventricular pressure, whereas vascular resistance describes how different rates of ejection influence ventricular pressure. In fact, vascular resistance is the absolute value of the rate of change of pressure with flow (Shroff *et al.* 1985).

The above parameters, which include preload, afterload and stroke volume, allow the stroke work, power output and efficiency of energy conversion of the ventricle to be evaluated (Tan 1986, 1987; Waaler *et al.* 1987; Geddes & Babylak 1991), thus providing insight into the functional state of the myocardium. In the case of skeletal muscle ventricles, on the other hand, the mechanical properties of the muscles are well documented. Can the mechanical properties be used to determine the hydraulic behaviour of SMVs formed from these muscles?

1.9.2. Optimization of SMV function

Several studies have been carried out on the function of SMVs presented with different preloads and afterloads (Bridges *et al.* 1989a, b ,c; Guldner *et al.* 1991; Oda *et al.* 1993). These investigators used stroke work to quantify SMV function. Oda *et al.* (1993) have studied the effect of size and configuration on the function of skeletal muscle ventricles by constructing different sizes of ventricle with either single- or double-layered wraps in mongrel dogs. Given the numerous parameters that need to be optimized in SMVs,

studies that simply focus on constructed SMVs may not be the ideal way forward, as the investigations may be tedious and lack flexibility. However, combining such studies with numerical models, based on the well-documented linear mechanical properties of skeletal muscles, would allow parameters that could not be optimized by experimentation to be investigated. Interestingly, Bridges *et al.* (1989a) used the mechanical properties of an SMV to develop a mathematical model of the ventricle, and concluded that such studies are likely to improve significantly the mechanical pumping efficiency.

As reviewed by Moriarty (1980), several mathematical models have been developed to study left ventricular mechanics, including the Laplace and the Lamé model. The Laplace model uses thin wall approximations and so is largely inconsistent with the thick-walled left ventricle; however, some investigators have employed a modified version that considers wall thickness (Spotnitz *et al.* 1966, 1974; Oda *et al.* 1993). Although the Lamé model, which assumes small deformations and linear stress-strain, is not entirely consistent with left ventricular mechanics, it may still be appropriate for use in SMVs as it takes into account the wall thickness. It must be noted, however, that the left ventricular wall is very inhomogeneous compared with an SMV wall, so that more complex models may be needed to adequately describe the left ventricular mechanics. Lamé's equations (Hearn 1985), which offered simplicity, have been used to calculate the instantaneous wall stress in a cylindrical model of an SMV. Even if qualitative results alone were obtained from the use of these equations, the information could prove very informative to surgeons involved in skeletal muscle cardiac assist (Salmons & Jarvis 1990a).

1.9.3. Limitations of the SMV approach

Although it has been shown unequivocally that SMVs have the potential to provide cardiac assist, the approach still suffers from a number of problems. Firstly, the technique increases the risk of thromboembolic complications as the blood is exposed to a new surface. Therefore, biocompatible surfaces need to be developed in order for effective use

of SMVs. Secondly, in common with other approaches of skeletal muscle cardiac assist, stimulation regimes that allow the most power to be harnessed from the muscle are yet to be determined. Thirdly, it remains unclear what an optimal size of ventricle is, or how best to define it. The SMV approach is therefore limited by the size, shape and fibre orientation of the latissimus dorsi forming the pumping chamber and by the lack of optimal stimulation regimes. If these parameters were optimized, then considerable power could be harnessed from the muscle in the SMV configuration, as the surgeon will have greater control over several parameters. At present, though, the approach remains largely empirical.

1.10. Other applications of electrical stimulation of muscle

Apart from cardiac assist, skeletal muscles may be stimulated electrically to utilize their force-generating capacity in a variety of other clinical applications, grouped together under the heading of functional electrical stimulation (FES). FES of skeletal muscle enables the restoration of function in upper (Hambrecht & Reswick 1977; Cybulski *et al.* 1984; Jaeger *et al.* 1989; Kralj & Bajd 1989; Jaegar 1992) and lower (Miller *et al.* 1989; Nathan 1989; Billian & Gorman 1992; Peckham & Keith 1992) extremities of individuals paralysed by spinal cord injury or stroke. Also, FES of skeletal muscle allows the augmentation of ankle dorsiflexion for cases of foot drop (Liberson *et al.* 1961; Waters *et al.* 1975). In addition, stimulation can be applied to restore function to the diaphragm (Glenn *et al.* 1980). A muscle may be grafted, with the motor nerve intact, to form a replacement for the external anal sphincter (Baeten *et al.* 1988; Williams *et al.* 1989). FES is also used in orthotics (Marsolais & Kobetic 1988) and in the replacement of sensory function in cochlea implants (Davis *et al.* 1984; Davis & Emmonds 1992).

To achieve the above tasks requires interdisciplinary knowledge not only of muscle and nerve physiology, but also of biomechanical and control principles. Moreover, improved basic knowledge on electrically stimulated skeletal muscle will result in enhanced

prediction of some FES parameters, such as stimulation protocols, through modelling instead of the present speculative approaches. For example, constant-frequency bursts are conventionally used in clinical applications for no better reason than that they are easy to generate. Such stimulation, with the associated high aggregate rate of impulse delivery, is likely to result in premature muscle fatigue in the short term, loss of muscle power in the long-term, and reduced lifetime of the internally implanted stimulation systems (Baeten *et al.* 1988; Keith *et al,* 1989 ; Jarvis *et al.* 1993; Kwende *et al.* 1995) that deliver these patterns. It would be beneficial, therefore, if patterns that maximised the muscle output with fewer impulses (optimal stimulation patterns) were used. Such patterns would deliver a lower aggregate number of impulses over time, resulting in less muscle fatigue. Moreover, these patterns would hold out the prospect of preserving muscle power more effectively in the long term. Also, burst patterns maintain (Ferguson *et al.* 1989; Jarvis *et al.* 1991b) or even increase (Kernell *et al.* 1987a) muscle mass, which is necessary for sustained power output, as discussed above. Because optimal stimulation patterns are similar to burst patterns (Zajac & Young 1980a), similar preservation of muscle weight would be anticipated. Furthermore, because optimal patterns use fewer pulses to achieve a desired output, they would also prolong the life span of the battery-powered internally implanted systems.

This thesis describes work designed to optimize systematically, from basic studies of skeletal muscle properties and mathematical modelling, the parameters that would lead to the design of efficient skeletal muscle ventricles. Cardiomyoplasty, as an application of skeletal muscle cardiac assist, has developed in an empirical way, and many aspects of the protocol at present could also benefit from a process of systematic optimization. The present work, though aimed primarily at skeletal muscle ventricles, could provide information of value to cardiomyoplasty, as the two approaches have quite a number of similarities: both approaches involve the wrapping of the latissimus dorsi (LD) muscle to provide circulatory assist.

1.11. Aims of the present study

The present study was primarily aimed at elucidating the biomechanics of skeletal muscle ventricles for circulatory assistance of patients in end-stage heart failure. Although chronic electrical stimulation of skeletal muscle leads to fatigue-resistance, the accompanying loss of mass and slowing of the muscle, which result in loss of power and difficulties of synchronization with the cardiac cycle, present the need for optimizing the output of SMVs in order to harness adequate power to provide useful cardiac assist. This can only be achieved if the mechanics of SMV function are well understood. The well documented muscle mechanical properties, which change with long-term electrical stimulation, were thus used, both in a numerical model and in acute experiments, to establish optimal parameters of SMV function.

A muscle that is configured either as a ventricular pump or a cardiomyoplasty wrap experiences complex loads against which it operates with changing mechanical advantage. The muscle in this new configuration may have different optimal loading conditions owing to the complex forces to which it is now subjected. These forces may increase wall stress and thus reduce blood flow to the muscles. Furthermore, mobilisation of the muscle leads to loss of blood capillaries, which may result in diminished function because of reduced viable muscle tissue, with an overall reduction in available power. The power capability of the muscle is further compromised by chronic electrical stimulation, which is necessary to produce a fatigue-resistant muscle. Consequently, the power capacity of the muscle graft is reduced greatly even before the muscle has begun providing an assist. It is therefore vital to optimize systematically several parameters of the entire procedure of skeletal muscle cardiac assist. This work addresses important aspects of SMVs, including optimal configurations and stimulation paradigms.

The optimum geometry for an SMV is crucially dependent on the nature of the contractile tissue from which it is formed. Therefore, one of the important challenges

posed by this technique is to establish the geometrical configuration that will be most efficient in the harnessing of power available from the skeletal muscle. An optimal configuration should allow the muscle to work as close as possible to the peak of its power curve. In addition, as the time available for the SMV to contract in one heartbeat is limited to about 250 ms for heart rates of up to 100 bpm, an efficient configuration should provide an adequate stroke volume to provide the metabolic needs of the body. Moreover, the ejection fraction should be high enough to minimize the volume of stagnating blood in the ventricles in order to reduce the risk of thromboembolism.

Since preload determines the contractile state of the muscle, it is important to study the effects of preload on volume (pressure-volume curve or elasticity) and ejection fraction, an indication of the contractility of the muscle in its new configuration. The hydraulic power of SMVs, measured as in the case of the heart, can then be compared with the linear power of the muscles forming the ventricular wall to determine power losses that may occur through changing the geometrical configuration of the skeletal muscle.

Another important consideration in the use of skeletal muscle as an assist is the relationship between neural input and muscle output. Electrical stimulation is essential not only in the use of skeletal muscle for cardiac assistance but also in a variety of other clinical applications (see above). Inappropriate use of electrical stimulation leads to premature muscle fatigue and loss of function. Therefore, patterns of stimulation need to be developed that allow the force profile to be controlled and also maximise muscle output per neural input. This will increase the life span of the implantable stimulators that provide such stimulation, and retain muscle mass and speed, and thus muscle power.

1.12. Summary

This thesis is part of a programme working towards the development of a new surgical treatment for end-stage cardiac failure. In the procedure, circulatory assistance will be provided by an auxiliary ventricle fashioned from the patient's back muscle. An important

challenge posed by this technique is to establish the geometrical configuration that will be most efficient in the harnessing of power available from the skeletal muscle. An efficient geometrical configuration must be able to generate sufficient stroke volume in the limited time available for the ventricle to contract during cardiac diastole, and produce good turnover of blood (maximal ejection fractions) in order to reduce the risk of thromboembolism. It must also allow the skeletal muscle to work as close as possible to the peak of its power curve.

Long-term electrical stimulation of muscle results in fatigue-resistance, a necessity for skeletal muscle cardiac assist. Present stimulation regimes, however, result in undesirable concomitant changes such as loss of muscle mass and speed of contraction, with an associated reduction of muscle power, and the activation bursts that are used deliver more impulses than are needed to generate force, leading to premature muscle fatigue. Therefore, muscle transformation and activation need to be optimized to minimize muscle fatigue, maintain muscle mass, speed of contraction, and consequently power. In addition to maintaining muscle power, a high speed of contraction is also essential to allow the muscle to relax quickly during cardiac systole so as not to present an extra load to the already frail heart. Furthermore, as pacemakers require battery power for operation, optimized stimulation patterns, which use fewer pulses to produce a desired output, will increase battery lifetime.

Therefore, a number of important questions must be answered before skeletal muscles can be used successfully as a surgical biomaterial to configure vascular pumps. What is the best geometry for a pouch or tube ventricle? What is the best pattern of activation? How should the muscle be loaded to function to best advantage? Is there any hope of reducing muscle fatigue by optimizing the patterns of stimulation?

Hence, the main aims of this work were as follows. First, to predict, from measurements of power output and fatigue resistance, the optimum conditions of shortening and loading

for skeletal muscle configured as a pumping chamber. Second, to test these predictions in a physical model of an assisted circulation in which it is arranged for muscles to perform hydraulic work. The model could then allow evaluation of strategies for feedback control of SMVs. Third, to determine the principles of optimization of stimulation patterns for FES applications.

1.13. Chapter introductions

Chapter 1. *General Introduction.* This chapter reviews the background work that has led to skeletal muscle cardiac assist, and the problems facing present methodologies of circulatory assist.

Chapter 2. *Apparatus and Software.* In this chapter, the apparatus specially designed for the determination of muscle mechanical properties, and the software developed to control the apparatus is described. Also, the basis of the mock circulatory system for the measurement of the hydraulic properties of SMVs is included.

Chapter 3. *Linear Mechanical Properties of Skeletal Muscle.* Muscle mechanical characteristics measured using the servo motor system are presented. The basis of using the muscle mechanical relations in numerical models of SMVs is established.

Chapter 4. *Optimization of SMV Configuration - A Mathematical Model.* In this chapter, a numerical model and a part physical-part numerical model are developed and used to study the function of SMVs.

Chapter 5. *Hydraulic Properties of Acute SMVs in Sheep.* SMVs are constructed from sheep LDs and their pumping function measured. These are then compared to the predictions from the numerical model.

Chapter 6. *Optimisation of Activation.* The neural input-output properties of skeletal muscles are studied with a view to developing optimal patterns.

Chapter 7. *Conclusions and Further Work.* A summary of the work presented in this thesis and the conclusions arrived at are presented. Ideas for further work are then presented.

Chapter 2

2. Apparatus and Software

2.1. Summary

Two set-ups were used for data acquisition, and the software for the control of one apparatus was written by the author. The first set-up was a computer-controlled servo system (CCSS) developed for measuring the linear mechanical properties of skeletal muscles. Software was written to control the servomotor transducer arm and for data acquisition so that experiments were automated in real-time, resulting in greater reliability. Furthermore, the experimenter was relieved of routine tasks and timing, which allowed more time for looking after the animal under anaesthesia. The second set-up was a mock circulation system designed for measuring the hydraulic function of acute ventricles constructed in sheep. The bulk of the mock circulation was developed in collaboration with the Department of Clinical Engineering. The CCSS functioned well, and is now routinely used in Professor Salmons' laboratory for various measurements of skeletal muscle properties.

2.2. The computer-controlled servo system

The computer-controlled servo system (CCSS) was able to characterize a skeletal muscle by setting and measuring muscle lengths and forces, controlling muscle stimulation, and collecting and analysing data. In a typical procedure, the length at which the muscle produced the peak twitch or tetanic force, the optimal length (Lo), was first determined. All subsequent measurements were carried out with the muscle initially set at Lo. Next, the relationship between force and frequency of stimulation was determined: this provided a value for the peak isometric force (Po). The muscle was then stimulated with a tetanus (200 Hz) to contract against increasing loads on the servomotor arm from zero newtons up to Po, and the initial velocities of contraction were evaluated. A force-velocity relationship was thus obtained from which a power-velocity curve was derived.

Force-length, force-frequency, force-velocity, and power-velocity curves were then plotted to complete the characterization of the muscle.

Software was developed that controlled the servomotor for each stage of the characterization procedure above, and for studies of other muscle properties. These included automated fatigue tests, cyclic control of the lever arm for work-loop measurements, post-tetanic potentiation routines, and complex loading of a linear rabbit muscle as though it formed part of the wall of a skeletal muscle ventricle. The software was written in Borland Turbo C++.

2.2.1. History of the system

Although a variety of muscle ergometers have been reported in physiological literature, Jarvis and Salmons (1991) recently designed an electrohydraulic system that addressed some of the problems associated with earlier systems. All of these ergometers enabled the length of a muscle and the tension it produced to be recorded to obtain its static and dynamic physical properties. These properties include the relationship of force to length, force to frequency, and the functionally important relationship between force and velocity during shortening or lengthening.

In many varieties of these ergometers, isotonic apparatus was used to supply a predetermined load to the muscles by means of weights (Fenn & Marsh 1935; Jewell & Wilkie 1958; Sréter *et al.* 1975), springs (Wells 1965; Ranatunga 1982; Hatcher & Luff 1988), pneumatic pressure (Fales *et al.* 1958), or servomotors (Gordon *et al.* 1966; Claflin & Faulkner 1989). Because these systems were developed primarily for single fibres or small muscles, serious measurement problems arise when larger forces are measured. Heavy loads introduce measurement errors because the effective mass must be accelerated toward the velocity at which the muscle can maintain a constant tension. These inertial effects have been minimised in some designs by giving considerable mechanical advantage to the muscle. However, any gains so achieved have been

compromised by the need to move large weights or springs (Fenn & Marsh 1935; Fales *et al.* 1958).

In other ergometer designs, the force generated by an activated muscle was measured in fixed-velocity release experiments (Hill 1970; Julian *et al.* 1986). The fixed-velocity release approach, by using feedback-controlled electromagnetic muscle loading systems, overcomes many of the inertial effects associated with isotonic apparatus. However, the constructed devices are limited both in excursion range and in the period of continuous use.

The electrohydraulic system designed by Jarvis and Salmons (1991), with a 20-mm excursion, provided up to 28% fibre shortening in a 3-kg rabbit and was able to function continuously for periods of up to 7 hours. Nonetheless, the system still suffered from the isovelocity problem of when best to release the muscle after stimulation. In addition, most controls were manually set, and the data were analysed post-acquisition so that it was a demanding process to determine the mechanical properties of a muscle. It could take up to a week of data analysis to complete the characterization of a muscle. Moreover, the system lacked isotonic control, since it was designed for isovelometric measurements.

In 1989, a versatile lever system, designed specifically for muscle, became available from Cambridge Technology, Inc., Watertown, MA, USA. This system could control forces up to 50 N, and was thus suitable for whole rabbit muscles. The system offered both isometric and isotonic modes of operation. However, control software was required to exploit fully the capabilities of the transducer system, and this called for expert help. Hence, a suite of software was specified that would (a) control the servo motor, (b) provide programmable stimulation for evaluating the effects of pattern on work output, and (c) provide for efficient data collection and on-line analysis. This task was contracted to Strathclyde University.

The system as delivered had several deficiencies. Despite efficient data acquisition, the control and data analysis aspects of the system software only partially worked and the stimulation hardly worked at all. The system was therefore unusable as it stood. The flaws were resolved as part of this thesis, and the software expanded to include other useful features already mentioned above. A highly schematic diagram of the system is shown in Figure 2.1.

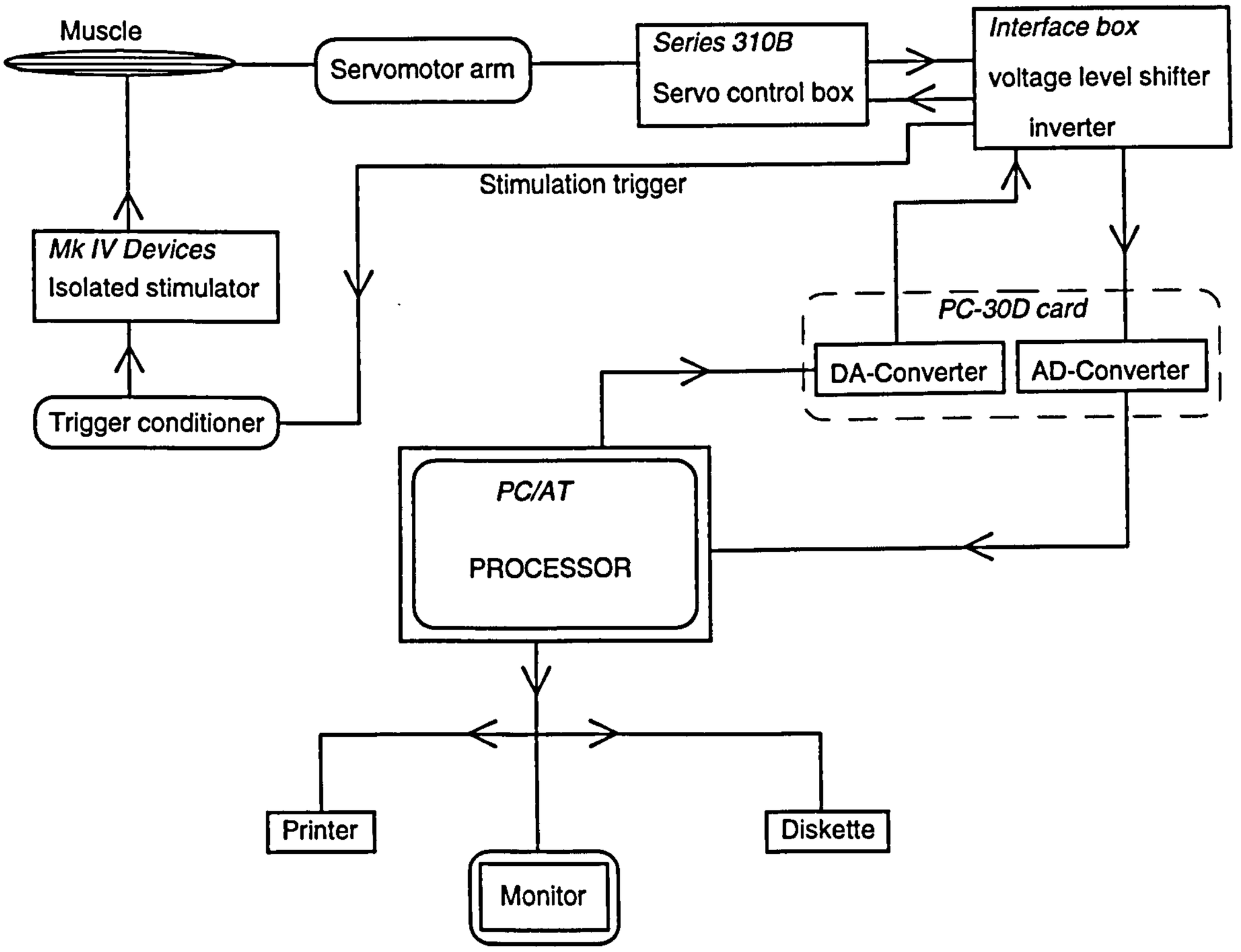

Figure 2.1. *A schematic diagram of the experimental set-up incorporating the CCSS: interconnections of the various components of the operational system.*

2.2.2. Hardware

The apparatus consisted of two servomotors, incorporating force and length sensors, two data acquisition cards, and two personal computers (PC's) for control of the servomotors, data acquisition and analysis. Two replica systems were built so that both tibialis anterior muscles of an anaesthetized rabbit, for example, could be characterized simultaneously, independently and under identical systemic conditions. Other equipment, such as

oscilloscopes (CRO) and frequency generators, were incorporated as necessary to monitor and improve certain aspects of the apparatus.

2.2.2.1. The series 310B lever system

2.2.2.1.1. General description

The lever system was a Dual Mode Servo System (Cambridge Technology, Inc., Watertown, Massachusetts, USA, Model 310B), a force and length controller designed specifically for muscle measurements (Figure 2.2). The heart of the system is a very high performance rotary moving coil motor. Precision ball bearings, having very low friction, support the rotor of the motor. Length is sensed by a high performance capacitive position detector. The motor is protected against overload partly by electronics and by mechanical stops inside the rotor housing to prevent gross over-travel. Figure 2.1 is a highly schematic representation of the series 310B lever system incorporated into the experimental set-up.

The model 310B lever system allows both length control (isometric) and force control (isotonic) modes of operation. In isometric control, the lever arm holds the muscle at a set length while it is stimulated: this is achieved by setting a lever force higher than the muscle can produce. On the other hand, isotonic control is achieved by setting a constant load lower than the peak isometric force on the lever arm and stimulating the muscle to pull this fixed load. When the muscle develops the set force, the lever arm moves while maintaining this set force level.

Associated with the 310B lever system is a control circuit which accepts analog voltages to control the tension on and the displacement of the lever arm, and provides the measured tension and displacement as analog voltages. Force and length offset controls allow the force and length to be varied manually. However, BNC connections to "force in" and "length in" enable the force and length to be controlled remotely from a PC.

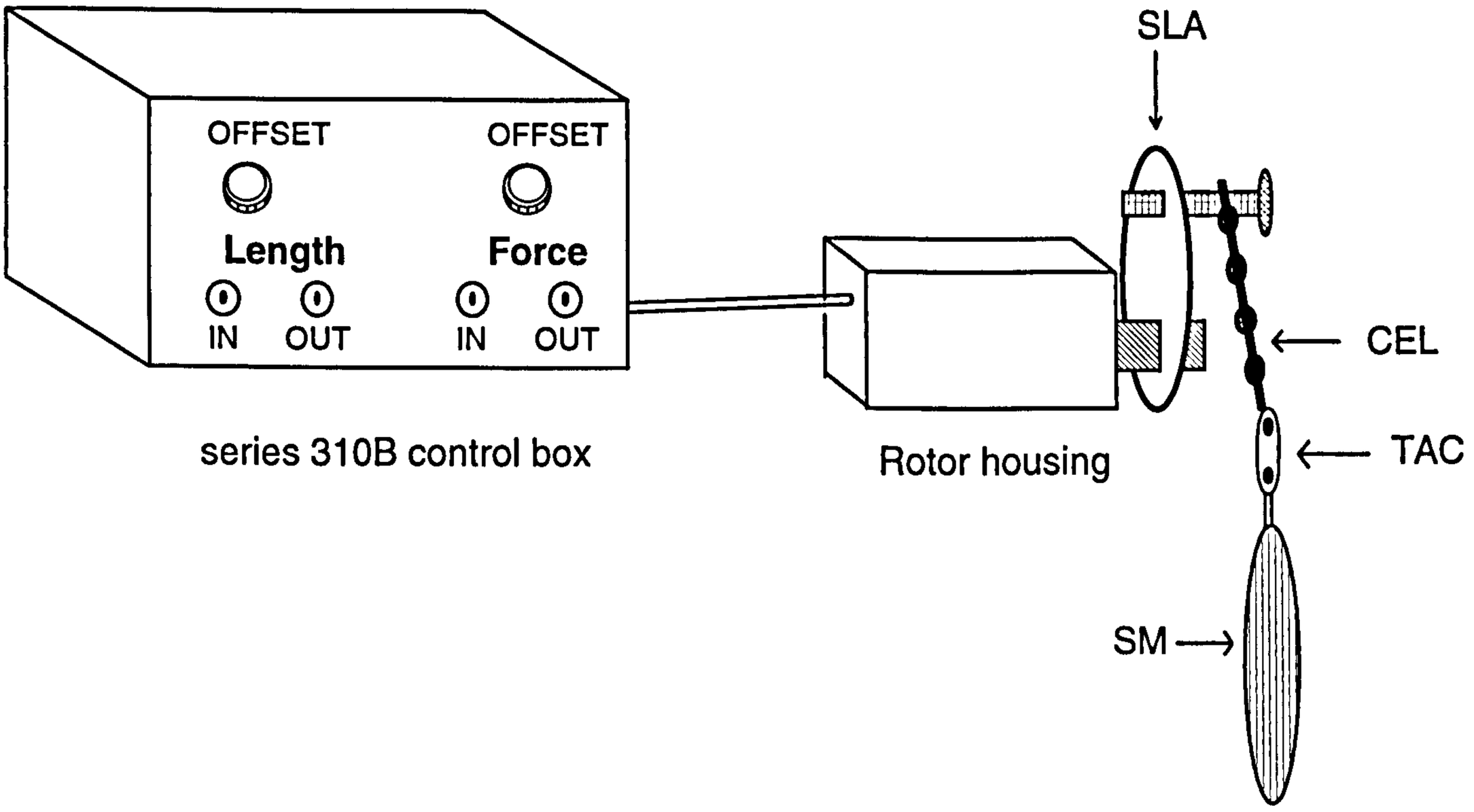

Figure 2.2. *The series 310B control box and lever arm. SM = skeletal muscle; TAC = miniature titanium alloy clamp; CEL = light carbon-epoxy link; and SLA = servo lever arm. In the experimental arrangement, the CEL, TAC and SM are aligned.*

2.2.2.1.2. Force control

The "force offset" setting and the input voltage at "force in" are summed internally to set the total isotonic force level. If, however, the "force offset" is zero, then the force level is controlled exclusively by the input voltage level at "force in"; the force offset is zero when its control is fully anti-clockwise. Both "force in" and "force out" are positive going voltages when muscle tension is increasing, with a voltage range of 0-10 V and a scale factor of 1 V per 5 N.

2.2.2.1.3. Length control

To allow complete remote control of the length, the "length offset" is set to zero by turning it first fully clockwise, and then five revolutions anti-clockwise. This action sets the servo arm at the centre of the mechanical range, the central position, which is the midpoint of the most accurately controlled part of the entire range; the center 20 mm has five times better length signal linearity and half the friction of the rest of the range. In the length control mode, a +1 change in "length in" results in a +1 change in "length out". To lengthen a muscle, therefore, "length in" must be driven with a positive going voltage.

Both "length in" and "length out" have a voltage range of -10 to +10 V, with a scale factor of 0.5 V per millimetre.

2.2.2.1.4. Specifications of the system

The servomotor system specifications are detailed in Table 2.1. These values are contained in the series 310B manual.

Table 2.1. *System specifications obtained from the series 310B servomotor manual.*

	LENGTH	FORCE
Length excursion or force range	40 mm	0 to 50 N
Signal resolution	4 micron	0.01 N
Scale factor	0.5 V per millimetre ±2%	2.0 V per 1 N ±2%
Step response time (1% to 99%)	10 ms, critically damped	10 ms
Signal non-linearity	0.1% over the center 20 mm 0.5% over the entire 40 mm	0.2% of force change
System friction	0.01 N over any 20 mm 0.02 N over full 40 mm	
Warm up time	1 minute to rated accuracy	
Power requirements	120V AC ±10%, 60 Hz, 5 amps max.	

2.2.2.1.5. Advantages of the system

The transducer is capable of generating controlled forces of up to 50 N and length excursions of 20 mm to either side of its central position. Other important features of the

system include a length measurement error that is negligible, transient-free mixed-mode operation, electronic cancellation of mechanical error contributions, fast step length change response, and force signals that are generated electronically without an external transducer. The transient-free mixed-mode operation allows the lever to be controlled auxotonically, i.e. the length and force can be varied simultaneously.

2.2.2.2. The computer system

IBM-compatible PCs (Viglen 386/486) were used to provide synchronized control of the servo motor, muscle stimulation, and data acquisition, the latter via an analog I/O board (Amplicon Liveline, Brighton, UK, PC-30D). The Viglen Genie 3SX is an MS-DOS machine with an 80386sx based motherboard operating at 16 MHz, with 4 megabytes of system memory, 3 megabytes of which is extended memory. The Genie Executive 4SX25 has an 80486 processor that runs at 25 MHz with 124 Mbytes hard disk space. These machines were used because of their high processing speeds, memory expansion capabilities, and large hard disk for data storage. Moreover, they were compatible with the PC-30D data acquisition card.

2.2.2.3. The PC-30D data acquisition card

The PC-30D card, a high performance analog I/O board, was utilised for data acquisition. It is a plug-in card designed for use in PC/AT- and AT-compatible computers. The card comprises a monolithic analog-to-digital converter (ADC) and a digital-to-analog converter (DAC).

The ADC converts analog voltage inputs from sensors into 12-bit digital codes, with a resolution of 1 in 4096, for processing by the host processor. Sixteen single-ended analog inputs were available, and could be configured for unipolar (input range of 0 to 10 V) or bipolar (input range of ±5 V) operation. The ±5 V range was used, and the following equation enabled the analog voltage signal to be converted into a digital value:

$$\text{Digital value} = 409.6(\text{Voltage} + 5) \tag{2.1}$$

The ADC was operated in continuous conversion mode at a frequency of 1 kHz and the conversions were monitored by interrupts (see below).

The DAC subsystem consists of two 12-bit DAC converters, DAC0 and DAC1, and two 8-bit DAC converters, DAC2 and DAC3, with resolutions of 1 in 4096 and 1 in 256, respectively. DAC0 was used for force and DAC1 for length because of their higher resolution, while DAC2 was used to provide a stimulation trigger and DAC3 a sampling trigger pulse prior to data sampling. The conversion equations for the +/-10 V range for the 12-bit ports (2.2) and the 0-10 V range for the 8-bit ports (2.3) are shown below. Note that the bipolar voltage range in (2.2) is inverted.

$$\text{Voltage} = -(\text{Digital value} - 2048)(10)/2048 \tag{2.2}$$

$$\text{Voltage} = (\text{Digital value})(10)/256 \tag{2.3}$$

2.2.2.4. The interface box

The interface box, which accompanied the delivered servo system, was a custom-designed unit that linked the PC-30D card in the PC to the Series 310B lever control box, providing signal level matching between the two. The 0 to 10 V range for "force-out" and the -10 to +10 V range for "length-out" had to be converted to the -5 to +5 V range of the ADC. Also, the -10 to +10 V range of the DAC output had to be converted to the 0 to 10 V range for "force-in". The interface box therefore housed circuitry that carried out the above signal conditioning. Moreover, this box provided BNC connections for the stimulation and start-of-sampling triggers from the PC so that the system could be synchronized with external apparatus.

2.2.2.5. Powering up the transducer system

A sequence of steps were necessary to power up the CCSS in order to avoid an uncontrolled vibration of the lever arm that would occur if the system was powered otherwise. Such vibration could damage an experimental muscle attached to the servo arm. First, the interface box and the PC were switched on. The desired program to run the servomotor arm was then started, eliciting an initialization routine that checked if the PC-30D data acquisition card was present and, if so, set the default parameters - the force on the lever arm was set to 40 N, and the arm moved to the central position. The default parameters for the various experimental routines were also set. The real-time display mode, a facility that enabled real-time monitoring of the lever force and position, was then started. In this facility, the vertical arrow keys controlled the force and the horizontal arrow keys the lever position, each press of a key representing one newton or one millimetre, respectively.

The arrow keys were then used to set the lever force first to zero and then to about 10 N, and the lever arm at its central (0) position - these actions overrode the default settings. The force offset control on the series 310B transducer was turned fully anticlockwise (0 N) so that the only force set on the lever arm was that from the PC. Next, the length offset control was first turned fully anti-clockwise, and then five revolutions clockwise, so that the lever was near its central position. At this point, the lever arm was manually held close to its central position and the series 310B transducer switched on. The lever arm therefore moved a minimal distance to get to the central position, the default start-up position, resulting in little or no vibration. Because the software assumed that the lever was at its central position on power-up, a right arrow key press, interpreted by the software as +1 mm lever position, followed by a left arrow key press set the lever arm to a software-recognised zero position. The muscle could now be attached safely to the lever arm.

2.2.2.6. Stimulation and synchronisation

Supramaximal stimulus pulses, with a pulse width of 0.05 ms and of about 20 V amplitude, were generated by an isolated stimulator (Devices Sales Ltd., Hertfordshire, UK, Mk. IV) that was triggered by pulses from the DAC2 port. Triggering of the isolated stimulator required a positive-going 10 V amplitude pulse with a rise time of 2 μs or smaller, from a source impedance greater than 1.5 kΩ. The pulses from the DAC2 did not satisfy the 2 μs rise-time criterion. These pulses were therefore processed in a pulse generator (Devices Sales Ltd., Hertfordshire, UK, Digitimer D4030) before making them available to the isolated stimulator. The sampling trigger pulse was useful in either synchronizing data acquisition to commercially available data acquisition software or triggering a pulse generator, as in fatigue testing routines (see later).

2.2.3. Software Development

Software development entailed initially debugging the original code to provide proper function of the servomotor arm, and subsequently developing new code for other control aspects. The software was written in Borland Turbo C++, which is now becoming the standard language for many applications programmers. On the one hand, C++'s flexibility in data and program structures, and its extensive library of functions, standard graphics, and disk and input/output routines allows programs to be written quickly. Its basic nature, on the other hand, means that code has to be very explicit. Code debugging could therefore be tedious, and much time was spent in debugging the intricate original code.

2.2.3.1. Special IDE settings

To ensure proper function of the compiled code, some special options were activated in the integrated development environment (IDE). The **huge** memory model was used for compilation, as the program code and data were each greater than 64 K. In addition, the **stack size** was increased to 48 (56) K using the stack-size variable **_stklen**, and some compile-time options including **Stack-Frame Checking** were turned off to allow correct

operation of the interrupt routines. Since most of the software details are included in the manual that accompanied the original software, emphasis here will be on general program flow and the improvements that were necessary to get the system fully functional.

Some drastic measures were necessary to ease the debugging procedure. Because problems arose with compilation memory, all graph-drawing routines in the original code were removed, as commercially available software (Easyplot and Cricketgraph) could be used for this purpose. As the memory problems persisted, the next step was to split the software so that each executable file only addressed one or two experimental aspects. Thus, different executable programs were compiled for the force-velocity and for the force-length and force-frequency experimental routines. However, the general program flow was essentially the same.

2.2.3.2. General program flow

Figure 2.3 is an illustration of the general program flow. After power-up, the desired program was started and the parameter entry option selected. The experiment type was then entered to allow the software to determine whether servo control was isotonic, isometric or auxotonic. Next, appropriate force and position parameters were entered and used to calculate muscle lengths and forces: these values were stored in global structures (see below) for later use. Other parameters required included the sampling time, data storage base file name and extension, and the time between tests.

When program execution starts, the software first checks to see if all the required stimulation files are found on the hard disk and, if they are, allocates a 100 kilobytes memory block, which is used to manipulate the data during an experiment. Program execution stops on failure either to allocate the memory area or locate any stimulation files; the names of the missing files are then printed on the screen. Otherwise, the muscle length and force for the first test are set and stimulation delivered to the muscle. The data is then captured and analysed on-line, with a data pointer used to manipulate the data in

memory. Sampling commences 50 ms before onset of stimulation for the resting length and force of the muscle to be determined.

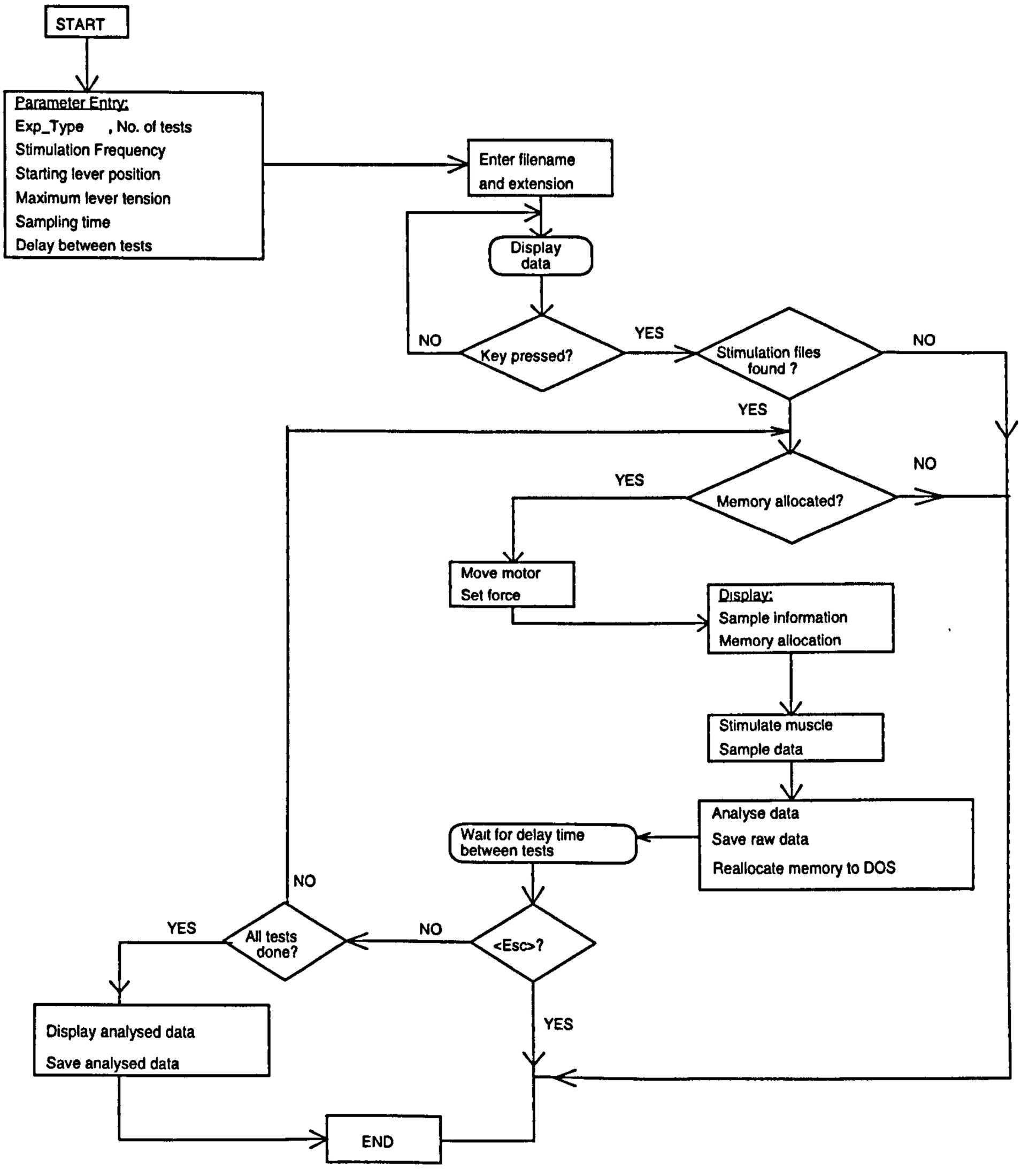

***Figure 2.3.** General program flow.*

The analysed data are stored in a global result structure while the raw data, the force and displacement records in time, are saved on disk for further analysis. The raw data file name is formed by concatenating the test number with the end of the base file name and then adding the file name extension, so that each set of test data is stored in a unique file. Also, a header is included in the saved data file that contains the parameters used,

including the date and time of the test and details of the experimenter. Data is saved as a comma-delimited ASCII file, and it takes about 10 s to save a file of 13 Kbytes.

The memory block is then reallocated to DOS, and the execution pauses for the period allowed between tests. This rest period is to allow the muscle to recover from possible fatigue and the effects of potentiation. The above routine is then repeated until all the tests are performed. Execution then stops. If, however, any key is pressed during the rest period, the program execution would stop prematurely. The analysed data, previously stored in global structures, is now displayed on the screen for saving to disk.

2.2.3.2.1. Interrupt handling

Interrupt-based I/O allow the PC's central processing unit (CPU) to perform other tasks at known intervals while the PC-30D card acquires data. For instance, the PC controls muscle stimulation while the PC-30D card samples the data. Thus, an interrupt routine, which is called an interrupt handler and is driven by the PC system clock at a rate of 1 kHz, was used to control the stimulation and data sampling. During an interrupt routine, however, mathematical calculations may not be performed and floating-point variables cannot be handled. Therefore, all parameters needed during an interrupt must already be saved in memory: this was achieved by the use of global variables.

2.2.3.2.2. Global variables

Global variables, as the name implies, may be used by multiple functions in a C++ program, and so were particularly useful in reducing the amount of code generated and for the interrupt handling routines. Stimulation variables, for example, were common to all experiment types and were thus assigned a global variable structure, resulting in reduced code size. At the start of an experiment, the parameters for each test were evaluated and stored in global variables so that they could be accessed during an interrupt routine.

Of particular interest was the use of global variables to store the current force and position of the lever arm each time the force was changed or the lever arm was moved. Because there were many functions that could change the lever force or position, it was crucial to keep track of the lever position for proper control. Hence, each function that affected the lever force or position saved the final values in global structures that could be accessed by other functions.

2.2.3.2.3. Data sampling

The sampling procedure provided with the original software was adequate for most of the system needs. The PC-30D card was initialized and the channels required for sampling loaded. 100 Kbytes of memory was then allocated and the required gains set on the card. The digital I/O ports were then configured as inputs, the A/D subsystem was cleared, and the A/D sampling rate set. Data sampling was initiated by software strobes, and up to 8 channels could be sampled sequentially. If sampling of all the channels was required, then 8 successive start A/D conversion pulses were generated. Each conversion took 5 μs to complete, so that 40 μs would be needed for all 8 channels. An on-board FIFO (First In First Out) buffer, which was cleared prior to start of sampling, was used as a temporary store for converted results that were then transferred to the computer's memory (an A/D sample buffer) by polled I/O, the simplest possible method of data transfer. [For a complete description, see PC-30D User Manual.]

Because of its extremely simple nature, polled I/O is limited to a sampling frequency of 3 kHz, which was more than sufficient in this case as the sampling frequency used was only 1 KHz - similar to that of the interrupt routine. The A/D sample buffer size was determined by the sampling rate, the number of sampled channels and the sampling time. If all 8 channels were sampled simultaneously, the memory storage requirement would be 64 K.

2.2.3.2.4. Stimulation control

2.2.3.2.4.1. Generation and storage of stimulation files

Software was written that enabled stimulation files with a known burst length to be created and stored to disk. A stimulation file contained the frequency of stimulation, the number of pulses in the burst and a sequence of 1's and integer values intervening between them: a 1 represented the presence of a pulse and the following integer the period in milliseconds before the next pulse. The burst duration (in ms) was therefore the sum of the sequence of numbers. When only constant-frequency bursts were required, the sequence of numbers representing the burst length was replaced by a single value, which was then used to determine the pulse sequence from the burst frequency.

2.2.3.2.4.2. Delivery of stimulation

Prior to the start of a test involving muscle stimulation, the desired stimulation file was converted and stored in global variables as a stream of digital values representing the presence (1) or absence (0) of a trigger in millisecond time slots. 50 ms of no stimulation was added at the start of the sequence to allow the resting conditions of the muscle to be determined during data sampling. The stimulation pulse sequence was then accessed by the interrupt during the experiment to generate stimulation triggers.

A stimulation pulse was represented by a digital value equivalent to 10 V and the absence of a pulse by an equivalent of 0 V. For some bizarre reason, a digital value of 256 (equal to 10 V, see equation (2.3)) was unable to provide a trigger for the isolated stimulator. By trial and error, a digital value of 2304 provided the desired trigger and so was used instead. In retrospect, it would have been wise to check the voltage level from the stimulation port of the PC-30D.

2.2.3.2.5. Motor control

When changing position, the series 310B lever arm is capable of high step speeds that could severely stress, and therefore damage, a muscle attached to it. The manufacturers recommended that the length be ramped slowly from one position to another.

A software routine was provided with the original software to accomplish smooth change of lever position. First, the "force in" is set to a value higher than the muscle can produce. The desired length change is then divided into 50 equal step lengths, which are delivered to the lever arm every 10 ms; hence it took half a second to accomplish any length change. A maximum length step change of 0.8 mm was possible, but seldom necessary. However, this step change could still allow smooth movement of the lever arm.

2.2.3.2.6. Disk input/output

The software provided a facility for storing data files to the hard disk or floppy drives. Such files contained a header with the time and date of the data collection, the experiment title and details of the experimenter. It also contained a record of the stimulation pulses delivered to the muscles. A separate program allowed stored data files to be reloaded and analysed. Stimulation files could also be created and stored to disk.

2.2.3.3. Summary

The experimental set-up was fully automated and could run all day providing that memory requirements were satisfied. Commercially available data acquisition software could be synchronized to the system with the aid of the sampling trigger. Furthermore, frequency generators could be incorporated to provide constant-frequency muscle stimulation. On the whole, the CCSS was a highly adaptable set-up. However, there were some shortcomings, which are addressed with respect to the individual experimental routines.

2.2.3.4. Force-length and force-frequency experiments

Muscle function is crucially dependent on its loading conditions, which include its initial length and frequency of stimulation. Force-length (F-L) and force-frequency (F-F) measurements determine a muscle's optimum loading conditions. In the experimental procedure, the muscle was first stimulated isometrically at various lengths to determine the length at which the maximum twitch or tetanic force was produced, the optimum length (Lo). The muscle was then set at this length and stimulated with bursts of increasing frequency and the developed force measured. F-L and F-F curves were then plotted.

Software was developed that automatically set the muscle at increasing lengths, stimulated the muscle, collected and analysed the data on-line, and displayed the analysed data for saving to disk. The data was then plotted with commercially available software.

2.2.3.4.1. Program flow

To determine the force-length curve, the minimum test length of the muscle, the step length size, the number of tests and the isometric force were entered. The sampling time (default 600 ms), the delay between tests (default 1 min), and the name of the stimulation file of a desired frequency (default 1 Hz) were also provided (Figure 2.4). Under automated control, the muscle was set at the minimum test length, stimulated, and the data sampled and analysed on-line. The raw data was saved to disk and the analysed data to a global structure. The system then paused until the delay time between tests had elapsed. The test length was incremented by the step length to a new test length at which the muscle was stimulated and the data sampled and analysed. The muscle was then reset to the shorter minimum start length to prevent prolonged stretch during the rest period. At the end of the delay between tests, the muscle length was again incremented to a new test length and the above procedure repeated until all the tests had been completed. The

analysed data was then displayed on the monitor screen, the optimum length noted, and the data saved to disk.

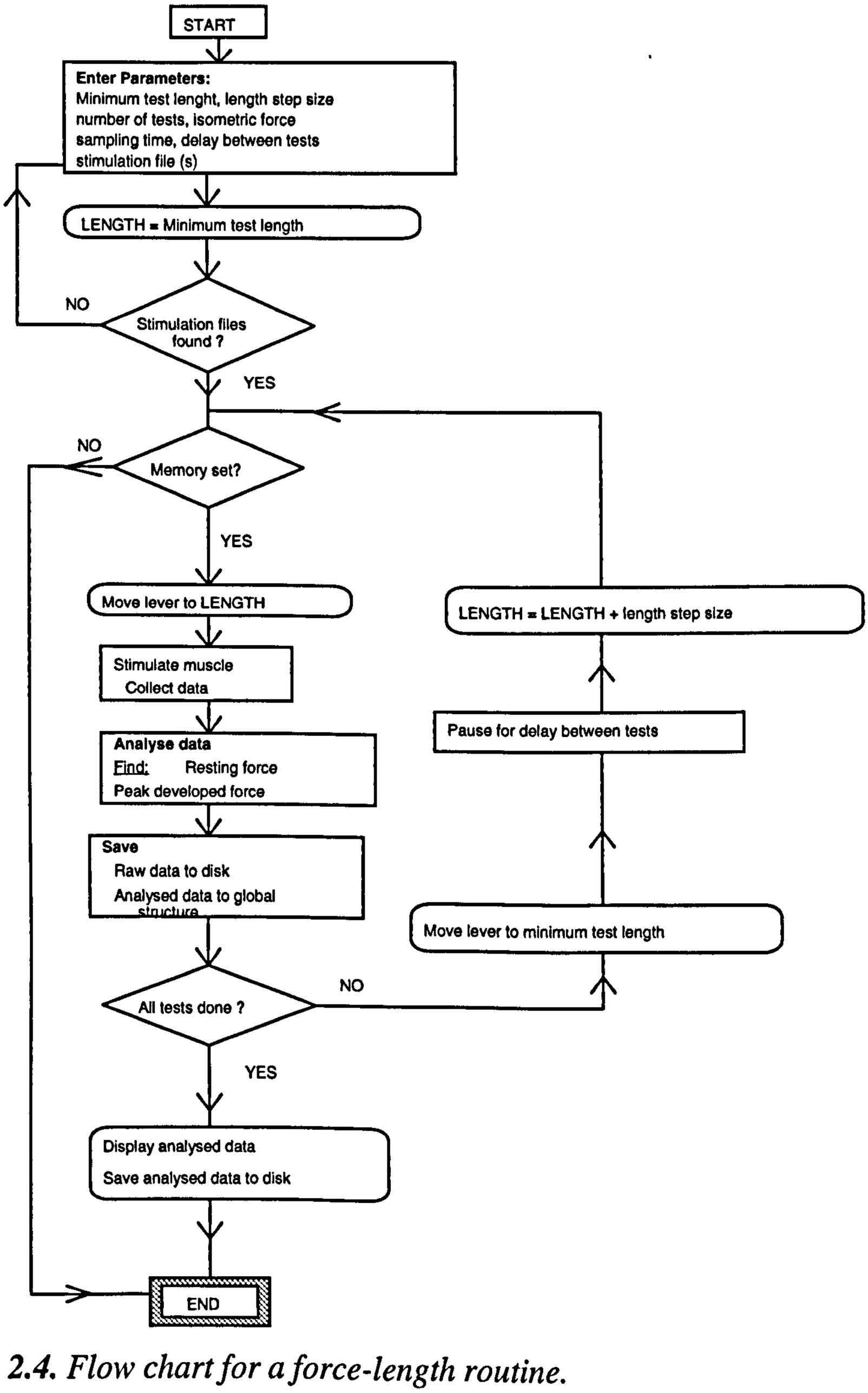

Figure 2.4. *Flow chart for a force-length routine.*

2.2.3.4.2. Data analysis

The resting force of the muscle was evaluated by finding the mean of the first 50 force samples that were obtained prior to muscle stimulation. The maximum force was then digitally determined. The resting force and the peak developed force, the difference

between the former and the maximum force, were saved against the corresponding length.

To determine the force-frequency relationship, the muscle was set at Lo and a force greater than the muscle could produce set on the servo arm. In an iteration routine, constant-frequency bursts of 400 ms duration with frequencies of 1, 10, 20, 40, 70, 100 and 200 Hz were delivered to the muscle (Figure 2.5).

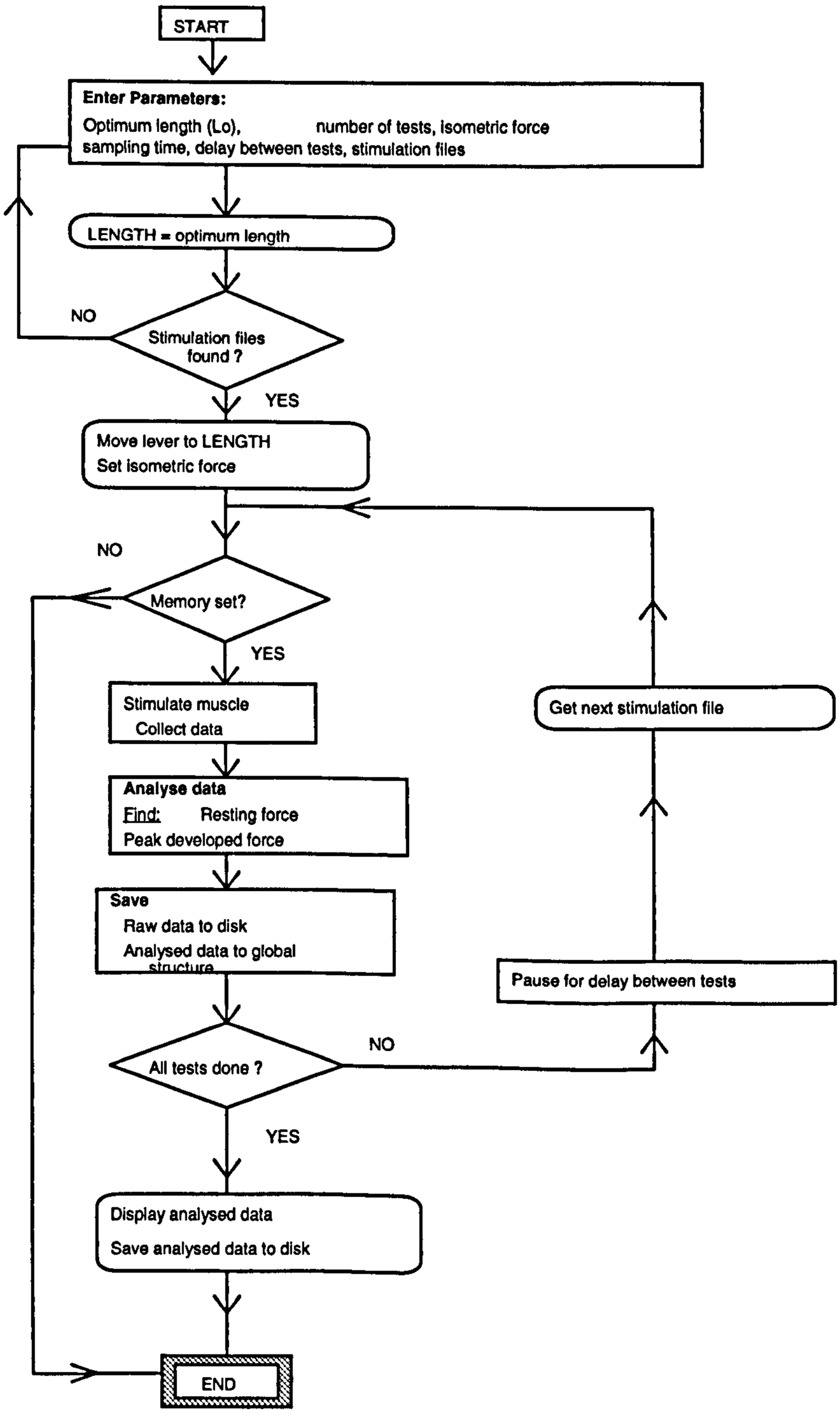

Figure 2.5. *Flow chart of a force-frequency routine.*

The iterations were separated by a delay period that allowed the muscle to recover from the effects of fatigue and potentiation. The data was collected, analysed and saved as above. The peak tension at each frequency was determined and used to plot a F-F curve. The peak isometric tension (Po) was then determined as the peak of this curve.

2.2.3.4.3. Difficulties encountered

There were no real problems with these experimental routines. The compiled program allowed both the force-length and the force-frequency measurements to be conducted in a single experimental run. This option was useful in two main ways: first, it still allowed the two routines to be run independently; secondly, it saved time, as the experimental parameters were only entered once. Moreover, the relationship between stimulation frequency and suboptimal muscle lengths could be investigated with no extra effort; a routine force-frequency curve measurement was usually done only at a single length, Lo say.

2.2.3.5. Force-velocity and power-velocity experiments

A functionally important property of skeletal muscle is the relationship between the load on the muscle and the speed at which it can contract against the load. Muscle power output is the product of speed of contraction and the load. It is therefore important to be able to measure easily the relationship between force and velocity of contraction of a muscle.

Software was developed that loaded a muscle with a series of increasing loads, stimulated the muscle, collected and analysed the data on-line, and thereby determined its force-velocity relationship.

2.2.3.5.1. Program flow

The following parameters were prompted for: the optimum length (Lo), the isometric tension (Po), number of tests (< 20), stimulation frequency (200 Hz default), delay

between tests (60 s default) and sampling time (Figure 2.6). The force step size was determined by dividing Po by the number of tests. With the muscle set at Lo and the lever force set to 0 N, the muscle was stimulated and the data sampled and analysed. After the time between tests had elapsed, the lever force was incremented by the step force and the above routine repeated in an iterative procedure until all the tests were done. The analysed data was then saved to disk and used to plot the force-velocity relationship. The power-velocity relationship was then determined by multiplying the force and velocity axes.

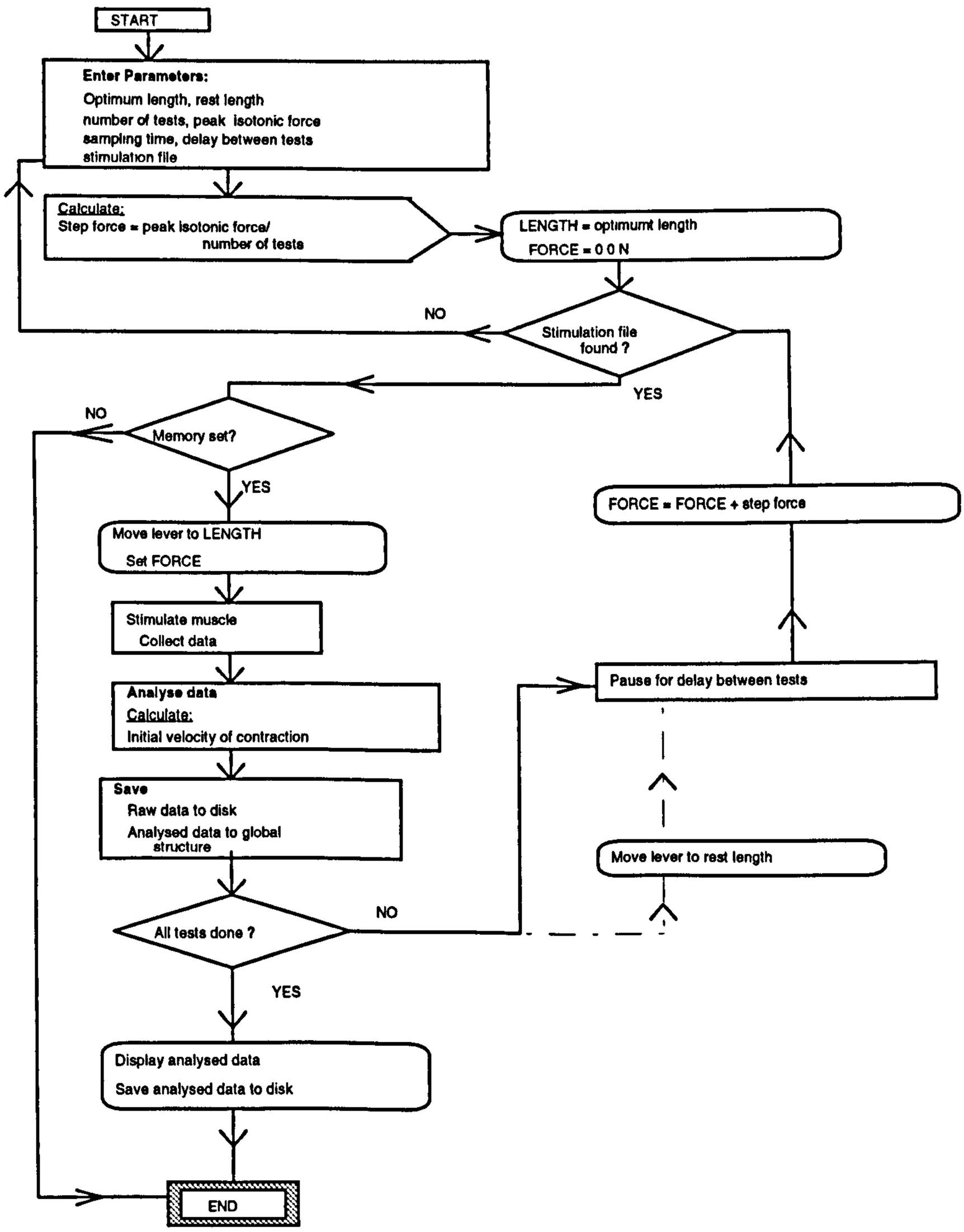

Figure 2.6. *Force-velocity program flow chart. The broken line indicates the preferred path of program flow.*

2.2.3.5.2. Data analysis

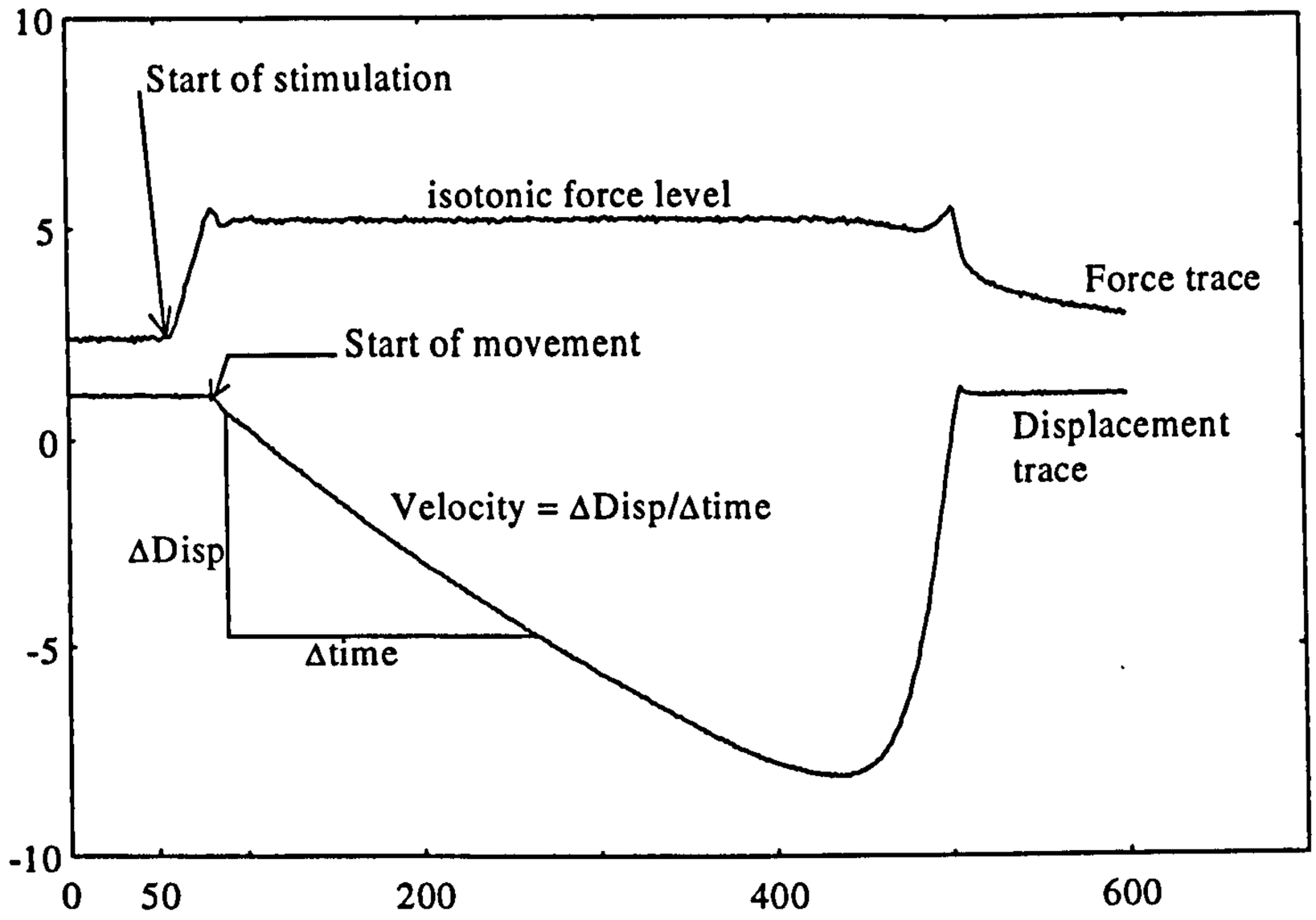

(a)

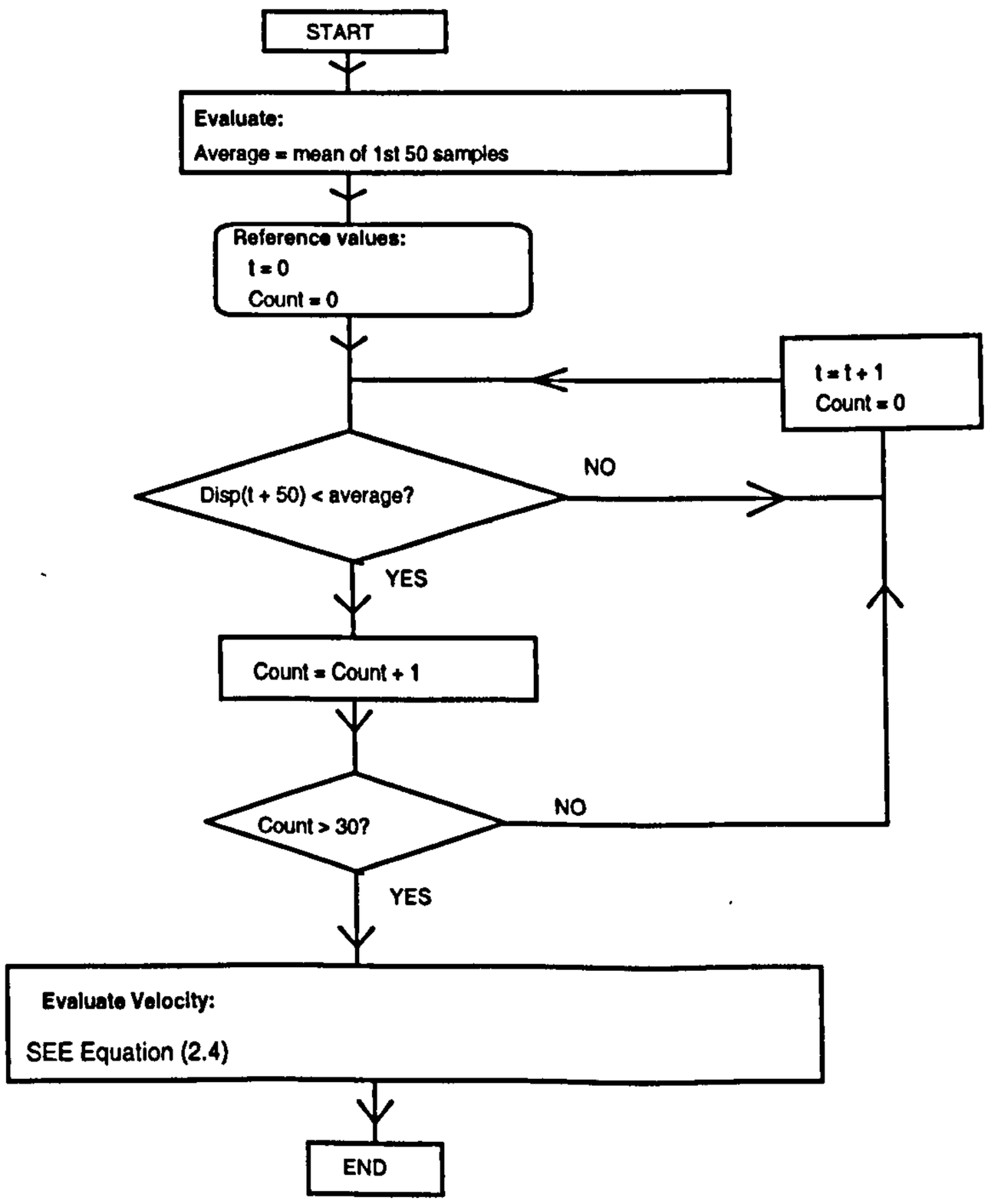

(b)

Figure 2.7. *(a) Calculation of initial velocity of contraction from the displacement trace. The velocity of contraction at the constant force level indicated is the gradient of the displacement trace at the start of movement. (b) Velocity analysis routine.*

Figure 2.7a, a plot of force and displacement against time from a rabbit tibialis anterior muscle, illustrates how the velocity at a particular force level was evaluated. Before the start of stimulation, there was a resting force on the muscle at Lo. When muscle stimulation started, the force rose while the muscle length stayed at Lo. When the force reached the isotonic force level, the muscle contracted isotonically until the end of stimulation. It was then reset to Lo.

The initial velocity of contraction at the isotonic force level was obtained by calculating the slope of the displacement record at the start of movement, which could easily be detected if the displacement trace was plotted in commercially available data analysis software, as in Figure 2.7a.

For on-line analysis, however, the start of movement was not immediately obvious. As illustrated in Figure 2.7b, this time-point was located digitally as follows. The resting length of the muscle was determined by digitally averaging the first 50 samples of the displacement record, the samples that were obtained prior to muscle stimulation. As sampling was done at 1000 Hz, a sample was collected every 1 ms. For a clear understanding of how the velocity of contraction was obtained, a function Disp(t) is defined as the muscle length at time t from the start of the sampled data. Displacement values from t = 50 (Disp($t \geq 50$)) were compared with the adjusted resting length, and a Count incremented from zero if the latter was greater; Count was reset to zero if a displacement was greater than the resting length. If the Count reached a desired value, which was chosen as 30, then it was taken that the start of movement was 30 ms earlier. Assuming that t_o was the time for start of movement, the gradient of the displacement trace was then evaluated in 10 ms intervals to give the initial velocity of contraction (mm/s) as

$$Velocity = \frac{1000}{Count - 10} \sum_{n=1}^{n=Count-10} \frac{\left(Disp(t_0 + n) - Disp(t_0 + n + 10)\right)}{10} \qquad (2.4)$$

where Count > 10. Taking the means of several gradients, as in equation (2.4), ensured that a better estimate of the velocity was obtained.

2.2.3.5.3. Difficulties

The muscle progressively slackened if it was left at Lo for a whole force-velocity experiment, which lasted more than half an hour. This was detrimental to the force-velocity measurements, which should be elicited from Lo. This drawback could have been overcome by ensuring that the muscle was set at a length at least 5 mm short of Lo during the delay period between tests, indicated by the broken line in Figure 2.6. However, this improvement was not implemented because of problems that later arose with the PC's compiler, a problem that has been attributed to a bug in the new MS-DOS 6 that was installed during the software development. The slack problem was, however, not significant because the developed force-length curve was fairly flat near Lo.

Another problem encountered arose when the passive force at Lo was greater than the desired isotonic force level on the lever arm: the resting length was then changed substantially prior to stimulation so that the movement was not initiated at Lo. This problem was solved by setting a force higher than the problematic isotonic forces, and unloading the lever only at the start of stimulation. The lever therefore had little time to move from Lo.

2.2.3.6. Complex load experiments

The aim of this experimental routine was to load rabbit tibialis anterior (TA) muscle linearly as though it formed part of a functioning skeletal muscle ventricle (SMV) wall. This would allow the effects of changes in SMV configuration on ventricular function to be studied. The measurements could then be compared to a purely numerical model based on the mechanical properties of the same muscles.

As explained in Chapter 4, Lamé's Equations (Hearn 1985) can be used to evaluate the stress acting in the walls of a cylindrical SMV of given dimensions and intraventricular pressure. In particular, the stress (force per unit area) in the walls of the SMV can be defined as a function of the circumference. This relationship was fitted by a mathematical equation so that it was defined by known constants. The constants were then incorporated into software that calculated the force on a linearly contracting muscle, based on its length (monitored in real-time) and cross-sectional area, as though it were incorporated into the SMV wall. The equations used to calculate the forces are explained in Chapter 4.

2.2.3.6.1. Program flow

Figure 2.8a illustrates the program flow for the auxotonic real-time control of the force on a contracting muscle attached to the lever arm. The software used the appropriate parameters to calculate and set the force required on the lever arm at the initial muscle length. The rabbit TA was then stimulated to contract. When the developed force reached the set value, the lever arm started to move. Every millisecond, the new lever position was obtained and used to calculate the corresponding force, which was then set. This continued until the cessation of stimulation. Hence, the load on the muscle could be varied as a function of changes in muscle length to simulate the relationship between wall stress and the radius in SMVs of different initial sizes, pumping against different internal pressures.

The maximum shortening of the muscle was equivalent to the change in circumference of the nominal SMV and so could be used to evaluate stroke volume and ejection fraction. Figure 2.8b shows data captured by CODAS (Dataq Instruments, Inc., Ohio USA) for auxotonic contractions. The top trace is the force and the bottom trace the displacement. As the initial force increases owing to higher intraventricular pressures, the amplitude of the displacement trace falls, resulting in falling stroke volumes.

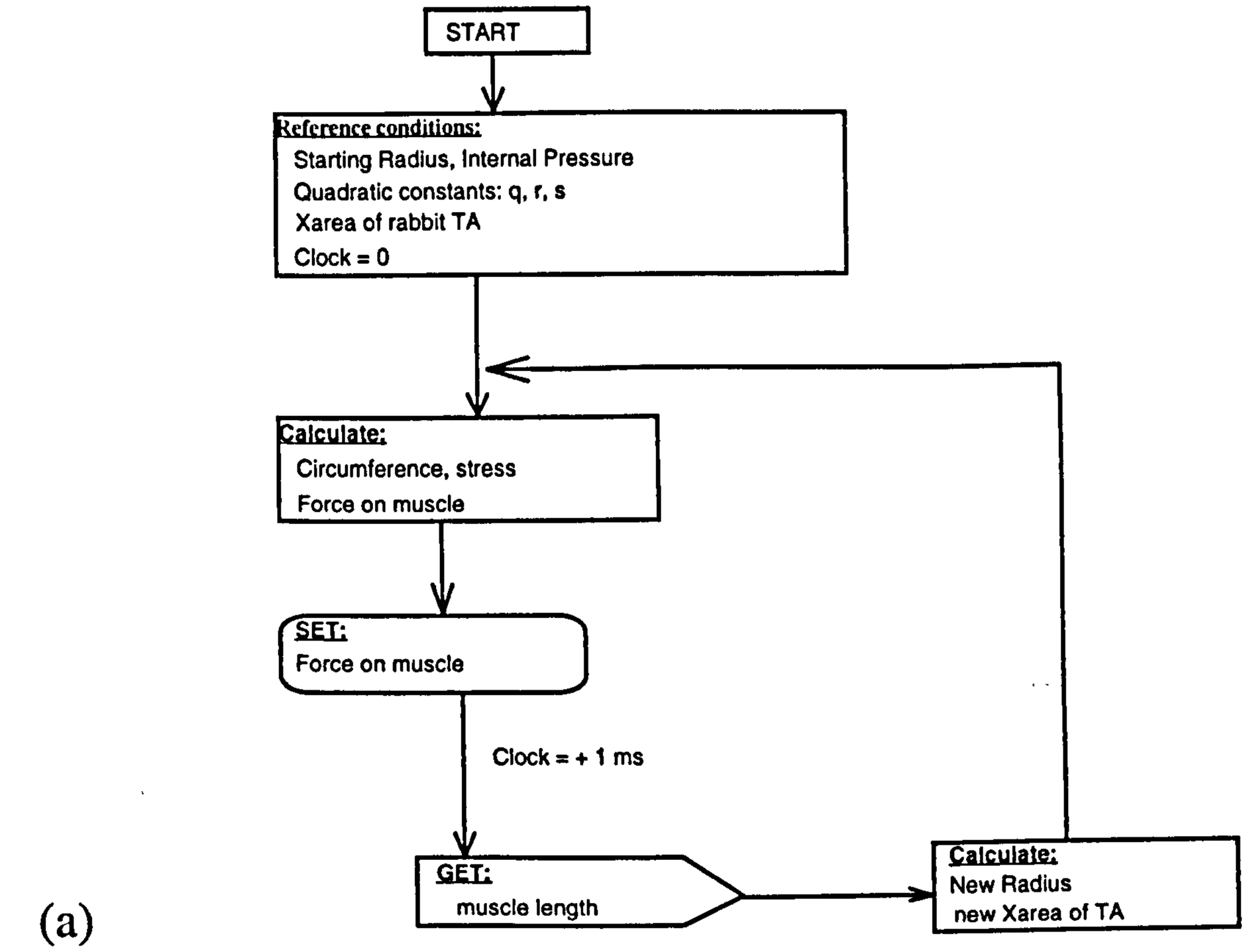

(a)

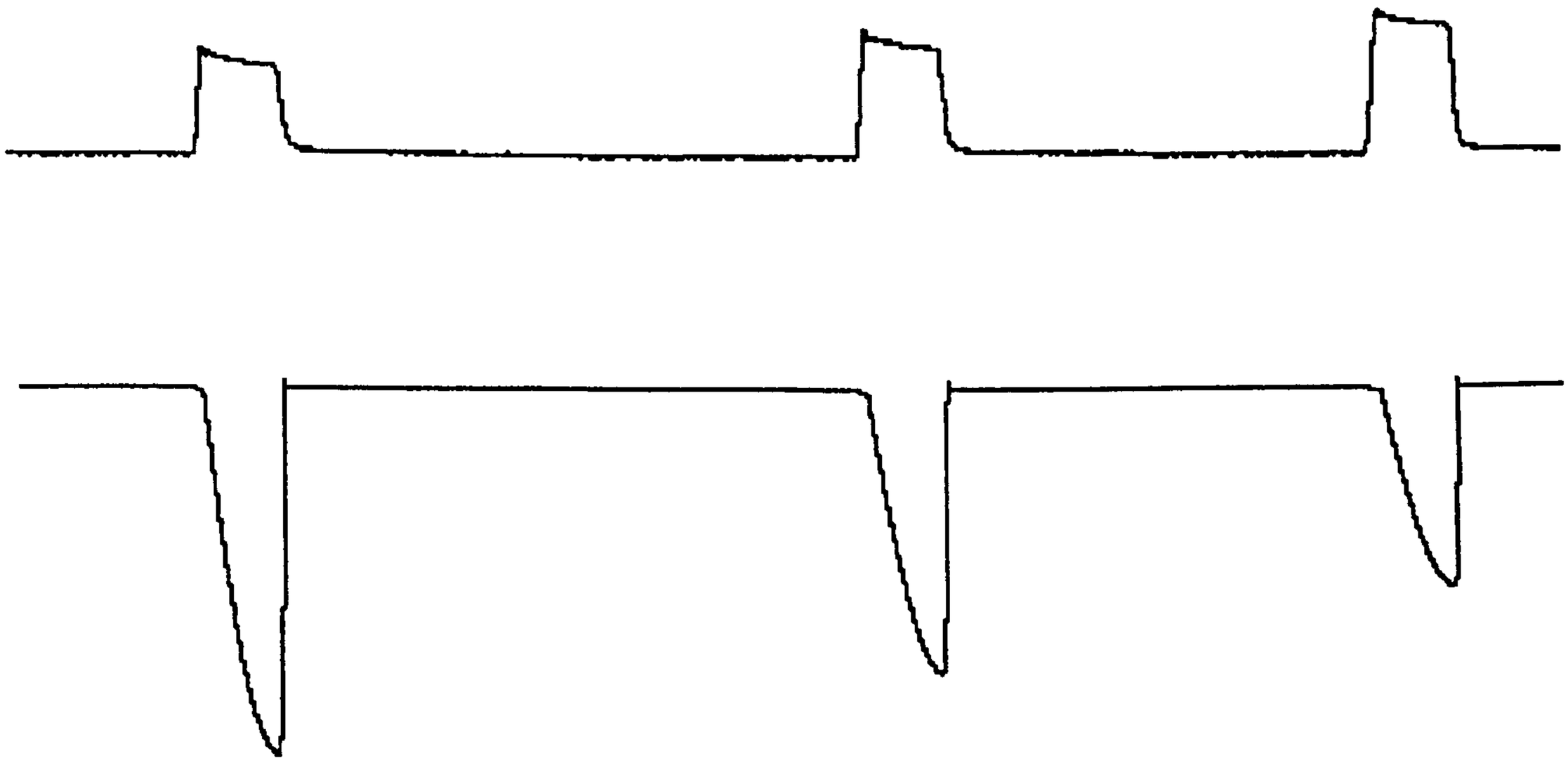

(b)

Figure 2.8. *(a) Real-time auxotonic control of the lever arm. The force and displacement are varied simultaneously. (b) Auxotonic contractions captured with CODAS. Note that this mode of behaviour is different from the conventional mode of operation of the servo system as in Figure 2.7a (isotonic contractions).*

2.2.3.6.2. Difficulties encountered

Since floating-point calculations were performed at each length to obtain the lever force, interrupts could not be used in this routine, as these computations are not allowed within an interrupt. Real-time control was thus a problem since the forces had to be updated every millisecond. This problem was overcome by incorporating purpose-written code (provided by Dr A Arowojulu of the Electrical Engineering Department) that controlled the system's internal clock. This code enabled the forces to be updated as desired.

2.2.3.7. Optimization of activation

The aim of this experimental routine was to investigate the input-output characteristics of muscle. The program delivered both random and constant frequency bursts of stimulation to the muscles. Thus, the mechanical response of muscles to various stimulation bursts could be studied.

2.2.3.7.1. Program flow

With the muscle set at Lo, a random or constant frequency burst was delivered from a saved file on disk. The force and displacement traces were sampled and the muscle set to a resting length shorter than Lo. The area under the force-time curve was calculated under software control to yield the force-time integral (FTI) as follows. The resting tension, obtained by averaging the force trace over the first 50 ms, during which there was no stimulation of the muscle, was multiplied by the total sampling time to give the passive FTI. The force trace was then summed over the entire sampling time and the passive FTI subtracted from this value to obtain the developed FTI of the burst. This value was divided by the total number of pulses in the burst to give the FTI per pulse (FTIpP). The peak developed tension was also obtained as in the force-length routines. The analysed data was saved to a global result structure and the sampled raw data was saved to disk. After the delay period of 60 s between tests had elapsed, the muscle was reset to Lo and stimulated from a different stimulation file. The above procedure was

repeated. When all the stimulation files had been delivered, the analysed data was displayed on the screen for saving to disk.

2.2.3.7.2. Difficulties encountered

As with the force-velocity routine, keeping the muscle at Lo over the two-and-a-half hour duration of these experiments would be undesirable. The muscle was thus returned to a rest length shorter than Lo, where it stayed during the period between tests.

2.2.3.8. Fatigue tests

There are several ways of measuring muscle fatigue resistance. In the various approaches, contraction of the muscle is initiated at Lo. In one approach, corresponding to the Burke fatigue test, a force far in excess of the peak muscle tension is set on the lever arm and the muscle stimulated to contract isometrically. The developed force is then monitored over time as an indicator of muscle fatigue. In another approach, the muscle is set to contract repeatedly against the load that corresponds to optimal power and the resultant displacement is monitored over time. This is an isotonic fatigue test. In a third method, the muscle is stimulated to contract during the shortening phase of a constant-velocity ramp. The last two approaches, in which the muscle moves a load and therefore does external work, are more representative of a muscle that is providing assistance, for instance in cardiac assist. Software was written to implement the third method of fatigue measurement.

2.2.3.8.1. Program flow

The muscle Lo and optimal velocity (Vopt) were determined. With the muscle initially set at Lo, a 20 mm ramp was generated at Vopt from lever position +10 mm to -10 mm. The time (t) needed to accomplish this length change must be such that Vopt (mm s^{-1}) = 20/t. Hence,

$$t\ (ms) = \frac{20}{1000 * Vopt} = \frac{1}{50 * Vopt} \qquad (2.5)$$

The 20 mm step was then divided into smaller length steps of 20/t mm. Implementation of the ramp involved decrementing the lever position by the length step every millisecond from the +10 to the -10 position of the lever. After a short duration at the -10 mm position, the lever arm then ramped back to the +10 position, ready for the next constant-velocity ramp. The ramps could be repeated at any frequency, provided that there was adequate time within the cycle period for the constant-velocity ramp to run and for the muscle to be ramped back to the starting position (+10 mm) in time for the next ramp. Figure 2.9 is a flow chart for the ramp implementation.

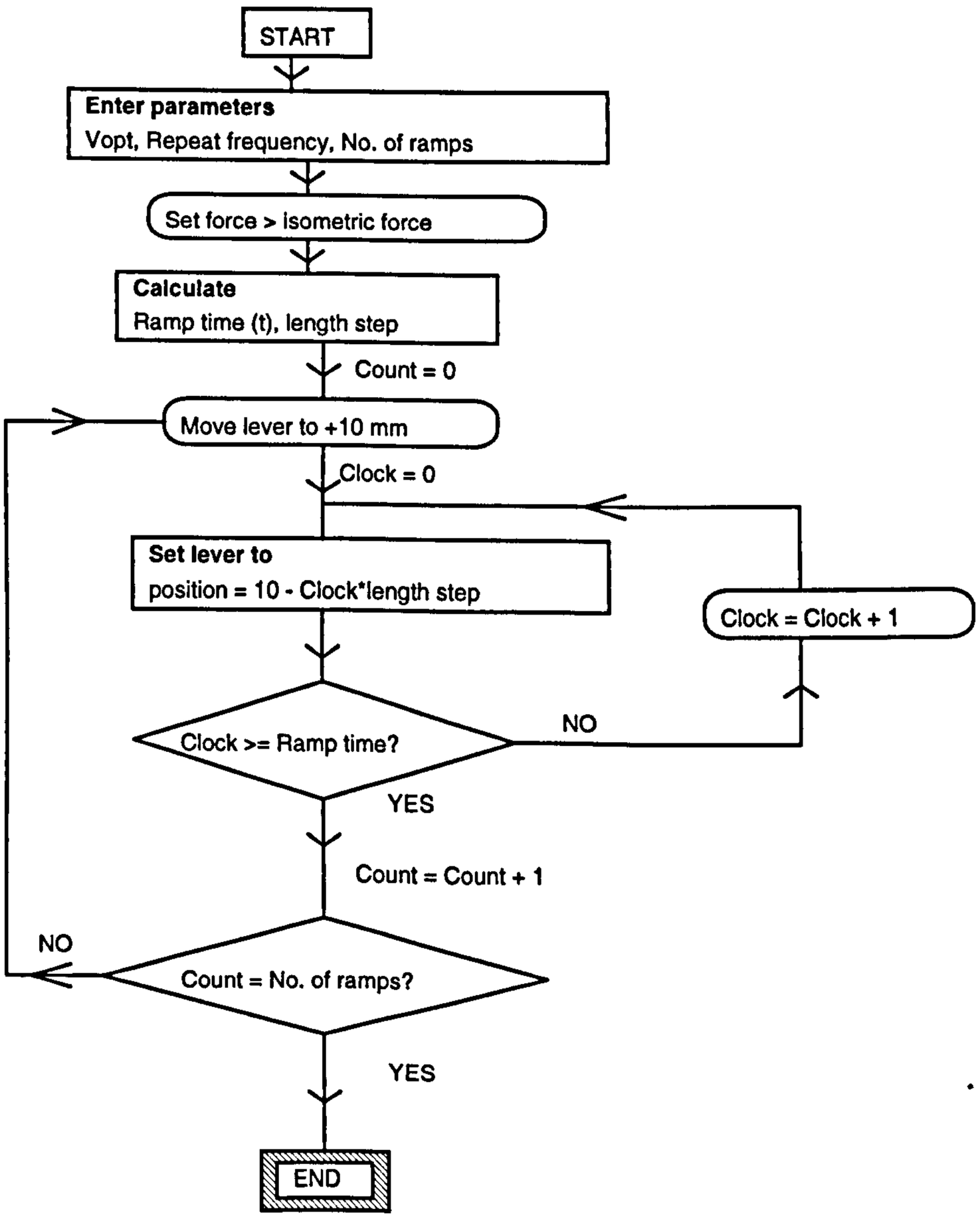

Figure 2.9. *Flow chart of constant-velocity ramp program for muscle fatigue measurement.*

Muscle stimulation was initiated by a trigger provided by the software just prior to the start of the constant-velocity ramp. The trigger was then used to set up a desired

stimulation burst from a constant-frequency generator (Devices Sales Ltd., Hertfordshire, UK, Digitimer D4030). The output from the latter was fed into the isolated stimulator for muscle stimulation. Using the Digitimer, the stimulation duration was adjusted during the shortening ramp so that the contraction force was as constant as possible. The force and length traces were then captured by CODAS for post-acquisition analysis.

2.2.3.8.2. Data analysis

The initial objective was to determine the ramp cycle frequency that allowed the muscle to work at a rate of 10 W/kg. Once the stimulation had been adjusted so that a suitable force trace was obtained (Figure 2.10), the stimulation was switched off and a few ramp cycles captured. The stimulator was then turned back on and further ramp cycles were sampled.

The area under the force record from the start to the end of the shortening ramp was measured and then multiplied by Vopt to obtain the active work; the passive work was determined from the force traces with no stimulation. The developed work (DevWork), the difference between the active and passive work, was then used to calculate the repetition rate of the shortening ramps to achieve the desired working level of 10 W/kg as shown in (2.6). Thus,

$$\text{Power (mW / g)} = \frac{\text{DevWork (Nmm)}}{\text{muscle mass (g)}} * \text{f (Hz)} \qquad (2.6)$$

where f is the repeat frequency. Substituting for the power level of 10 W kg^{-1} (equivalent to 10 N mm/g) into (2.6) and rearranging,

$$f = \frac{10 * \text{muscle mass (g)}}{\text{DevWork (Nmm)}} \qquad (2.7)$$

The fatigue test was then performed with the ramps set to repeat at the above frequency and the developed work measured over time to quantify muscle fatigue.

2.2.3.8.3. Difficulties

With such an approach, it may not be easy to set the muscle stimulation to give the force output. Also, because data was analysed post-acquisition, it was a time-consuming routine. However, this should be a useful method of quantifying skeletal muscle fatigue.

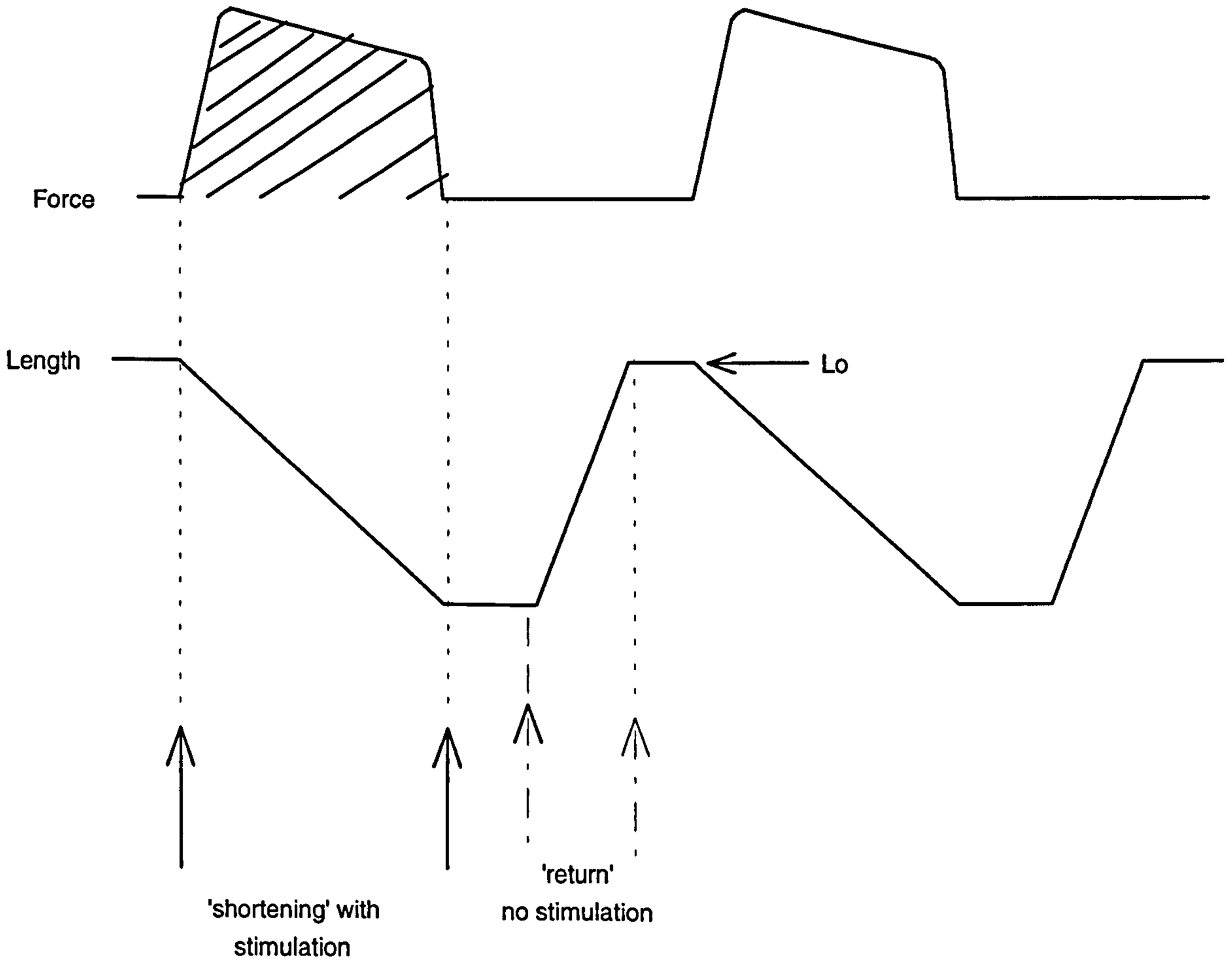

Figure 2.10. *Schematic representation of force and length traces of constant-velocity ramps.*

2.2.3.9. Cyclic control of the lever arm

Most of the control routines of the lever arm thus far mentioned have been for either isometric or single isotonic shortening contractions, except for the complex loads. However, muscle function involves cyclic shortening and lengthening contractions in activities such as flying, running, or swimming (Johnson & Altringham 1988; Johnston 1991; Josephson 1993). Moreover, a skeletal muscle providing circulatory assist is also subjected to cyclical loading. It was therefore necessary to develop software that would

allow us to investigate of parameters of cyclical function of muscle: such parameters include frequency of oscillation, stimulation frequency, phase at which stimulation is initiated and the duration of the stimulation. Data from such studies are usually analysed by producing work loops, which are the result of plotting the force versus the muscle length. Muscle power measured in this mode of operation reflects the important considerations necessary to take into account in the use of skeletal muscle for circulatory assistance.

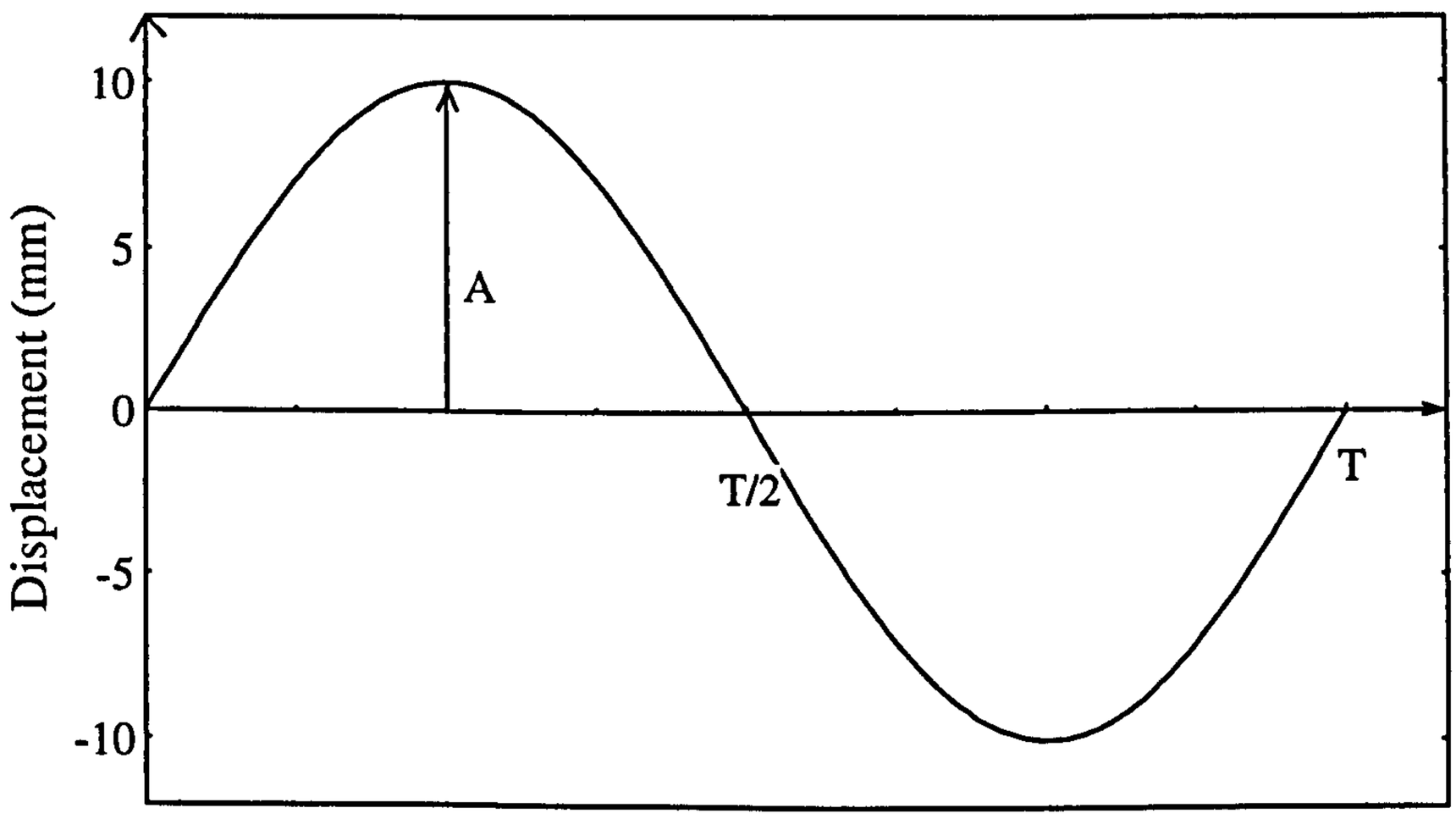

Figure 2.11. *A sinusoid depicting the parameters required for cyclic control of the lever arm. A = amplitude and T = period of oscillation.*

To afford cyclical control of the muscle, software was developed that allowed the muscle to cycle at a prescribed frequency, and enabled stimulation to be introduced at a desired phase of the movement. This was based on a sinusoidal function (Figure 2.11) with the lever oscillating about its central position, from which movement was initiated. The displacement as a function of time was therefore represented by

$$\text{Displacement (mm)} = A \sin(wt) \tag{2.8}$$

where A is the amplitude, the maximum displacement from the central position, ω is the angular velocity ($\omega = 2\pi f = 2\pi/T$; f = frequency (Hz) and T = period (in seconds) of oscillation) and t is the time (in seconds) from the start of the oscillation. Equation (2.8) could thus be represented as

$$\text{Displacement (mm)} = A \sin(2\pi ft) = A \sin\left(\frac{2\pi t}{T}\right) \tag{2.9}$$

2.2.3.9.1. Program flow

Given the frequency of oscillation, the amplitude of the movement, the stimulation phase angle (θ) and the number of oscillations (N), cyclic movement was implemented by first calculating the displacements for each time point over the whole duration of the cycle and storing the values in a global structure. The displacement was then updated every millisecond to achieve cyclic control of the lever arm (Figure 2.12).

In the protocol, the total oscillation time (in ms) was obtained by multiplying the number of cycles by the period of the oscillation (1/f). The displacement values for each millisecond from 0 to the total oscillation time was calculated by substituting the time and frequency in (2.9) and then storing the displacement values against the corresponding times in a global structure. The lever position was then updated every millisecond until all the cycles were completed.

A stimulation trigger was generated by converting the phase angle to a time point within the cycle period. Since a whole cycle (2π radians) is equivalent to the period (T) of the cyclic movement, a phase angle of θ radians in the Nth cycle will correspond to a time t_θ given by

$$t_\theta = \frac{N\theta T}{2\pi} = \frac{N\theta}{\omega} \tag{2.10}$$

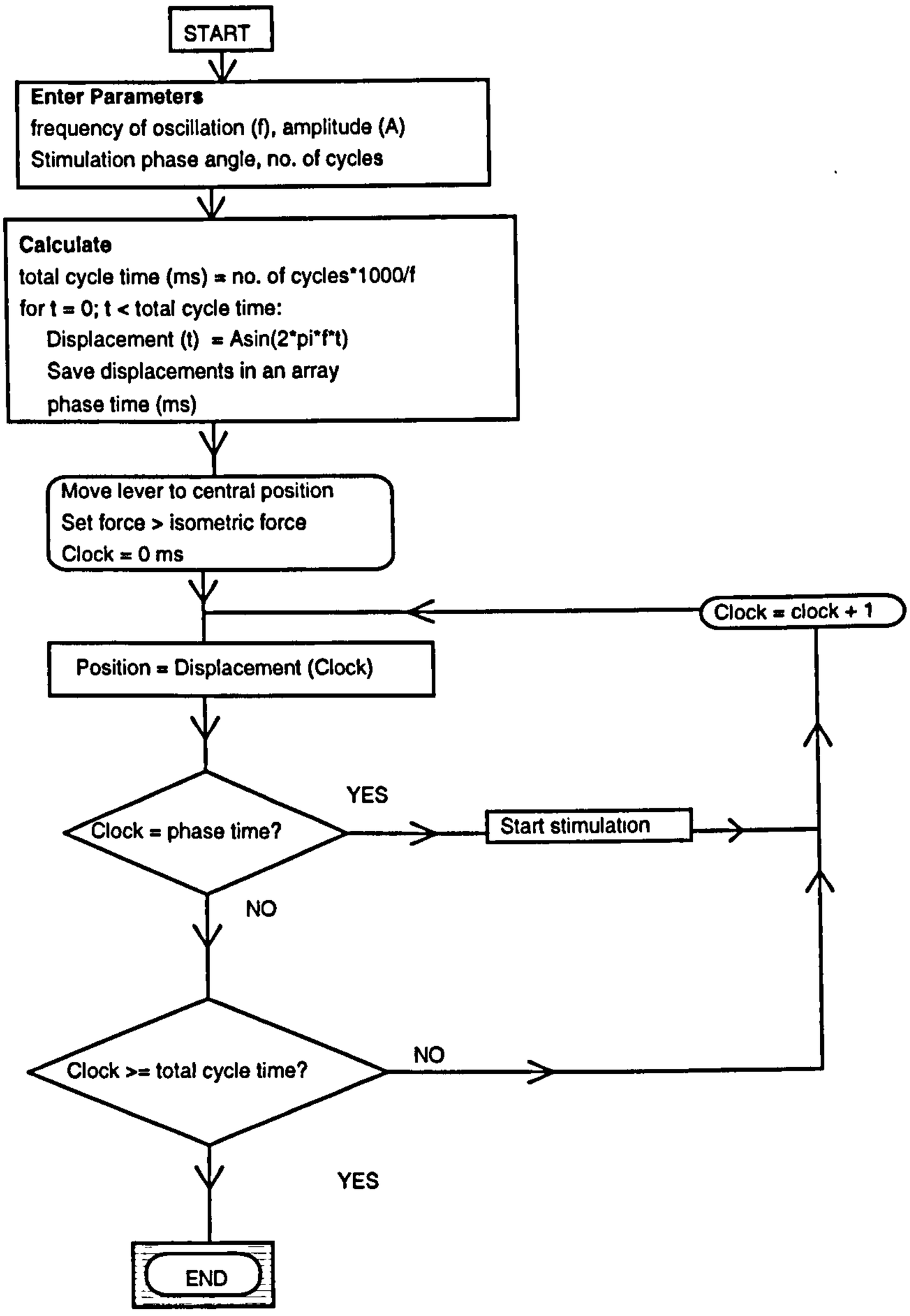

Figure 2.12. *Program flow for cyclic lever arm control.*

2.2.3.9.2. Difficulties encountered

The system clock had to be accessed in order to achieve correct timing. Thus, software similar to that used for the complex load routines was employed here to control the system's clock.

2.2.3.10. Post-tetanic potentiation

Electrical stimulation of skeletal muscle results in potentiation or depression of the muscle output on repeated tetanic stimulation. Such effects must be taken into account when the force profile of a muscle is controlled in FES. Experimental routines were

therefore developed that allowed studies of the effects of post-tetanic potentiation on stimulation patterns, especially optimal stimulation patterns, in control and chronically stimulated muscles. The idea was to deliver frequency bursts before and after a tetanic burst and then to compare the muscle outputs. This was achieved in two steps: the first to determine if there was an optimal post-tetanic delay interval at which muscle output was maximum, and the second to compare the effect on muscle output of stimulation bursts delivered at this optimal post-tetanic delay interval to those delivered pre-tetanically. Software was written to implement the above.

2.2.3.10.1. Program flow

2.2.3.10.1.1. Determination of optimal post-tetanic interval

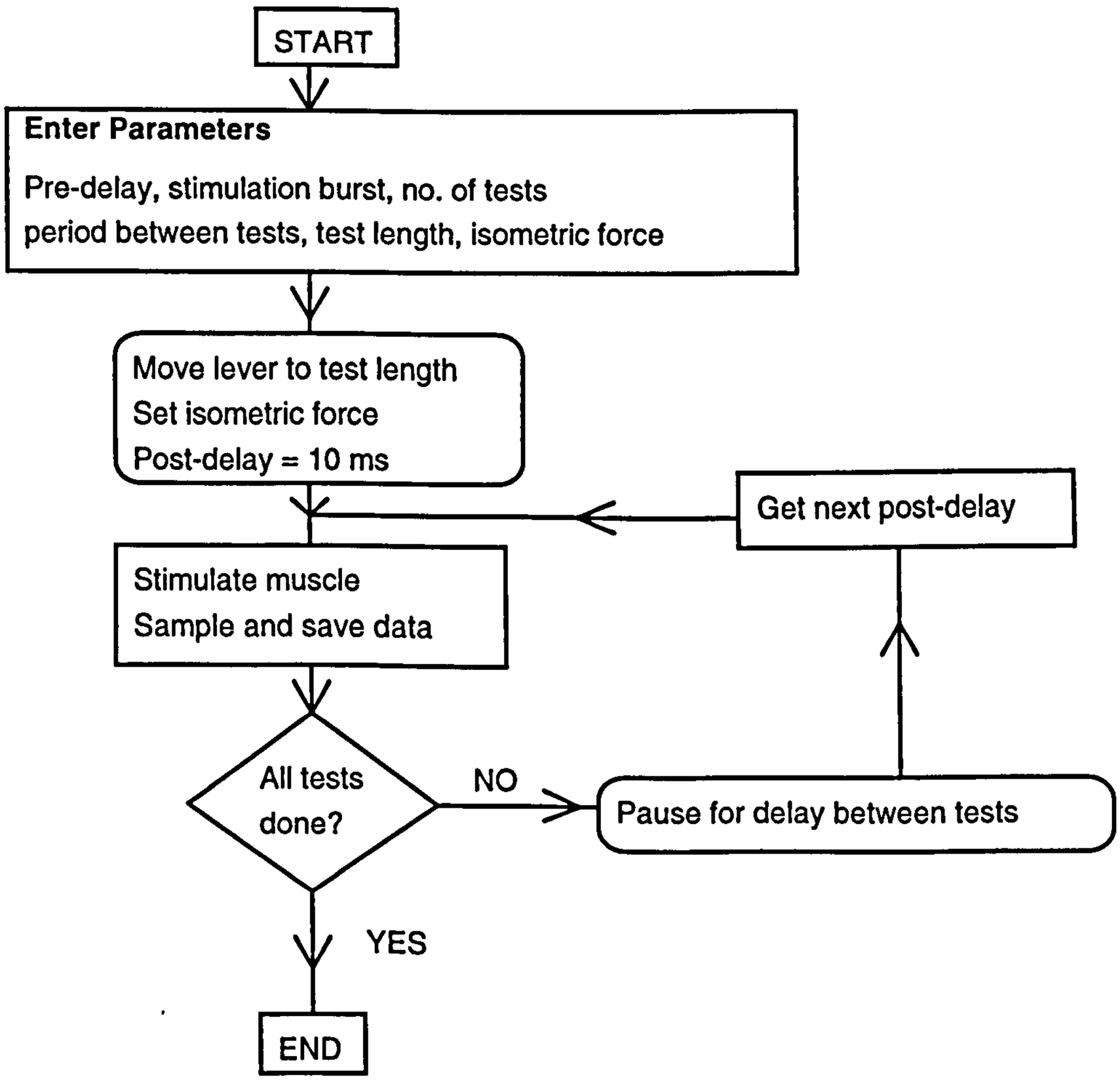

Figure 2.13. *Flow chart for determination of the optimal post-tetanic interval.*

The required experimental parameters, which included the pre-delay period (100 ms default) to the tetanus, the test burst file name, the number of tests, the muscle test

length, the isometric force and the period between tests, were entered. The software then set the muscle test length and the isometric force (Figure 2.13).

The test burst was delivered to the muscle and, after the pre-delay period had elapsed, a 200 Hz tetanic burst of 300 ms duration was also delivered. After the first post-tetanic delay interval had elapsed, the same test burst was again delivered. The sequence of post-tetanic delays was as follows (ms): 10; 20; 50; 100; 200; 500; 800; 1000; 2000; 5000; 10,000. The force and displacement traces were sampled from 50 ms prior to the first test burst delivery to about 100 ms after the end of the post-tetanic test burst delivery, resulting in a long data capture time. The data was captured and stored to disk using CODAS, which was triggered remotely by a 5 V TTL signal generated by the Digitimer. This was in turn triggered by pulses from the software. At the end of the period between tests, the next post-tetanic delay was used and the above routine repeated until all the tests were completed. The data was then analysed post-acquisition: the force and the force-time integral at the different post-tetanic delays were measured. The delay with the maximum muscle output was then used in the subsequent experiment.

2.2.3.10.2. Difficulties

Because of limitations on remote triggering of the CODAS system, the data sampling period, which increased with both longer post-tetanic delays and test burst duration, could not be varied for individual tests. Therefore, a sampling period of 11 s, covering the longest possible sampling requirement for a post-tetanic delay of 10 s, had to be used in the determining the optimal post-tetanic interval. Such an excessive sampling period in all tests meant that some memory was wasted. However, the CODAS system can record for very long periods on hard disk.

2.2.3.10.2.1. Effects of post-tetanic potentiation on burst output

A burst with a given number of pulses was delivered to the muscle pre- and post-tetanically as above. However, the post-delay interval was set to the optimal post-tetanic

delay period determined above. The procedure was then repeated, but with bursts of varying frequency and number of pulses. CODAS was used to capture and analyse the data after acquisition. The pre- and post-tetanic outputs were compared.

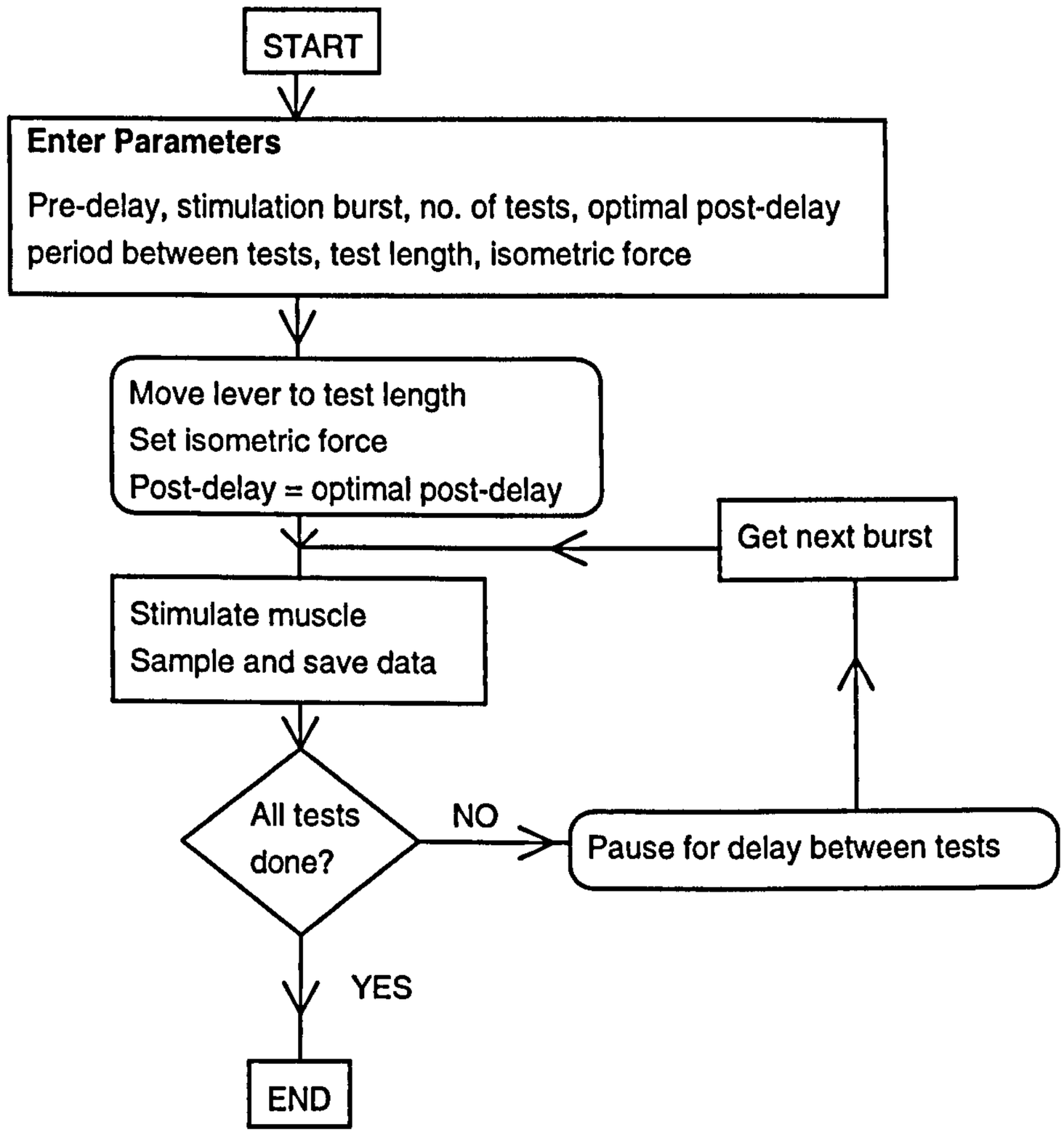

Figure 2.14. *Flow chart for varying stimulation burst delivery.*

2.2.4. Validation, refinement and reliability of the CCSS

The CCSS was found to be a very reliable and accurate system. The series 310B lever system was factory-calibrated and the manufacturers state that recalibration is not required over the lifetime of the instrument. With the high resolution and linearity of the length and force signals, and with negligible measurement errors, the CCSS measurements were very accurate (see below). Furthermore, the PC-30D card had manufacturer-supplied software to calibrate the ADC and DAC subsystems for reliable voltage conversions. However, the system still had to be calibrated for a particular force applied to the lever arm.

2.2.4.1. System validation

Known forces were applied to the lever arm and the corresponding voltages noted. This was achieved by placing the series 310B rotor housing on its side so that the lever arm could move in a vertical direction. The force offset was turned fully clockwise to set a force of 50 N on the lever arm, and so fix its position. Standard weights were then hung by means of light elastic bands to the servo arm and a voltmeter used to measure the resulting voltages on the "force out" signal. The computer monitor also displayed the force value as measured by the CCSS. Figure 2.15 is a plot of the weights and the corresponding system outputs. The linear regression fit of the data shows perfect correlation ($r^2 = 1.0$) between the input and output of the CCSS.

2.2.4.2. Reliability

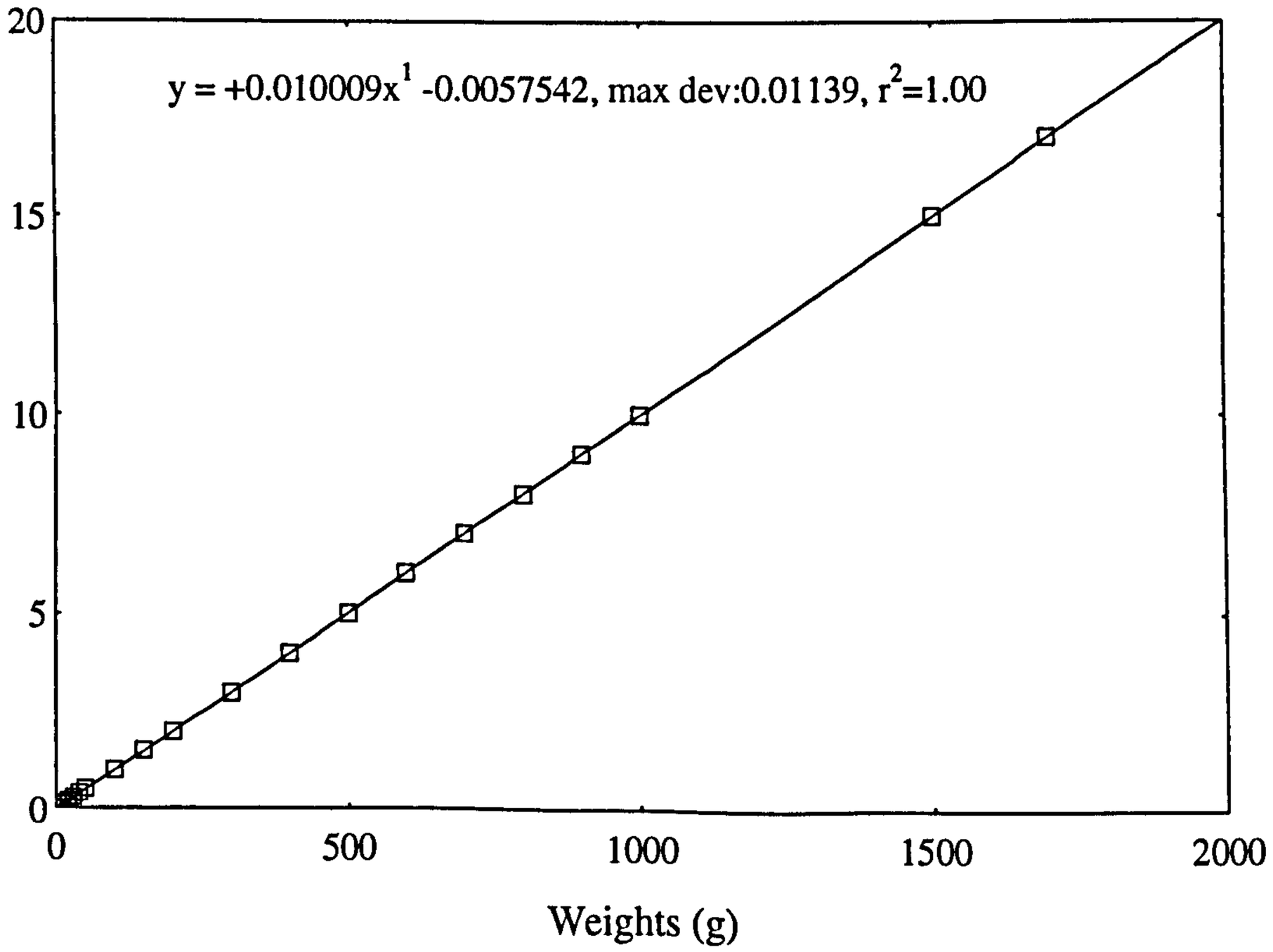

Figure 2.15. *Validation of force measurements. The linear regression fit shows that there is perfect correlation between input and output of the CCSS.*

The system was able to give reproducible results all the time, apart from discrepancies resulting from changes in the state of the muscle. The data analysis routines worked well,

but sometimes analysed data had one or two spurious data points. When this occurred, the raw data file was re-analysed using commercially available software.

Unfortunately, the force signal could disappear. This was particularly troublesome as a whole experiment could be ruined by the loss of the force signal. Therefore, a CRO was often used to monitor the force signal during an experiment. If the signal disappeared, the experiment was stopped and the system reset by pushing the lever arm out of range. Sometimes, it was necessary to replace one or more of the chips in the interface box. However, loss of the force signal was rare.

2.2.5. Summary

The CCSS provided a means of measuring accurately and quickly the mechanical relationships of skeletal muscle. Because of its versatility, it was adapted to automate several other measurements of muscle mechanical properties. The system also allowed the force on the muscle to be changed auxotonically, i.e. with both length and force changing simultaneously under computer control. This enabled software to be written to control the force on a linearly contracting muscle as though it formed part of the wall of a skeletal muscle ventricle; such control has not been reported previously. In conclusion, the CCSS is a reliable and versatile system, and was used extensively to investigate the biomechanics of skeletal muscle for use as a contractile surgical biomaterial.

2.3. Measurement of hydraulic performance of ventricles

2.3.1. Introduction

Since the work of Acker *et al.* (1987c), the study of SMV function has always involved the use of mock circulation systems, which mimic the human circulation. As reviewed by Bowles *et al.* (1991), there are several types of mock circulation system. Because these devices simulate physiological parameters, they allow experimental ventricular assist devices to be loaded as though they were providing cardiac assist in circulation. The

hemodynamic function of these assists can then be studied to improve their function and efficiency of energy conversion.

In the present work, a mock circulation device was developed in-house and used to measure the hydraulic function of acute SMVs constructed from sheep LD muscles. Because the system was built in-house, it was constantly being updated in the course of the experiments. Nonetheless, it was a very adaptable and reliable system, and allowed useful measurements of SMV function. The hydraulic system consisted mainly of two parts: a data acquisition system and a mock circulation.

2.3.2. The hydraulic data acquisition system

The system consisted of an adaptable mock circulation, a servomotor pump and a PC for control and data acquisition. The software aspects of this system were developed by Dr Adam Shortland of the Department of Clinical Engineering. The pump was controlled by utilizing a feedback signal from a linear displacement transducer (Linear potentiometer, 100 mm, 4K, Penny & Giles Position Sensors Ltd., Christchurch, UK) to ensure precise positioning of the piston head. The piston could be made to advance or retreat by depressing the computer's arrow keys. The pump had a volume resolution of 0.5 ml and a capacity of 300 ml. A highly schematic drawing of the hydraulic testing system is shown in Figure 2.16.

Two Luer-fitting pressure transducers (Gaeltec Ltd., Isle of Skye, Scotland) measured preload and afterload pressures, and an in-line ultrasonic flow probe (Model HT107, Transonics Systems Inc, USA) measured outflow from the ventricle. The cannulating flow probe used throughout the experiments had a 19 mm bore. Pressure and flow transducers were calibrated prior to conducting an experimental procedure.

2.3.3. Adaptable mock circulation

The apparatus was constructed largely from perspex. It consisted of a T-shaped section which incorporated a port for the 'ventricular' or preload transducer. The side arm of the T-piece led to the servomotor volume control system. At the distal end of the T-section, a one-way valve led to a voluminous pressurised afterloaded chamber - 10 cm high - that contained a small volume of water. This served both to keep the system airtight and to provide a liquid environment for best performance of the pressure probes. The air space in the afterload chamber was connected to a 40-litre air chamber that was pressurised to any desired afterload by means of a cylinder pump. Since the volumes ejected from the ventricle were small compared to the air chamber volume, the afterload was practically constant during ejection. A perspex block was placed at the bottom of the afterload chamber so that the cross-sectional area available to the fluid was very small. The side of the chamber was marked in this region so that one could accurately return to the ventricle the fluid ejected from it during the previous contraction. This volume also served for comparison with the ejected volume calculated by the software by integration of the flow.

2.3.4. Data acquisition and analysis

Flow and pressure traces were recorded by a 12-bit multichannel A/D converter (DASH 16, Metrabyte Corp., USA.) and simultaneously displayed on the host computer. The sampling frequency of data acquisition was 100 Hz per channel. Data recording was triggered at the onset of muscle stimulation. Data records were post-processed for calculation of flow, pressure, stroke volume and work. The output power efficiency of the SMVs could then be calculated.

2.3.5. Limitations of the system

The long length of non-uniform tubing leading from the ventricle to the afterload chamber, whose resistive properties may be difficult to account for because of its non-

uniformity, should be shorter to decrease resistance to flow. The fact that the system was updated progressively meant that earlier measurements were not as accurate.

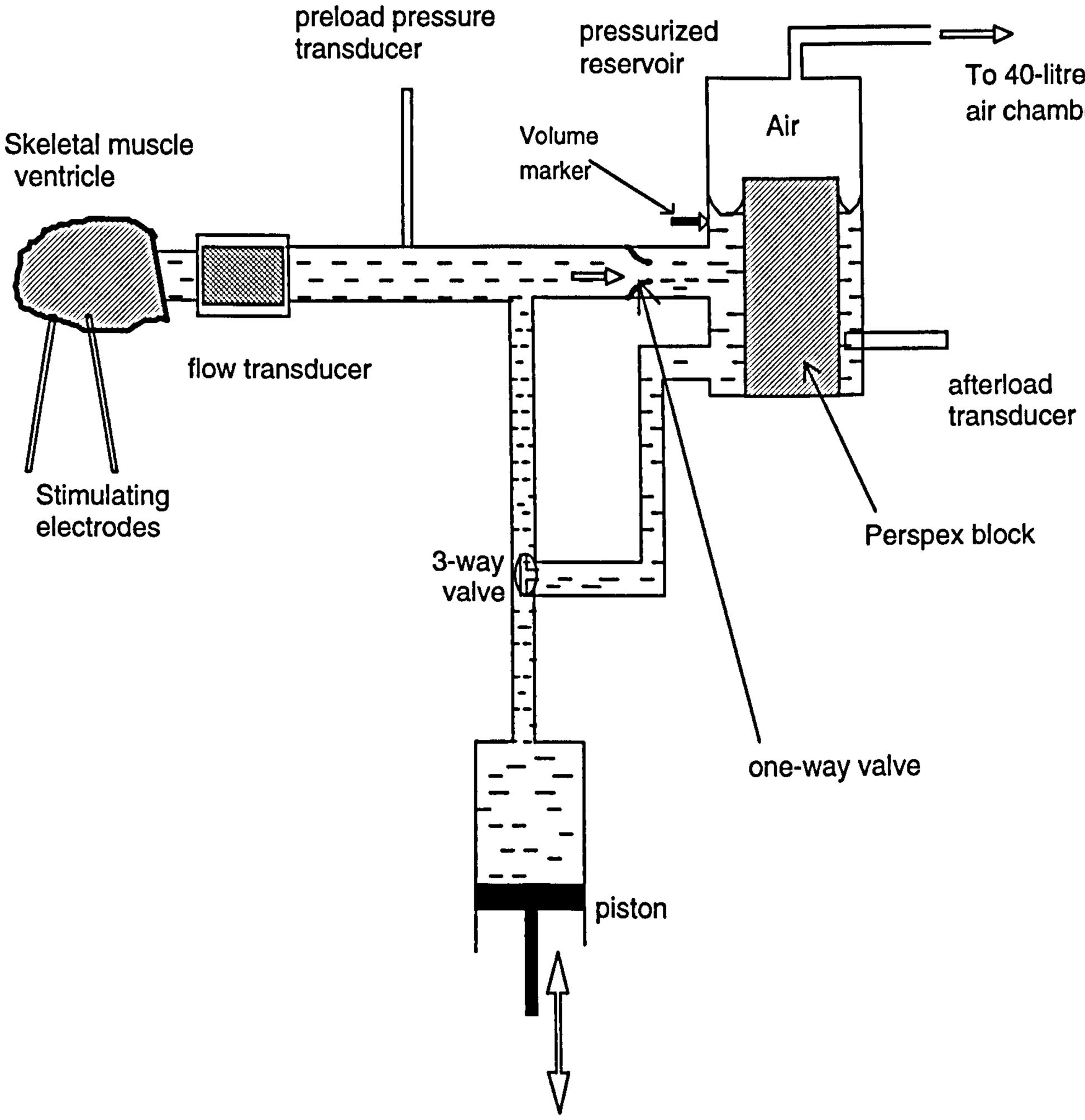

Figure 2.16. *Schematic diagram of the adaptable mock circulation. The flow, preload and afterload transducers were connected to a PC, and the piston was controlled by another PC.*

2.4. Conclusion

The CCSS for the measurement of muscle linear mechanical properties and the hydraulic system for the measurement of hemodynamic properties of SMVs worked well. Despite a few problems, they allowed skeletal muscle to be characterized as a ventricular assist device. In fact, the electrohydraulic system previously used in Prof. Salmons' laboratory for measurement of muscle mechanical characteristics (Jarvis & Salmons 1991b; Jarvis *et*

al. 1991c; Jarvis 1993) has now been replaced by the CCSS, as is evident from recent publications (Jarvis *et al.* 1993b, c; Kwende *et al.* 1995). The CCSS is therefore a useful research tool, and its potential has certainly not been exploited fully yet.

3. Linear Mechanical Properties of Skeletal Muscle

3.1. Summary

The mechanical properties of rat, rabbit and sheep skeletal muscles were measured using the servomotor system described in Chapter 2. The system performed satisfactorily and was able to measure accurately the linear properties of muscles with different mechanical characteristics. Thus, muscles that had undergone chronic low-frequency stimulation could be compared with unstimulated control muscles. The implications of the differences in terms of cardiac assistance are discussed. Furthermore, the basis for using the mechanical properties in a mathematical model of skeletal muscle ventricles is established.

3.2. Introduction

As an actuator, skeletal muscle properties are governed by a series of curves relating force to length, force to frequency, force to velocity of shortening, and power to velocity (see Chapter 1). These relationships determine the power that the muscle can deliver, and the working conditions under which it can be loaded to perform most efficiently. Following the work of Hill (1938), several investigators have measured muscle mechanical characteristics, both in single fibres (Edman *et al.* 1976; Sweeney *et al.* 1986; Curtin & Woledge 1988) and in whole muscles (Kernell *et al.* 1987; Salmons & Jarvis 1990a, b, 1992; Jarvis 1993), in order to elucidate muscle function (Wilkie 1985). However, with the discovery of skeletal muscle fatigue resistance, which reopened research into the use of such muscle for cardiac assist, these measurements have been geared towards unravelling, and therefore modifying, the changes associated with chronic electrical stimulation. A detailed knowledge of these changes is being exploited in strategies to load skeletal muscle to function to its maximum capacity in providing cardiac type work (Salmons & Jarvis 1990a, b, 1995; Jarvis 1993).

A skeletal muscle (latissimus dorsi) mobilised for cardiac assistance is usually wrapped either around the heart in cardiomyoplasty (Carpentier & Chachques 1991), or around a

mandrel (Pochettino *et al.* 1991) that is subsequently removed to form an SMV. The fibre architecture in this new configuration is alien to the muscle and so may result in impaired function of the muscle graft, as discussed by Salmons and Jarvis (1990b, 1991a). This is because sarcomeres on the outside of the wraps may be over-stretched while those on the inside are at suboptimal, or even non-functional, lengths. The wrapping of the muscles may also result in increased intramuscular pressure due to increased fibre curvature; this may lead to decreased blood flow to the muscle (Van Leeuwen & Spoor, 1992) and thus to a lowered oxygen supply. Consequently, the maximal sustainable muscle power would be reduced. Moreover, though chronic electrical stimulation is necessary to produce fatigue-resistant muscle, it also results in a further loss in muscle power due to a reduction in both muscle bulk (Pette *et al.* 1976; Salmons & Henriksson 1981; Eisenberg & Salmons 1984; Jarvis et al. 1991b) and maximum speed of contraction (Salmons & Vrbová 1967, 1969; Al-Amood *et al.* 1973; Pette *et al.* 1973). Although the function of a skeletal muscle in an SMV configuration may be compromised by chronic electrical stimulation and surgery, loading conditions could still be determined to allow this muscle to provide maximal cardiac assist.

It is, however, not known whether an optimal configuration of skeletal muscle in its new cylindrical configuration allows it to function as efficiently as in its linear configuration. It certainly is important, at least, to gain knowledge of how much power is lost merely by changing the muscle's physiological configuration, and how these losses vary for muscles in different states of transformation. Such information will be invaluable in optimizing muscle power output for circulatory assistance. Certainly, it is crucial in cardiac assist to load the muscle to function as close as possible to its peak performance, which, in the linear configuration, is usually related to the peak of its power-velocity curve. Hence, the use of skeletal muscle as a surgical biomaterial should be guided by a detailed understanding of its linear mechanical properties.

3.3. Aims

The aim of the work described in this chapter was to measure the linear mechanical properties of rat, rabbit and sheep muscles that had a history of low-frequency chronic electrical stimulation and to compare them with measurements in unstimulated controls. These measurements would allow the sensitivity of the servomotor system, in terms of differentiating between muscles with different mechanical properties, to be tested. These properties would then form the basis for a numerical model to optimize the function of SMVs.

3.4. Materials and methods

3.4.1. Chronic electrical stimulation

3.4.1.1. Implantable stimulators

Miniature electronic stimulators were designed and constructed as described previously (Jarvis & Salmons, 1991a). The devices were encapsulated in silicone rubber (Dow Corning 3140RTV, Midland, MI) and were 35 mm in diameter and no more than 8 mm thick. A Dacron mesh extending from the encapsulant facilitated suturing. The output from the device was taken via multistrand PVC-insulated stainless-steel wires (Cooner Sales Company, Chatsworth, CA, USA) to loop electrodes formed from the bared wire and a Dacron velour pad. The implantable pulse generator incorporated a photosensitive switch which enabled it to be turned on and off remotely by light flashes through the skin. The output pulses were of 0.2 ms duration and 3.2 V amplitude at various frequencies set during construction (2.5 - 20 Hz). This protocol provides supramaximal stimulation of all the motor axons in the common peroneal nerve.

The devices were sterilized by immersion in benzalkonium chloride (10 g l^{-1}) for 24 h and implanted into either adult New Zealand White rabbits or adult male Wistar rats, under deep anaesthesia. Full aseptic precautions were taken.

3.4.1.2. Anaesthesia and Surgical Procedures

3.4.1.2.1. Rat

Rats were anaesthetised with intraperitoneal fentanyl/fluanisone (Hypnorm: fentanyl citrate, 0.315 mg ml^{-1} and fluanisone, 10 mg ml^{-1}, Janssen Pharmaceutica, Grove, Wantage, Oxon; 1 ml kg^{-1}) immediately after intraperitoneal administration of atropine sulphate (Sigma Chemical Co. Ltd., UK; 1.5 mg kg^{-1}) and diazepam (Roche Products Ltd., UK; 5 mg kg^{-1}). The miniature stimulators were placed in the abdominal cavities of the rats, and in closing the muscular wall of the abdomen the Dacron mesh was entrapped, suspending the stimulator from the wall, to avoid migration. Leads were passed subcutaneously from the flank to the common peroneal nerve; one lead was placed proximal to the nerve and the other was placed in the lateral head of the gastrocnemius muscle. The rats were allowed to recover from surgery for one week before the stimulator was switched on by a pulse of light directed through the skin and subjacent tissues to a phototransistor in the device (Brown & Salmons 1981). Stimulation of the left common peroneal nerves was then continuous at 10 Hz or 20 Hz for 55-61 days.

3.4.1.2.2. Rabbit

Implantation of stimulators into the rabbits took place under deep anaesthesia with fentanyl/fluanisone (Hypnorm: fentanyl citrate, 0.315 ml kg^{-1} and fluanisone, 10 mg ml^{-1}, Janssen Pharmaceutica, Grove, Wantage, Oxon; 0.3 mg kg^{-1}, I.M.) after premedication with atropine sulphate (Sigma Chemical Co. Ltd., UK; 3 mg kg^{-1}) and diazepam (Roche Products Ltd., UK; 5 mg kg^{-1}) given subcutaneously. The device was placed subcutaneously and sutured lightly to the abdominal wall; leads were taken subcutaneously to the lower hind limb. One electrode was placed in a slip of the gastrocnemius muscle immediately beneath the common peroneal nerve. The other electrode was placed 20-30 mm distally on the surface of the lateral head of the gastrocnemius muscle. The wounds were closed with Prolene sutures (Ethicon Ltd., Edinburgh, UK) and the rabbit left to recover for 1 week before the stimulator was

switched on. Stimulation of the common peroneal nerve was then continued without interruption until the terminal experiment.

3.4.1.2.3. Sheep

Sheep, maintained under deep anaesthesia with 1.5% fluothane in 1:1 oxygen/nitrous oxide after induction and intubation with intravenous sodium thiopentone (approx. 10 mg kg^{-1}), were implanted with clinical neuromuscular stimulators (Medtronic Itrel), which were placed in a pocket under the rectus abdominis muscle. Electrodes from the stimulators were tunnelled under the skin, interlaced into the proximal portion of the LD near to the motor nerve branches and secured with titanium ligation clips. Full aseptic precautions were taken. The stimulators were programmed to deliver 210 μs pulses at a continuous frequency of 2 Hz for 6-8 weeks.

3.4.2. Terminal procedure

3.4.2.1. Rat

In terminal experiments, the rats were anaesthetised with urethane (Sigma Chemical Co. Ltd.; 30% solution, 5 ml kg^{-1}). Without disturbing any existing electrodes, new electrodes were placed near to the common peroneal nerve on both sides and the nerve was cut proximal to the electrodes. The muscle and skin were then closed over the electrodes. The tibialis anterior (TA) muscle was carefully displaced laterally from the extensor digitorium longus (EDL) muscle, cutting only the fibrous attachments between the two muscles. The proximal tendon of the EDL was exposed by an incision that ran a few millimetres into the knee capsule. The proximal tendon was held firmly in a modified artery forceps and the heel was supported in a small toothed clamp. The distal tendon of the EDL muscle was tied to a light steel hook, that was in turn connected to the servomotor arm. The muscles were kept moist with liquid paraffin and warmed with electric heating lamps to maintain their temperature at 37 ± 1 °C.

3.4.2.2. Rabbit

In terminal experiments, the rabbits were anaesthetized with urethane (Sigma Chemical Co. Ltd.; 300 g/l; 600 mg/kg body weight) and pentobarbitone sodium (Sagatal, May & Baker Ltd., Manchester, UK; 30 mg/Kg), administered via a 25 g butterfly catheter in the marginal ear vein. Supplementary doses of pentobarbitone sodium were given throughout the procedure as needed, to maintain deep anaesthesia. The trachea was cannulated, but it was seldom necessary to provide mechanical respiratory assistance. In animals that had been subjected to chronic stimulation, the leads were cut at this stage. Flap electrodes (Barnard *et al.* 1986) were implanted around both common peroneal nerves without disturbing the chronic stimulation electrodes on the left side. The nerve was then cut centrally, proximal to the electrodes. The TA tendon was transected below the extensor retinaculum and threaded through a miniature titanium alloy clamp, leaving a minimum of unclamped tendon. The alloy clamp was connected by a non-compliant carbon fibre-epoxy link to the servomotor arm (see Figure 2.2). The muscles were kept moist and their temperature maintained as above.

3.4.2.3. Sheep

Sheep were maintained under deep anaesthesia with 1.5% fluothane in 1:1 oxygen/nitrous oxide after induction and intubation with intravenous sodium thiopentone (approx. 10 mg kg^{-1}). The LD muscle of the anaesthetised sheep was exposed. In the stimulated muscles, the electrodes were disconnected from the implantable stimulator. Electrodes were then introduced into unstimulated muscles as described above, and connected to the isolated stimulator in both sets of muscles. With the muscle *in situ*, i.e. with the forelimb in its normal standing position, marker sutures were placed at 5 cm intervals, starting from the distal myotendinous junction, proximally in the midline of the muscle. The resting muscle length was measured before freeing the muscle by cutting through the distal attachments. Care was taken to maintain the blood and nerve supplies intact at the proximal end. Some

fat was retained on the top surface of the muscle to keep it warm. It was necessary to perform as complete a proximal dissection of the muscle as possible so that the muscle could be lifted away from the costal surface in order to achieve reliable mechanical measurements. The free distal portion was wrapped and sutured around a light aluminium tube (about 15 cm long) grooved at each end. Velcro strips were used as pledgets to provide sufficient mechanical support. A flexible steel wire, with small blocks at both ends to hook into the grooves, connected the muscle to the arm of the servomotor, which was attached to a steel frame that was lifted over the sheep. The humerus, to which the LD was still inserted at its proximal end, was fixed by strapping it to the frame. Electric heating lamps were used to maintain the temperature of the LD at 37±1°C.

3.4.3. Mechanical measurements

With the muscles attached to the servomotor arm, the loading of the muscle, stimulation, collection and analysis of force and displacement records was achieved under automated control, as described in Chapter 2. Mechanical measurements were carried out to determine the force-length, force-frequency, force-velocity and power-velocity relationships of the rat EDL, rabbit TA and sheep LD muscles. The time to peak force and the half-relaxation time of the twitch response, and the maximum tetanic force were also recorded. At the end of the mechanical measurements, other tests, such as the construction of SMVs in sheep LD, were carried out on the muscles as necessary. Finally, the muscles were removed and weighed.

3.4.4. Curve fitting

The passive force-length and the force-velocity curves were fitted by the least squares fitting routine, using EasyPlot (Spiral Software, Brookline, MA, V.3), to the exponential equation (1.4) suggested by Pinto and Fung (1967) and to Hill's equation (1.5), respectively, so that these curves were defined by equations with known constants. To obtain good fits, the procedure was carried out in two steps. An initial curve-fitting

routine used arbitrarily chosen starting values for the constants. A second fit then used the constants obtained from the initial fit as starting values, resulting in good fits to the experimental data.

3.5. Results

3.5.1. Characteristic curves

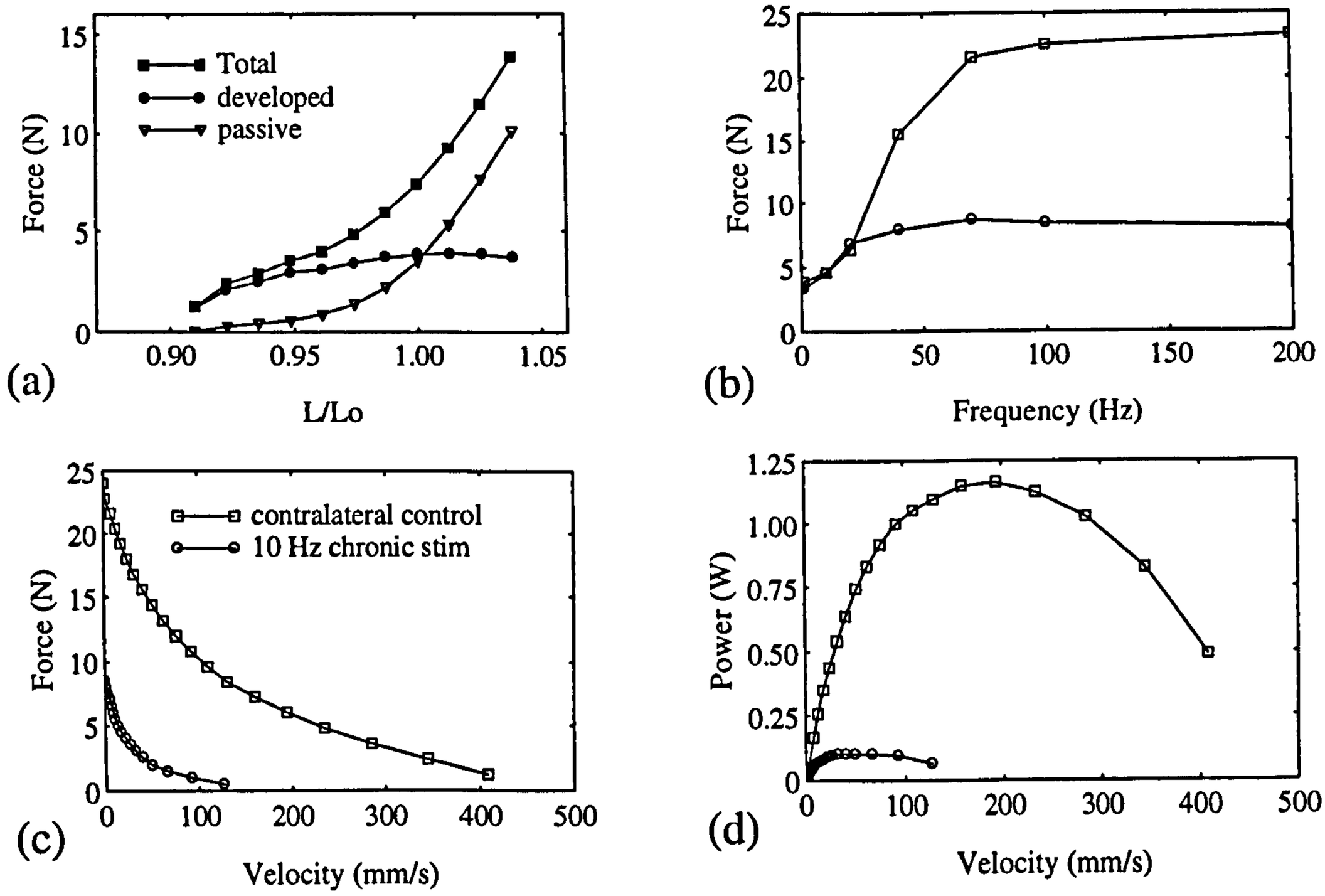

Figure 3.1. *Typical linear mechanical relationships of skeletal muscle obtained using the servomotor system. These curves are for rabbit tibialis anterior muscles. (a) Force-length curves for a control muscle. (b) Force-frequency, (c) Force-velocity and (d) Power-velocity curves. See panel (c) for legend for panels (b) and (d). The data points are joined by straight lines.*

Figure 3.1 shows the characteristic curves of rabbit TA muscles measured by the servomotor system. The passive curve in Figure 3.1a shows the typical exponential relationship between force and fractional stretch in skeletal muscle. The mechanical properties of chronically stimulated muscles are compared with those of the contralateral controls in Figures 3.1b, c and d. Similar force-length, force-frequency, force-velocity and power-velocity curves were obtained for the rat and sheep muscles.

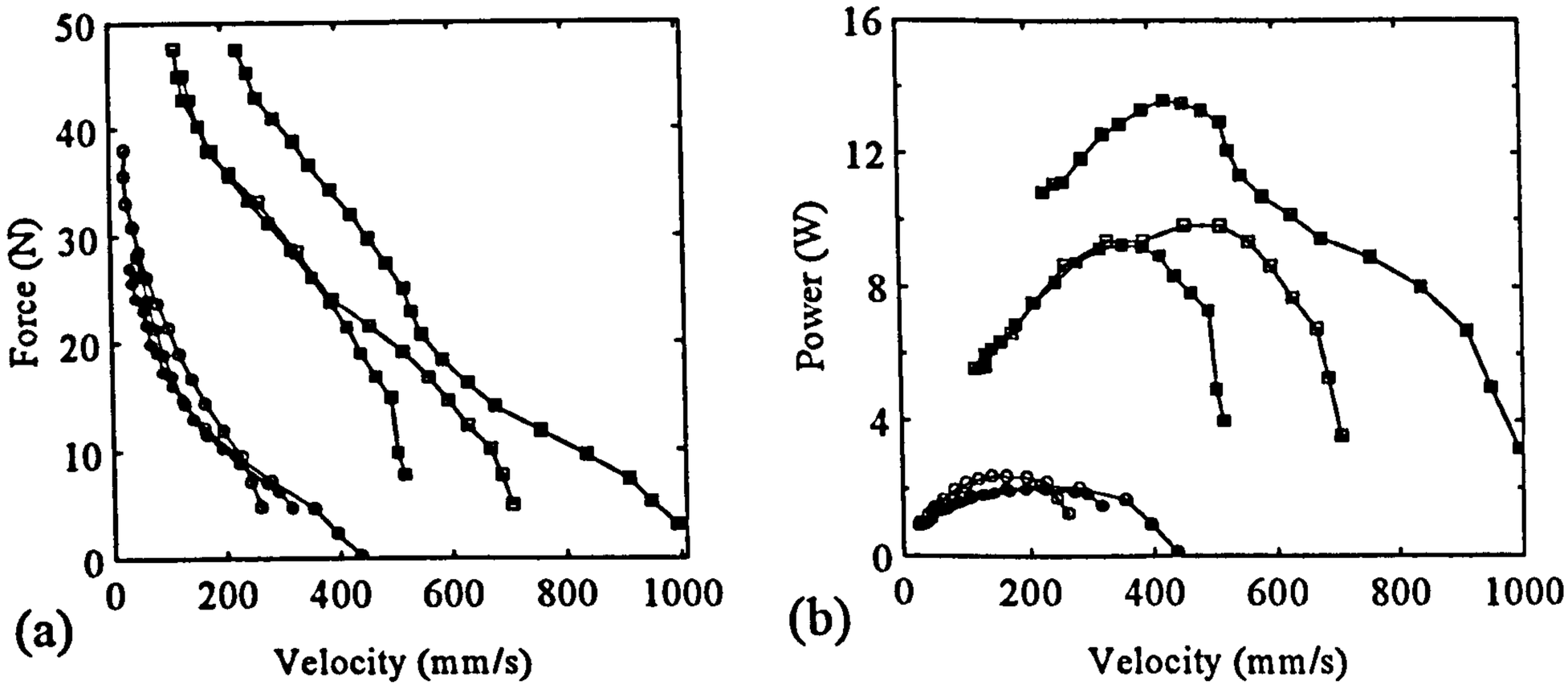

Figure 3.2. *Plots of force-velocity and the corresponding power-velocity curves for control (square symbols) and chronically stimulated (circle symbols) sheep LDs. The data points are joined by straight lines. The irregularity of the curves in places is due in part to problems with the limited force range of the servomotor and also to difficulties of attaching the LDs to the servo arm.*

The force-velocity and the corresponding power-velocity curves from control and chronically stimulated sheep LD muscles are shown in Figure 3.2. The faster control muscles did not give smooth hyperbolic curves, probably due to the nature of the experimental preparation. In addition to the fact that the sheep LD is long and compliant, it also has fibres of different lengths, which necessitated the addition of a cloth material to the LDs to enable their attachment to the servo arm. Some force records therefore contained oscillations due to lateral vibrations of the muscle and linkage between the muscle and the servomotor. However, the quality of the records were sufficient to determine the mechanical properties of the sheep LDs. Although the 0 to 50 N force range of the servomotor system used to determine sheep LD mechanical properties was limited, it covered a sufficient range to identify the peak of the power-velocity curve (Figure 3.2b), and thus allowed these properties to be compared to those measured in the rat and rabbit muscles (see later). Stimulated LDs produced a maximum power output of about 2 W, and control muscles about 10 W; these correspond to about 90 W kg^{-1} and 15 W kg^{-1}, respectively. These represent the instantaneous power output of the muscles, and should not be taken to indicate the sustainable power output.

Changes in the characteristic properties of the muscles following long-term electrical stimulation were dramatic. In rabbit TA muscle, there was a reduction in the fusion frequency from 70 Hz in the control muscle to 30 Hz in the stimulated muscle (Figure 3.1b), accompanied by a 60% drop in the peak isometric tension (Po). Furthermore, there was about a three-fold fall in the maximum velocity of contraction (Figure 3.1c), which, together with the 60% fall in Po, translated into a 90% drop in peak power output (Figure 3.1d).

3.5.2. Twitch versus tetanus

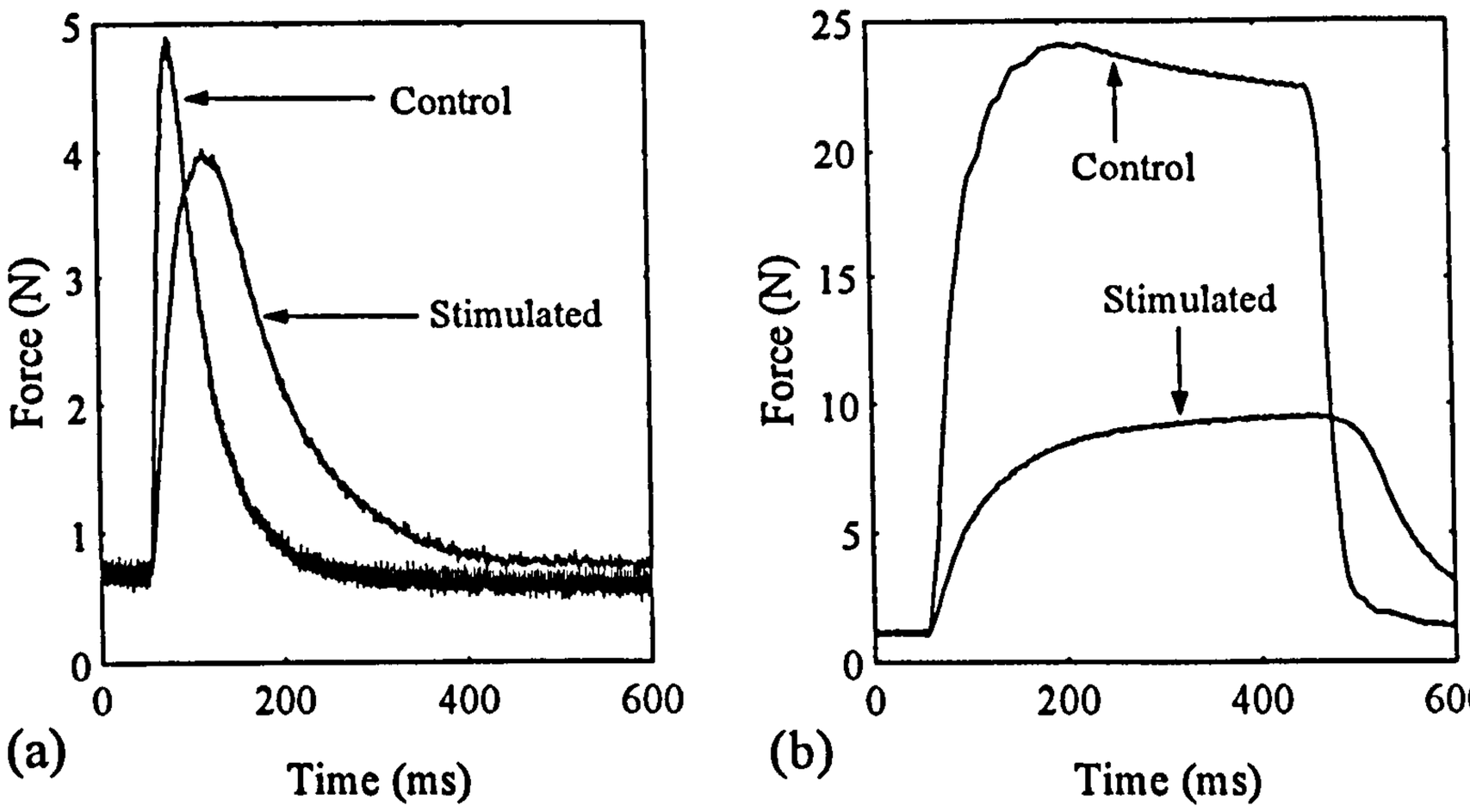

Figure 3.3. *Comparison of twitch and tetanic force responses in control and chronically stimulated rabbit TA muscles. (a) Twitch response. (b) Tetanic response to a 400 ms, 100 Hz burst.*

Figure 3.3 shows the twitch and tetanic force responses for a rabbit TA muscle that had been chronically stimulated at 10 Hz and its contralateral control. Long-term electrical stimulation resulted in a slower-rising, longer-lasting twitch response (Figure 3.3a), and a greatly reduced peak tetanic tension (Figure 3.3b). As a result, the twitch:tetanus ratio (TW:TET) is 1:2 in the chronically stimulated muscle and 1:5 in the control muscle, respectively. Chronic stimulation therefore leads to an increase in the TW:TET ratio, an observation that has been reported previously (Salmons & Vrbová 1969).

3.5.3. Summary of mechanical properties

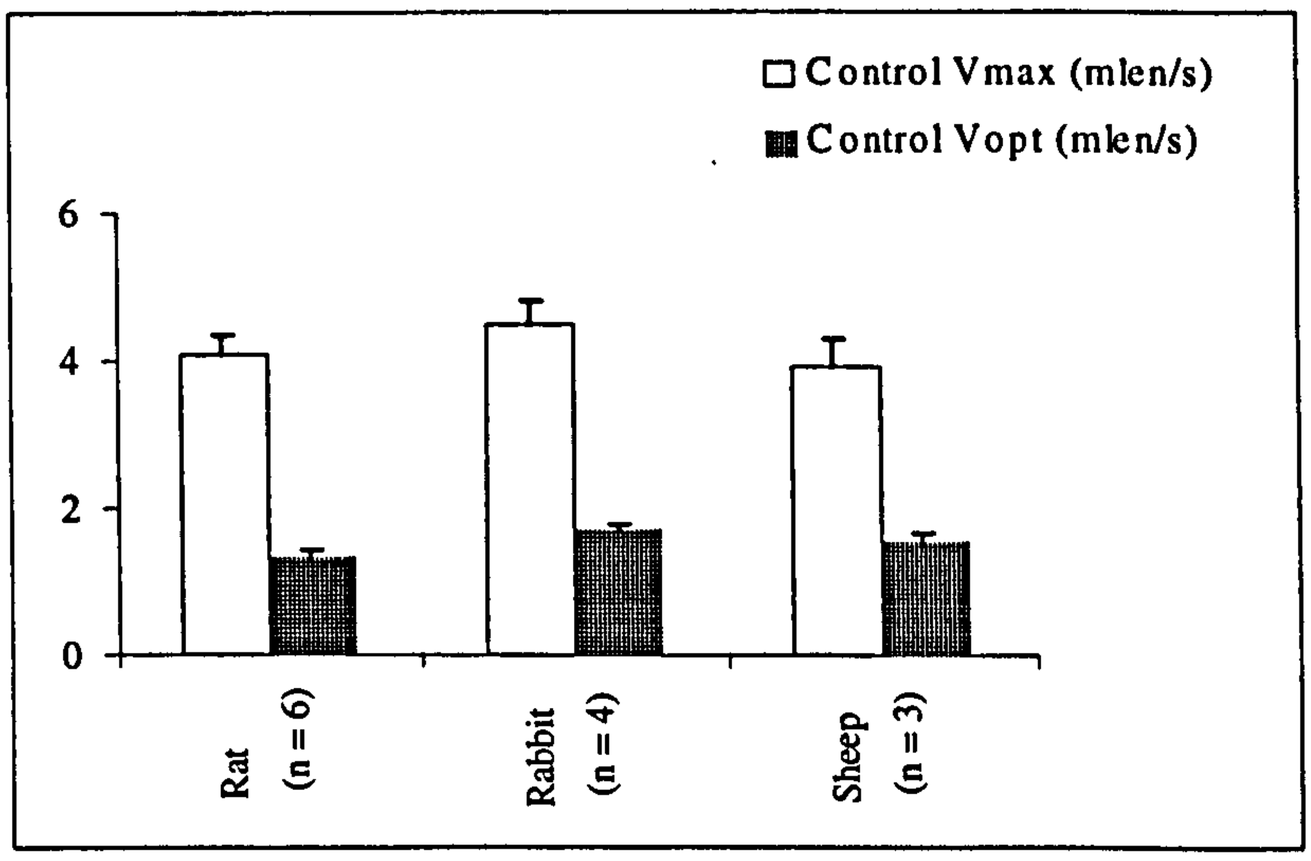

Figure 3.4. *Comparison of maximum velocity of contraction and velocity for optimum power in unstimulated muscles. Vopt is about a third of Vmax, and the latter is not significantly different in all three muscles (p>0.05).*

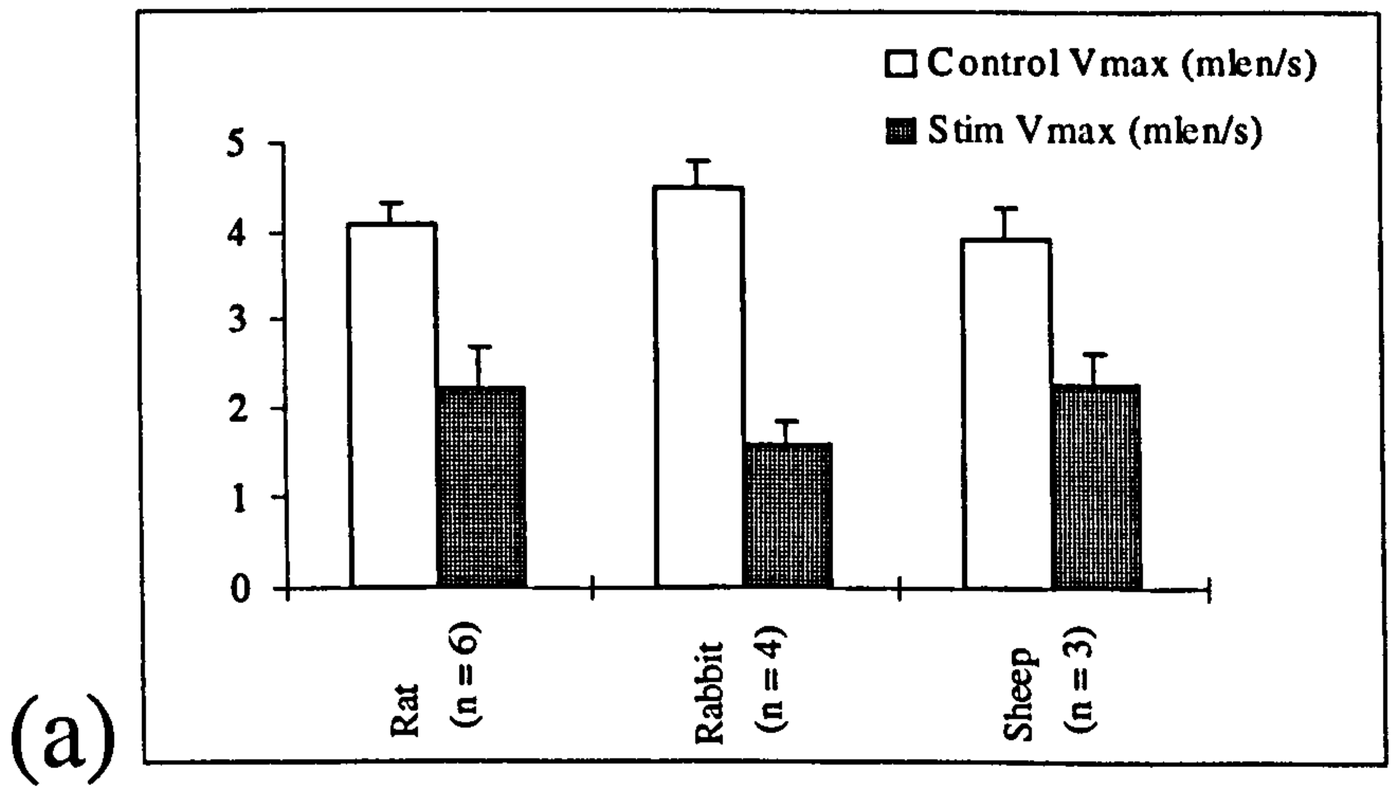

Figure 3.5. *Comparisons of the effect of chronic electrical stimulation on maximum velocity of contraction and peak power output of rat, rabbit and sheep skeletal muscles. Stim = stimulated muscle.*

The mechanical properties of the rat, rabbit and sheep muscles were pooled, and are summarised in Figures 3.4 and 3.5. For comparisons between the different animals, the velocities are expressed in muscle lengths per second (mlen/s), obtained by dividing the velocity by the optimum length. As expected, the velocity for optimum power (Vopt) was about one-third of the maximum velocity of contraction (Vmax) in the control muscles (Figure 3.4), and Vmax was not significantly different in all three muscle types ($p > 0.05$).

Although the muscles from the rat, rabbit and sheep muscles were stimulated chronically at different frequencies and duration, the conditions were sufficient to result in fibre type transformation. The effects of chronic electrical stimulation of these muscles are therefore summarised in Figure 3.5. On the whole, there was about a 50% fall in Vmax (Figure 3.5a), with a corresponding drop in Vopt. This, coupled with the drop in Po, resulted in a fall of the peak power level to 50% in the rat muscles and to about 15% in both the rabbit and the sheep muscles. Long-term electrical stimulation therefore reduced substantially the power capability of the skeletal muscles, as has been observed previously (Jarvis 1993).

3.5.4. Effect of a lower frequency of chronic stimulation

Chronic stimulation of rabbit TA with a frequency of 5 Hz, which is intermediate between the 2.5 Hz and 10 Hz frequencies previously studied (Jarvis *et al.* 1991b), resulted in a muscle with mechanical properties similar to those of the 2.5 Hz muscles. The CT and 0.5RT of the 5-Hz stimulated muscles were intermediate between those of the control and the 10-Hz stimulated muscles (Figure 3.6a), and were similar to those reported by Jarvis *et al.* (1991b) for the 2.5-Hz muscles. Also, the velocity for maximum acute power Vopt and the maximum acute power output, as a percentage of the control values, were similar in the 2.5 Hz and 5-Hz stimulated muscles. Although fatigue tests were not carried out on the muscles stimulated at 5 Hz, they would be expected to be as fatigue-

resistant as the 2.5 Hz or 10-Hz stimulated muscles. Muscle mechanical properties could therefore be modulated by varying the stimulation pattern for chronic stimulation.

(a)

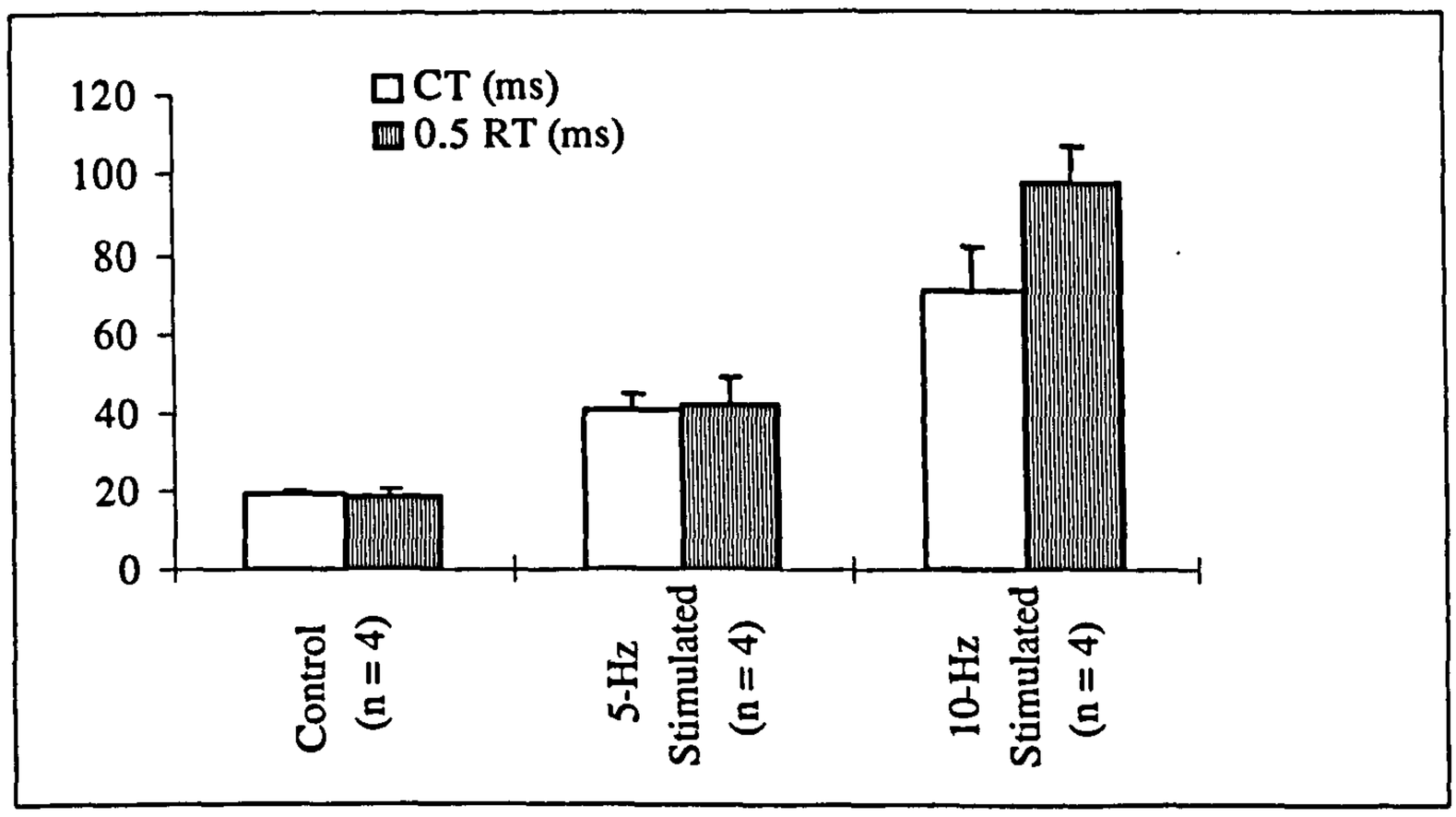

(b)

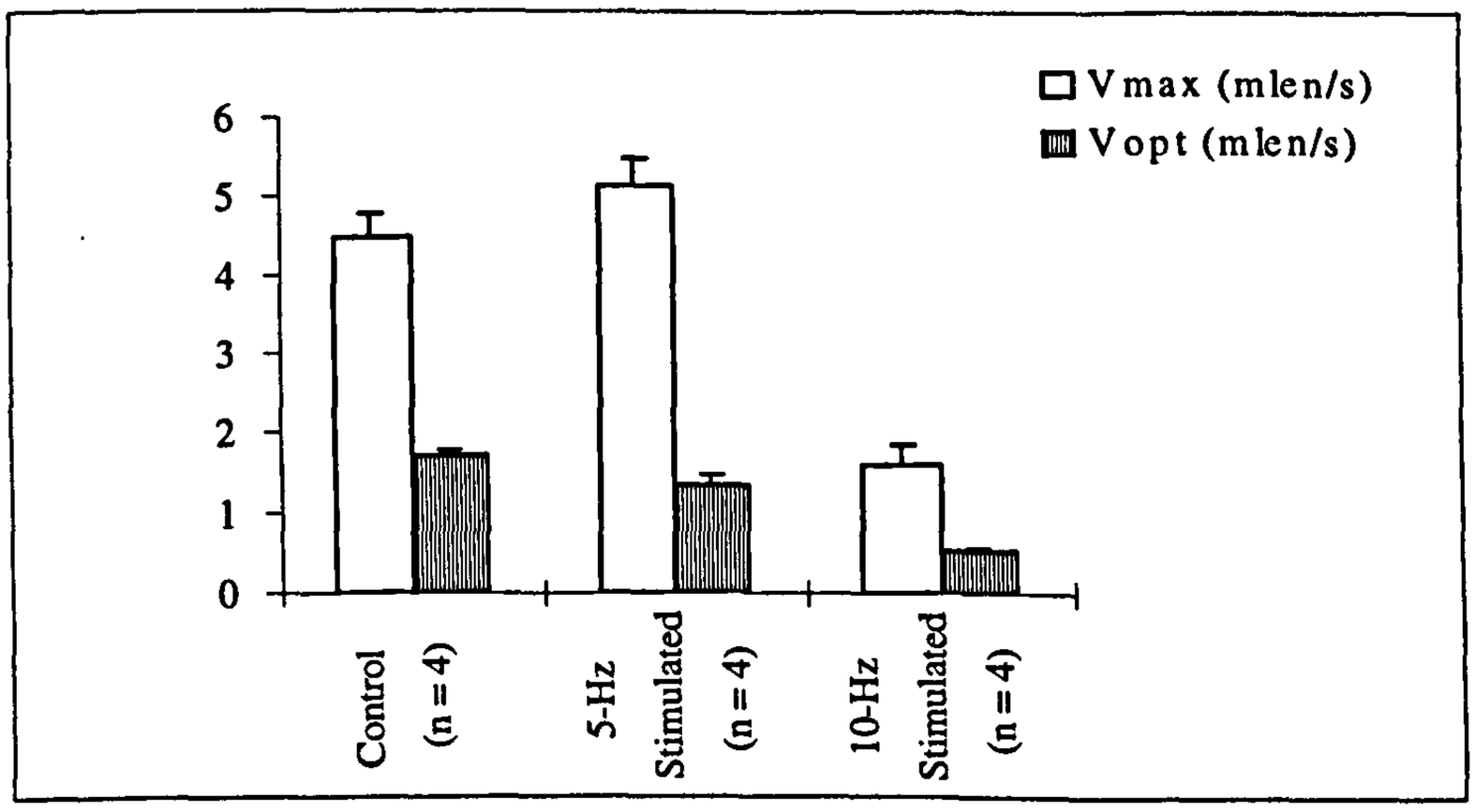

(c)

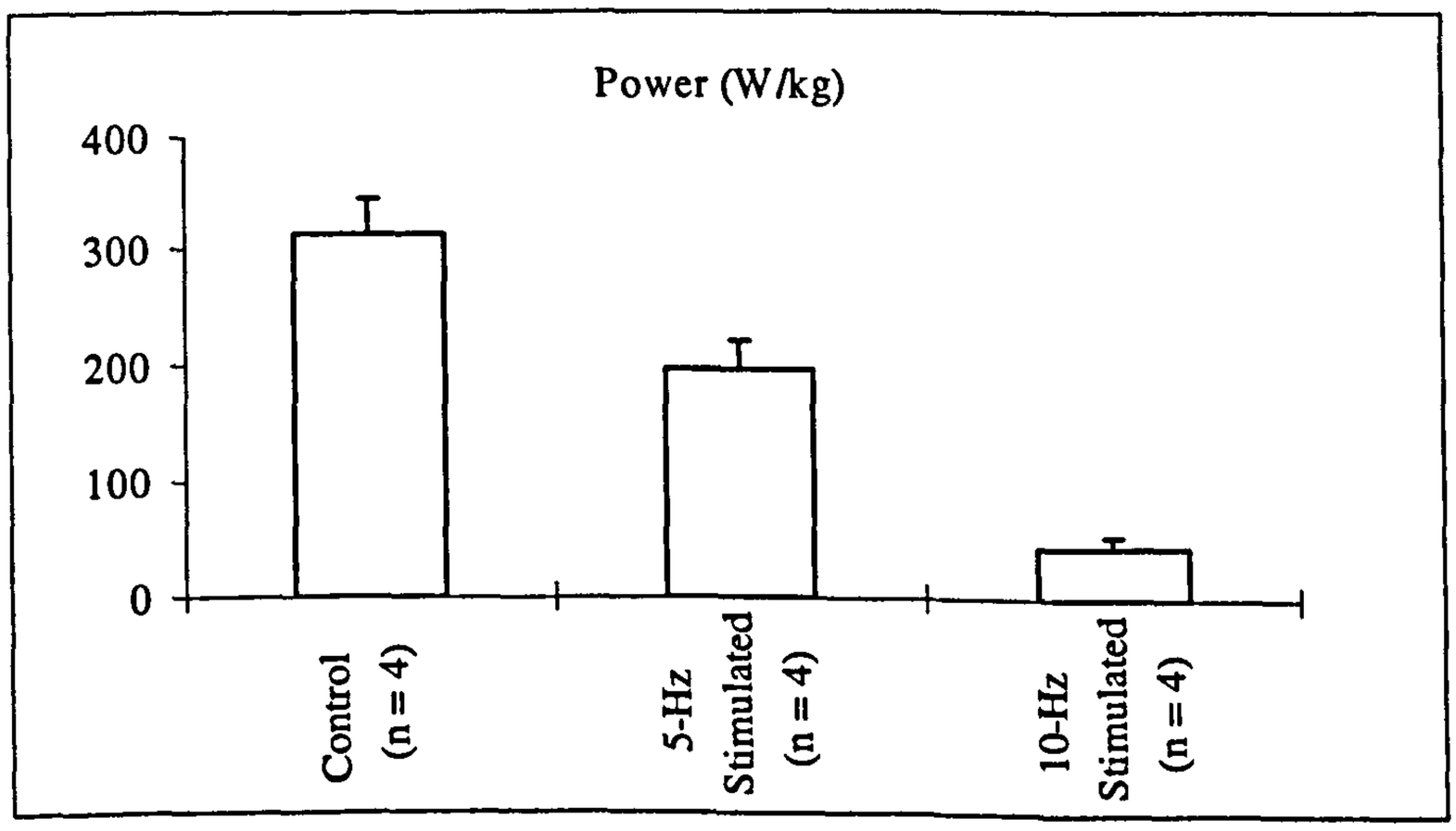

Figure 3.6. *Effects of an intermediate frequency of chronic stimulation on rabbit TA mechanical properties. (a) CT and 0.5RT. (b) Vmax and Vopt. (c) Peak power output.*

3.5.5. Curve-fitting

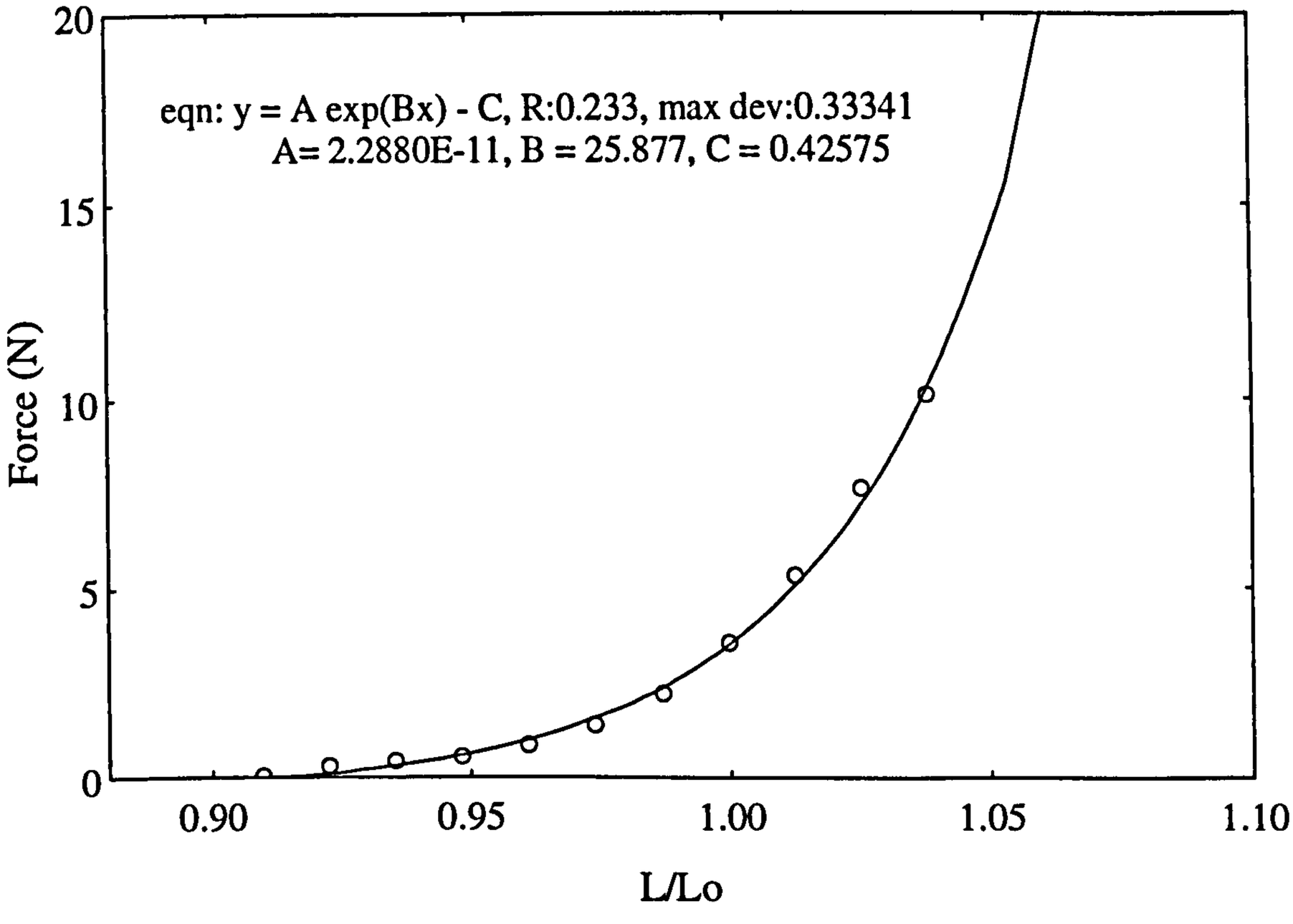

Figure 3.7. *Least squares curve-fitting of the passive force-length curve of rabbit TA.*

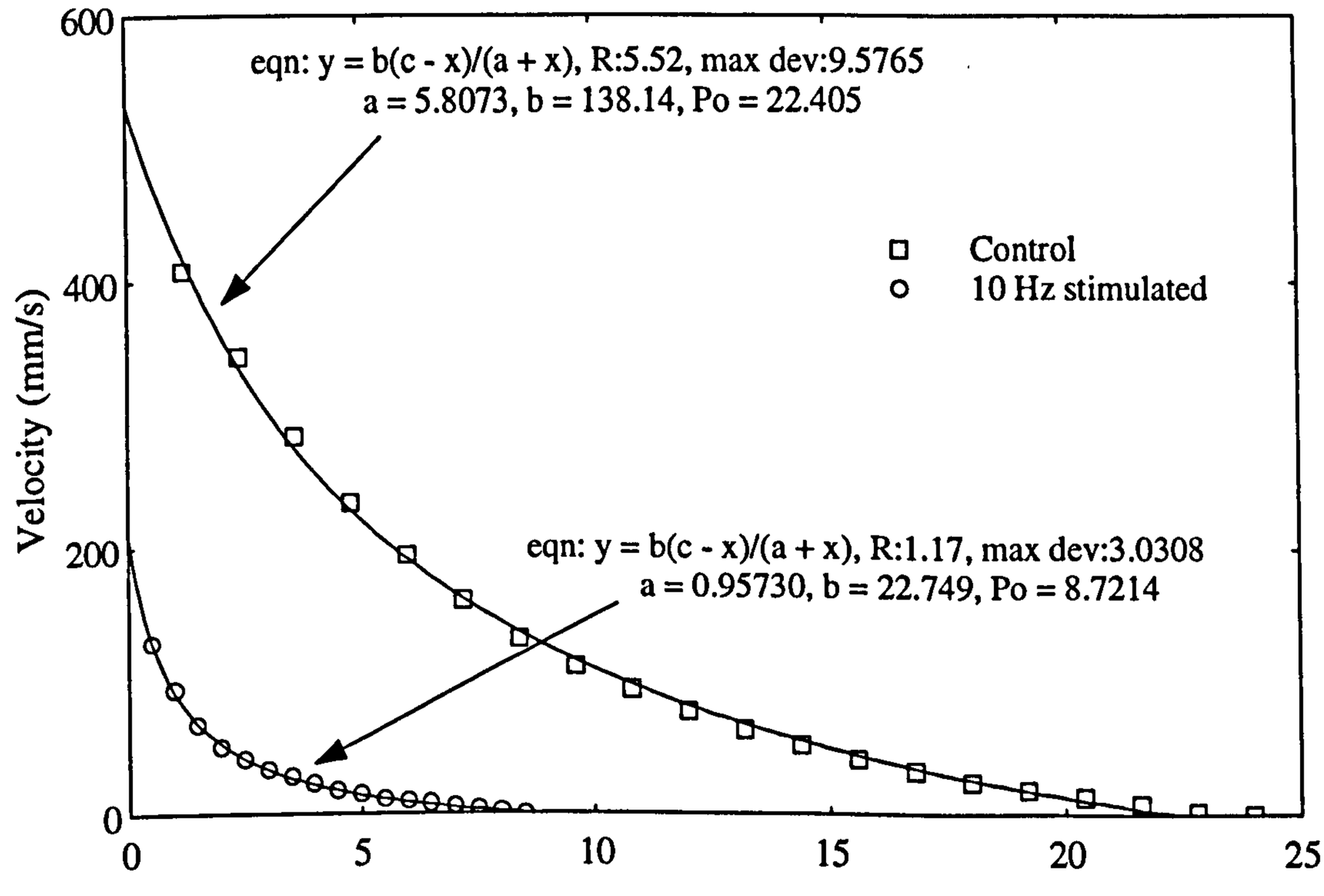

Figure 3.8. *Least-squares curve-fitting of the Hill's equation to the experimental force-velocity curve.*

Figure 3.7 is a least-squares fit of the exponential equation proposed by Pinto and Fung (1.4) to the experimental passive force-length curve. The force-velocity curve was similarly fitted by the Hill's equation (1.6), so that the F-V curve was defined by the Hill's constants (Figure 3.8); both control and stimulated muscle force-velocity curves were fitted. The experimental data was well fitted by the above equations. The force-length and the force-velocity curves could thus be represented by equations with known constants.

3.6. Discussion

The primary aim of the work described in this chapter was to test the performance of the servomotor system by measuring the linear mechanical properties of skeletal muscles. These measurements would allow further studies of the use of skeletal muscle as a contractile surgical biomaterial for cardiac assist, as discussed in later chapters.

3.6.1. Servomotor performance

The servomotor system was a very effective means of determining the linear mechanical properties of skeletal muscles. The system performed reliably and could operate completely automatically for most of the measurements. Consequently, it cut down considerably the time required to measure and to analyse data: muscle characterization could be completed within two hours of surgical preparation. Although the servomotor system was developed primarily for the determination of rabbit TA characteristics, it was adapted successfully for measurements of both rat and sheep muscle mechanical properties.

However, the limited force range of the servomotor posed difficulties when measuring sheep LD properties, resulting in irregularities in parts of the force-velocity curves (see Figure 3.2). Estimation of the LD Vmax and Po from the hyperbolic fitting of the force-velocity curve was therefore somewhat unreliable. But the limited force range might actually have been useful in obtaining a good fit of the Hill's equation to the experimental data, since it has been observed that better fits result for forces much less than Po (Edman

et al. 1976; Curtin & Woledge 1988). Further difficulties were encountered in attaching the LD to the servo arm, and in fixing the forelimb of the sheep to the metal frame to which the servomotor was attached, leading to vibration of the servo arm at high forces. Nevertheless, the servomotor measurements were of sufficient quality in the region of optimum velocities for maximum power output in the sheep LDs.

The computer-controlled servomotor system is therefore a versatile set-up, despite its shortcomings, and is now routinely used in Prof. Salmons' laboratory for the study of skeletal muscle mechanical characteristics. Further software has been written to exploit fully the capabilities of the servomotor system, such as cyclic control for work-loop measurements.

3.6.2. Significance of chronic electrical stimulation

The differences in the mechanical properties of control and chronically stimulated muscles observed here have been reported previously by several investigators, and have important bearing on the use of skeletal muscle for heart assist. The slowing of the muscles, the loss of force production and the accompanying loss of power following long-term electrical stimulation are detrimental to the use of the muscle in cardiac assist: a slowly contracting muscle may pose problems of synchronization with the cardiac cycle, leading to the already frail heart being subjected to an extra load during the pumping cycle. In order to address these problems, therefore, several studies have been carried out to elucidate the properties of useful chronic stimulation regimes (Ferguson *et al.* 1989; Badylak *et al.* 1990; Jarvis *et al.* 1991c; Jarvis 1992).

Work from Professor Salmons' laboratory has shown that fatigue resistance, the reason for chronic stimulation, does not require complete fibre type transformation, with the undesired accompanying extreme slowing of the muscle contraction speed, that results from chronic 10 Hz stimulation (Jarvis 1992; Jarvis *et al.* 1994; Mayne *et al.* 1994). In fact, the use of lower frequencies retains muscle speed of contraction and power output,

as is evident from Figure 3.6. Moreover, rabbit fast skeletal muscles stimulated with a lower frequency of 2.5 Hz are as fatigue-resistant as 10-Hz stimulated muscles (Jarvis *et al.* 1991b, 1994). Some regimes of chronic stimulation even result in gain in muscle mass (Kernell *et al.* 1987a), thus making the muscle better suited to performing cardiac-type work, as there is enough mass to produce adequate stroke work. The last chapter of this thesis describes experiments to determine the properties of optimal stimulation patterns that could be useful for muscle transformation and activation to provide assistance in the whole field of functional electrical stimulation (FES).

3.6.3. Curve-fitting

Several investigators have successfully fitted the force-length and the force-velocity curves of muscle with an exponential function (Baratta *et al.* 1993) and the Hill's equation (Edman *et al.* 1976; Petrofsky *et al.* 1981; Curtin & Woledge 1988), respectively. In fact, a comprehensive review is provided by Josephson (1993) in which the Hill's constants from a wide variety of animal muscles are presented. It is clear that a good fit of the Hill's equation to the experimental data is obtained with forces much lower than Po (Edman *et al.* 1976; Curtin & Woledge 1988); using values greater than 0.78Po can result in more than 30% overestimation of Po (Edman *et al.* 1976). Thus, the limited range of the servomotor in measuring the force-velocity curve of sheep muscles had little effect on the ability to obtain the correct Hill's constants from curve-fitting.

The ratio a/Po is used to indicate the curvature of the force-velocity curve (Curtin & Woledge 1988; Josephson 1993). It has a typical value of 0.25; a low value indicates a strongly curved force-velocity relation and a high value a nearly linear relation. For the control rabbit TA fit in Figure 3.8, a/Po is 0.26, which is consistent with the typical value above; similar values were obtained for the other muscles. The 10-Hz stimulated muscle curve, which has a visibly greater curvature than the control curve, has an a/Po value of 0.11. This indicates that chronic electrical stimulation leads to increased curvature of the

force-velocity plot. In terms of the a/Po values, the force-velocity measurements presented here are consistent with those in the literature. Thus, the Hill's constants obtained from these measurements appear accurately to represent the force-velocity curves.

3.6.4. Basis for a numerical model

The measurement of sheep LD mechanical properties could allow the development of a good experimental model with which to study of the effects of chronic electrical stimulation on the function of SMVs, as ventricles of a realistic size can be constructed from this muscle. Moreover, as the mechanical properties are well-fitted by mathematical equations so that they are defined by equations with known constants (Figures 3.7 and 3.8), the linear muscle characteristics can easily be incorporated into software to model such muscles as if they constituted a contracting SMV wall. Such an approach would allow optimization of important parameters of SMV function that may not be readily available to experimental investigation, and the model may give clues as to the direction of changes in these optimal parameters following chronic electrical stimulation. The above mathematical approach was suggested by Salmons & Jarvis (1991a), and is the subject of the next chapter. Even if such a model study only gave qualitative predictions of SMV function, this information could be very useful in providing a guide to the many surgeons constructing SMVs.

3.7. Conclusion

The servomotor system is reliable and versatile. It was used for extensive measurements of muscle mechanical properties in various states of transformation, and is therefore a useful research tool. In the following chapter, these mechanical properties have been employed in a numerical model to study the hemodynamics of SMVs.

Chapter 4

4. Optimization of SMV Configuration - A Mathematical Model

4.1. Summary

The mechanical properties of rabbit and sheep skeletal muscles measured in Chapter 3 were used in a mathematical model to predict the pumping function of SMVs. A linearly contracting rabbit TA was then loaded as though it formed part of the cylindrical wall of an SMV, and its performance evaluated and compared with the mathematical predictions. Both approaches predicted that there is an optimum size of ventricle at which maximum stroke volume (SV) is produced. However, the size for maximum ejection fraction (EF) is smaller than that for maximum stroke volume; EF indicates the amount of stagnant blood in the ventricles and hence the risk of thrombus formation. The numerical models were extended to chronically stimulated muscle with similar results, but the size of ventricle for optimum function was reduced considerably. These studies thus suggest that a compromise has to be made in the design of SMVs: for adequate function, SMVs should be constructed at a size less than that required for maximum stroke volume in order to reduce the risk of thromboembolism. Moreover, the optimum size might change if the ventricle is formed and then stimulated chronically.

4.2. Introduction

The use of SMVs for heart assist is still in an experimental stage because of the many parameters that need optimizing before SMVs could be used satisfactorily in clinical practice. These parameters include the shape and size of the ventricle, the fibre orientation in the wrap, and the connection of the ventricle to the circulation. It is crucial to optimize these parameters, under physiological loading conditions, to obtain SMV configurations that make the best use of the limited power available from skeletal muscle for cardiac assist. As mentioned in the previous chapter, there are two main sources of skeletal muscle power loss: the first is associated with chronic electrical stimulation, resulting in loss of speed and muscle mass, and the second is due to wrapping of the

muscle to form the SMV, resulting in a limited number of fibres operating at their optimal length at any instant. The model presented here uses the well-documented muscle mechanical properties to predict the optimum SMV size, and to study the effects of changes in the optimal configuration following chronic electrical stimulation.

The LD muscle predominantly used to form SMVs in cardiac assist varies in size from one patient to another (Sola *et al.* 1991). It is important to establish the geometrical configuration that will be most efficient in harnessing the power available from the skeletal muscle graft. Should the graft be used as a single- or multi-layered ventricle, and is there an optimum size of ventricle that would allow it to function to its maximum capability? The answers to these questions are particularly important as energy requirements in skeletal muscle cardiac assist can be difficult to meet (Salmons & Jarvis 1992). Studies addressing the entire question of optimizing SMV configuration have involved both experimental and numerical approaches.

4.2.1. Experimental approach

As reviewed by Pochettino *et al.* (1991), most of the early experimental SMV work concentrated on the long-term feasibility of this mode of skeletal muscle cardiac assist while paying little attention to optimizing its function. It has been shown unequivocally that SMVs have the potential to perform in a cardiac assist role (Acker *et al.* 1986, 1987; Anderson *et al.* 1988; Bridges *et al.* 1989a, b, c, 1991; Pochettino *et al.* 1991; Fietsam *et al.* 1993) under physiological loading conditions. But some of these studies noted that maximum power output from SMVs could only be achieved at fairly high (> 40 mmHg) preload pressures (Spotnitz *et al.* 1974; Acker *et al.* 1986, 1987).

Although these experimental studies were useful in establishing the feasibility of the approach, few investigators have focused on optimization of SMV configuration. Depending on the geometry of the mandrel around which the muscle is wrapped and the

amount of muscle flap available, SMVs can be configured as cones, cylinders, ellipses or spheres of a variety of sizes (Bridges *et al.* 1989a). In dynamic cardiomyoplasty studies in mongrel dogs, Kao *et al.* (1990) showed that the preferred orientation of skeletal muscle fibres for best performance in a wrap is circumferential. Lu *et al.* (1993) concluded that a configuration to pump blood from the left ventricular apex to the aorta with two valved conduits may be particularly appropriate for cardiac assist. By constructing two sizes of SMVs in beagle dogs, Hammond *et al.* (1990) showed that the smaller ventricles could reach greater passive pressures; however, the larger SMVs performed better in terms of generating work per unit mass of muscle. It should, however, be noted that large ventricles may produce a greater stroke volume, and thus more work, but are less desirable as they may have lower EFs than smaller ventricles. Oda *et al.* (1993) studied the performance of single- and double-layered ventricles under physiological preload in mongrel dogs: they showed that small single-layered ventricles performed better than, or at least as well as, small double-layered or large single-layered ventricles. However, experimental studies alone may not be the best way forward because of the large number of parameters that need optimizing and the great expense in terms of money and of animal lives. A numerical model may lead to a better understanding of the hemodynamics of SMV function and also promote experimental studies to determine the optimal parameters of skeletal muscle cardiac assist.

4.2.2. Numerical approach

Several numerical models have been developed to optimize SMV function. Bridges *et al.* (1989a) designed a mathematical model of an SMV based on large deformation elasticity theory. Using experimentally derived elastic stiffness in systole and diastole, their model predicted an optimal size of ventricle for hemodynamic performance under physiologic loading conditions (Bridges *et al.* 1989a; Hammond *et al.* 1990): maximum stroke volume was produced at a particular SMV size; however, this model took no account of

time or velocity of shortening. Also, a time-varying elastance model, which characterizes the pump function of the heart by the ratio of intraventricular pressure and volume (Suga & Sagawa 1974), was used by Suguira *et al.* (1993) to analyse cardiomyoplasty function. They were able to predict an improved end-systolic elastance which they also measured experimentally. However, this latter approach assumes that the elastance function of skeletal muscle is not dependent on preload or afterload. In addition to the several assumptions made, the choice of muscle properties (time-varying elastance and elastic stiffness) used in the above models may not be easily differentiated in control and chronically stimulated muscles. These models would therefore be unsuitable for studying the effects of chronic electrical stimulation of skeletal muscle on the optimal configurations of SMVs. Hence, models based on the well-documented linear relationships of skeletal muscle, such as the force-length and force-velocity curves, may be more useful in the above regard.

In fact, muscle mechanical properties have been used in mathematical models to characterize the heart as a pump (Arts *et al.* 1982, 1991; Bayer & Sideman 1984, Bovendeerd 1990), but these models used idealised versions of cardiac activation, force-length and force-velocity relationships. Moreover, Spotnitz *et al.* (1974) utilized isometric force-length relations of rectus abdominis muscles to predict the developed pressure, using a modified form of the Laplace expression, in composite ventricles formed from the same muscles. It is therefore feasible to use the linear mechanical characteristics of skeletal muscles in a numerical model to determine optimal SMV configurations.

The optimum geometry for an SMV is crucially dependent on the nature of the contractile tissue from which it is formed. The mechanical properties of a skeletal muscle determine the power that the muscle can deliver, and the loading conditions for optimum performance, as discussed in Chapter 3. Although early surgical work has been extremely important in demonstrating the feasibility of the general approach of skeletal muscle

cardiac assist, it has not been guided by a knowledge of these fundamental relationships. Moreover, we need to find out the effects of the slowing that is associated with long-term electrical stimulation on the geometry of SMVs. Furthermore, because a linearly contracting muscle wrapped around to form a ventricular pump is subjected to complex loading conditions during a pumping cycle, its performance would depend on the initial loading conditions (preload), its speed of contraction, and the load it has to pump against (afterload). The effect of these parameters on SMV function need to be understood before SMVs can be introduced in circulation. Because of the numerous parameters involved, a combination of both a numerical and a physical model would be most appropriate (Spotnitz *et al.* 1974; Bridges *et al.* 1989a).

The original concept of SMV configuration optimization in our laboratory was to develop a muscle-driven pump incorporating mechanical arrangements to vary the loading conditions, but this approach lacked flexibility. A purely mechanical approach would be cumbersome, since every adjustment to the model would require a newly-manufactured component. Two models were developed: a) a purely numerical and b) a part numerical-part physical model.

4.2.3. Aims

The aim of the work presented in this chapter was to develop models of SMVs based on experimentally measured linear muscle mechanical properties. These models would be used to make predictions of SMV function, including effects of changing the size of the cavity volume and the wall thickness under different loading conditions. More importantly, the numerical model would allow a study of the effects of changes in the muscle mechanical properties, following chronic electrical stimulation, on ventricular function.

4.3. Materials and methods

4.3.1. The SMV model

The SMV was modelled as a thick-walled cylindrical vessel based on the linear mechanical characteristics of both rabbit TA and sheep LD muscles. The model consisted of two parts: a) a purely numerical model based simply on muscle mechanical properties and, b) a part physical model in which a rabbit TA was loaded as though it formed part of the wall of a contracting cylindrical ventricle. In essence, the purely numerical model was the same in both the TA and the LD, with minor variations to account for the physical differences between the two. For instance, the sheep LD, which is large enough to form a realistic-sized ventricle, was loaded differently from the rabbit TA, which could only form part of the cross-section of the ventricular wall. The models were implemented in Turbo C++.

The model was based on the following assumptions:

1. SMV modelled as a thick-walled cylindrical ventricle.

2. The SMV wall is incompressible and homogenous, with uniform wall mechanics.

3. The mechanics of the ventricular wall are equivalent to those of either the rabbit TA or sheep LD muscles.

4. Stress in the walls of the ventricle is due only to the internal pressure (assumed constant in a single contraction).

5. Muscle fibres are concentric, that is, they lie along the circumference of the ventricular wall.

The Lamé's Equations (Hearn 1985) define the radial stress (σ_R), and the circumferential stress or the so-called "hoop stress" (σ_θ) acting tangentially at a given radius (r) within the walls of a thick-walled cylindrical vessel of internal pressure P, internal radius R_i and external radius R_o as

$$\text{Hoop stress, } \sigma_\theta = \frac{PR_i^2}{\left(R_o^2 - R_i^2\right)}\left[1 + \frac{R_o^2}{r^2}\right] \tag{4.1}$$

$$\text{Radial stress, } \sigma_R = \frac{PR_i^2}{\left(R_o^2 - R_i^2\right)}\left[1 - \frac{R_o^2}{r^2}\right] \tag{4.2}$$

Since the muscle fibres are assumed to be concentric, one is mainly concerned with the hoop stress (4.1), which is not constant but drops monotonically from the inside to the outside of the cylinder wall. Because Arts *et al.* (1991) have shown that circumferential stress in the wall of a chamber is dependent strongly on geometry, this model should allow the optimization of SMV geometry.

4.3.2. Simulation of an SMV wall by linear muscle

The SMV was simulated both as a passive wall that stretched with increasing intraventricular pressure (P), and as an active wall in which the ventricle pumped fluid against a constant P. The former simulation was based on the passive force-length characteristics of the linear muscle, and the latter simulation on the force-velocity characteristics. The general simulation method is detailed first, and then rabbit TA and sheep LD muscles are used as case examples.

4.3.2.1. Simulation of a passive SMV wall

The constants A, B and C, obtained by curve-fitting the passive experimental force-length data of muscle into (1.4), give a universal description of the muscle as a spring (see Chapter 3). These constants were then incorporated into software that calculated the stress in the walls of an SMV of internal radius R_i, and thus the pressure P, resulting from volume changes that stretched the ventricular wall. When a linear muscle of optimal length Lo is used to form a ventricle of radius R_{io} such that $Lo = 2\pi R_{io}$, then R_{io} is

referred to as a nominal radius. If fluid is then introduced to change the ventricle volume by stretching the muscle to a new radius R_i, the fractional stretch is given by

$$\frac{L}{Lo} = \frac{R_i}{R_{io}} \tag{4.3}$$

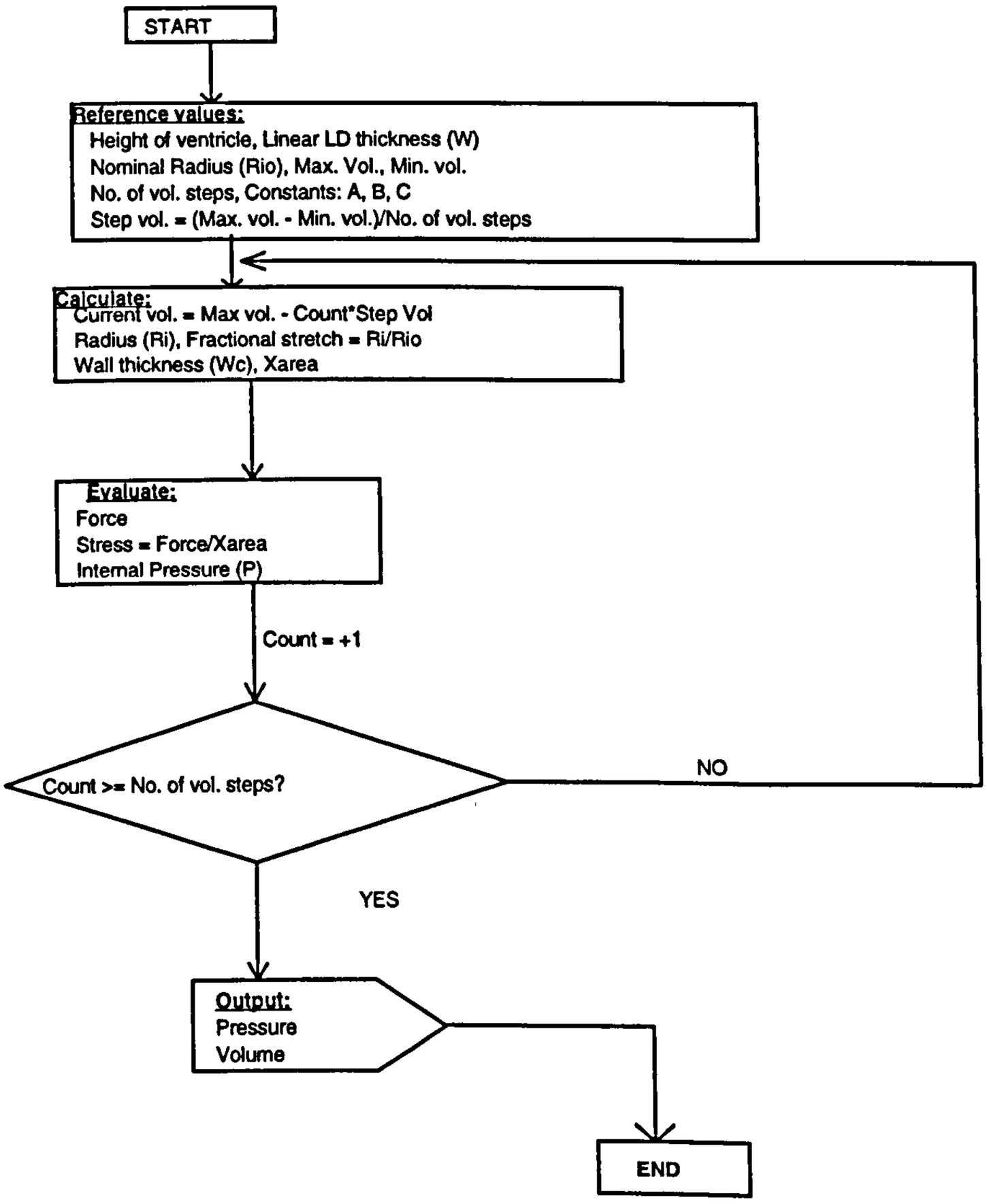

Figure 4.1. *Program flow for pressure-volume curve prediction.*

where L is the length corresponding to R_i. The fractional stretch was evaluated at different values of R_i and substituted into (1.4) to determine the force (F), and hence the stress (force per unit cross-section), acting in the walls of the ventricle:

$$\bar{\sigma} = \frac{F}{Xarea} \tag{4.4}$$

where Xarea is the ventricular wall cross-sectional area and $\overline{\sigma}$ is the mean stress in the ventricular wall (see Section 4.3.3 for the rationale for using the stress at the inner radius for a mean wall stress). The mean stress was then used in the Lamé's Equation (4.1) to determine P inside the ventricle as

$$P = \overline{\sigma} \frac{\left(R_o^2 - R_i^2\right)}{\left(1 + \frac{R_o^2}{R_i^2}\right)} \tag{4.5}$$

Figure 4.1 illustrates the program flow to implement these calculations. Pressures were then obtained and plotted against the volume (given by πHR_i^2, where H is the height of the ventricle) to yield the predicted passive pressure-volume relationship of the SMV.

4.3.2.2. Simulation of a contracting SMV wall

The Hill's constants derived from fitting the experimental force-velocity data into (1.6) were used in the model of the active or contracting SMV wall to predict ventricular performance. The flow chart for this simulation is shown in Figure 4.2.

4.3.2.2.1. Stroke volume and ejection fraction

The Lamé's equation (4.1) was incorporated into software that calculated the circumferential wall stress in a cylindrical SMV from its internal radius, wall thickness and internal pressure (P, assumed constant), and derived the speed of contraction of the muscular wall (4.7) from the Hill's constants. The default wall thickness of the linear muscle flap used to form the ventricle was taken to be 12 mm, as the mean thickness reported for the human LD muscle is 11-13 mm (Chachques *et al.* 1986).

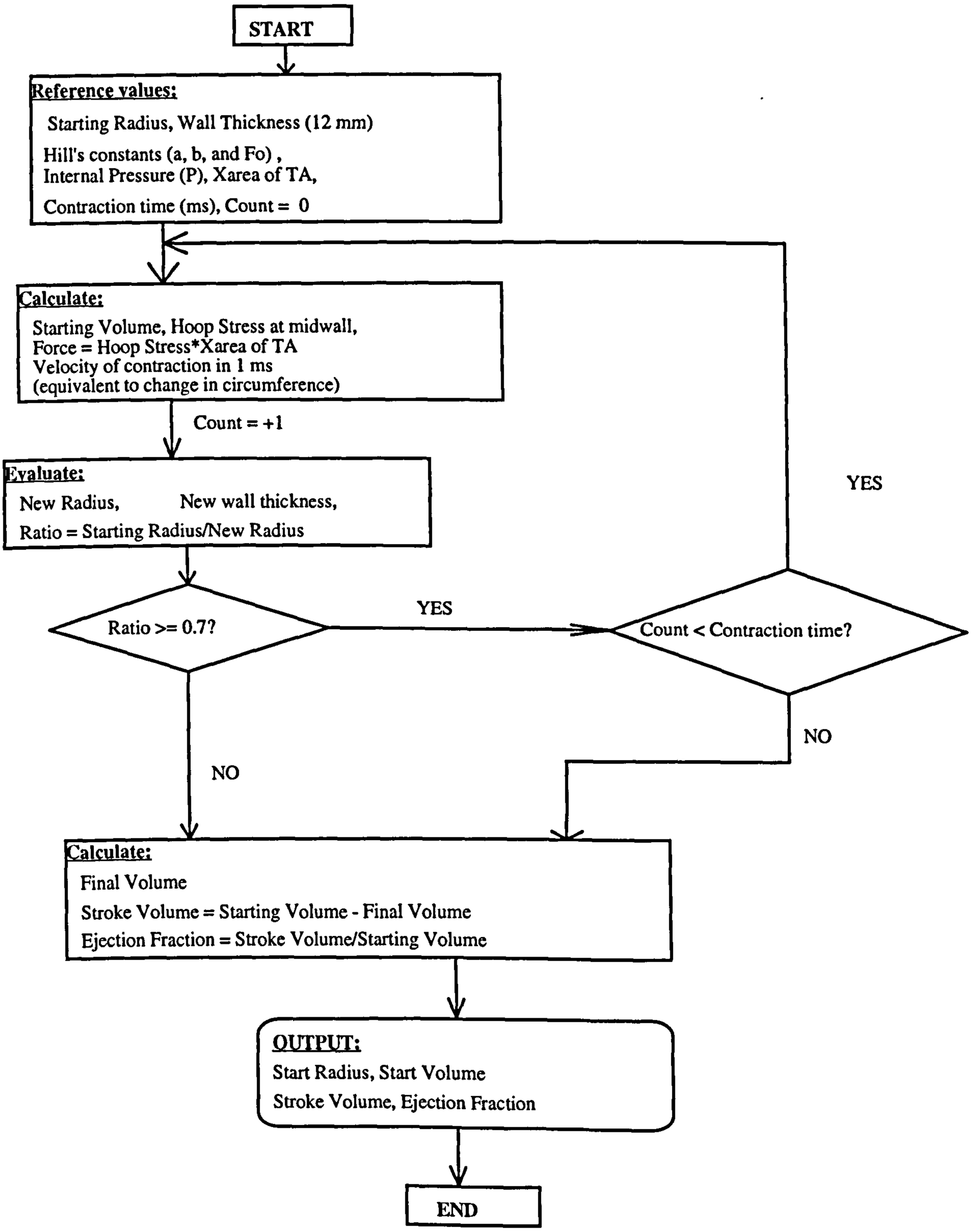

Figure 4.2. *Program flow to simulate a contracting SMV wall.*

As the muscle fibres in the SMV wall are assumed to be concentric, equation (4.1) defines the stress acting on them. The equivalent force on the muscle was thus evaluated as the product of the mean stress ($\bar{\sigma}$) and the cross-sectional area (Xarea),

$$F = \bar{\sigma} X \text{area} \tag{4.6}$$

Since stress is a function of radius with a constant P (4.1), the stress in the walls of the ventricle falls as it contracts and reduces in size. Assuming that ventricular contractions are in 1 ms time steps, and that the velocity during each millisecond of contraction is instantaneously constant, the change in ventricular circumference in a step contraction was obtained by substituting the force (4.6) into (1.6), yielding

$$V = \frac{b\left(P_o - \bar{\sigma} X \text{area}\right)}{\left(a + \bar{\sigma} X \text{area}\right)} \tag{4.7}$$

The resulting radius of the SMV from the above 1 ms change in circumference is calculated and then used to evaluate the new stress in the walls of the ventricle, and hence the force on the muscle fibres for the next step contraction. Using an iterative technique with 1 ms time-steps, the end radius was determined in a stroke contraction of the ventricle. The stroke volume (SV), calculated as the total change in volume in a full contraction, and the corresponding ejection fraction (EF), the ratio between the SV and the starting volume, of SMVs of various resting sizes were predicted for a given contraction time of the muscular wall. For heart rates of up to 100 bpm a skeletal muscle graft can be stimulated to contract for a period of 250 ms during each cycle (Salmons & Jarvis 1990a, 1991a). SV and EF were therefore obtained for ventricles pumping against different intraventricular pressures (afterloads) in both control and chronically stimulated muscles.

4.3.2.2.2. Pressure-flow curve

Theoretically, a contracting SMV should have a pressure-flow relationship similar to the force-velocity curve in a linearly contracting muscle constituting the ventricular wall (Spotnitz *et al.* 1974). The flow value would be that at the start of the ventricular contraction. Software was written to predict this relationship.

For a ventricle of a given height, radius and wall thickness, a series of values of force from the peak muscle tension (Po) to 0 N, assumed to be acting circumferentially in the ventricular wall, were used to calculate the stresses in the cross-section of the wall based on the Lamé's equation. The corresponding intraventricular pressures were then evaluated using (4.5). The forces were also used to calculate the volume change in a 1 ms of ventricular contraction to yield the flow (volume change per second). The flows were then plotted against the corresponding internal pressures to obtain the pressure-flow curve, from which a power-pressure curve could be obtained by multiplying the pressure by the flow.

4.3.2.3. Global corrections to the model

4.3.2.3.1. Muscle contraction limited to 30%.

Skeletal muscle can only contract to about 30% of its optimal length. Hence, in the SMV model pumping fluid, the maximum fractional change in circumference was limited to 30%. Circumference is linearly related to radius so that a change in circumference results in the same fractional change in radius. Thus, the 30% limitation of circumferential contraction will mean that

$$\frac{\left(R_i - R_{new}\right)}{R_i} \leq 0.3$$

where R_i is the initial radius and R_{new} the radius at the end of contraction. Rearranging the above equation yields

$$\frac{R_{new}}{R_i} \geq 0.7 \qquad (4.8)$$

Limitation on the extent of muscle contraction in the numerical model was therefore satisfied by ensuring that (4.8) was true throughout a full contraction. The consequence was an upper limit on EF, which is theoretically 51% (Salmons & Jarvis 1990a, 1991a).

4.3.2.3.2. Constant muscle wall volume

Jan Swammerdam, circa 1663, showed that a contracting muscle did not change its volume (McMahon 1984), a demonstration which supports the assumption that the SMV wall is incompressible. Wrapping a linear graft of muscle to form a ventricle leads to a change in graft length as the inner fibres become shorter than the outer ones; hence the linear graft thickness changes in the ventricular configuration to maintain the muscle volume. Consider the case where a linear muscle graft of length L and thickness W_L is used to construct a cylindrical ventricle of wall thickness W_c and internal radius R_i so that the inner circumference is equal to the graft length (i.e. $L = 2\pi R_i$); assume the height (H) of the muscle in both configurations is the same (Figure 4.3).

The linear graft volume – depicted as a rectangular block in Figure 4.3 of thickness W – is equal to the ventricular wall volume – represented by an annulus of thickness W_c and inner radius R_i – constructed from the graft. Equating the muscle volumes in both configurations gives

$$2\pi WHR_i = \pi H\left(R_o^2 - R_i^2\right) \tag{4.9}$$

But $R_o = R_i + W_c$ so that $W_c = R_o - R_i$. Substituting W_c in (4.9), and rearranging, gives

$$2WR_i = W_c\left(2R_i + W_c\right) \tag{4.10}$$

Equation (4.10) is a quadratic in W_c, and solving yields

$$W_c = \sqrt{\left(R_i^2 + 2WR_i\right)} - R_i \tag{4.11}$$

When the ventricular size decreases during contraction, the wall thickness must increase. If the ventricle of radius R_i and wall thickness W_c (4.11) changes in a millisecond contraction to a new radius R_{new} and wall thickness W_{new}, then the muscle volume is

maintained by substituting R_i and W_c with R_{new} and W_{new}, respectively, in the right-hand-side of (4.10), resulting in

$$W_{new} = \sqrt{\left(R_{new}^2 + 2WR_i\right)} - R_{new} \qquad (4.12)$$

In (4.12), R_i now represents a nominal radius (see above). During a contraction, therefore, the new wall thickness was calculated after every millisecond using (4.12).

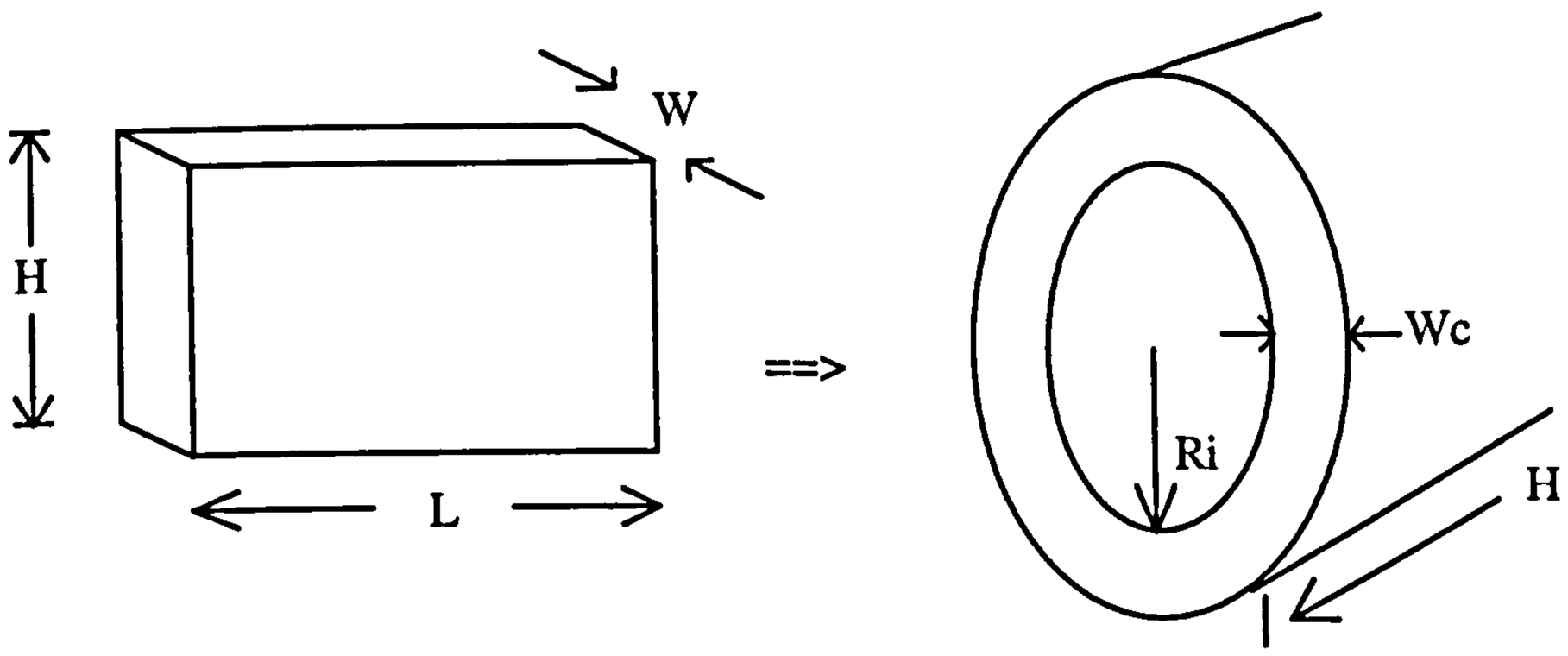

Figure 4.3. *Change of configuration from a linear muscle flap to a cylindrical ventricle. The cylindrical ventricle is lying on its side.*

4.3.2.3.3. Rabbit TA only forms part of the ventricular cross-section

Considering rabbit TA as part of the SMV wall (Figure 4.5), the stress on the TA cross-section was taken to reflect that of the entire ventricular wall. A change in the internal radius, due either to passive stretch from an internal pressure P or to active muscle contraction, leads to a corresponding change in the cross-sectional area of the ventricular wall in order to maintain muscle volume. The TA cross-section must change proportionally, i.e. as a constant fraction of the ventricular cross-section. For the muscle block in Figure 4.3, therefore, if the TA has a cross-sectional area in this wall of X_{lin}, say, and X_{cyl} in the annulus of thickness W_c, then

$$\frac{X_{lin}}{WH} = \frac{X_{cyl}}{W_c H}$$

so that the following equation was satisfied throughout a single contraction,

$$X_{cyl} = \frac{W_c}{W} X_{lin} \tag{4.13}$$

Equation (4.13) is the cross-sectional area that was used in the case of the rabbit TA to calculate the force on the muscle during simulations of ventricular wall contraction.

4.3.3. Model refinement

Two important questions needed resolving before any sensible model predictions could be made. The first involved adjusting the ventricular wall thickness during a contraction to maintain a constant wall volume. In a step contraction, for example, it is unclear how the final internal radius should be determined, since this depends both on simple muscle contraction and on adjustments of the wall thickness to maintain muscle volume. Should the extra thickness be added to the inside or outside of the inner radius? The second question concerned the radius within the ventricular wall at which the stress should be calculated. This stress, calculated using (4.1), is not constant but falls monotonically from the inner to the outer radius according to the Lamé's equations. What single radius would reflect the loading of the entire ventricular wall? An attempt to resolve these vital questions is outlined below.

4.3.3.1. Addition of the extra wall thickness

Consider that in a 1 ms step contraction of the SMV, the wall thickness remained constant at the initial value. Using (4.7), a new internal radius was obtained based simply on muscle contraction. The extra muscle volume required to maintain ventricular wall volume was then calculated and added as a uniform extra thickness to the new internal radius of the ventricle. In a preliminary model, the stroke volume outputs resulting from adding the extra thickness to the inside or to the outside of the new inner radius were determined and compared with outputs from a constant wall thickness consideration. SMV flow modelling engineers from City University (London) had indicated that the

inner radius defined the ventricle size, thus suggesting that the extra muscle thickness be added to the outside of this radius.

4.3.3.2. Radius for stress evaluation

In a preliminary model, stroke volume outputs obtained by calculating the stress at the inner and mid radii were compared. The wall thickness was then doubled to determine if both options still maintained similar outputs.

Intuitively, the use of the inner radius for stress evaluation would be preferred as its surface is in direct contact with the ventricular fluid. By the Lamé's equation, stress distribution in a thick-walled cylindrical ventricle is highest at the inner radius, where the fibres are assumed to be at their optimal length in this model, and falls constantly to the outer radius. In a real situation, attributing the higher inner wall stress to the outer fibres will, in effect, limit their contractility; this may be equivalent to overstretching the outer fibres. If, however, these fibres were stretched beyond their optimal length, they would contract less forcefully according to the force-length curve of skeletal muscle. Because of the distribution of stress in a ventricular wall by the Lamé's equations, the outer fibres should ideally contract against forces lower than those seen by the inner fibres. Therefore, a single stress value could be used for all the muscle fibres in the ventricular wall, allowing the entire wall to contract at a single velocity. In fact, models of myocardial wall mechanics have predicted uniform transmural distribution of fiber shortening as well as fiber stress during the ejection phase (Arts *et al.* 1982, 1991). However, the uniform myocardial fibre stress distribution may have been due to the complex fibre geometry in the myocardium.

4.3.4. Applications of the model

Predictions of the passive and active characteristics of SMVs were made using the linear mechanical properties of both rabbit TA and sheep LD muscles. Predictions from

ventricles whose walls consisted of muscles with fast, slow or intermediate mechanical properties, pumping against different afterloads, were compared. Using the computer-controlled servomotor (see Chapter 2), linearly contracting rabbit TA was loaded as though it formed part of the wall of a cylindrical ventricle.

4.3.4.1. Simulation of an SMV wall by rabbit TA muscle

4.3.4.1.1. Purely numerical predictions

In the rabbit TA, ventricular relationships investigated included the passive pressure-volume, stroke volume and ejection fraction against starting radius, and preload versus stroke volume relationships. These predictions were compared in muscles with different histories of chronic stimulation.

4.3.4.1.2. Complex loads

To increase the predictive power of the SMV simulations with the rabbit TA, the purely numerical model was extended to a part physical/part numerical model that still allowed the freedom to examine the effects of altering the geometry. Rabbit TA muscle was loaded in a way that simulated the variable relationship between wall stress and intraventricular pressure during ejection from an SMV. This was achieved using software that provided full control of the load on the muscle in real-time (see Chapter 2). So this part of the model neither assumed the mechanical properties of the muscle nor assumed that the pressure-volume relationship was obeyed instantaneously.

4.3.4.1.2.1. Real-time control of the load on a muscle

Lamé's equation (4.1) was used to determine the relationship between radius and hoop stress in cylindrical ventricles contracting from initial radii of 35, 25, 20 and 15 mm, considering a constant muscle wall volume and internal pressure P. The initial linear thickness of the muscle flap used to form the SMV was taken to be 12 mm, similar to that measured in humans.

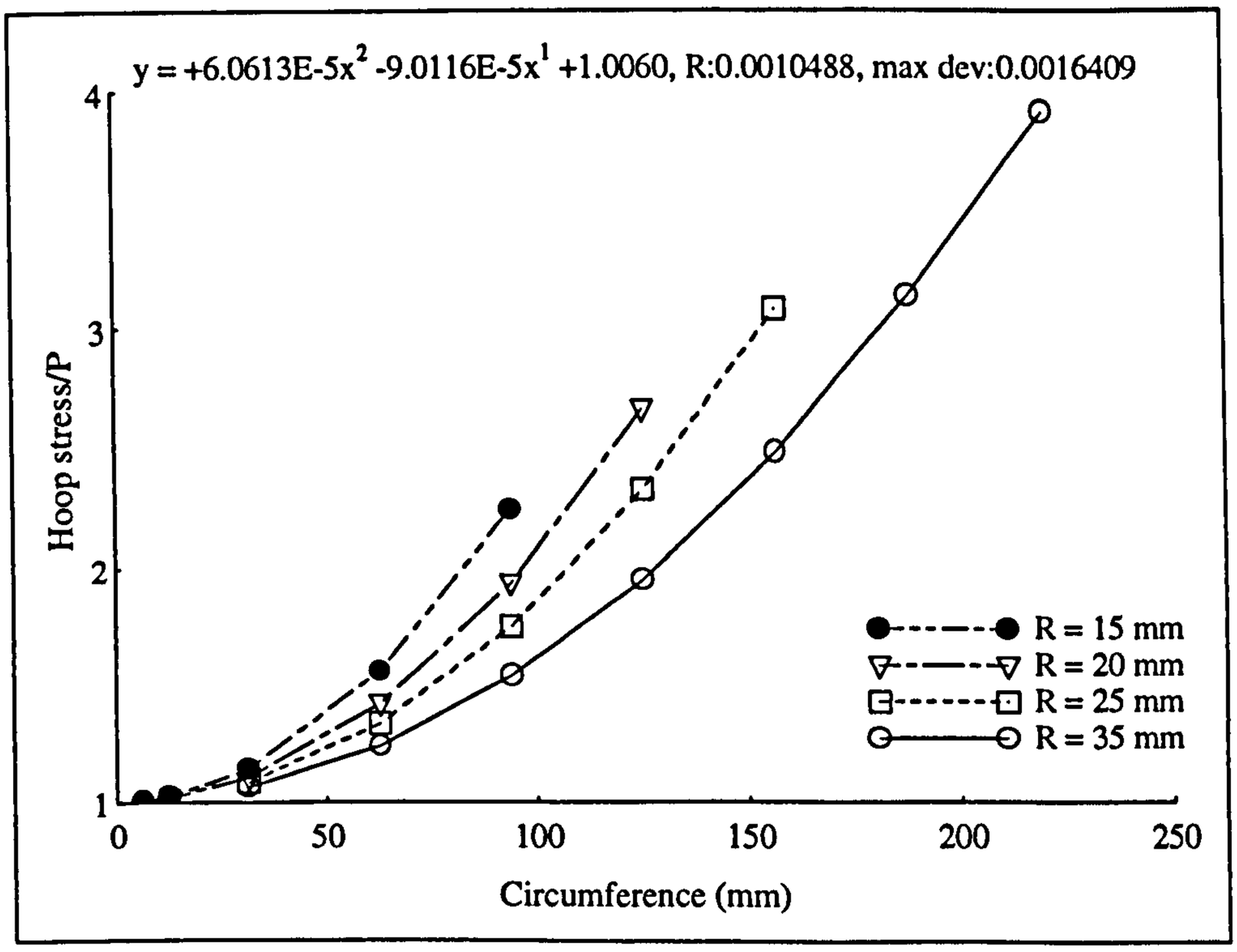

Figure 4.4. *The relationship between stress/P and circumference in SMVs of different initial sizes and a starting linear muscle thickness of 12 mm. The stresses are calculated at the inner radius, with constant volume considerations taken into account. The fitted equation is for the 35 mm radius ventricle.*

For a given initial radius, stress/pressure (σ/P) was determined from (4.1) and then plotted against circumference ($C = 2\pi R$), with due consideration of a constant ventricular wall volume (Figure 4.4). The plots were well fitted by a quadratic equation of the form

$$\sigma/P = qC^2 + rC + s \tag{4.14}$$

where q, r and s are constants. These constants were then incorporated into software to determine the force acting on a cross-section of a linearly contracting rabbit TA muscle as though it was within the walls of an SMV (Figure 4.5) with intraventricular pressure P. The use of the constants in (4.14) instead of the original equation (4.1) in calculating ventricular stress certainly reduced the computation time and thus allowed more accurate real-time force update.

The force on the muscle was updated every millisecond as the muscle shortened following electrical stimulation, as discussed in Chapter 2 (Figure 2.8a). Thus, the load on

the muscle could be varied as a function of changes in muscle length (equivalent to circumference in Figure 4.4) to simulate the relationship between wall stress and the radius in SMVs of different initial sizes pumping against different internal pressures. The maximum shortening of the muscle (see displacement trace in Figure 2.8b), taken to reflect a change in ventricular circumference, was then measured and used to evaluate the SV and EF.

4.3.4.1.2.2. Experimental procedure

Rabbits were anaesthetized as explained in Chapter 3. The resting (90°) length (L) of the exposed TA was measured *in situ*. The active and passive force-length relationships of the muscle were measured to determine the optimum length (Lo). The mass (in grams) of the TA (estimated as 90% of t

he rabbit's weight in kilograms) was used to estimate the cross-sectional area of the muscle. As skeletal muscle density, stated as 1.072 g/cm^3 (Gollnick *et al.* 1981), is close to unity, if the rabbit TA at L (cm) has an average cross-section of Ao cm^2, then the density

$$1 = \frac{mass}{AoL}$$

and the mean cross-section is given by

$$Ao = \frac{mass}{L} \tag{4.15}$$

However, rabbit TA does not have a uniform cross-section, but can be assumed to be widest around its centre. It can thus be considered as two cones, each of length L/2, joined end-to-end at the base of maximum cross-section Xmax. The volume of a cone is given by one-third of the base area multiplied by the height, so that

$$\tfrac{1}{3} X\max\left(\tfrac{L}{2}\right) \times 2 = AoL \tag{4.16}$$

Substituting (4.15) into (4.16), and rearranging, yields the maximum muscle cross-section as

$$X\text{max} = \frac{3 \times mass}{L} \tag{4.17}$$

As rabbit TA is not long enough to form a realistic-sized ventricle, a variable K was defined as the ratio of the circumference of a realistic-sized ventricle to the TA length (Figure 4.5) at the start of contraction. The size of the human LD allows construction of SMVs of up to 33 mm in radius, equivalent to a circumference of more than 200 mm; thus, for TA lengths of about 70 mm, K values of up to 3 were used. If a muscle of length L constitutes part of a ventricle of internal radius R_i (Figure 4.5), then

$$KL = 2\pi R_i \tag{4.18}$$

During a contraction, the K value was kept constant so that the muscle was a constant fraction of the circumference in the complex force calculations. The muscle was set at a series of lengths, from the resting length to a few millimetres above the optimal length, and the active and passive tensions measured. The passive force-length relationship was then used in the passive wall model described above to determine the corresponding pressures. A series of pressure-volume curves were then determined for different sizes (i.e. a series of values of K) of ventricle.

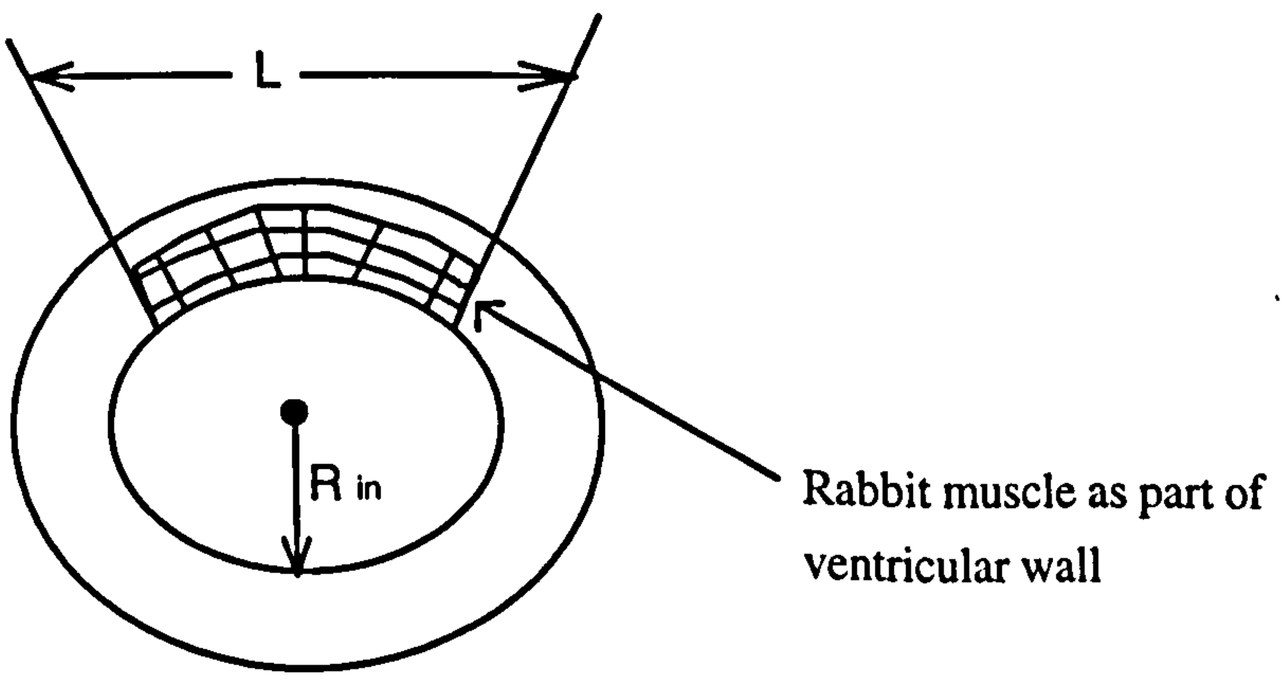

Figure 4.5. *Rabbit TA of length L as part of a ventricular wall of an SMV of internal radius R_i. Muscle stress was calculated at the inner radius.*

For the above values of K, a series of afterloaded contractions (single contractions with complex loads) ejecting against pressures from 80 to 160 mmHg were performed. The frequency of muscle stimulation was 200 Hz. SV and EF of SMVs pumping against the above afterload pressures in 200 ms were determined and plotted against radius. Work done in a single contraction was calculated at different initial muscle lengths as the product of the SV and the difference between the afterload and preload, which was obtained by converting the passive force at the various lengths into pressures. The work done was then plotted against preload for different afterloads.

4.3.4.2. Simulation of an SMV wall by the sheep latissimus dorsi

The sheep LD mechanical properties, measured in Chapter 3, were fitted in the same way as the rabbit characteristics so that they were defined by equations with known constants. These constants were then used in the numerical model to predict the passive pressure-volume curve, the pressure-flow relationship, and the stroke volume and ejection fraction versus starting radius curves.

4.4. Results

4.4.1. Model refinement

Results from preliminary model predictions are presented in this section to determine the single radius for stress evaluation and the radius for addition of the extra wall thickness in the simulations.

4.4.1.1. Extra wall thickness addition

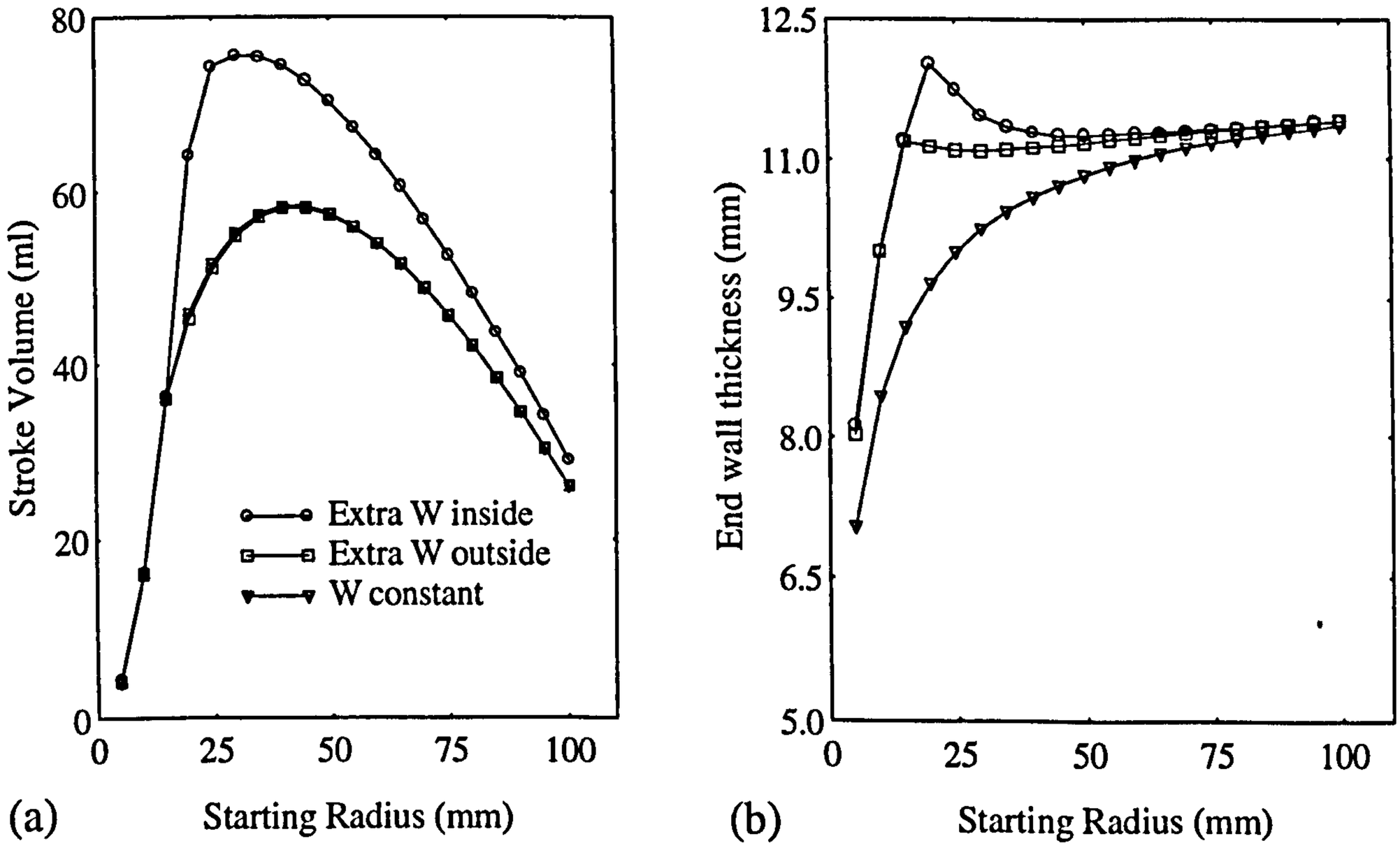

Figure 4.6. *(a) Preliminary model results showing stroke volume output for adding the extra wall thickness (W), either to the inside (∇), outside (□), or leaving the wall thickness constant (○). (b) The wall thickness at the end of contraction; for the constant W case, the indicated wall thickness is the starting value for the other two cases.*

Adding the extra thickness to the outside gave similar outputs to leaving the thickness constant, while adding the extra W to the inside exaggerated the stroke volume output (Figure 4.6a). However, for large radii, for which the effect of wall thickness is minimal, the outputs from all three options converged. This is to be expected from the Lamé's condition for a thin-walled ventricle consideration, which stipulates that the ratio of the diameter to the wall thickness be greater than 15. This value is approached here for radii

greater than 100 mm, at which changes in wall thickness during a contraction are negligible (Figure 4.6b). Adding the extra wall thickness to the outside was adapted because it predicted values similar to a thin wall consideration (i.e constant wall thickness), and because it was recommended by SMV flow modelling engineers from City University (London).

4.4.1.2. Radius for stress evaluation

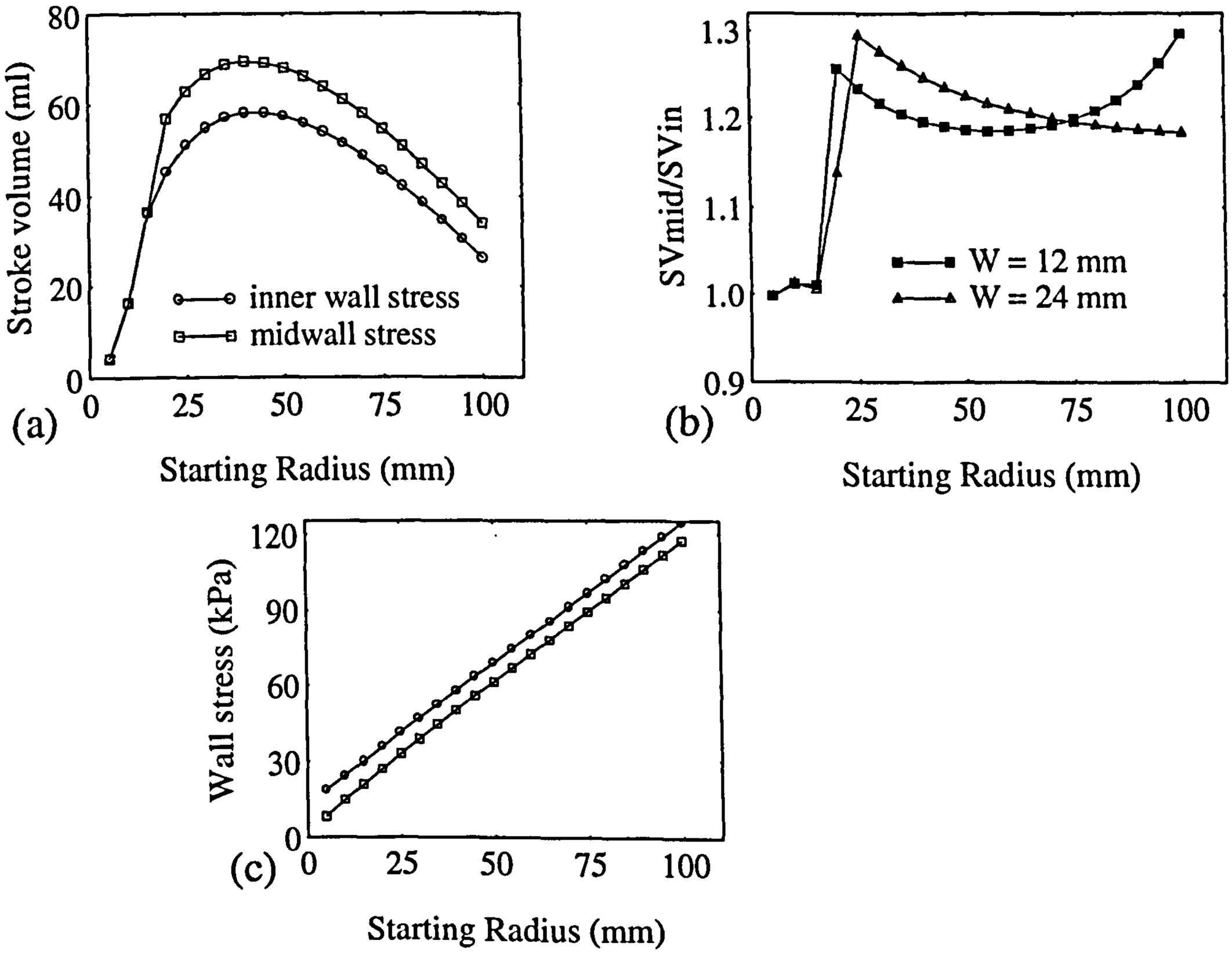

Figure 4.7. *Preliminary predictions with stress evaluated at the inner radius and at the midwall of the ventricle.*

In order to determine a single radius within the SMV wall at which stress could be evaluated to reflect that of the entire wall, SV outputs from a preliminary model with stress computed at both the inner radius and the midwall were compared (Figure 4.7a).

Table 4.1. *Typical muscle mechanical properties used in the model predictions.*

Muscle	Hill's constants	F-L fit constants	X-area or thickness
Control rabbit TA	a = 4.17 b = 133.8 Po = 21.67	A = 6.7E-10 B = 22.34 C = 0.79	151.52 mm^2
Rabbit 2.5 Hz (12 weeks)	a = 2.17 b = 65.28 Po = 18.99	A = 5.7E-12 B = 26.39 C = 0.27	127.93 mm^2
Rabbit 5 Hz (12 weeks)	a = 1.68 b = 45.78 Po = 14.72	A = 1.77E-7 B = 16.77 C = 19.5	104.18 mm^2
Rabbit 10 Hz (4 weeks)	a = 0.96 b = 22.75 Po = 8.72	A = 4.13E-12 B = 26.0 C = 2.1E-2	75.90 mm^2
Control sheep LD	a = 59.05 b = 1062 Po = 54.78	A = 33.74 B = 0.771 C = 60.30	6.0 mm
Sheep LD 2 Hz (8 weeks)	a = 11.22 b = 178.6 Po = 34.28	A = 3.21E-2 B = 8.02 C = 0.28	3.89 mm

The evaluation at the inner radius gave lower SV outputs than that at the midwall, where the transmural stresses were lower (Figure 4.7c). However, the radius for maximum SV output was the same with either option. On doubling the wall thickness, the midwall option produced even greater outputs compared with the inner wall consideration (Figure 4.7b), indicating that the difference in the outputs of the two options varied with wall thickness. One of these options thus had to be adapted for the model predictions. The inner radius was chosen because it presented the highest possible loading of the ventricular wall and therefore the 'worst case' situation. Moreover, its surface was in contact with the ventricular fluid and so imparted its stress directly to this fluid. Furthermore, the model assumed that the linear mechanical measurements were made at fibre lengths equivalent to those at the inner radius (see Figure 4.3), which must therefore

be used in any predictions. Stress was therefore evaluated at the inner radius in the following predictions.

4.4.2. Purely numerical predictions

Table 4.1 shows typical muscle mechanical properties used in the numerical predictions. The constants defining the passive force-length and the force-velocity curves were obtained as explained in Chapter 3. Estimated rabbit TA cross-sectional areas, using (4.17), and the measured mean thickness of sheep LDs are also presented.

4.4.2.1. Passive SMV wall

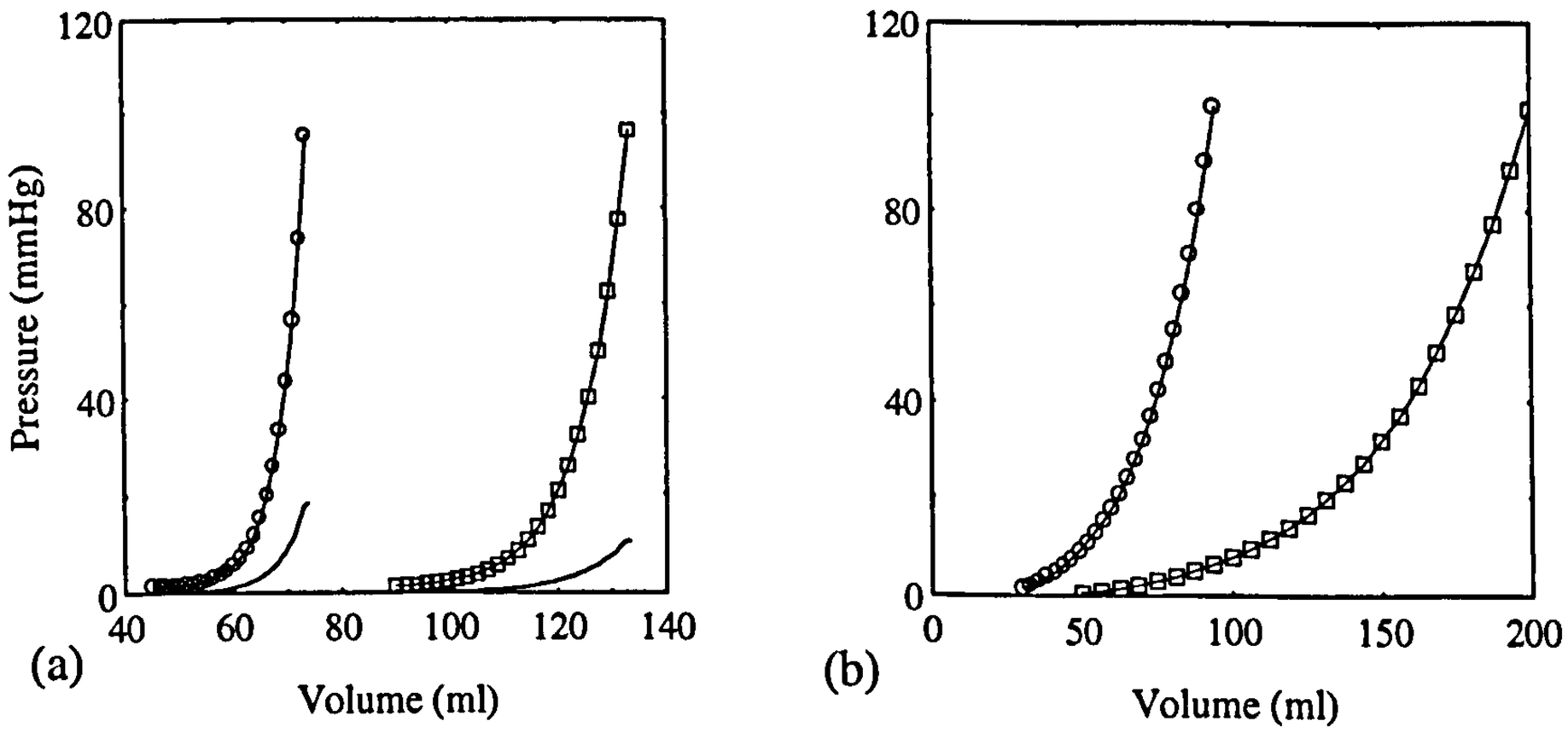

Figure 4.8. *Predicted passive pressure-volume curves for two sizes of SMVs of 10 cm height: Radius = 15 mm (○) and Radius = 20 mm (□). (a) From rabbit mechanical properties: the smooth curves are obtained by differentiating the predicted curves to give the dP/dV plots. (b) From sheep LD properties.*

The models predicted passive pressure-volume (P-V) curves in two sizes of ventricle, using rabbit TA (Figure 4.8a) and sheep LD (Figure 4.8b) force-length relationships. The predicted P-V curves in Figure 4.8a are differentiated with respect to volume (smooth curves), and indicate that change in pressure with increasing volume (dP/dV) is higher in the smaller ventricle. The model thus predicts that a small ventricle is stiffer than a large ventricle, which is therefore more distensible.

4.4.2.2. Active SMV wall

4.4.2.2.1. Pressure-flow predictions

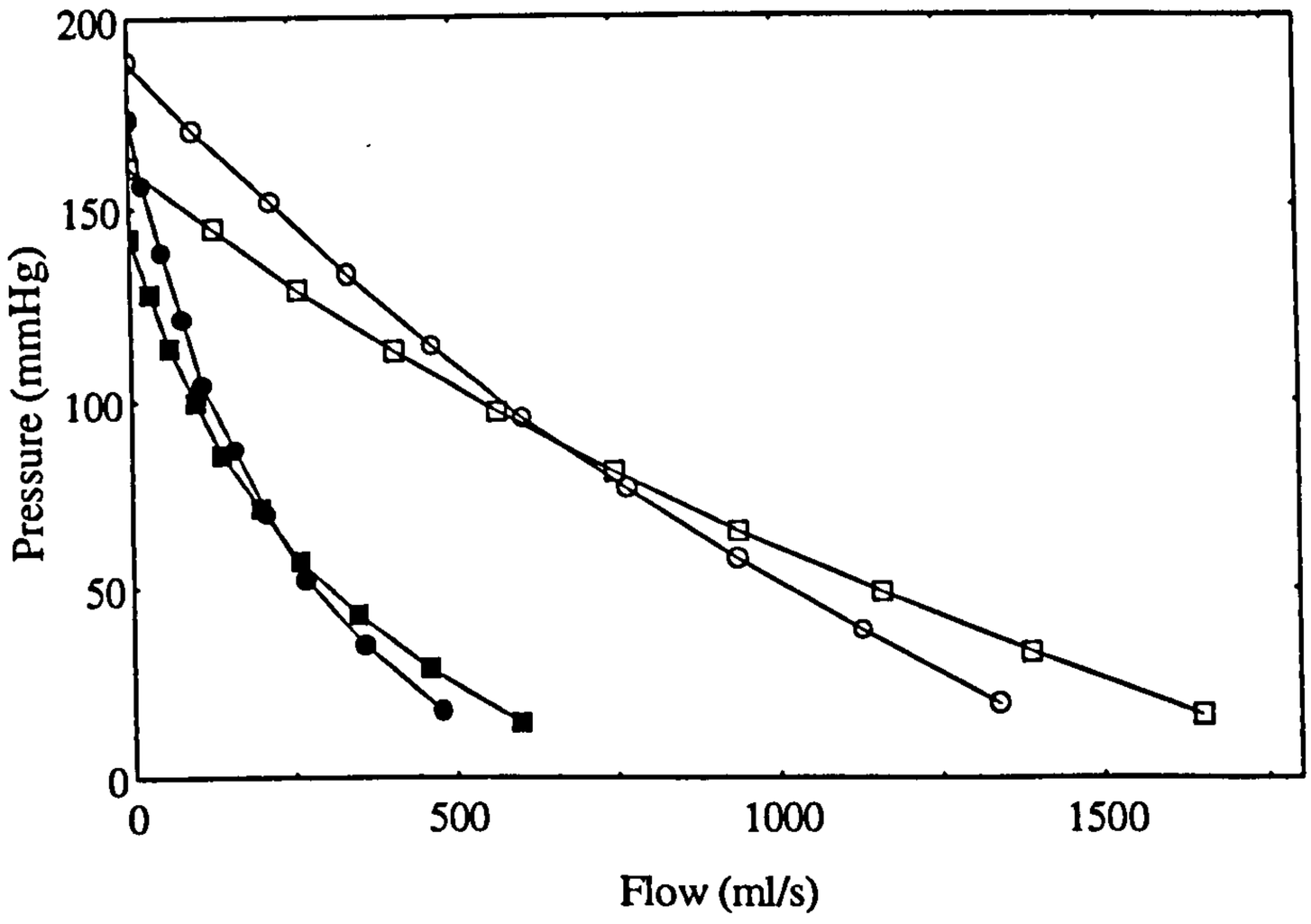

Figure 4.9. *Predicted pressure versus flow curves from the force-velocity relationship of control (open symbols) and chronically stimulated (closed symbols) sheep LD muscles. The predictions are for two sizes of ventricle: Radius = 15 mm (○) and Radius = 20 mm (□).*

In calculating the SV in a given contraction time of the SMV wall, volume changes in millisecond time steps (flows) were calculated and then summed. The rate of volume change at the start of contraction was greatest, and was thus used as an indication of the peak flow of fluid out of the ventricles. In sheep SMVs, the predicted flow was averaged over the first 5 ms of contraction, and the resulting pressure-flow curves are shown in Figure 4.9. The pressure is inversely related to flow, and the shape of the curve is similar to the force-velocity relationship of muscle. The control muscle produced three-fold more flow than the stimulated muscle, but the peak afterload pressures at which no flow occurred were similar.

4.4.2.2.2. Optimum size of ventricle

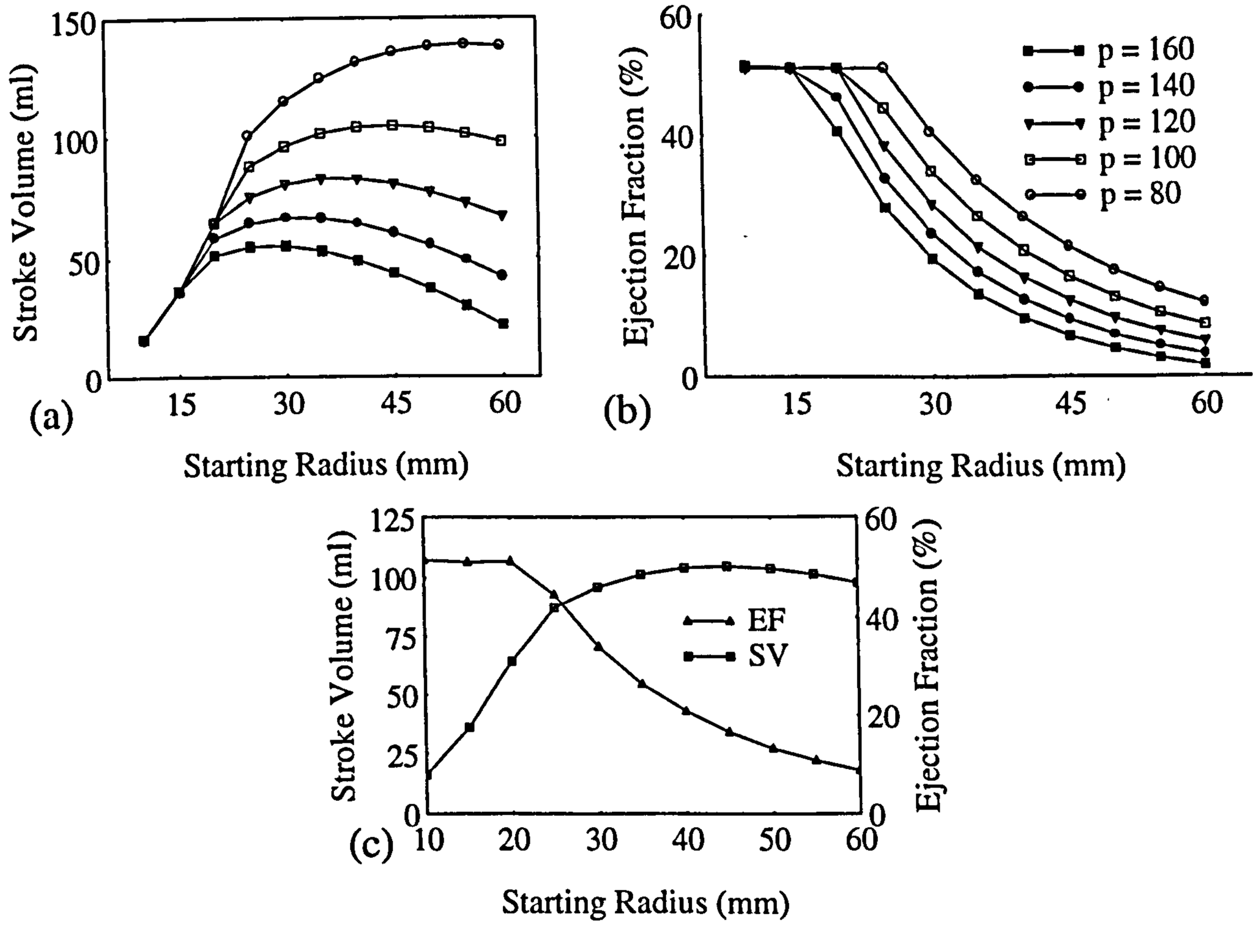

Figure 4.10. *Predicted stroke volume (SV) and ejection fraction (EF) versus ventricle size at different afterloads. (a) SV (ordinate) versus starting radius (abscissa). (b) EF versus starting radius. (c) Inverse relationship between SV and EF.*

The effects of increasing intraventricular pressure (P) on the predicted SV and EF in ventricles of increasing radii are presented in Figure 4.10. The higher the afterload pressure, the lower the SV output at a given radius (Figure 4.10a), with a corresponding fall in EF (Figure 4.10b). Figure 4.10a also indicates that the effect of afterload pressure on ventricular output is higher at large than at small radii. Also, the optimum radius for SV output shifts towards smaller radii with increasing afterload pressure. Stroke volume, however, is inversely related to EF (Figure 4.10c). Clearly, the maximum EFs occur at radii much lower than that for maximum stroke volume. Thus, in order to increase the ejection fraction, SMVs must be constructed at a size less than that predicted for maximum stroke volume output.

4.4.2.2.3. Effect of muscle transformation on ventricular function

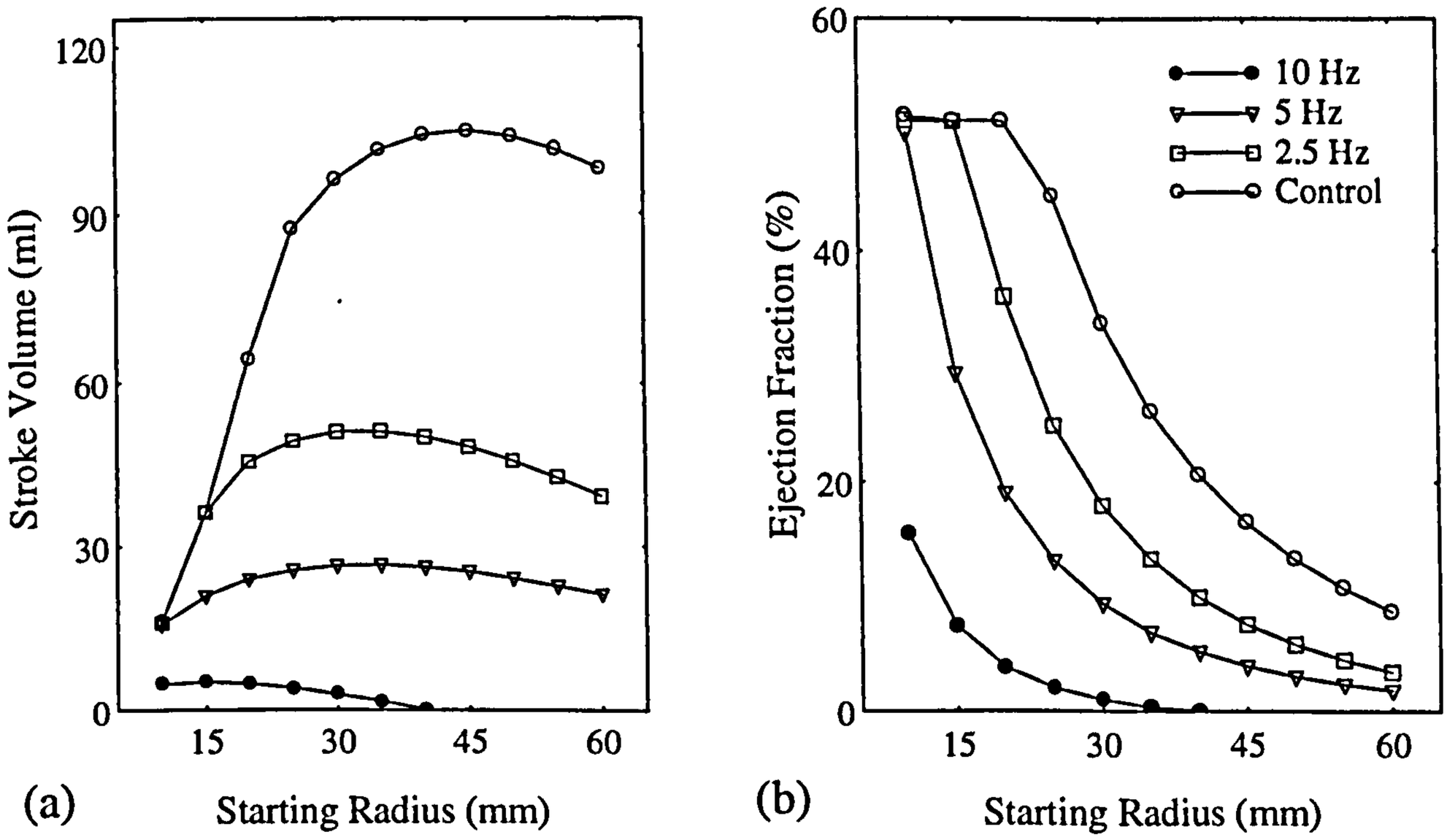

Figure 4.11. *Predicted SV and EF from rabbit TA at different stages of chronic transformation. The afterload pressure is 100 mmHg. (a) SV against starting radius. (b) EF versus starting radius. See panel (b) for legend.*

SV and EF outputs predicted from rabbit TA control muscles, and muscles stimulated chronically at 2.5 Hz, 5 Hz, and 10 Hz for more than 4 weeks are presented in Figure 4.11. The model predicted a concomitant decrease in SV and the radius for optimum output with increasing frequency of chronic stimulation (Figure 4.11a); the EF also fell in line with the SV. Thus, the SMV output is predicted to decrease as the muscle becomes more fully transformed to a slow state. Similar results were predicted for the sheep LD muscles.

4.4.3. Complex loads

Plots similar to those derived from the purely numerical predictions were obtained for the complex load measurements (Figure 4.12). The SV increased with increasing volume according to the Frank-Starling law, and the EF was inversely proportional to the SV (Figure 4.12c). In fact, the numerical predictions (broken lines, Figure 4.12a) were similar

in magnitude to the complex load outputs; the predictions were done for a shorter contraction time because some of the 200 ms of the complex load experiments was used for force generation. Thus, the complex load results were qualitatively and quantitatively similar to the numerical predictions. The maximum EF measured in the complex load experiments was under 50% (Figure 4.12b), though no restriction was placed on the extent of muscle contraction.

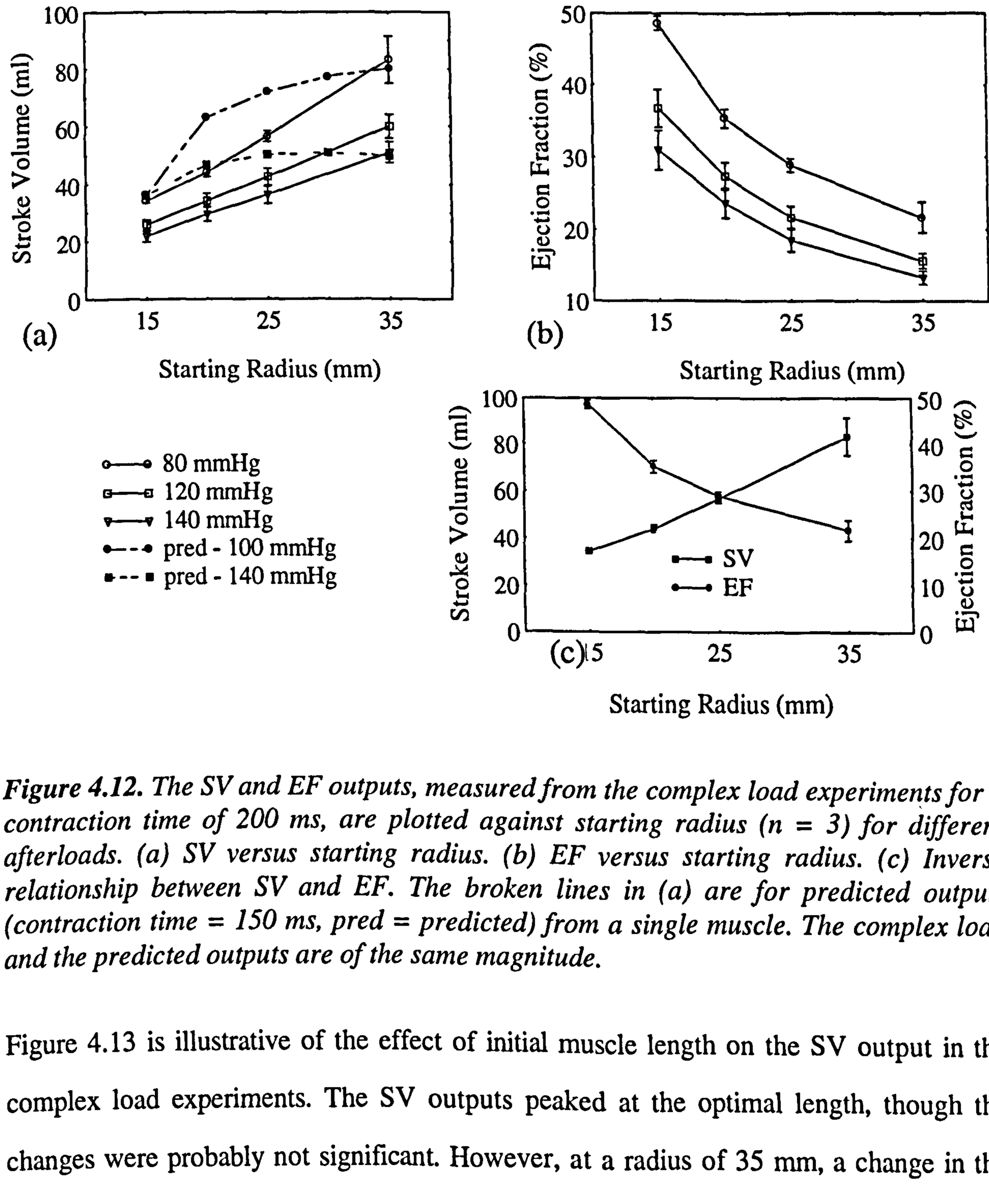

Figure 4.12. *The SV and EF outputs, measured from the complex load experiments for a contraction time of 200 ms, are plotted against starting radius (n = 3) for different afterloads. (a) SV versus starting radius. (b) EF versus starting radius. (c) Inverse relationship between SV and EF. The broken lines in (a) are for predicted outputs (contraction time = 150 ms, pred = predicted) from a single muscle. The complex load and the predicted outputs are of the same magnitude.*

Figure 4.13 is illustrative of the effect of initial muscle length on the SV output in the complex load experiments. The SV outputs peaked at the optimal length, though the changes were probably not significant. However, at a radius of 35 mm, a change in the

initial length to 5% below the optimal length (Figure 4.13a) led to a 15% fall in SV, while only a 9% drop was observed for a similar length change above the optimal length. As initial length in the complex loads is equivalent to preload, the outputs thus seemed to be more sensitive to smaller preloads.

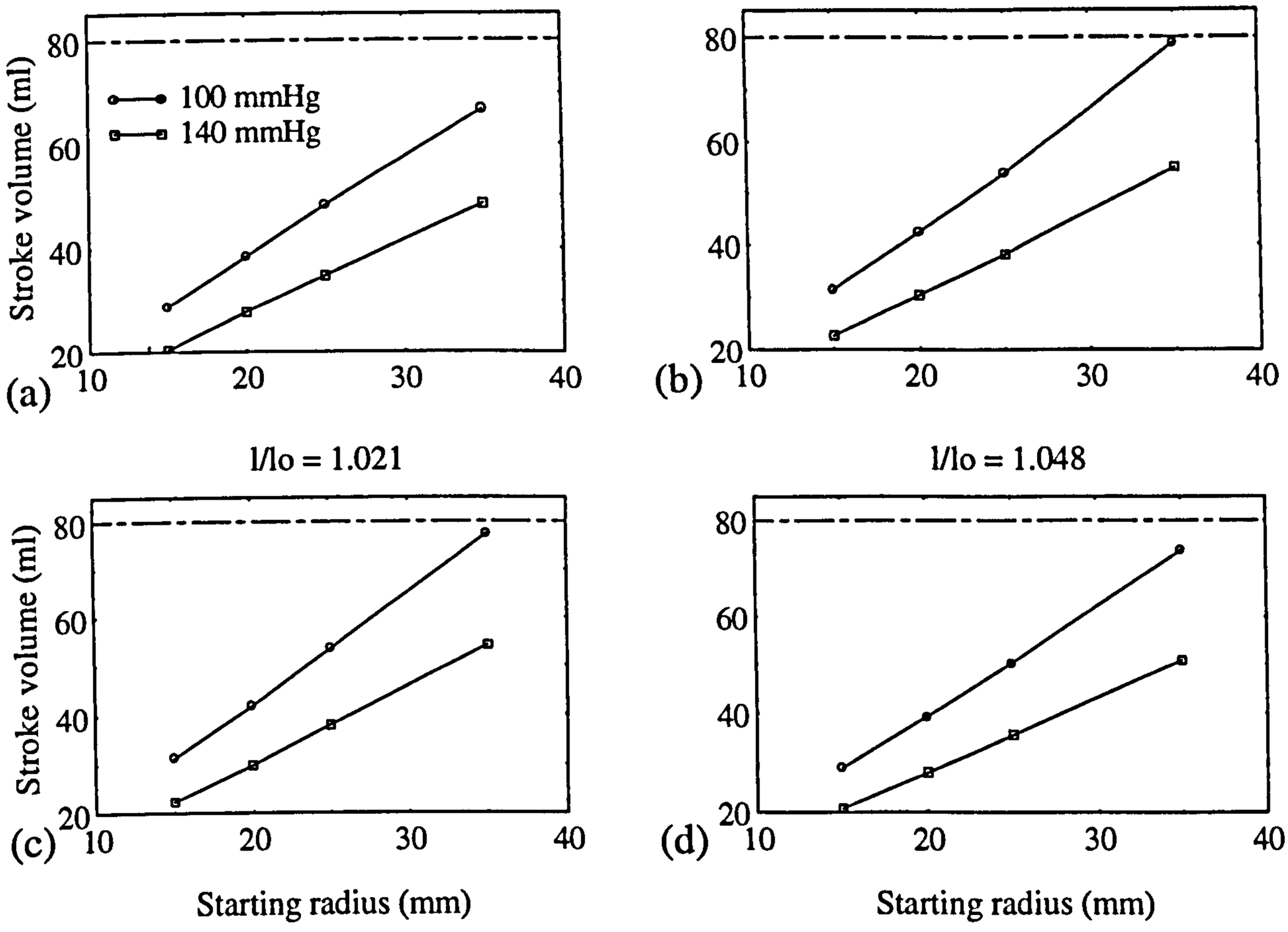

Figure 4.13. *Effect of initial muscle length (equivalent to preload) on output in complex load experiments. The peak output occurred at the optimal length (l/lo = 1.0, panel (b)). For legend, see panel (a). A broken line is drawn at a SV of 80 ml to ease comparison.*

For illustrative purposes only, stroke work measurements from a single rabbit TA, contracting under complex loading against different afterloads, are presented in Figure 4.14. This figure suggests that there was an optimum preload (> 0 mmHg) and afterload (120 mmHg in this case) against which maximum work was produced, with peak work output around 300 mJ. Also, the large ventricle (radius = 20 mm) produced more work than the small ventricle (radius = 15 mm) at all combinations of preload and afterload.

However, using the peak work outputs against the 120 mmHg afterload, the small ventricle produced work per unit mass (2.67 W/kg) similar to the large ventricle (2.59 W/kg). Thus, in terms of normalized work, small ventricles may be similar to large ventricles; however, small ventricles produce higher ejection fractions, thus reducing the risk of thrombus formation. SMV configuration optimization therefore requires compromises in the various parameters.

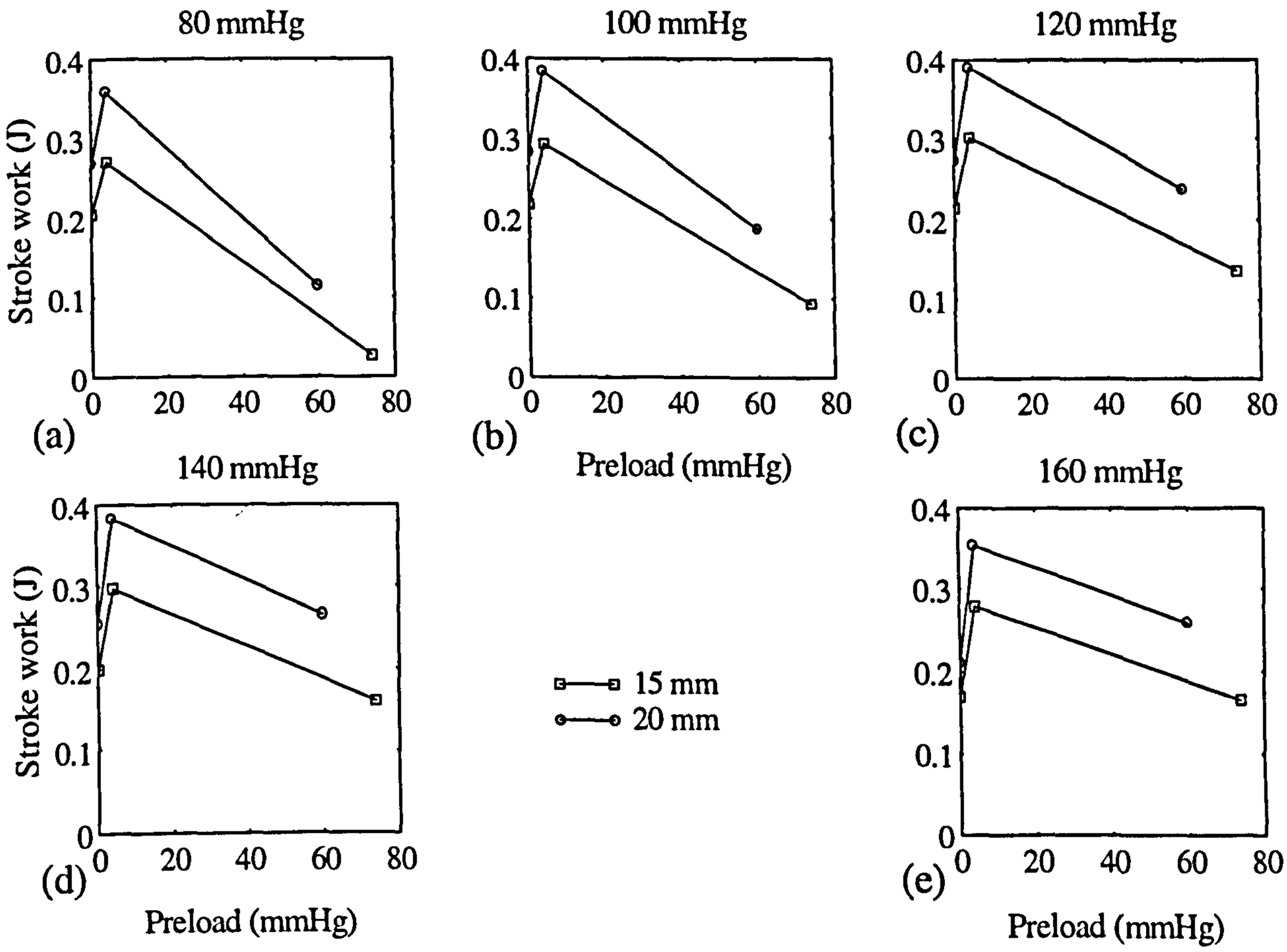

Figure 4.14. *Illustrative results of work calculated from complex load experiments. Stroke work for two sizes of SMVs pumping against different afterloads are plotted against the preload (calculated from the initial muscle lengths). Legend indicates the radii.*

4.5. Discussion

A mathematical model was developed to predict SMV function from the linear mechanical properties of skeletal muscle. A part physical-part numerical model in which a linearly contracting rabbit TA muscle was loaded to contract against complex loads as

though it formed part of the wall of an SMV was also developed. Both models predicted optimal ventricular sizes for stroke volume output of ventricles pumping against various loading conditions and for muscles in different states of transformation. But would this model be of much use to the many surgeons providing skeletal muscle cardiac assist?

4.5.1. Pressure-volume predictions

The model predicted passive pressure-volume curves similar in shape to those measured in intact canine and feline hearts (Spotnitz *et al.* 1966, 1979), to those predicted and measured from the rectus abdominis muscle in mongrel dogs (Spotnitz *et al.* 1974), and to those measured in acute SMVs constructed with canine LD muscles (Oda *et al.* 1993). The small ventricle (radius = 15 mm) was stiffer (a steeper dP/dV curve, Figure 4.8a) than the large ventricle. This prediction is in agreement with pressure-volume curves measured by Oda *et al.* (1993), who found that larger ventricles were more distensible. The difference in slope of the pressure-volume curve in the small and large ventricles may be explicable in terms of sarcomere response to stretch (Spotnitz *et al.* 1966): a similar change in volume in both a small and a large ventricle represents a higher fractional length change in the former, and thus a much higher ventricular wall stress and a correspondingly higher pressure. Thus, the model is able to predict, at least qualitatively, that a large ventricle is more distensible or more compliant than a smaller ventricle.

4.5.2. Optimal ventricular size

For each afterload pressure and a set of the Hill's constants, the numerical model clearly predicted an optimum size of ventricle at which peak stroke volume occurred (Figure 4.10a and 4.11a). But the ejection fraction was greater for a smaller size of ventricle, with the peak value occurring at a size less than that for peak stroke volume output (Figure 4.10c). The complex load measurements confirmed the numerical predictions (Figure 4.12). A similar relationship of stroke volume versus ventricular size has been predicted

in a mathematical model of SMVs based on large deformation elasticity theory (Bridges *et al.* 1989a; Hammond *et al.* 1990). Hammond *et al.* also showed that large ventricles generated more work than smaller ventricles of the same mass over varying loading conditions, an observation that would tend to favour the use of larger-sized ventricles. Although large SMVs may always produce more work, as was confirmed in the present study from the complex load measurements (Figure 4.14), they may just be as energy efficient as smaller-sized ventricles, which usually have the advantage of higher EFs. In fact, the calculated work output per kg from Figure 4.14 was similar for both sizes of ventricle; the work output from the small ventricle formed by Hammond *et al.* (1990) may have been reduced by the thicker ventricular wall that resulted from the use of the same mass of muscle as for the larger ventricle. Ventricular wall thickness can significantly affect the performance of an SMV (see below). The purely numerical and the complex load models also showed that EF is inversely related to stroke volume for increasing ventricular size. The predicted ventricular sizes for maximum SV output therefore have low EFs, which are associated with an increased risk of thrombosis, arising from an insufficient turnover of blood, or high residence times, within the ventricle. The above predictions are therefore suggestive of a design compromise in the construction of SMVs: for efficient function, SMVs should be constructed at a size less than that required for maximum stroke volume in order to reduce the risk of thromboembolism.

The results also showed that chronic transformation of the muscles had a very large effect on the optimum size of ventricles. The extreme slowing of the muscles led to a 90% drop in stroke volume (Figure 4.11, control versus chronic 10 Hz), and a reduction in the optimum radius from 45 mm to 15 mm, with a similar fall in ejection fraction. These changes would mean that there is less blood available to provide cardiac assist, a situation that is worsened by difficulties of synchronization of such slowly contracting ventricles to the heart cycle. Better hemodynamic performance of SMVs would result if chronic

stimulation regimes that maintained muscle speed were developed (compare the 2.5 Hz and 5 Hz outputs, Figure 4.11a). It is therefore crucial to optimize ventricular size in chronically stimulated muscles in order to exploit the limited power available for circulatory assist.

4.5.3. Effect of multi-layered wraps

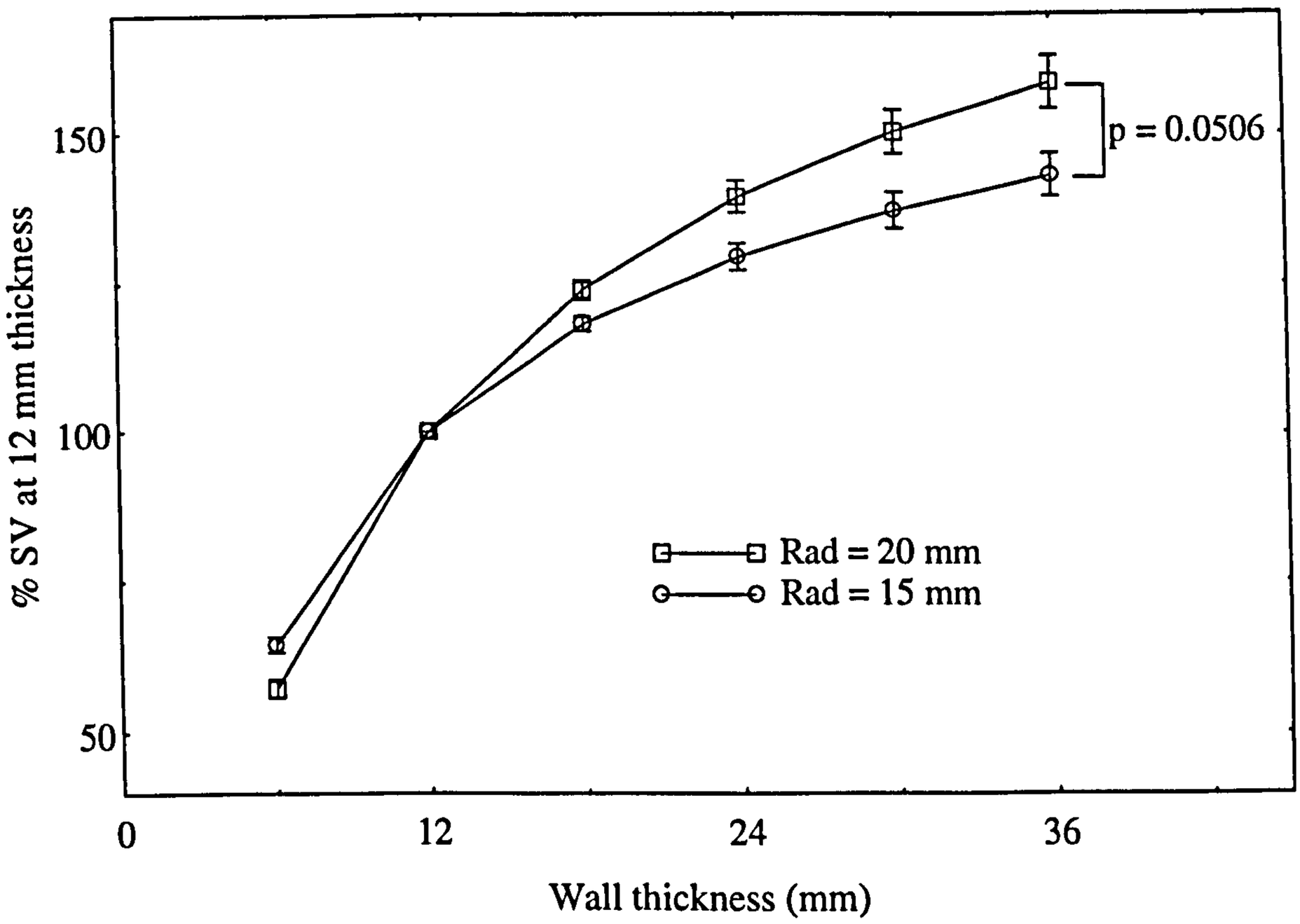

Figure 4.15. *Predicted effect of wall thickness on ventricular output at an afterload of 100 mmHg. The SV output (ordinate) is plotted as a percentage of that at a wall thickness of 12 mm. The Hill's constants from three control rabbit TA muscles were used.*

Because of the complex nature of transmural stresses (Spotnitz *et al.* 1966; Beyar & Sideman 1984), ventricular wall thickness could play a very important role in the function of an SMV. However, models of myocardial wall mechanics have predicted uniform transmural fiber stress distribution during the ejection phase (Arts *et al.* 1982, 1991). The present model used the stress at the inner wall as representative of a uniform transmural stress distribution, and so could be used to investigate the effect of wall thickness on

ventricular function. Feigl and Fry (1964) measured the instantaneous and continuous left ventricular wall thickness in dogs, reporting a change by as much as 21% during systole.

They concluded that myocardial wall thickness changes during the cardiac cycle may be important in some considerations of the heart's performance. The wall thickness change predicted using fast rabbit TA mechanical properties in Figure 4.6a (25 mm radius) are similar to the above value, and so it would be interesting to establish any other similarities of the model predictions to actual left ventricular indices of performance during contraction.

Figure 4.15 shows the predicted SV outputs for two sizes of ventricle with increasing wall thickness using rabbit TA mechanical properties (n = 3). The large ventricles perform better for larger thicknesses: trebling the wall thickness (from 12 mm to 36 mm, Radius = 20 mm) increases the SV output by as much as 60% for the same size of ventricle and contractility (the same set of the Hill's constants); the difference in the two sizes of ventricle approaches significance ($p = 0.0506$) at this thickness. On the other hand, the small ventricles perform better with smaller wall thicknesses (< 12 mm). With regards to wall thickness, the difference in performance between the large and the small ventricles may be explicable in terms of the functional state of the sarcomeres in the ventricular wall. A thicker wall in a large ventricle would allow most of the many sarcomeres to function close to their optimal length due to the limited curvature of the ventricular wall. In a small ventricle, on the other hand, a thinner wall would yield the same advantage above. The model therefore suggests that ventricular performance is largely influenced by wall thickness in relation to radius. The radius/thickness (R/Th) ratio is equivalent to the volume/mass (V/M) ratio, both of which are useful indices of ventricular performance (Gaasch 1979; Oda *et al.* 1993). The V/M ratio determines how appropriate the mass of muscle is for a particular ventricular volume. Both the R/Th and

V/M ratios calculated at the predicted optimum radii for stroke volume output for various wall thicknesses at an afterload of 100 mmHg are presented in Table 4.2.

Table 4.2. *Radius/thickness and volume/mass ratios at predicted optimum radii for different wall thicknesses, pumping against an afterload of 100 mmHg. The SMV thickness is calculated from the linear wall thickness assuming constant muscle volume (see text).*

Linear wall thickness (mm)	SMV wall thickness (W, mm)	Predicted radius for peak SV (mm)	Radius/W	Volume/mass
6.0	5.3	20.0	3.8	1.7
12.0	10.6	40.0	3.8	1.7
24.0	20.9	70.0	3.4	1.5
36.0	31.6	115.0	3.6	1.6
		mean ± SEM	3.6 ± 0.1	1.6 ± 0.1

The predicted V/M ratio of 1.6 ± 0.1 (Table 4.2) for maximum SV output compares favourably with the value of 1.53 ± 0.14 measured by Oda *et al.* (1993) for their large single-layered ventricle (LSLV) constructed from control canine LD muscle. This ventricle produced significantly higher SV at the appropriate loading conditions than either the small single-layered (SSLV) or the small double-layered (SDLV) ventricles that were formed. However, the SSLV and the SDLV ventricles produced significantly larger ejection fractions than the LSLV ventricle under all loading conditions; these ventricles had V/M ratios of 0.76 ± 0.06 and 0.30 ± 0.02, respectively. Oda *et al.* (1993) concluded that the smaller ventricles were less affected by loading conditions because of their lower V/M ratios. These observations support the model predictions, which recommend construction of SMVs at a size less than that which gave maximum stroke volume. The

overall effect will be ventricles with lower V/M ratios, which are capable of generating adequate pressures but with a volume large enough to provide useful cardiac assist, as was recommended by Oda *et al.* (1993).

An interesting finding from the model was the fact that the R/Th ratio of 3.6 ± 0.1 (Table 4.2) for optimum performance was similar to the value of 3.0 ± 0.7 reported in the normal hearts of children and adults (Gaasch 1979). This suggests that when contractility is not at issue, the R/Th ratio is a very important index of ventricular function. For the 10 Hz stimulated muscles, the R/Th and the V/M ratios for optimum performance were 1.59 ± 0.01 (n = 6) and 0.60 ± 0.01 (n = 6). It may thus be concluded that there is a unique R/Th ratio for optimum performance of an SMV with given contractility: the slower the muscle, the lower the R/Th ratio for optimum performance. The low V/M ratio obtained for the 10-Hz stimulated muscle is associated with low EFs (Oda *et al.* 1993), so that SMVs formed from chronically stimulated muscles would function less efficiently, and therefore increase the risk of thrombus formation. However, the function of these ventricles with low V/M ratios may be less influenced by the loading conditions, as was the case for the SDLV and the SSLV (Oda *et al.* 1993). Hence, as concluded by Oda *et al.* (1993), construction of SMVs entails a compromise between a low enough V/M ratio to enable adequate pressure generation to overcome the afterload, and a V/M ratio high enough to allow loading of the ventricle with sufficient volume to provide an adequate SV output for heart assist.

Another interesting finding from the model was the prediction of the relationship between R/Th ratio and afterload pressure. Figure 4.16 is a plot of the R/Th ratio for the ventricular size predicted for maximum SV output versus the afterload pressure against which the SMV pumps. The curve obtained using control rabbit TA mechanical properties is identical to that determined by Ford (1976) for approximating the normal inverse relation between R/Th (end-diastolic) and systolic pressure. In humans, this

relation reflects the degree to which left ventricular muscle mass is appropriate or adequate for chamber size. When stimulated TA mechanical properties were used, the predicted curve was shifted in a direction that is referred to as inappropriate hypertrophy (Ford 1976; Gaasch 1979), despite the fact that the muscle mass was essentially the same.

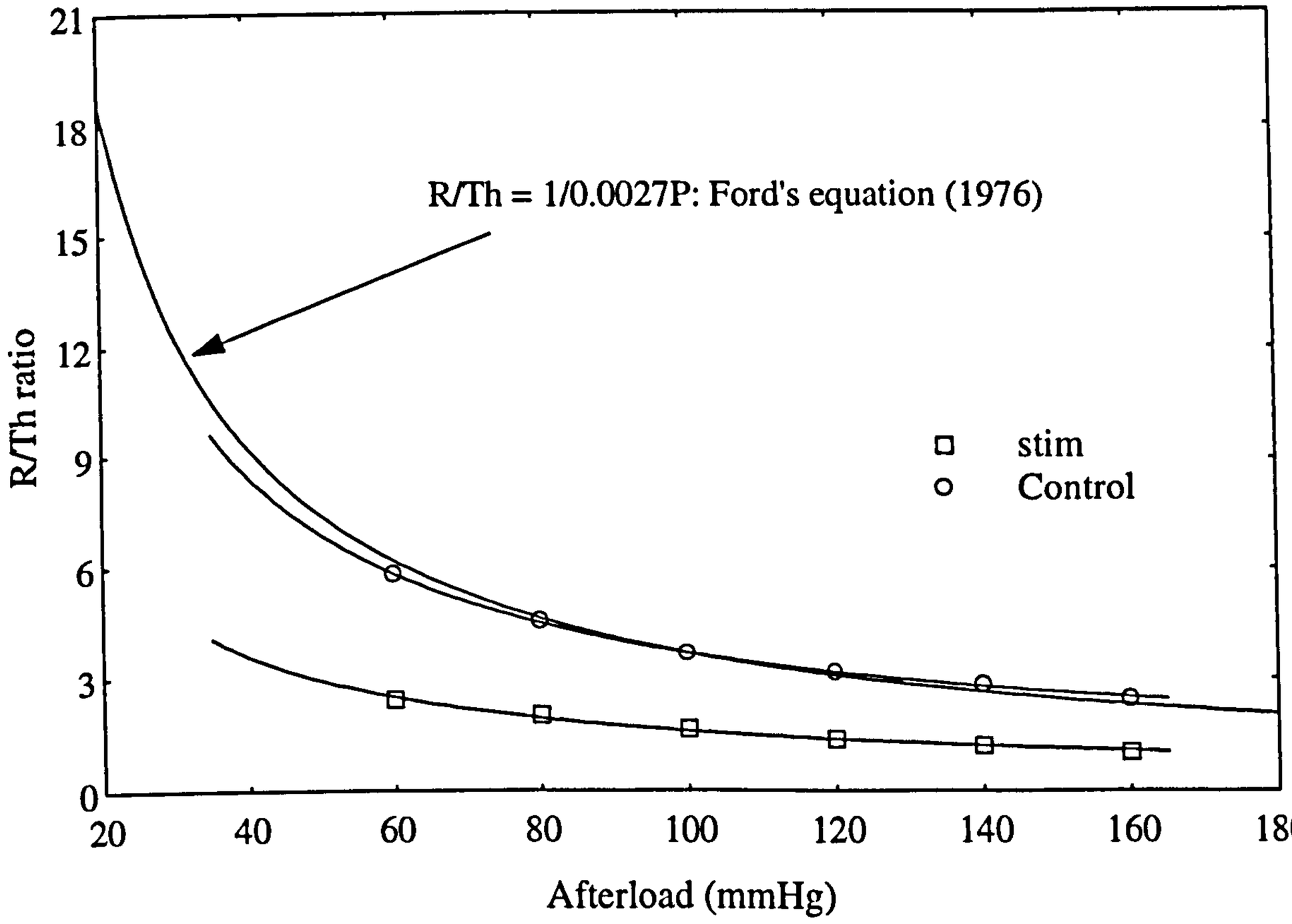

Figure 4.16. *Predicted R/Th versus afterload curves for control (○) and stimulated (□) muscles. The Ford's equation (1976) is also plotted for comparison. [P = systolic pressure.]*

It may therefore be possible to configure slowly-contracting chronically stimulated muscle to provide cardiac assist more efficiently by simply adjusting the R/Th ratio of the constructed ventricle. However, the ability to achieve the desired ratios would be limited by the amount of LD muscle available, and the function of these ventricles would be hampered by difficulties of synchronization with the cardiac cycle.

4.5.4. Possible mechanism of function of cardiomyoplasty

The predicted increase in function of SMVs with increasing wall thickness, despite the fact that the contractility of the muscle is the same, may partly explain the mechanism of cardiomyoplasty (CMP). As indicated by recent reviews (El Oakley & Jarvis 1994; Hooper & Salmons 1994), there is controversy surrounding the hemodynamic evidence of CMP: although clinical improvement is clearly evident, results of active systolic assist are inconsistent. Though a recent study using beat-to-beat analysis of left ventricular pressure-volume and stroke volume in CMP patients has shown that such careful analysis is important in demonstrating an improvement in cardiac function (Schreuder *et al.* 1995), this improvement may not be necessary for adequate CMP performance (Kass *et al.* 1995).

From Figure 4.15, it is clear that the difference in performance between the small and large ventricles is more discernible at larger wall thicknesses, only nearing significance ($p = 0.0506$) at a wall thickness of 36 mm. However, doubling the wall thickness from 12 mm to 24 mm results in a significantly greater SV output in the large ventricle compared with the small ventricle ($39.33 \pm 2.67\%$ versus $29.33 \pm 2.19\%$; $p < 0.05$). A greater improvement in function may thus be expected by wrapping a highly dilated heart with extra muscle, with no associated increase in cardiac contractility. It is therefore not surprising that the only studies of CMP that have shown consistent results were reported by a group from Sao Paulo, Brazil, whose studies were on patients with dilated cardiomyopathy (Moreira *et al.* 1990, 1991). Recent work (Kass *et al.* 1995) proposes that CMP may act more passively to help reverse heart chamber remodelling, lending support to the view that the contractility of the myocardium may not be crucially important if the R/Th ratio, for example, was optimal. Increasing the wall thickness of a dilated heart with the CMP procedure would tend to restore this ratio, which has been shown to be a very important index of left ventricular function (Gaasch 1979).

4.5.5. Summary

Although the numerical model was made as simple as possible, it seems to be able to predict reasonably well several important parameters of ventricular function. The model predictions indicate that the R/Th ratio is a very important index of ventricular performance, and so needs to be paid particular attention. It would certainly be useful to test the ability of this model in predicting the function of real ventricles. This is the subject of the next chapter, in which the function of acute SMVs, constructed from sheep LDs whose mechanical properties are presented in Chapter 3, are compared with predictions made with this model.

4.5.6. Limitations of the model

There are a few limitations to the numerical model presented here. Firstly, it is a static model because it does not take account of force generation by muscle, but simply concentrates on the limited period in an SMV contraction when there is flow. Therefore, the model does not take into consideration the effect of different preloads and the ability of the ventricle to generate pressure. Secondly, in using the force-velocity curve, the model neither accounts for the velocity changes that would occur as the muscle shortens and thus slows down due to deactivation during ventricular contraction, nor is it able to predict the pumping function from a different initial length other than the optimal length at which the force-velocity curve was measured. However, the initial velocity of contraction of rabbit TA can be maintained for long periods (up to 300 ms, Figure 2.7a), reducing the impact of slowing due to shortening deactivation. The relationships between different initial lengths and the Hill's constants proposed by Petrofsky and Phillips (1981) could be incorporated in the model to predict the pumping function for different starting lengths or preloads. Although the complex loads considered different starting lengths, the outputs near the optimal length were very similar (Figure 4.13). Thirdly, the afterload pressure, equivalent to the peripheral resistance, was assumed to be constant. However,

this is not the case as peripheral resistance increases with increased flow into the systemic circulation (Shroff *et al.* 1985). Some of the above limitations were unavoidable in an attempt to keep the model simple. Surely, a better model could be developed by eliminating the above limitations.

Despite these limitations, the model predicted indices of ventricular hemodynamics that have been reported in the literature and indicated that the radius/thickness ratio is a very useful index of ventricular function. It is therefore a useful model that can be used, at least, to predict qualitative properties of optimal SMV configurations following chronic electrical stimulation.

4.6. Conclusions

A mathematical model of SMVs developed using muscle mechanical properties demonstrated how large an effect the mechanical properties of the muscle had on the performance of SMVs of a realistic size. The model predicted an optimal volume at which peak stroke volume occurred. However, the ejection fraction at such optimal volumes was low. The function of ventricles could be better represented by the R/Th or the V/M ratios. The model revealed a design compromise: for optimal performance, the resting radius of the surgically-formed ventricle would have to be somewhat less than that which gave maximum stroke volume. As the predictions from the model were similar to the complex load experimental measurements, the model will be tested further in the next chapter by comparing predictions with actual measurements made in acute SMVs constructed from the same muscles in sheep.

5. Hydraulic Properties of Acute SMVs in Sheep

5.1. Summary

Sheep LD muscles, whose mechanical properties had already been determined (see Chapter 3), were used to form pumping chambers that were connected to a mock circulation. Two sizes of ventricle were constructed from the same muscle, one after the other, and their isovolumetric performance and pumping function measured. The measurements were compared in ventricles that were constructed from control muscles and from muscles that had undergone 2 Hz chronic electrical stimulation for 6-8 weeks. The hydraulic performance of the ventricles was also compared with numerical predictions made using the model derived in Chapter 4. The numerical model was able to predict reasonably well the isovolumetric function of the ventricles and the afterload for maximum power output. But the flow, and therefore the power available, was overestimated. The model therefore gave a qualitative and quantitative description of the hydraulic properties of the ventricles, with some discrepancies that could be attributed to the surgical formation of the ventricles. The results thus suggest that the surgical technique of SMV configuration is important in maintaining muscle power for cardiac assist. The function of the conditioned ventricles was poor because of the slow character of the muscles. Thus, the performance of SMVs can be improved through better surgical procedures and by the use of stimulation protocols that produce faster fatigue-resistant muscles.

5.2. Introduction

The mechanics of SMVs must be well understood before they can be used successfully in humans. The numerical model developed in the previous chapter, using muscle linear mechanical properties, predicted hydraulic relations of SMVs similar in shape to the corresponding muscle mechanical properties. However, the quantitative predictive

capacity of the model can only be assessed if the numerical predictions are compared to hydraulic relations measured in SMVs constructed from the same muscles. Such comparison would give an indication of whether the muscle functions less adequately in its new SMV configuration, and allow the associated power losses to be quantified. Moreover, it is not known by how much the surgical procedure reduces the maximum power output of the muscle wrap. Certainly, a knowledge of the amount of power lost following surgery alone would be necessary in deciding whether it needs to be given more attention. Furthermore, it would be useful to establish if one can entertain the hope of successful SMV circulatory assist following the combined power losses from chronic electrical stimulation and surgery.

In this chapter, surgically formed SMVs from sheep LD were compared in control and chronically stimulated muscles. The measured hydraulic properties were also compared with the linear mechanical properties of the muscles and with the predicted hydraulic relations. These comparisons should be useful in elucidating important parameters of SMV function that would allow the most power to be harnessed from the muscle for circulatory assist, and hopefully point to future investigations that may be necessary for a successful application of SMVs clinically.

5.3. Aims

The aim of the work presented in this chapter was to measure the hydraulic performance of acutely formed ventricles in sheep control and chronically stimulated muscles, and to compare them with the linear mechanical characteristics of the muscles used to form the ventricles. Numerical predictions made using the model presented in Chapter 4 would then be compared to the measured hydraulic relations of the SMVs. It would therefore be possible to establish important parameters of SMV configuration for optimal performance. Such knowledge would be useful to surgeons in the construction of functional SMVs.

5.4. Materials and methods

At the end of the mechanical measurements described in Chapter 3, the sheep LD muscle was taken down from its attachments to the servomotor, and the motor and frame removed. With the muscle held at its resting length so that the marker sutures were 5 cm apart (resting length), the muscle thickness at the anterior and posterior borders were measured and averaged to obtain a mean thickness. Such a measurement was complicated by the fact that some fat was retained over the LD to help keep it warm during the day-long experiment. However, a more reliable determination of the thickness was made during preparations of muscle sections for histochemical analysis (not presented here). A group of 8 sheep of weights between 61 and 71 kg were used; 4 of the LDs had been stimulated chronically at 2 Hz for 6-8 weeks (see Chapter 3).

5.4.1. Wrapping the muscle into an SMV

Velcro strips were placed at the level of the distal myotendinous junction, and 94 mm proximally, with the muscle still held at its resting length. The two velcro strips were then sutured together to make an approximately cylindrical ventricle of 15 mm radius. A polyester fabric conical ring, sewn to the anterior border of the muscle to forge the neck of the ventricle, formed the connecting piece between the ventricle and the hydraulic pumping apparatus (Figure 2.16). To the connecting piece was attached a latex condom, which was then inflated into the ventricle and pulled through its open apex. The condom was held in place within a purse string closure of the apex; this prevented the condom recoiling and avoided possible twisting that could impair the function of the ventricle. The mock circulation system (see Chapter 2) was then filled with water introduced via the servomotor pump. Once air was bled from the system, pressure and flow were measured at a range of fixed preloads and afterloads. The muscle was stimulated at 100 Hz for the active measurements: the duration of the stimulation burst was 300 ms for the control muscles or 500 ms for the stimulated (slower) muscles to allow both types of muscle to

reach their maximum force. Thirty seconds was allowed between contractions to prevent progressive muscle fatigue. When measurements from the 15 mm radius SMV were completed, another ventricle of 20 mm radius was constructed from the same muscle and the measurements repeated. Since the length of the ventricles was about 10 cm, the nominal volumes of the ventricles were 70 ml and 125 ml, respectively.

5.4.2. Pressure-volume relationship

5.4.2.1. Working the ventricle

Prior to any measurements on a ventricle, the following protocol was performed. The outflow to the reservoir was clamped and the ventricle slowly inflated by the action of the computer-controlled piston to approximately 100 mmHg and then deflated. This action was repeated several times to 'work' the ventricle. Such action would also rid the ventricle of any air that may be trapped in the condom.

5.4.2.2. Passive measurements

The ventricle was inflated by introducing fluid into it to a series of preloads from 5-80 mmHg. At each preload, the volume injected by the pump was noted. The preload was then plotted against the volume to yield a passive pressure-volume curve.

5.4.2.3. Active measurements

For the same values of preload above, the ventricle was stimulated while recording the pressure throughout the isovolumetric contractions. The ventricle was deflated after each contraction and refilled for the next preload. The peak pressure for each preload was obtained from the captured pressure trace; the peak developed pressure (PDP) was then the difference between the two. Peak pressure and PDP were plotted against volume to yield curves similar to the linear force-length characteristics of muscle.

5.4.3. Pumping function

The reservoir, with a marker to indicate the initial level of fluid, was pressurised to a known afterload and the ventricle inflated to a known preload. The outflow clamp was released and the ventricle stimulated to eject fluid into the reservoir. Flow and pressure were recorded throughout the contraction. The excess fluid pumped into the reservoir above the pre-calibrated marker level was drained by decrementing the position of the servomotor pump piston head - this excess fluid gave a direct measurement of the stroke volume (SV). Its recycling ensured that the starting volume was always known. The above procedure was repeated with pairs of preloads and afterloads from 5-80 and 40-140 mmHg, respectively. Usually, the preload was kept lower than the afterload so that the ventricle did not begin to pump fluid even before it was stimulated.

For each contraction, the flow trace, which looked rather noisy, was first smoothed and then digitally integrated to give a measure of SV. This value agreed well with that from the direct volumetric measurement. The work done in pumping fluid was evaluated as the product of the PDP and the SV. Power was calculated as the PDP during pumping times the peak flow. Several plots were produced to show the interrelations between these parameters.

5.4.4. Numerical predictions

Sheep LD mechanical relations (see for example Table 4.1) were used in the numerical model derived in Chapter 4 to predict the hydraulic relationships of the constructed SMVs. The predicted curves were then compared to the measured hydraulic properties of the ventricles. Although the constructed ventricles were more conical in shape, they looked cylindrical when stimulated to contract, and so could be reasonably modelled using a cylindrical configuration (Chapter 4).

5.5. Results

5.5.1. Pressure-volume relationships

5.5.1.1. Preload-volume

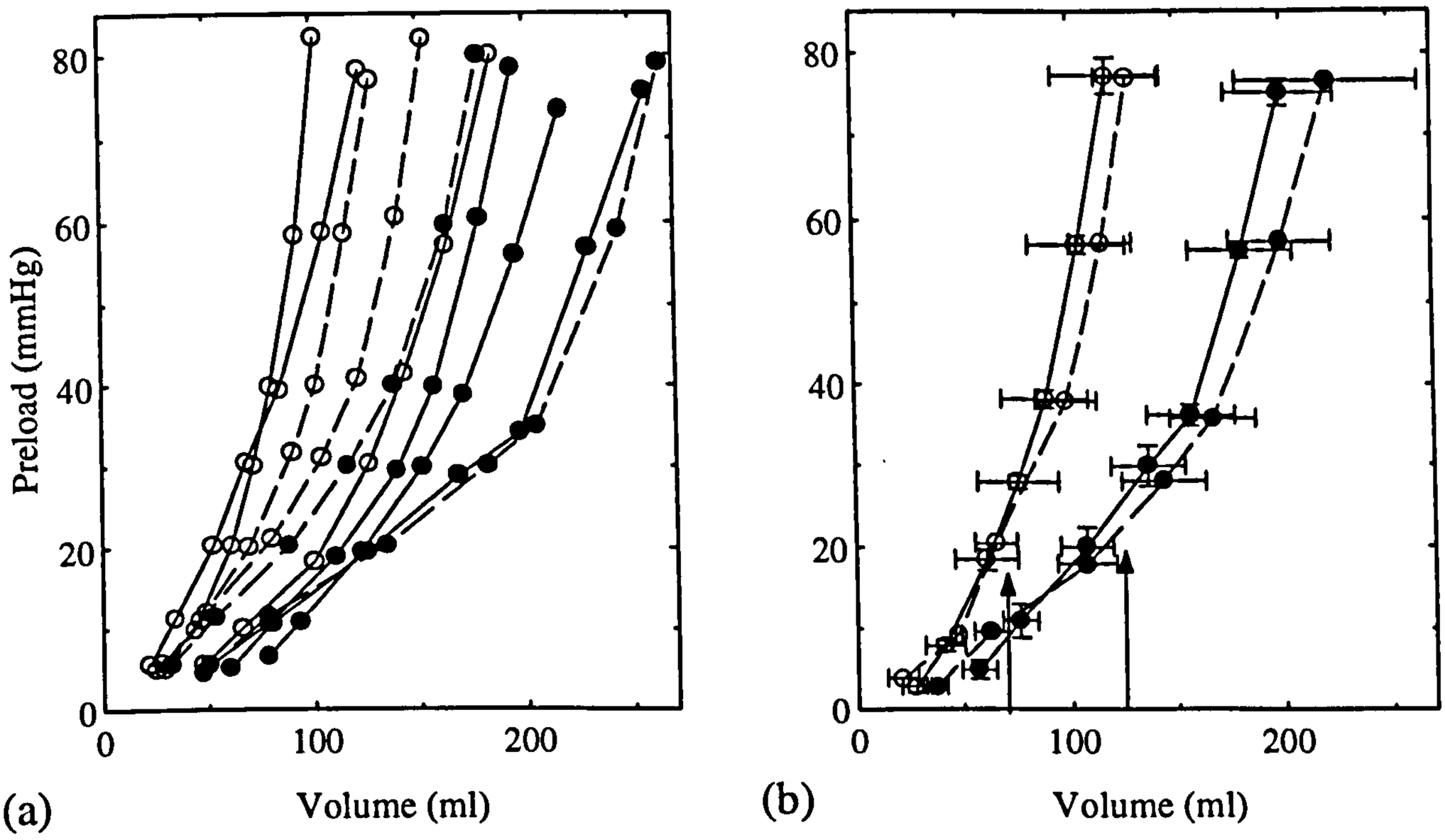

Figure 5.1. *Passive pressure-volume curves from various ventricles. (a) A continuum of curves from ten ventricles. (b) Mean ± SEM (error bars) for the small* (○) *and large* (●) *ventricles and for control (broken lines) and stimulated (continuous lines) ventricles (n = 3 in each group). Arrows in (b) indicate nominal volumes.*

The passive pressure-volume (P-V) curves from the various ventricles showed wide variation. Although the P-V curves formed a continuum (Figure 5.1a), with the ventricles of nominal radius 15 mm overlapping those of nominal radius 20 mm and with no clear distinction between ventricles from control and from chronically stimulated muscles, the mean data presented in Figure 5.1b show that, on average, two distinguishable sets of SMVs were successfully made from the LDs. However, there was very little difference in the mean curves for control and stimulated muscles. Thus, chronic stimulation had little effect on the passive muscle properties. From the mean curves, it is clear that the P-V curves of the small ventricles were steeper than those of the large ventricles. The large ventricles were therefore more compliant.

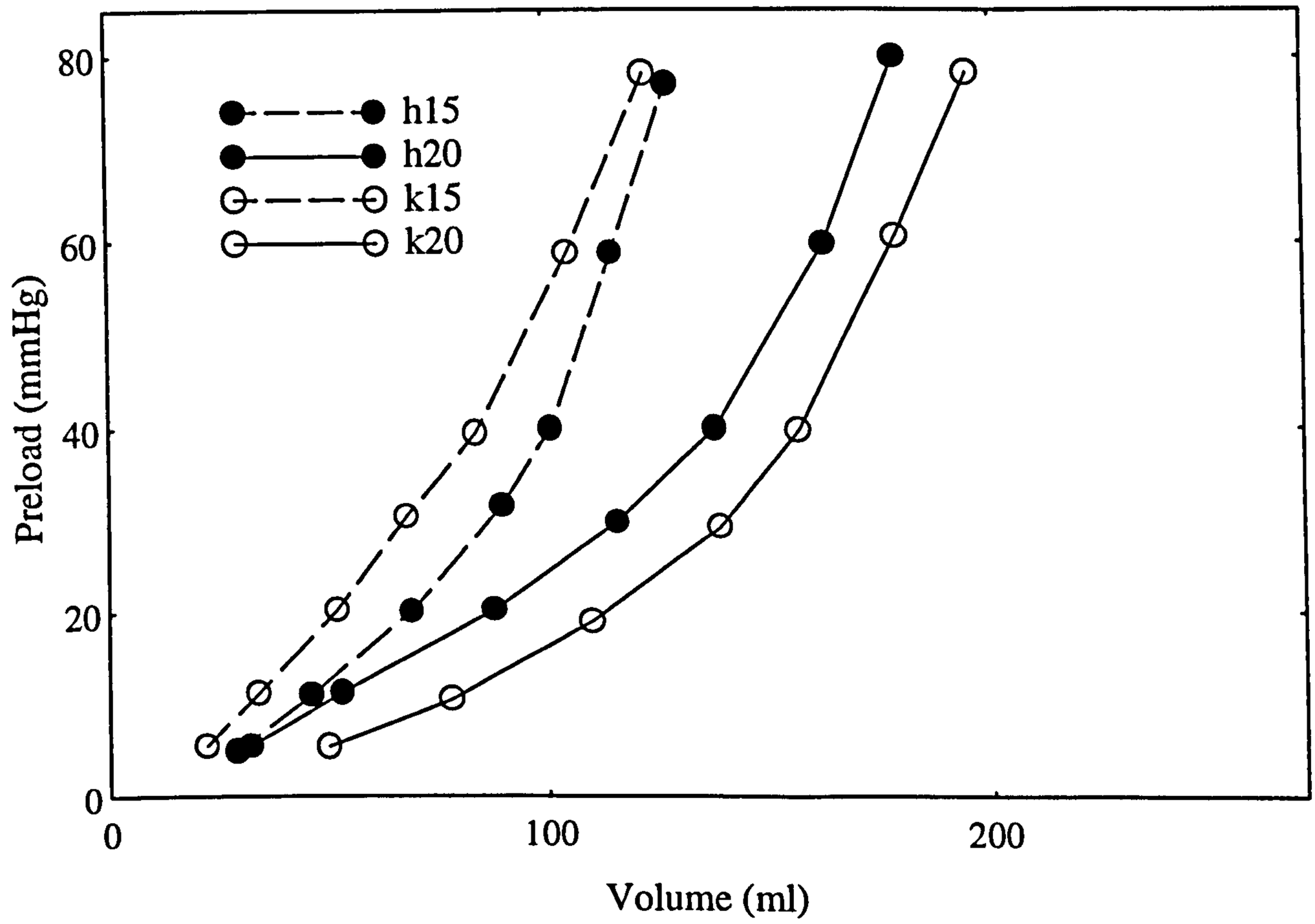

Figure 5.2. *Pairs of ventricles with similar passive pressure-volume curves: h is control and k is stimulated muscle.*

The arrows in Figure 5.1b indicate that the pressure inside the ventricles at the nominal volumes of 70 ml and 125 ml was similar, near to 20 mmHg. Because of the wide variation in ventricular construction, it was difficult to compare the pumping function of the ventricles. Therefore, data are presented from two groups of four ventricles (15 mm radius and 20 mm radius from one control and one conditioned muscle) whose passive pressure-volume curves were very similar (Figure 5.2). Since no difference was seen between the passive force-length properties of the control and chronically stimulated muscles, it is assumed that these pairs of ventricles were similar in terms of construction as possible so that the difference in performance could be attributed to the parameters under investigation, namely, size (15 mm or 20 mm radius) and contractile state (control or conditioned).

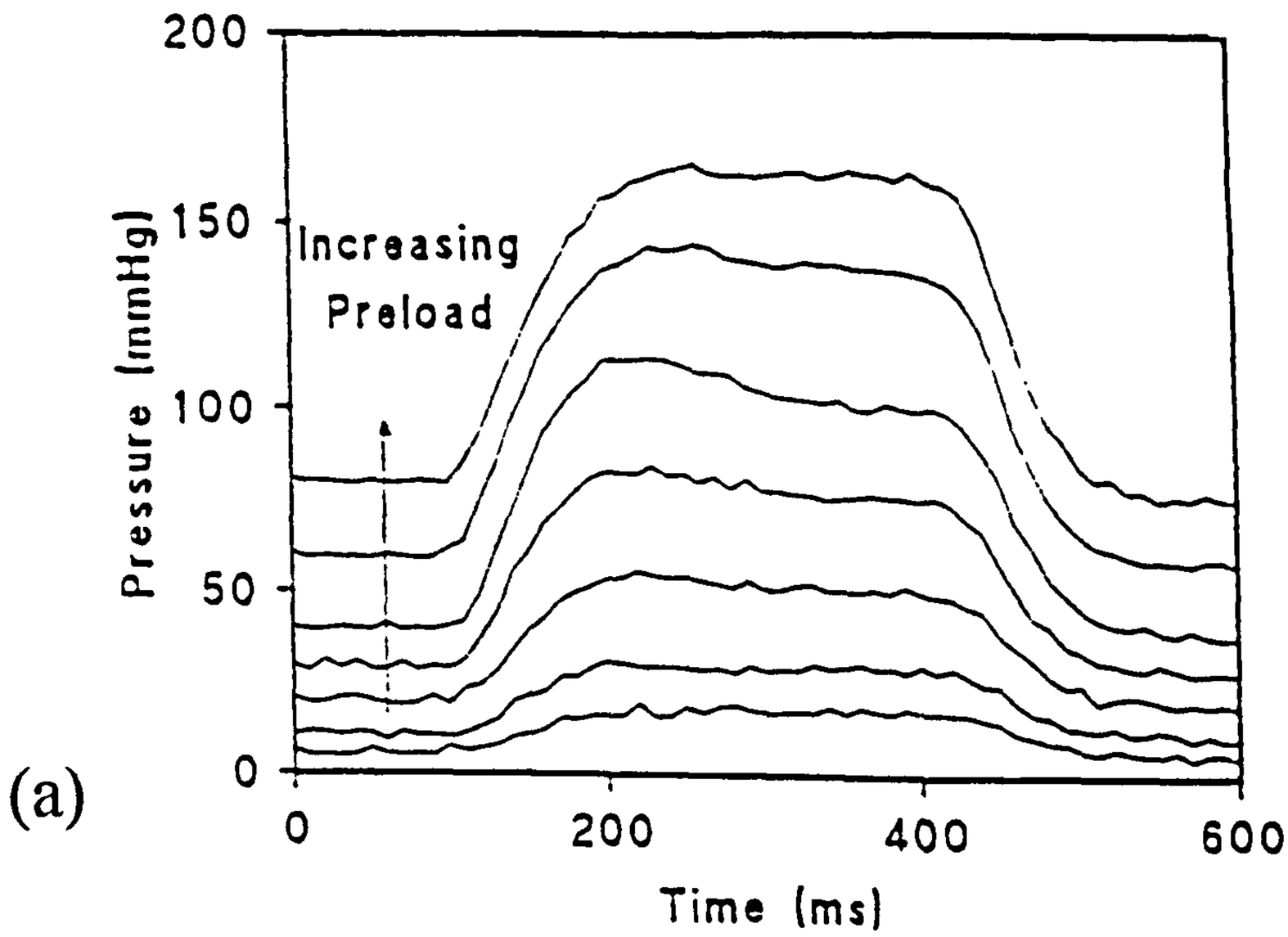

(a)

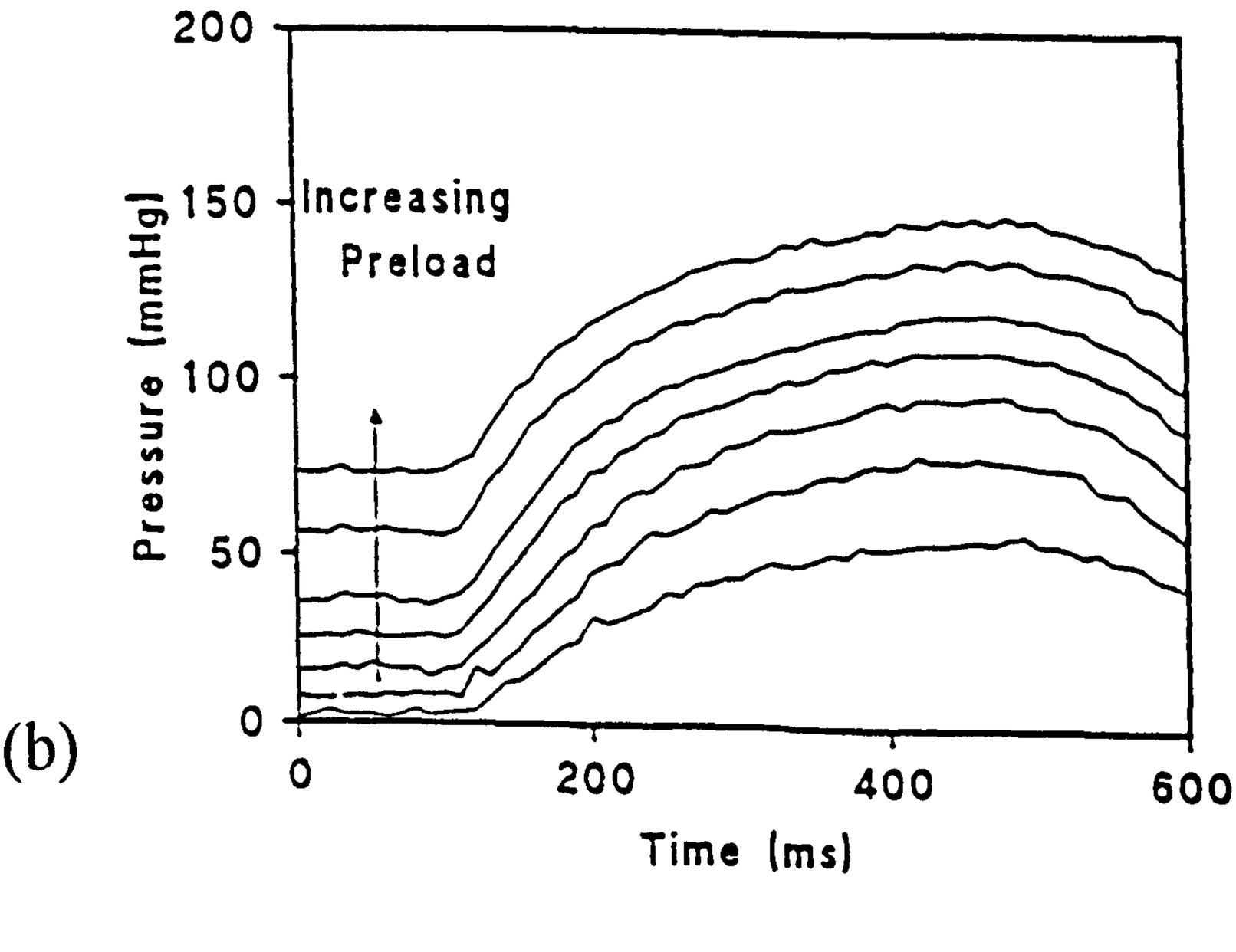

(b)

Figure 5.3. Isovolumetric pressure traces for a 20 mm radius ventricle. (a) Control ventricle. (b) Conditioned ventricle. The traces in (a) are more responsive to preload than those in (b).

The isovolumetric pressure traces in Figure 5.3 show that pressure generation is more sensitive to preload in an SMV constructed from control muscle (Figure 5.3a) than in one formed from conditioned muscle (Figure 5.3b). Preload, peak pressure and PDP, determined from such traces are plotted against volume in Figure 5.4: control ventricles (Figure 5.4a and b) are compared with stimulated ventricles (Figure 5.4c and d).

5.5.1.2. Isovolumetric performance

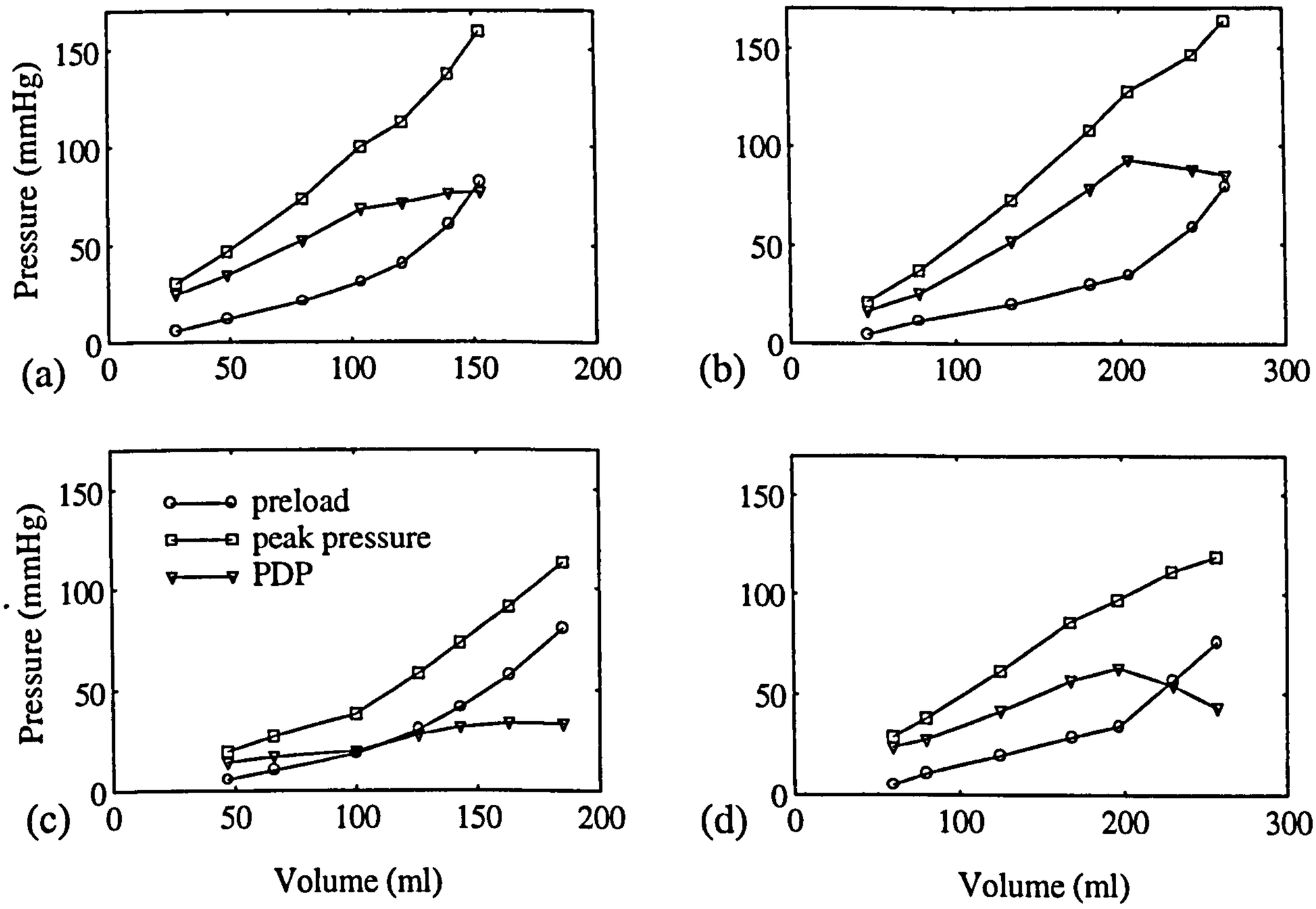

Figure 5.4. *Pressure-volume characteristics in sheep ventricles. See panel (c) for legend. (a) Control small ventricle. (b) Control large ventricle. (c) Conditioned small ventricle. (d) Conditioned large ventricle.*

The curves in Figure 5.4 are very similar to the linear force-length curves typical of skeletal muscles (see Figure 3.1a), and to the force-length curves of the sheep SMVs (not shown). PDP is produced at a volume greater than the nominal volume; the nominal volume is equivalent to the optimal length in the linear muscle. The isovolumetric relations of the SMVs are thus similar to the linear isometric relations of the LD; however, the optimal volume does not seem to correspond to the optimum length.

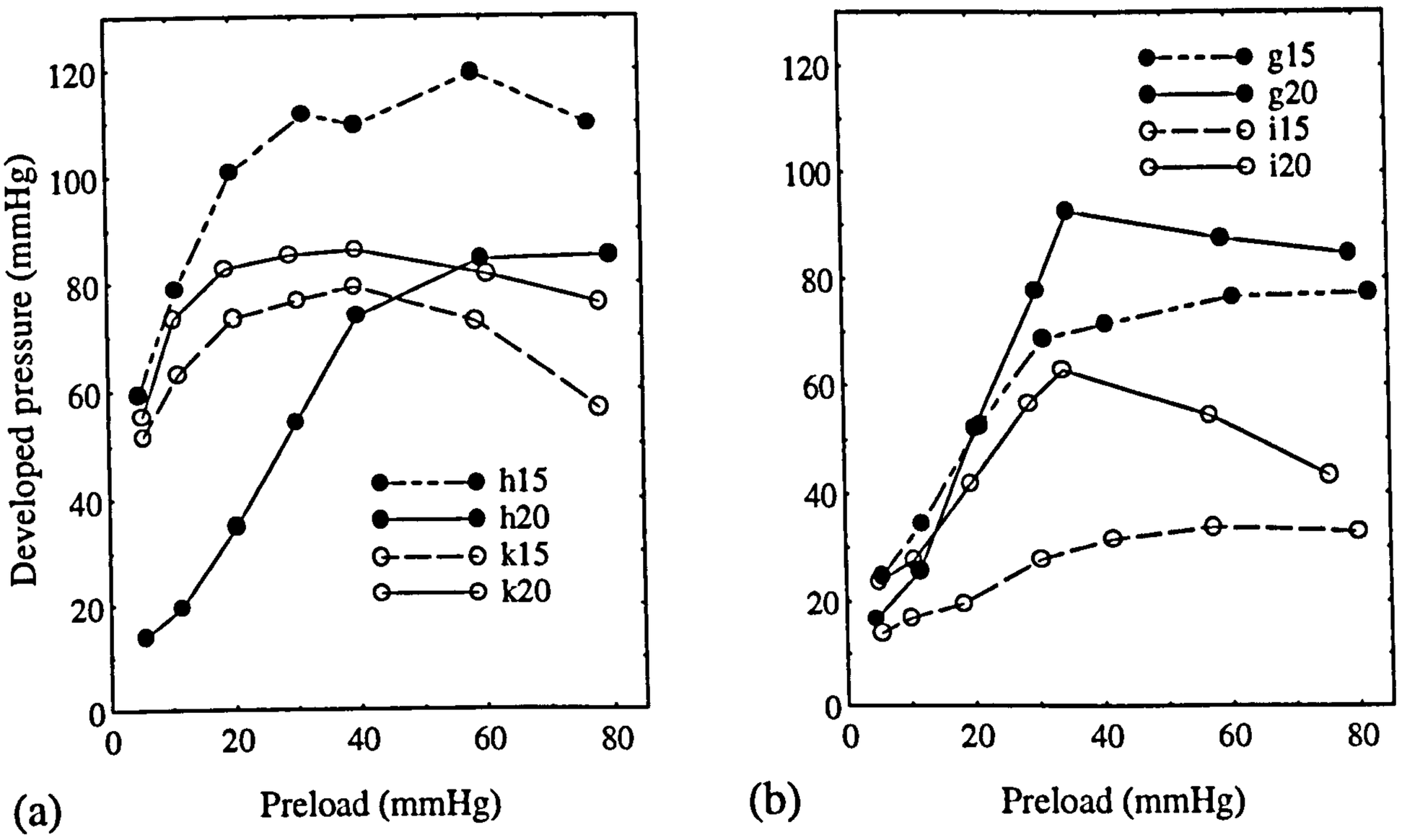

Figure 5.5. *PDP versus preload for pairs of ventricles with similar preload-volume characteristics : control (g and h) and conditioned (i and k) ventricles. Refer to legend convention in text.*

In Figure 5.5, the isovolumetric pressure developed from the pairs of ventricles with similar preload-volume curves (see Figure 5.2) are presented. Although this figure suggests that control ventricles (closed symbols) developed greater pressures at high preloads than the conditioned ventricles (open symbols), the picture is blurred by the anomalous output of the 20 mm radius control ventricle (h20, Figure 5.5a), which performed badly when stimulated to generate pressure. This abnormal function could be attributed to possible slipping of the condom through the sutures during activation of the ventricle.

To gain a clearer picture of the variation of developed isovolumetric pressure with preload, therefore, data from ventricles made from six muscles (3 control, 3 conditioned) are presented in Figure 5.6. Comparisons are made between the 15 mm and 20 mm radius ventricles, and between the control and stimulated muscles.

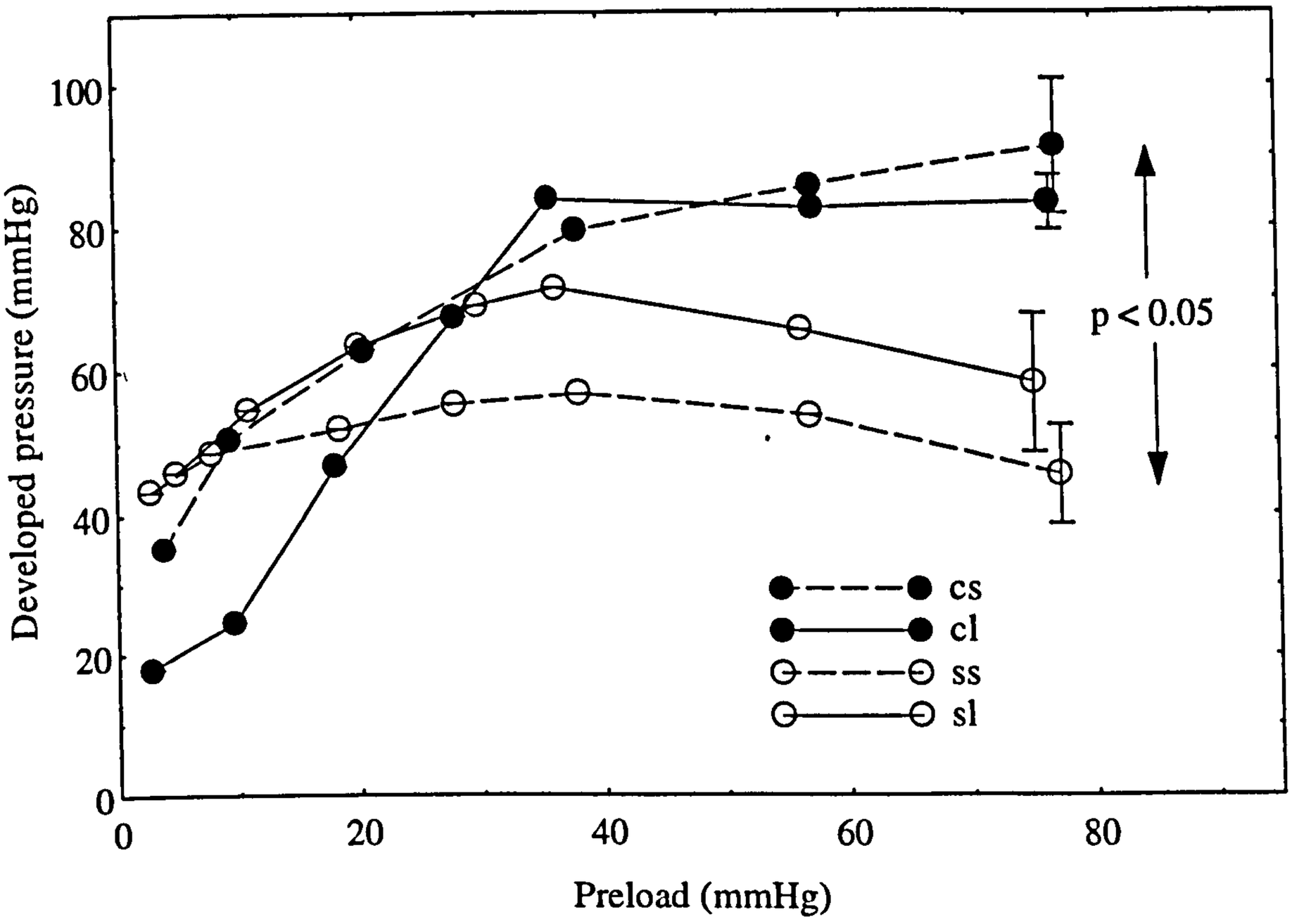

Figure 5.6. *Pooled PDP versus preload for control small (**cs**), control large (**cl**), stimulated small (**ss**) and stimulated large (**sl**) ventricles. For each group n = 3. The mean values are plotted and the error bars shown for the largest preloads are representative.*

No significant difference was observed at any preload between the pressure developed by the two sizes of ventricle made from the same group of muscles. However, the pressure developed by the control group of small ventricles (cs, Figure 5.6) was significantly greater than that developed by the stimulated group (ss) at 80 mmHg ($p < 0.05$), and approached significance ($p = 0.054$) for the two groups of large ventricles. The ability of the control ventricles to develop pressure was more dependent on preload than that of the conditioned ventricles: for the entire range of preloads, the control ventricles produced less PDP at low preloads, with the pressure rising more steeply with preload up to 40 mmHg, and thereafter more slowly; the PDP of the conditioned ventricles, on the other hand, remained relatively constant, with a broad peak around 40 mmHg. The contractile state of the ventricles (control or conditioned) and their preload therefore affected their ability to develop pressure.

5.5.2. Pumping function

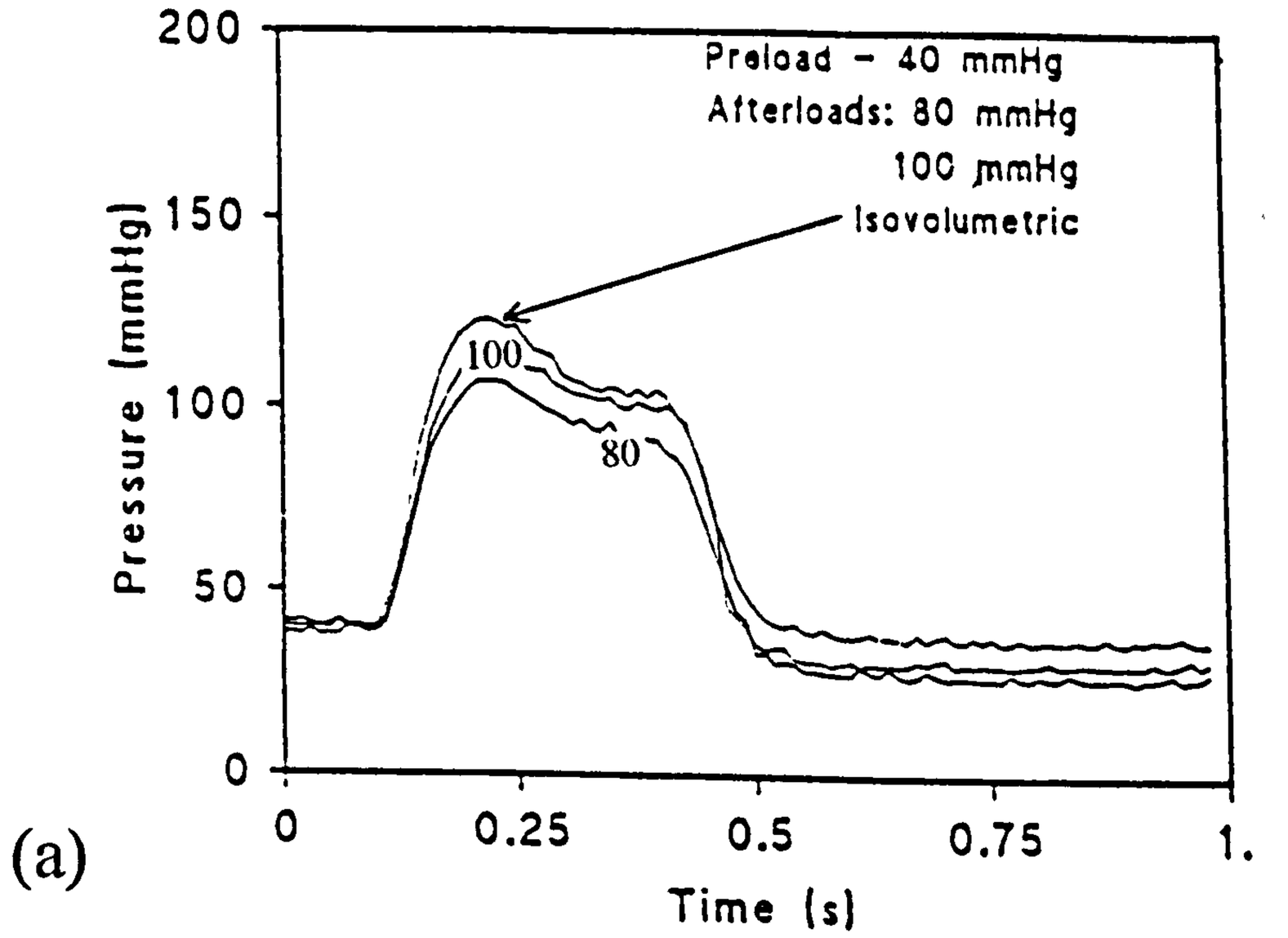

(a)

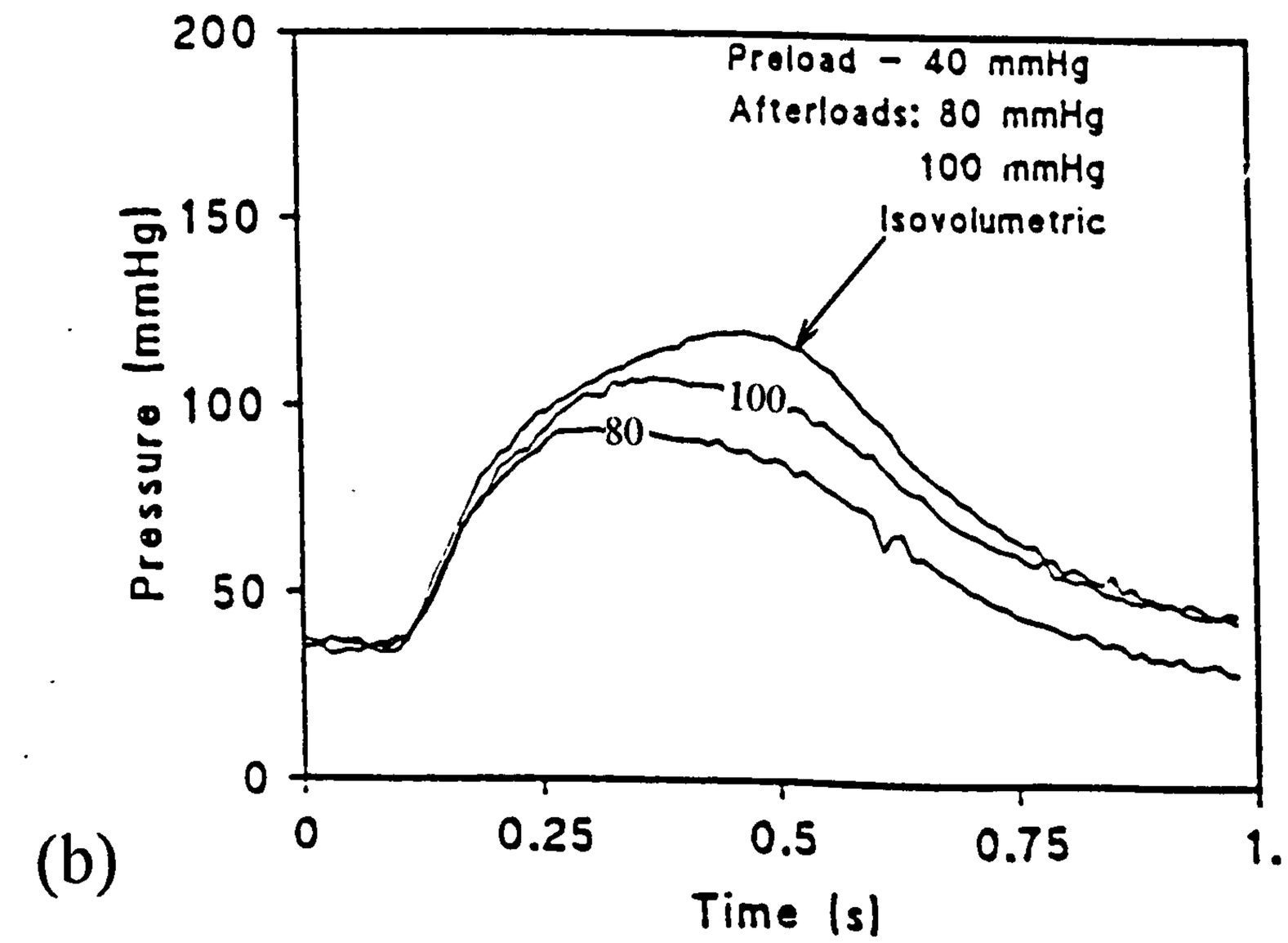

(b)

Figure 5.7. Isovolumetric and pumping pressure traces with a preload of 40 mmHg in 20 mm radius ventricles. (a) Control ventricle. (b) Conditioned ventricle. The isovolumetric trace reached the highest pressure in both control and stimulated ventricles. The control ventricle was activated for 300 ms and the conditioned ventricle for 500 ms to allow both ventricles to develop their peak pressure.

Pressure traces obtained when the ventricles pumped fluid are shown in Figure 5.7 for control and conditioned ventricles. The isovolumetric trace, which generates the highest

pressure, is added for comparison. The afterload chamber was able to maintain the pressure at the set value during pumping, although the pressure in the control ventricles initially rose above the set value (Figure 5.7a). In contrast, the stimulated ventricles quickly attained the set afterload pressure (Figure 5.7b). The conditioned ventricles were stimulated for longer because their isovolumetric traces did not attain their peak quickly.

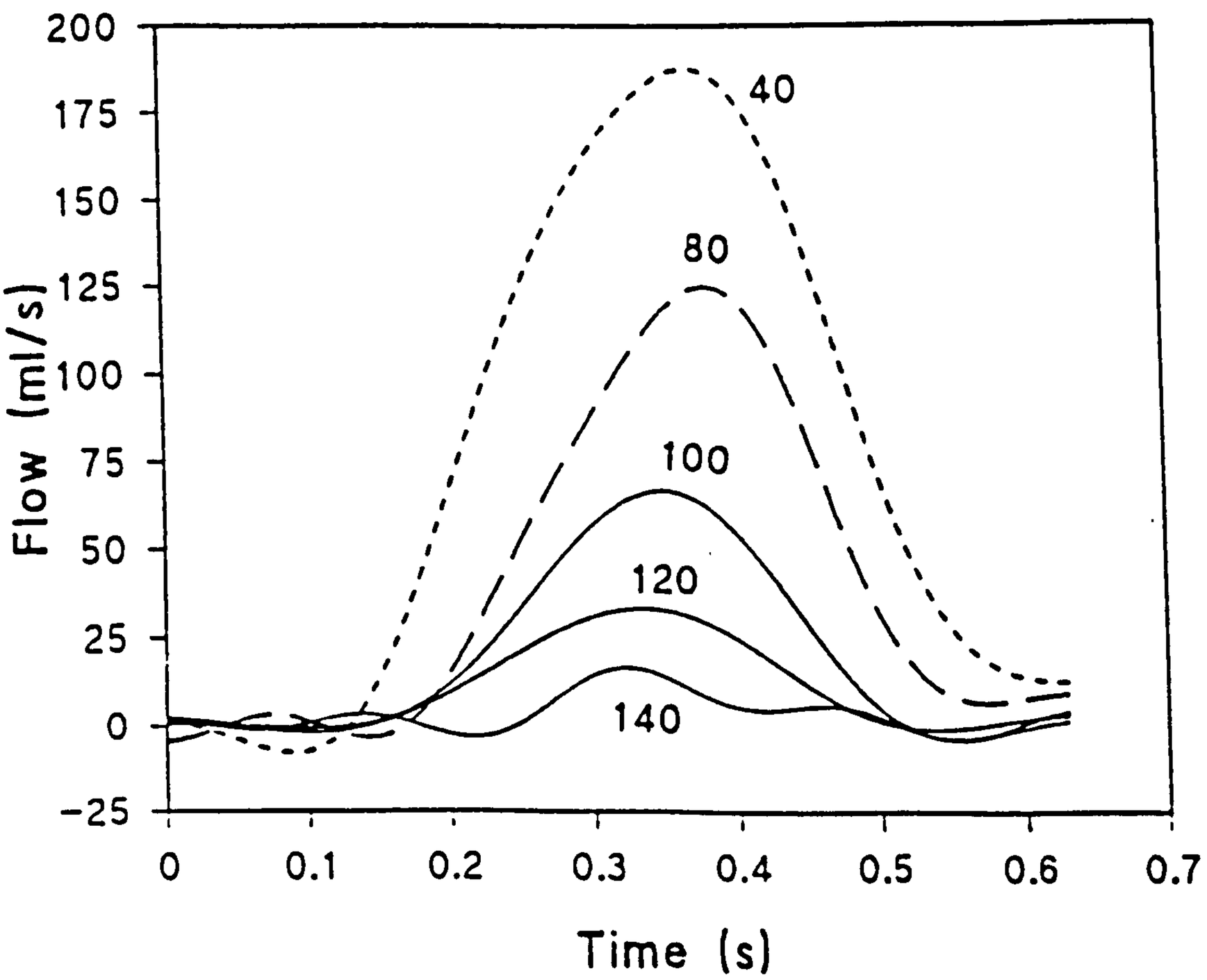

Figure 5.8. *Smoothed flow traces obtained from a 15 mm radius control ventricle at a preload of 30 mmHg, with different afterloads.*

The pressure (Figure 5.7) and flow (Figure 5.8) records for each ejection were analysed to determine the SV, peak power and work done in each individual contraction at each preload and against each afterload. Results are presented in Figure 5.9 for the two pairs of ventricles, as in Figure 5.5. Also, data from ventricles made in dogs (Oda *et al.* 1993) are replotted on the same axes for comparison.

By and large, the dynamic measurements showed a greater discrepancy between the control and conditioned ventricles than the isovolumetric measurements. This was to be expected since conditioning affects not only the strength, which determines the isovolumetric pressure production, but also the contractile state of the muscle tissue. The ability to produce hydraulic power is proportional to the product of these parameters.

5.5.2.1. Stroke volume

Figure 5.9 shows the SV output for the two sets of ventricles with similar preload-volume curves. The SV produced by the ventricles was highly dependent on preload when the afterload was small (Figure 5.9a and d). Also, there was a striking reduction in the performance of the SMVs made from the stimulated muscles (open circles) compared to those made from control muscles (filled circles). In general, the stroke volume of the larger ventricles (solid lines) was greater than that of the smaller ventricles (dotted lines); but an exception is shown in panels d, e, and f in which the large control ventricle performs poorly compared to the other ventricles at low preloads, but relatively well at high preloads. This is the same ventricle in Figure 5.5a that was anomalous in pressure generation.

Figure 5.9 also demonstrates the good correspondence between the SV outputs from the 20 mm nominal radius ventricles made with sheep LD (upper curves, panels a, b, and c) with results from SMVs made with dog latissimus LD (panels g, h and i, Oda *et al.* 1993), the ventricles referred to as large, single-layered (LSLV) in that paper. The LSLV

ventricles was made from the whole LD of mongrel dogs so nominal radius is not given, but the passive pressure-volume relationship (Figure 2, Oda *et al.* 1993) is similar to that shown in Figure 5.1b above.

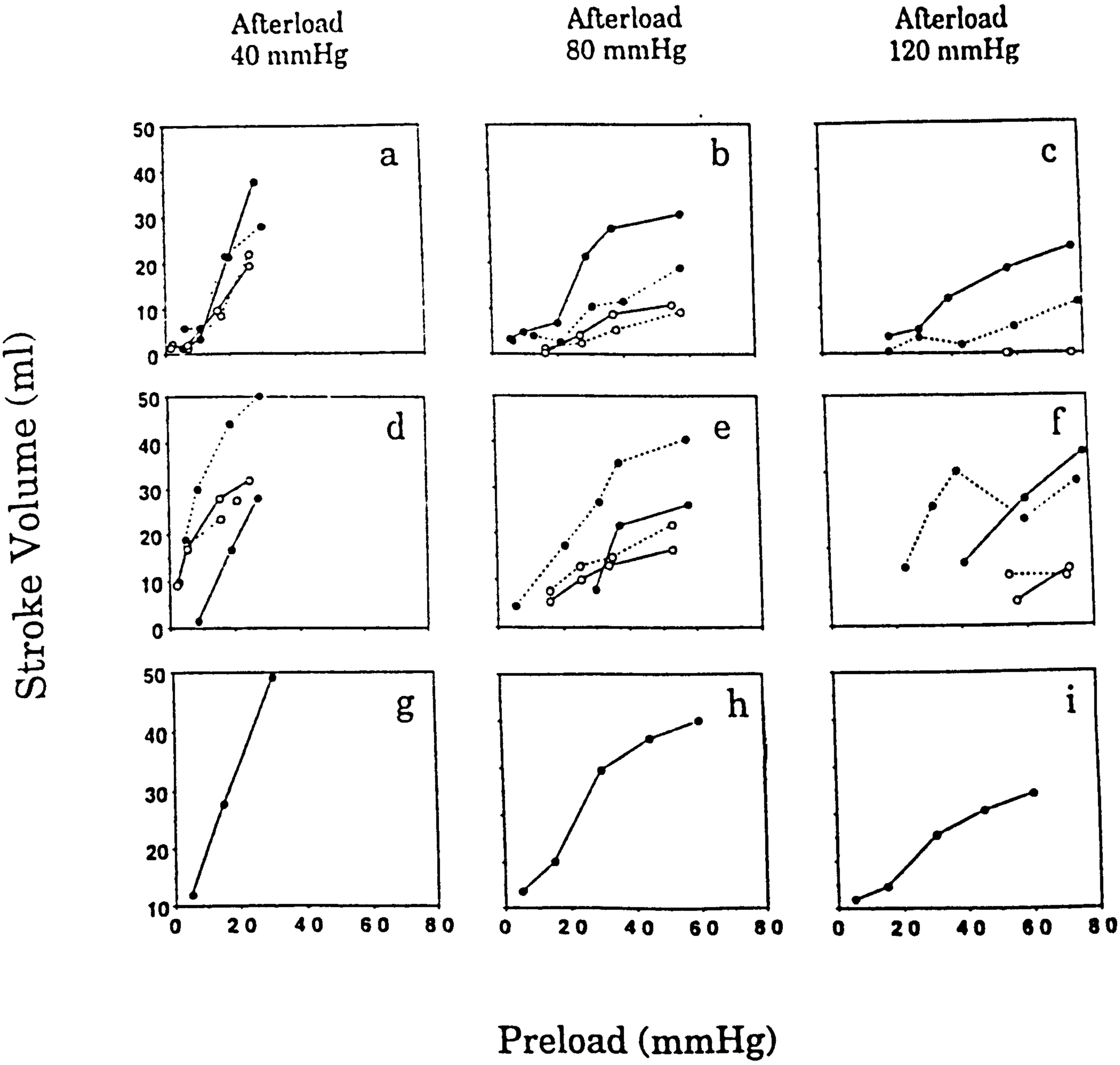

Figure 5.9. Graph of stroke volume output versus preload for different ventricles. In panels a - f, outputs are compared in ventricles of nominal radius 15 mm (dotted lines) and 20 mm (solid lines), constructed from control (●) *and conditioned* (○) *muscles. Panels g - i are data from the large, single-layered ventricle (LSLV,* Oda *et al.* 1993*) for comparison.*

This is perhaps the first time that comprehensive performance data on SMVs made in different laboratories has been compared. The SV of the ventricles made from conditioned muscle was lower than that of the control ventricles, and the conditioned ventricles did not eject at all against an afterload of 120 mmHg. The maximum ejection fractions were in the region of 40% for both sizes of ventricle.

5.5.2.2. Peak power

The calculation of power emphasizes the difficulties in making measurements of hydraulic performance. The equivalent measurement of the linear power of muscle (force × velocity) used a servo-controlled constant force that has no inertial component. Although the afterload was held constant in the hydraulic situation, there was a significant inertial component to the ventricular load, caused by the movement of the fluid in the T-piece. As a result, the pressure and flow traces were out of phase; the peak power of the ventricle could not therefore be determined by the peak value of "ventricular pressure × flow". Peak power was therefore calculated as "peak pressure during ejection × peak flow during ejection".

The peak power of the large, control ventricles was highly sensitive to preload but not to afterload (Figure 5.10, panels a, b and c). The peak power obtained from a control ventricle was just over 1 W at 40 mmHg preload and 80 mmHg afterload. Assuming that this ventricle was of height 10 cm and that the LD thickness was about 6 mm, the mass of muscle constituting the ventricular wall would be about 74 g (muscle density of 1 g cm^{-3}). Thus, the peak power output would be about 13.3 W kg^{-1} for the large control ventricle. From Figure 3.4 (Chapter 3), the mean peak linear power calculated for control sheep LD muscles was 90 W kg^{-1}, so that the control SMV only produced about one-sixth of the linear power of the LD. The maximum power output of the conditioned ventricle was 0.3 W, which would be equivalent to about 5.3 W kg^{-1} (calculated as above), about one-third of the mean peak linear stimulated LD power of 15 W kg^{-1} (Figure 3.4). Thus, when the

muscle is wrapped to function in a cylindrical configuration there is about a three- to six-fold drop of the linear LD muscle power, which is obtained with a non-inertial load and in the normal anatomical (linear) configuration.

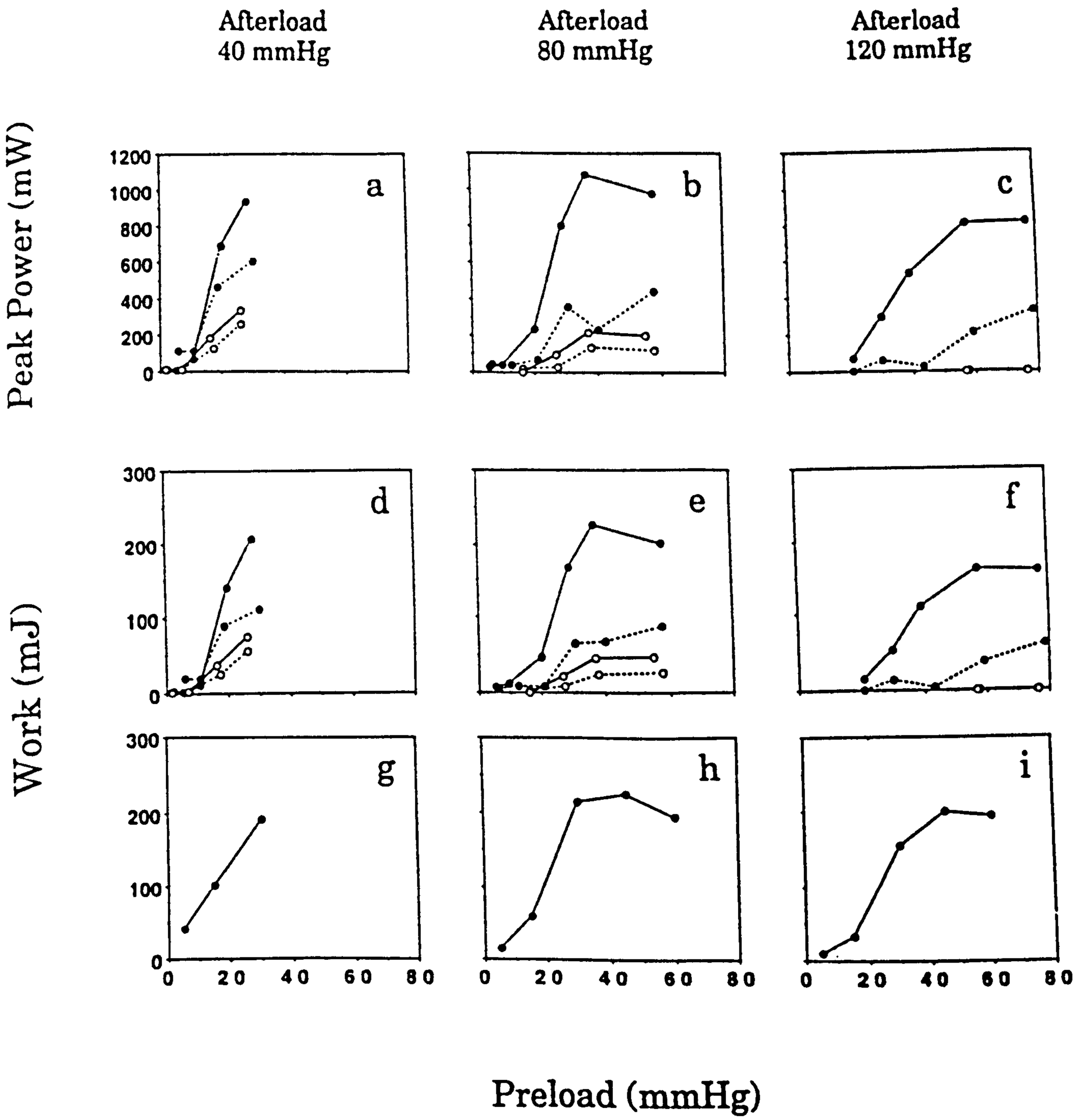

Figure 5.10. Plots of peak power (panels a to c) and maximum stroke work (panels d to f) versus preload for different afterloads. In panels a - f, outputs are compared in ventricles of nominal radius 15 mm (dotted lines) and 20 mm (solid lines), constructed from control (●) *and conditioned* (○) *muscles. Panels g to i are work data from the large, single-layered ventricle (LSLV,* Oda *et al.* 1993*) for comparison.*

5.5.2.3. Work

The maximum work done in a single contraction (Figure 5.10, panels d, e and f) varied similarly to the peak power (Figure 5.10, panels a, b and c). The stroke work of the large, control ventricles was very highly sensitive to preload but not to afterload. Interestingly, the peak stroke work of about 200 mJ was similar to that measured by Oda *et al.* (1993) in canine LSLV ventricles (Figure 5.10, panels g, h and i). It should, however, be noted that this work level in the control ventricles may not be sustainable in the repeated contractions that are necessary for heart assist. The large ventricles produced substantially more work than the small ventricles, and the stimulated ventricles produced under 50% of the stroke work of the control ventricles. These very low work levels of ventricles made from stimulated muscles would provide inadequate cardiac assist.

5.5.3. Comparisons with numerical predictions

5.5.3.1. Preload-volume

Predicted passive preload-volume curves using the force-length curve of sheep LDs is compared with the measured curves (Figure 5.11). Predictions from a stimulated muscle whose linear force-length curve fitted particularly well the exponential equation (see Chapter 3) corresponded strongly with the actual data (Figure 5.11a). Because chronic stimulation had little effect on the passive mechanical properties (see above), mean predicted preload-volume curves from both control and stimulated muscles were compared with the mean of the measured relations (Figure 5.11b). Although the predicted curves were steeper than the measured curves, suggesting that the constructed ventricles were more compliant than would be expected, the curves were not significantly different ($p > 0.05$ at 80 mmHg preload). The apparent greater distensibility of the constructed SMVs could be attributed to the greater range of movement (ROM) of the muscles in the cylindrical configuration: in the linear measurement of the mechanical

properties, the muscles were stretched by less than 20% (from about 200 - 240 mm) compared to the more than 35% (125 - 230 ml) range in the SMV configuration.

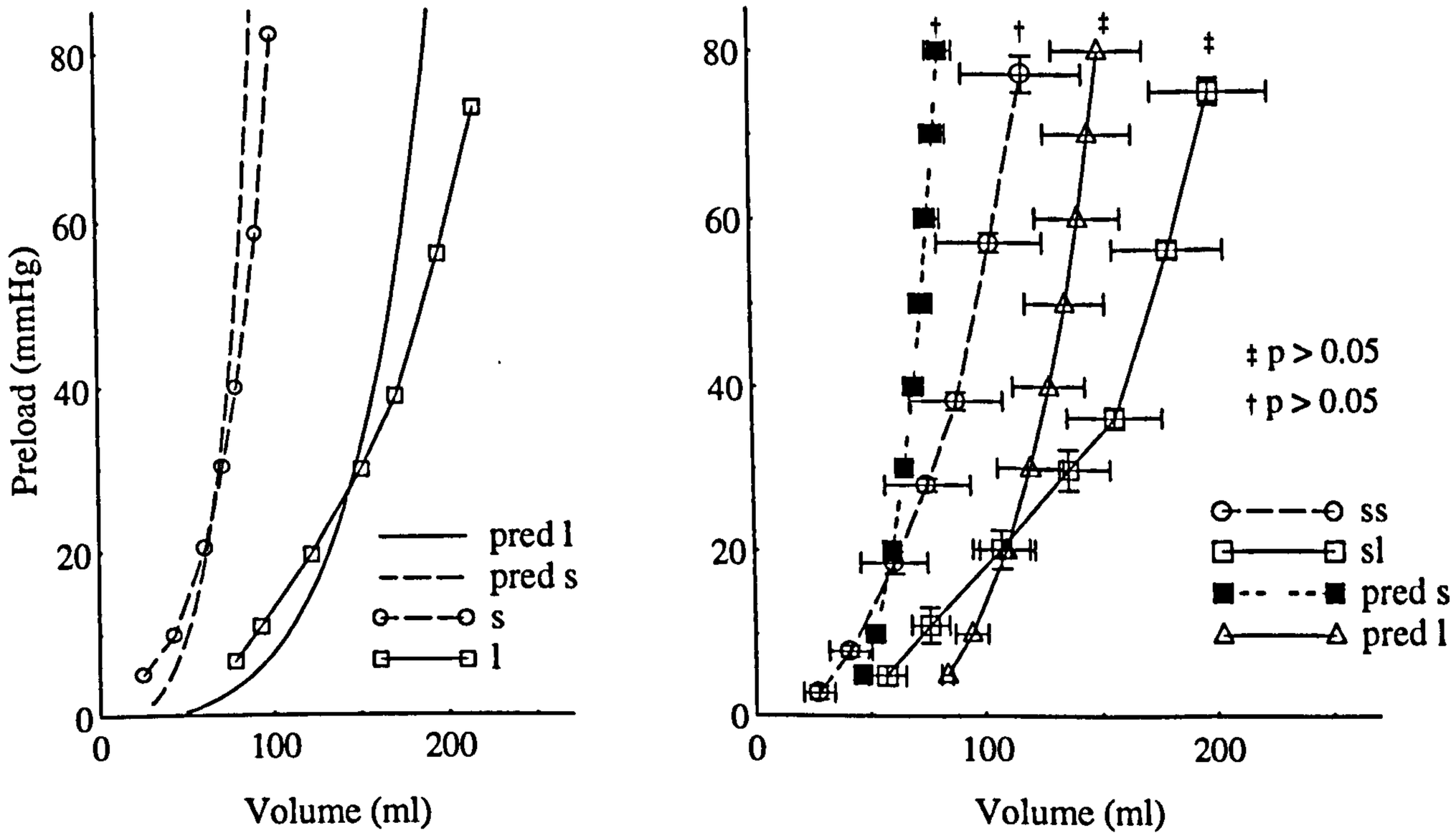

Figure 5.11. *Comparison of predicted and measured passive pressure-volume relations. (a) A single stimulated muscle. (b) Mean curves, n = 3; values are plotted as mean ± SEM. Legends follow convention in text. (s = small; l = large; pred = predicted; ss = stimulated small; sl = stimulated large).*

The predicted curves cross the actual curves at a preload pressure of 20 mmHg (Figure 5.11b), which corresponds to the pressure of the nominal volumes (see above). More accurate predictions could therefore be made if the nominal volume was appropriately related to the optimal volume, which was always higher than the nominal volume (see Figure 5.4). The discrepancy between predicted and measured preload-volume curves could also have been due to the inaccurate fit of the exponential to the force-length curve that was measured over a much smaller ROM compared to the measured hydraulic relations, which covered a much longer range. Nonetheless, the predictions fitted fairly well the measured data. The Lamé's equations, as used here, may therefore be useful in quantifying the load on a muscle formed into an SMV.

5.5.3.2. Pressure-flow predictions

Using the force-velocity characteristics of sheep LD muscles, pressure-flow curves were predicted for control and chronically stimulated muscles (Figure 5.12a, diamond symbols). The measured flow curves are also plotted for comparison. The product of pressure and flow, the power output, is plotted in Figure 5.12b.

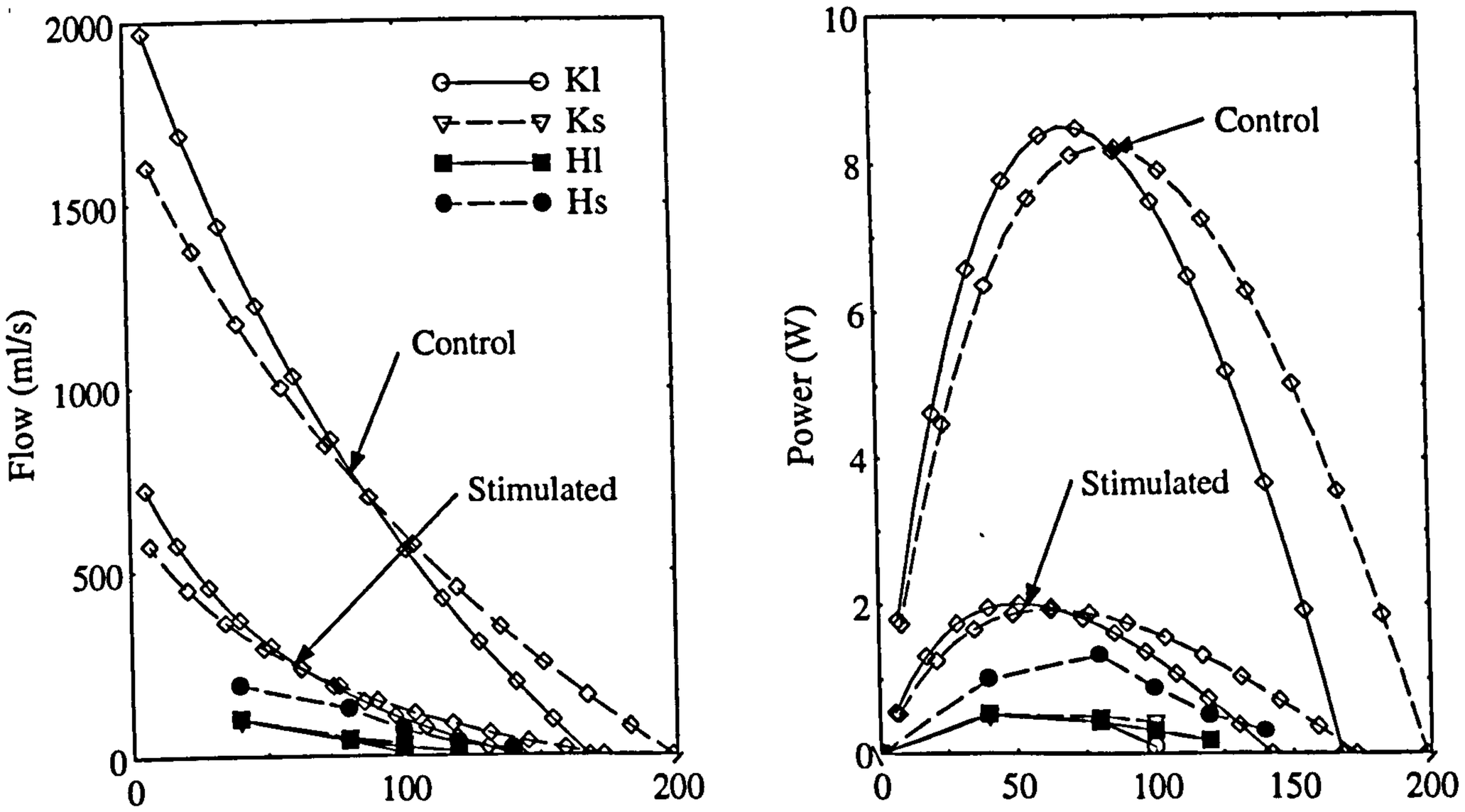

Figure 5.12. *Predicted and measured flow and power against pressure in the small and large ventricles. (a) Flow-pressure curves. (b) Power-pressure curves. The diamond symbols are the predicted curves. All other legends follow the convention in the text.*

The pressure is inversely proportional to the flow, and the shape of the pressure-flow curves is similar to that of the force-velocity curves (compare Figures 3.2a and 5.12a). Thus, skeletal muscles maintain the shape of their linear mechanical relations when formed into a ventricle. The predicted power in the control ventricles is about 8 W while that in the stimulated ventricles is about 2 W; these peak power levels are similar to those measured in the linear configuration (Figure 3.2b). But the measured peak power is about 1 W in the control ventricles and only 0.5 W in the stimulated ventricles. Thus, the predictions overestimate the actual hydraulic power of the ventricles. This is not at all

surprising, as the model clearly makes no allowance for power losses related to reforming the muscle into a cylindrical pumping chamber. Moreover, the linear power, which is measured with a non-inertial load, may overestimate the power of the linear muscle.

However, the predicted curves show some striking correspondences with the experimental data. First, the predicted isovolumetric pressure (zero flow) was quite close (compare Figures 5.4 and 5.12). Second, the model predicted little difference in the performance of the two sizes of ventricle made. Third, the model predicted the afterload range at which the power output of the ventricles was highest to be between 50 and 100 mmHg (Figure 5.12b).

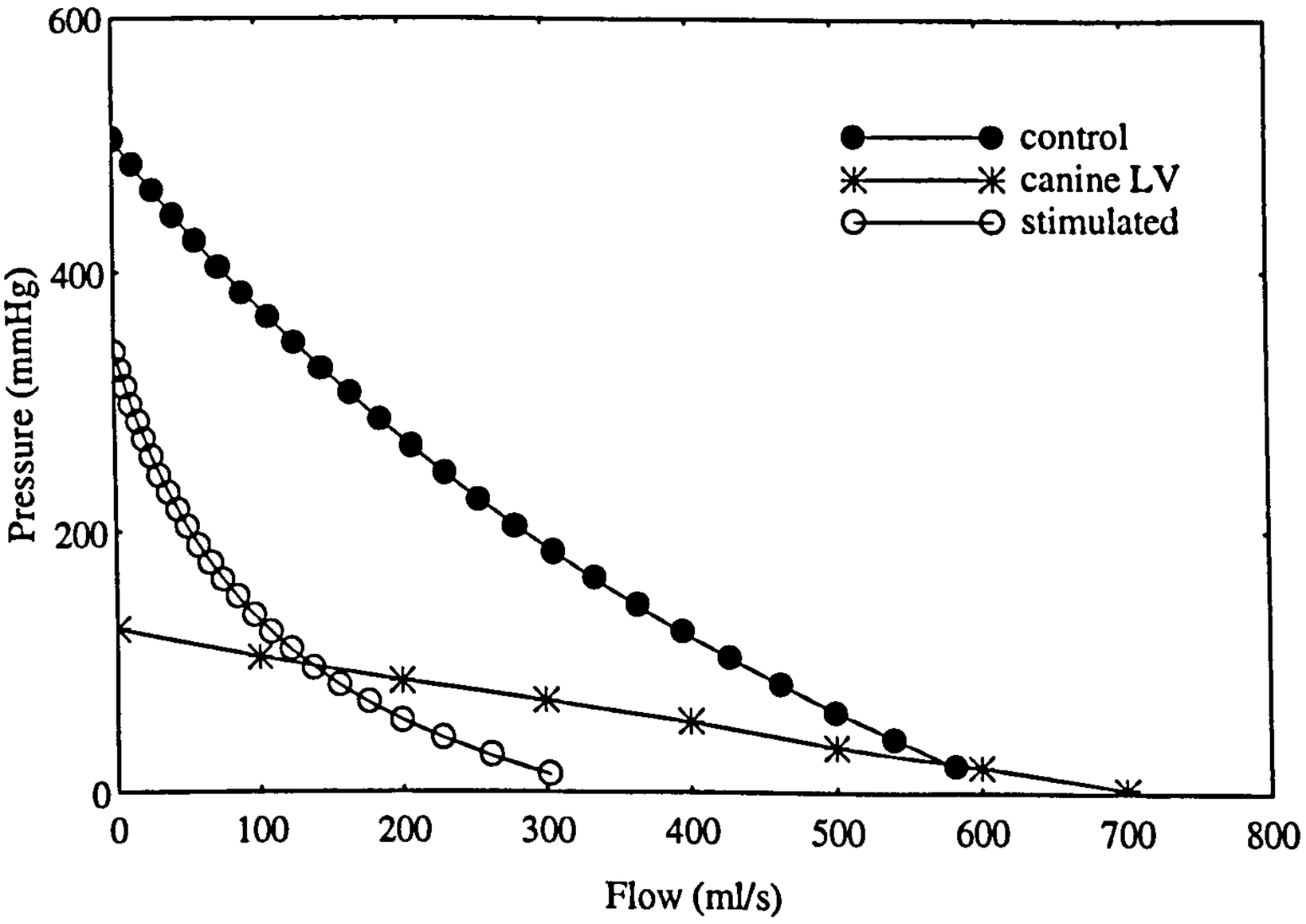

Figure 5.13. *Comparison of pressure-flow from canine left ventricle (LV,* Shroff *et el.* 1985*) with predictions from SMVs of the same size as the canine LV.*

The model was also used to predict the pressure-flow relationship for ventricles made of control and stimulated muscles at the size of a dog left ventricle (LV), for which the actual pressure-flow relationship is available (Shroff *et al.* 1985). The absolute slope of the pressure-flow curve can be interpreted in terms of internal resistance to flow, indicating the pressure drop due to a certain flow rate. Clearly, the resistance derived

from the predicted curves, in which no account was taken of any losses in wrapping the muscle into the SMV shape, is higher than that of the LV (Figure 5.13). Thus, the natural LV possesses the important characteristic of producing less resistance to flow than SMVs. This could account for the poor ejection of SMVs and their inability to provide heart assist, unless their function is improved. Since the shape of the force-velocity curve of papillary muscle is not greatly different from that of skeletal muscle, it may be that the complex fibre geometry of the natural ventricle contributes to its remarkable ability to minimize resistance to flow.

The greatest difference between the predicted and the actual performance of the SMVs was in their flow-generating capacity. Since the pressure-generating properties were modelled reasonably well, it is concluded that the greatest loss of power has to do with the effect of the wrapping procedure itself on the ability of the ventricle to move, rather than some aspect of geometry that was not adequately modelled. The reduced performance may be due to internal stresses within the curved muscle fibres and to a reduced blood perfusion in the SMV.

5.6. Discussion

The aim of the work presented in this chapter was to measure the hydraulic performance of acute SMVs constructed from control sheep LD and from muscle that had been stimulated chronically at 2 Hz for 6-8 weeks. Isovolumetric performance and pumping function were measured in two sizes of ventricle and compared to predictions made from the mechanical properties of the same muscles. The results obtained give an insight into the function of SMVs and point to areas that need particular attention.

The shape of the linear mechanical relations of the muscle was maintained in the ventricular configuration. Although chronic stimulation had little effect on the passive mechanical properties of the muscles, the large (20 mm nominal radius) ventricles were

more compliant than the small (15 mm nominal radius) ventricles. The pressure generation of the stimulated ventricles was independent of preload, while that of the large ventricles rose sharply for preloads up to 40 mmHg and then more slowly thereafter (Figure 5.6). The difference in pressure generation between the two sizes of ventricle was significant at a high preload (80 mmHg). The model predictions confirmed the measured data that there was little difference in the performance of the small and large ventricles. Thus, future experiments should use largely disparate sizes of ventricle for better comparison. In terms of pumping performance, SV output was dependent on preload for small afterloads, and the large ventricles always produced higher SVs than the small ventricles; the stimulated ventricles performed very poorly compared to the control ventricles. Power output was sensitive to preload but not to afterload, with peak hydraulic power of about 1 W. This power level was 3- to 6-fold lower than the actual linear power. The work generated varied similarly to the power. These considerable losses in work and power output could be attributed to the use of an inertial load in the hydraulic measurements and of only the distal part of the muscle to form the ventricles, and possible distal ischemia due to restricted blood perfusion. These problems must be overcome in future experiments. Although reproducibility was not really adequate for comprehensive numerical analysis, the main points are clear.

The numerical model predicted reasonably well the passive hydraulic relations, but it overestimated the flow, and therefore the power output of the ventricles. The fact that the model predicted peak power similar to the actual linear power was hardly surprising, as the model made no allowances for any losses. Since the passive relations were well predicted, the discrepancy between the predicted and measured power was attributed to the surgical formation of the ventricles.

The analysis therefore points towards the surgical configuration of the ventricles as the area in which most effort should be concentrated. In fact, data were highly variable, and

some of the ventricles had a performance considerably better than the mean values. Further work on SMVs in our laboratory suggests that a few refinements to the surgical technique appear to improve the reproducibility of hydraulic function, with indices of performance falling in the upper range of that found in the groups of ventricles analysed in the present study.

5.6.1. Problems encountered

Surgically, it was difficult to construct SMVs of 15 and 20 mm repeatedly with the floppy sheep LDs. Also, the nature of the wrap meant that the free end of the muscle that was sutured unto itself could not be sewn tightly together as this would impede blood flow. The condom could therefore slip out through the sutures at high preloads, leading to measurement difficulties. Although attempts were made to reduce the effect of the inertial load by recycling the pumped volume back into the reservoir, the long tubing that connected the ventricle to the afterload chamber increased the resistance to flow. Improvements in the mock circulation system will certainly lead to more reliable measurements. Better results could be obtained if the above difficulties were overcome.

5.6.2. Conclusion

The results obtained from the sheep LDs were fairly consistent with measurements performed using canine LD in another laboratory (Oda *et al.* 1993). The present work, however, extends to chronically stimulated muscle, and shows that it performs worse than control muscle, though the low outputs of the former would be maintained for longer. Better surgical procedures would certainly lead to improved ventricular performance and allow the model, from which useful information could be gathered, to be developed further. Also, further work is required to develop stimulation patterns that retain speed of contraction, and thus maintain the performance of stimulated ventricles. By and large, the mathematical model gives good qualitative and quantitative descriptions of the hydraulic

function of SMVs, and could therefore be extended to obtain useful information for constructed functional SMVs.

6. Optimization of Activation

6.1. Summary

Three approaches were used to determine stimulation patterns that maximize the isometric force-time integral per impulse (FTIpP) available from tibialis anterior muscles of the rabbit. Initially, the interval between two pulses was fixed at the value that gave the maximum force-time integral, and successive pulses were added at intervals that maximized the FTIpP. This iterative approach was checked by a second method, in which a computer-generated protocol was used to deliver randomized bursts to the muscles. These experiments confirmed that optimal stimulation patterns for fast muscles consisted of an initial high-frequency portion followed by a train of impulses at a lower frequency. However, for muscles that had been stimulated chronically at a constant low frequency, an initial high-frequency portion conferred no advantage. In a third set of experiments, constant-frequency bursts were used to generate contour surfaces that represented the dependence of FTIpP on the frequency and number of impulses. The results agreed with those from the earlier methods. Thus optimized patterns have potential for clinical use, but their value will depend strongly on the activation characteristics of the stimulated muscle.

6.2. Introduction

Skeletal muscles may be stimulated electrically to utilize their force-generating capacity in clinical applications. Stimulation can be applied to a muscle *in situ* to restore function to the diaphragm (Glenn *et al.* 1980) or to limb muscles (Hambrecht & Reswick 1977; Bajd & Jaeger 1994) that have been paralysed by spinal cord injury. Alternatively a muscle may be grafted, with the motor nerve intact, to replace the external anal sphincter (Baeten *et al.* 1988; Williams *et al.* 1989) or to provide cardiac assistance to a failing heart (Acker *et al.* 1987; Salmons & Jarvis 1992; Hooper & Salmons 1993).

It is conventional to use constant-frequency bursts in clinical applications, for no better reason than that they are convenient to generate. However, such patterns deliver more impulses to the muscles than are needed to maintain contraction; the associated high aggregate rate of impulse delivery results in premature muscle fatigue in the short term and loss of muscle power in the long term (Jarvis 1991b, 1993). Constant-frequency bursts actually bear no resemblance to physiological patterns of motoneurone firing, which consist of trains of action potentials with changing interpulse intervals (Marsden *et al.* 1971; Zajac & Young 1980b; Hennig & Lømo 1985). Would it be advantageous to adopt impulse trains that are closer to these physiological firing patterns for clinical applications of electrical stimulation?

The mechanical response of a muscle fibre is not a simple function of the frequency of action potentials delivered to it by its motor axon. Wilson and Larimer (1968) showed that the force exerted by a crayfish claw opener muscle could be maintained by less frequent stimulation than that required to generate it, a property known as 'catch'. A phenomenon somewhat analogous to 'catch' exists in mammalian skeletal muscle: Marsden *et al.* were able to simulate a maximal voluntary contraction in human muscle by an electrical tetanus whose frequency was progressively decreased (Marsden *et al.* 1976). Such a strategy minimized fatigue that resulted from prolonged contraction of the muscle, a phenomenon that they referred to as 'muscular wisdom' (Marsden *et al.* 1983). Burke and his colleagues found that, when slow-twitch (type S) muscle units were stimulated repetitively within a narrow frequency range (6 - 20 Hz), tension output could be increased significantly by adding a single pulse at a short inter-pulse interval (IPI) in an otherwise constant low-frequency train (Burke *et al.* 1970, 1976). This enhancement of force output could be elicited from both slow and fast motor units, the optimum timing depending only on the speed of the isometric twitch. Zajac and Young (1980a) determined the properties of stimulus trains that produced maximum force-time integral

per impulse (FTIpP) from single motor units in the gastrocnemius muscle of the cat. They concluded that an iterative technique could be used to obtain the optimum stimulation pattern for a muscle, and they went on to establish that the optimal initial IPI was 5-10 ms (Zajac & Young 1980b).

Chronic stimulation of rabbit skeletal muscle at 10 Hz for several weeks renders it fatigue-resistant, a property that is crucial to clinical applications that call for sustained levels of activity. However, muscles stimulated in this way also undergo a reduction in bulk (Salmons & Henriksson 1981; Pette *et al.* 1976) and contractile speed (Salmons & Vrbová 1969; Al-Amood *et al.* 1973; Pette *et al.* 1973; Salmons & Sréter 1976; Kernell *et al.* 1987), and this results in a substantial loss of power (Jarvis 1993). Chronic stimulation at 2.5 Hz and 5 Hz produces muscles that are significantly faster and more powerful than those stimulated at 10 Hz, yet just as resistant to fatigue in tests conducted at a fixed working rate of 10 W kg^{-1} (Jarvis *et al.* 1991a, 1991b, 1994; Mayne *et al.* 1994). Since an optimal stimulation pattern should enable the same mechanical response to be elicited by fewer impulses, it would deliver a lower aggregate number of impulses over time, and would therefore hold out the prospect of preserving muscle power more effectively in the long term. This would be a substantial benefit in applications such as cardiac assistance, in which the power requirements can be difficult to meet (Salmons & Jarvis 1992).

The aim of the study presented in this chapter was to use three different approaches to determine patterns of stimulation that optimize the response of both control and chronically stimulated rabbit TA muscles.

6.3. Materials and Methods

Nine adult New Zealand White rabbits were used in the study, of which three had undergone chronic 5 Hz and six chronic 10 Hz stimulation for more than four weeks.

Only the left TA was stimulated in each animal. At terminal experiments, data was collected from contralateral control muscles (n = 9) and the muscles stimulated at either 5 Hz (n = 3) or 10 Hz (n = 6). The procedures of chronic stimulation and terminal experiments were similar to those detailed in chapter 3.

The length at which the muscle developed the greatest isometric twitch force was determined and the muscle was maintained at this length for all isometric measurements, including the measurements of contraction time. Isotonic contractions were initiated from this length.

6.3.1. Optimization of stimulation pattern

In the context of these experiments, an optimal stimulation pattern (OSP) is defined as the sequence of nerve impulses that elicits from the muscle the maximum mechanical output per impulse. An appropriate measure of mechanical output is the isometric force-time integral (FTI), which has been shown to be highly correlated with energy utilization and with work output measured in terms of resynthesis of reduced nicotinamide-adenine dinucleotide (NADH) during oxidative recovery after activity (Jöbsis & Duffield 1967).

6.3.2. Iterative method

In a preliminary experiment (Jarvis 1991), isometric force was measured and converted to FTI by a Gould analog integrator (Gould Electronics, Cleveland, Ohio, Model 13-4615-70). The FTI obtained in response to two stimulating pulses was plotted against the interval between the pulses. The interval was then fixed at the value that gave the highest FTI, and an additional pulse was added to the train, optimizing the interval in the same way. The procedure was repeated for successive pulses, up to a total of six. The same procedure was used to produce a stimulus train that maximized force rather than FTI. Measurements were carried out on three muscles chronically stimulated at 10 Hz and on the contralateral controls. An approach of this type has been used previously (Zajac &

Young 1980a; Maxwell *et al.* 1993), but those experiments did not extend to chronically stimulated muscle.

6.3.3. Random pattern method

One hundred patterns were generated in which the IPIs were of quasi-random length. For control muscles, the response to an isolated single impulse was a twitch contraction with a time to peak (CT) of about 20 ms and a total time above resting force of about 80 ms. The maximum IPI used in the random patterns was therefore 70 ms (between three and four times the CT), since the mechanical responses to individual pulses would not interact if the intervals were any longer than this (Burke *et al.* 1970). The random pattern trains were generated by setting the first pulse and adding subsequent pulses at random intervals until the maximum burst length of 300 ms had been reached. Each random burst was then saved to disk as a stream of digital values representing the presence (1) or absence (0) of a supramaximal nerve stimulus (0.05 ms, 20 V) in one millisecond time slots, as explained in Chapter 2. The computer-controlled servomotor system delivered these digital values as triggers to the isolated stimulator, sampled and analysed the data on-line to obtain the FTIpP, and saved the results to disk. A one-minute rest period was interposed between stimulation bursts. Patterns were then placed in rank order according to the magnitude of the FTIpP that they elicited. A standard train of twelve pulses at 40 Hz was included at the beginning of the experiment ('rested' standard pulse train) and after every ten random burst trains, as a means of checking for possible deterioration or fatigue of the muscle preparation or, conversely, for signs of potentiation of muscle output. The preparations were in fact extremely stable (see below). Data was collected from three muscles that had undergone chronic stimulation at 10 Hz and from their contralateral controls.

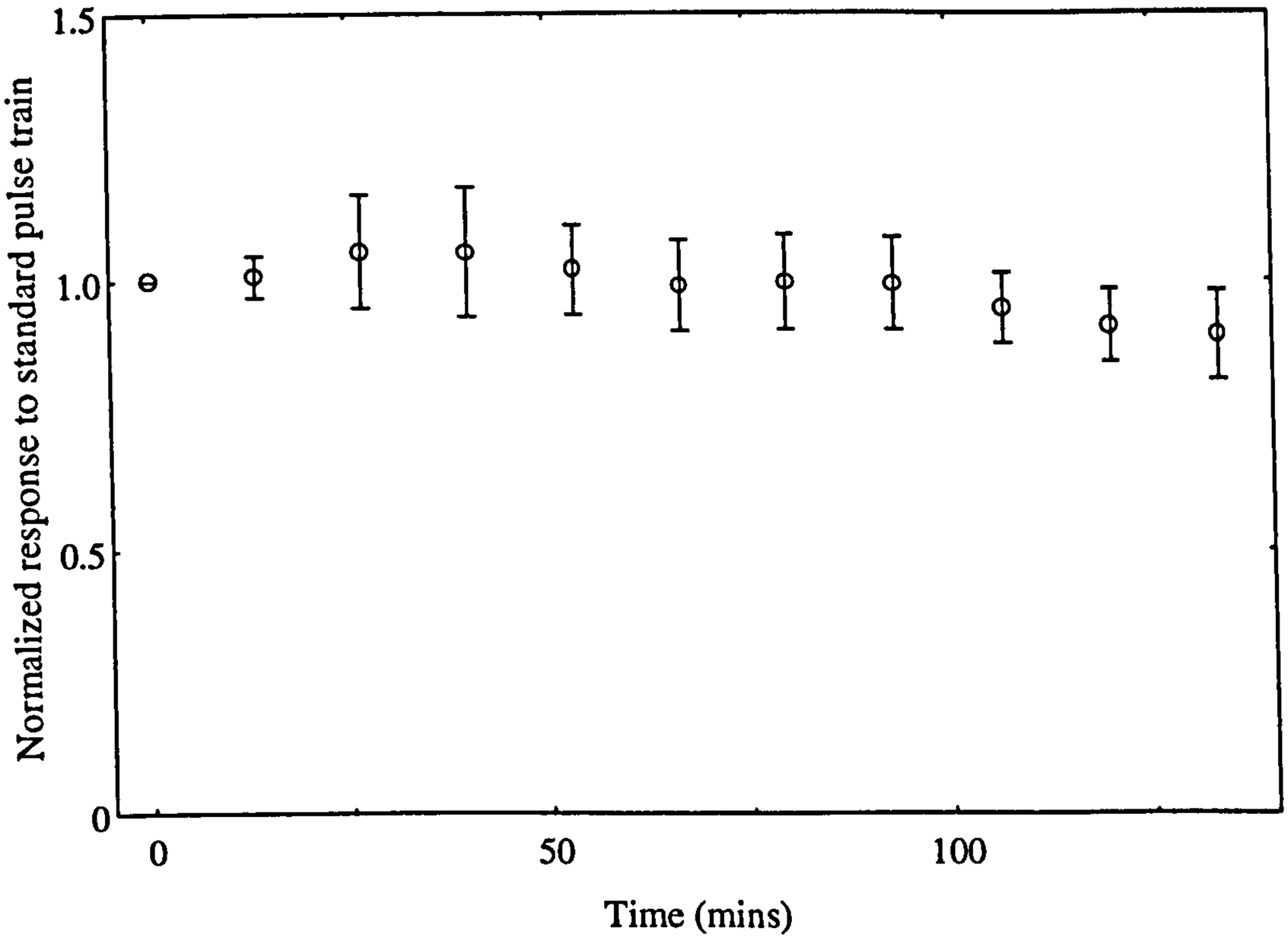

Figure 6.1. *The mechanical response to a standard pulse train plotted as a function of time in 9 experiments. The ordinate is normalized in terms of the response to the 'rested' standard train, and is plotted as the mean ± SEM.*

6.3.4. The FTIpP index

The effectiveness of the patterned impulse train may be assessed as the amount by which the FTIpP exceeds that for a single pulse (i.e., a twitch contraction):

$$\text{FTIpP} = \frac{\text{Burst FTIp}}{\text{Twitch FTI}}$$

However, this measure alone would not take account of systematic variation occurring during the two-and-a-half hour duration of the experiment. The standard pulse trains were used to compensate for this variation. In Figure 6.1 the ratio of the FTI of the standard trains to that of the 'rested' train is shown as a function of time for 9 different muscles. The graph shows that the muscle preparations were in fact rather stable: the maximum coefficient of variation in the mean was 3.8%.

This ratio was then used as a correction factor for the raw FTIpP index defined above:

$$\text{FTIpP index} = \frac{\text{Burst FTIpP}}{\text{Twitch FTI}} * \frac{\text{FTI of 'rested' standard train}}{\text{FTI of preceding standard train}}$$

If the mechanical response of a muscle increased in direct proportion to the number of pulses, the FTIpP index would always be unity. An index greater than unity for any pulse pattern represents a 'more-than-linear' summation of the mechanical response elicited by the impulses in that train. We refer to this as the 'doublet effect', since it occurs when at least two of the pulses are separated by a short IPI. A value less than unity reflects a reduced responsiveness of the chronically stimulated muscle to the second impulse; this phenomenon has not previously been observed in either control fast or slow muscle (Burke *et al.* 1976; Zajac & Young 1980a).

6.3.5. Constant frequency train method

To develop a more general basis for determining OSPs for any type of muscle, constant frequency bursts of 1 to 10 pulses were generated over a frequency range of 1 to 500 Hz and delivered to control rabbit tibialis anterior muscles and muscles that had been stimulated chronically at 5 Hz (n = 3) and 10 Hz (n = 3). The protocol of burst delivery to the muscles was the same as for the random pattern method.

6.4. Results

6.4.1. Iterative method

Figure 6.2 illustrates the results obtained with the iterative method for determining OSPs; for clarity this is shown only for the first 3 IPIs. In this figure a control muscle (a, c, e) is compared with a muscle that had been stimulated chronically for 4 weeks at 10 Hz (b, d, f). In control muscles, peak force and FTI were produced when the intervals between the pulses were short (Figure 6.2a and c).

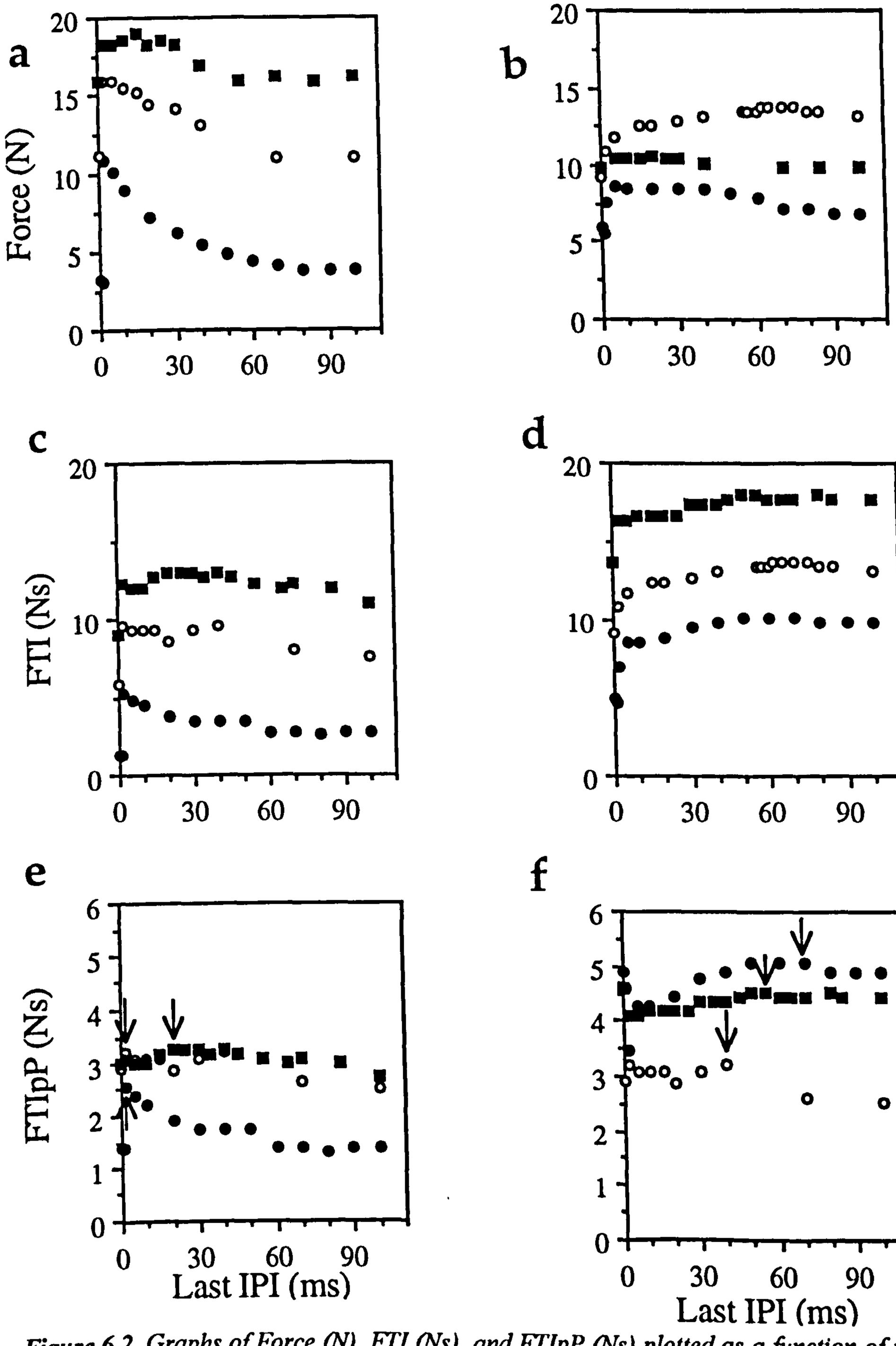

Figure 6.2. Graphs of Force (N), FTI (Ns), and FTIpP (Ns) plotted as a function of the last IPI for 2 (●), 3 (○) and 4 (■) pulses. The responses shown are typical of control muscles (a, c, e), and muscles stimulated chronically at 10 Hz for 4 weeks (b, d, f). The arrows in e and f show how optimal burst IPIs are determined by choosing the longest interval that gives the maximum FTIpP. Each curve is for a single muscle.

The patterns that produced the optimal mechanical responses were made up of the following IPIs: 3, 3, 20, 10, 10, 10 ms for force, and 3, 40, 35, 20, 30 ms for FTI. Stimulated muscles contracted more slowly (Table 6.1) and peak FTI occurred at intervals greater than 50 ms (Figure 6.2d). For these muscles, optimal force and FTI were generated for pulse trains of 30, 30, 20 ms and 70, 70, 50 ms, respectively. For the chronically stimulated muscle, FTIpP was highest for the twitch response (Figure 6.2f, filled circle on the ordinate) and was depressed by up to 20% by the addition of further pulses at very short IPIs. The maximum FTIpP index for this muscle was therefore close to unity. In contrast, the maximum FTIpP index for the control muscle (Figure 6.2e) was about 2.0, representing a doubling of the twitch output, for 2- and 3-pulse bursts.

Table 6.1. *Twitch contraction times (time from a single stimulus to the peak of the force response to that stimulus) for rabbit TA muscles stimulated chronically at 5 Hz or 10 Hz, and for contralateral control muscles (mean ± SEM).*

Muscle state	CT (ms)
Control (n = 6)	20.24 ± 0.92
5 Hz (n = 3)	27.35 ± 3.37
10 Hz (n = 6)	65.22 ± 4.70

6.4.2. Random pattern method

The random patterns that produced the highest FTIpP indices for the fast control muscles (Figure 6.3a) were characterised by one or more pairs of closely spaced pulses; thus short IPIs enhanced the response of the fast muscles. The average frequency of these bursts (Figure 6.3a) was about 45 Hz. On the other hand, the best patterns for the muscles stimulated chronically at 10 Hz for 6 weeks (Figure 6.3b) were characterized by long intervals between pulses, which reduced the average frequency to about 20 Hz. Figure 6.3d, which shows the worst patterns for this muscle, suggests that the incidence of short

IPIs within the burst was actually detrimental. The worst patterns for the control muscle (Figure 6.3c) were similar to the best patterns for the chronically stimulated muscles.

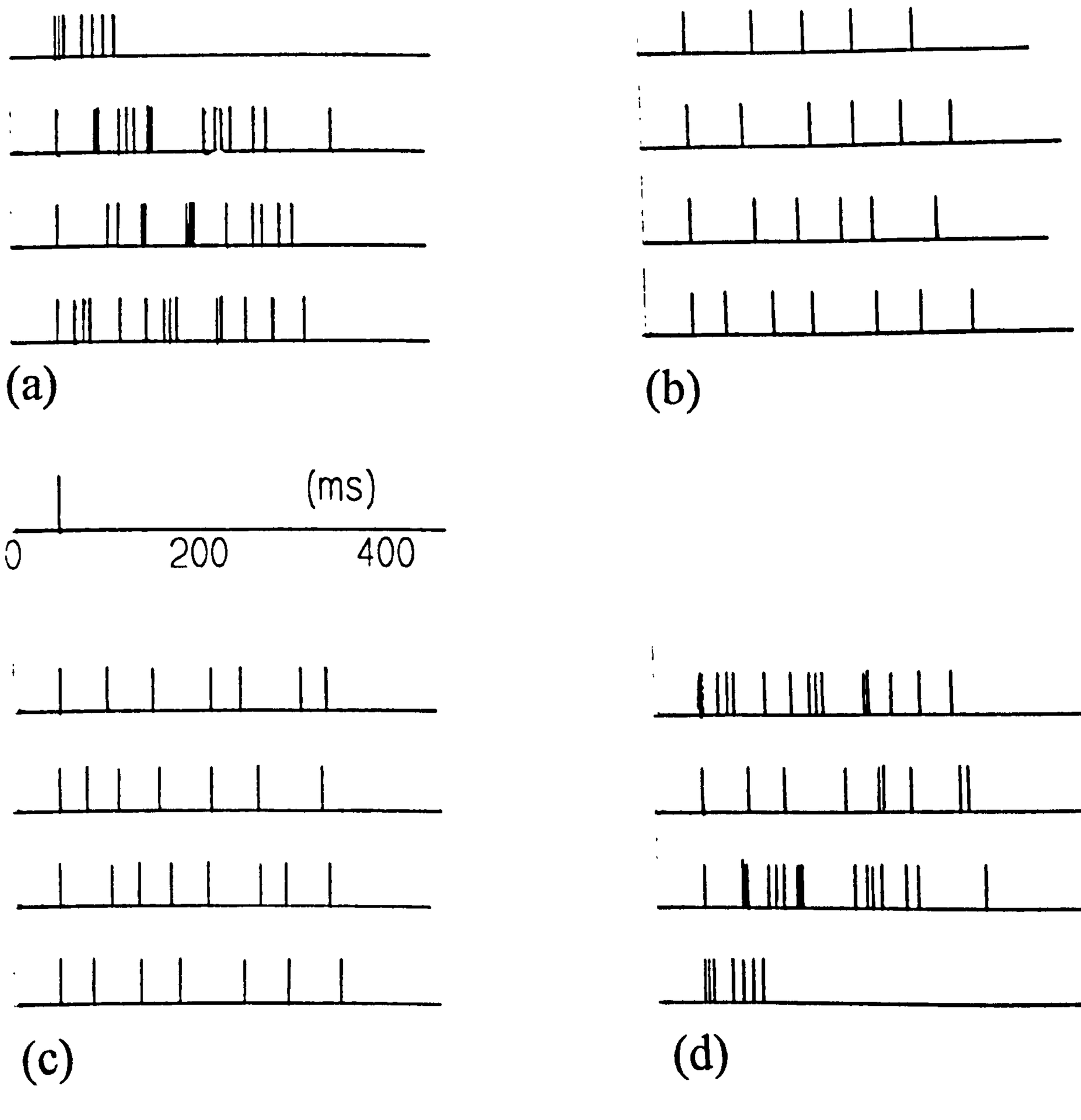

Figure 6.3. *The results of rank-ordering the FTIpP indices for the responses to 100 random patterns. a) 'Best' patterns for a control fast muscle. b) 'Best' patterns for a chronically stimulated muscle (6 weeks of stimulation at 10 Hz). c) 'Worst' patterns for a control fast muscle. d) 'Worst' patterns for the same chronically stimulated muscle.*

6.4.3. Constant-frequency train method

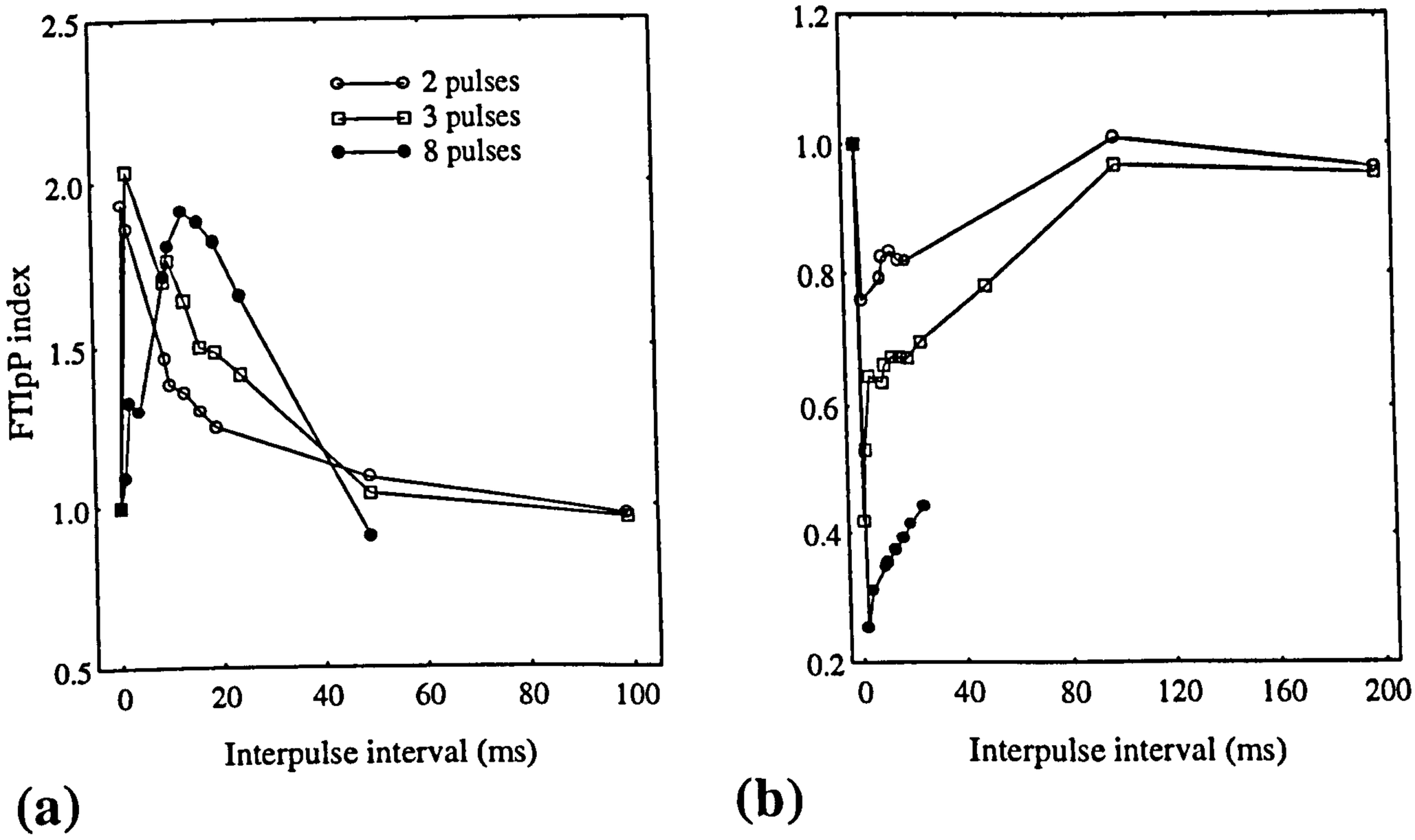

Figure 6.4. Graph of FTIpP index (ordinate) versus interpulse interval (abscissa) for 2- (○)*, 3-* (□) *and 8-pulse* (●) *constant-frequency bursts. (a) Control fast muscle. (b) Chronically stimulated muscle (6 weeks of stimulation at 10 Hz). See (a) for legend.*

When short, constant-frequency trains were delivered to control fast muscles, the 2- and 3-pulse bursts produced a peak in the FTIpP index for IPIs less than 5 ms (Figure 6.4a). Muscles that were chronically stimulated (Figure 6.4b) showed a trough for all bursts that contained very short IPIs. Nevertheless, these muscles showed a peak at a much longer IPI of 100 ms (10 Hz), a result that agrees with previous observations on slow muscle (Burke *et al.* 1970). Even at this peak value, the FTIpP index only approached unity, so the mechanical output per pulse never exceeded that for a single twitch.

The difference between control muscles and muscles stimulated chronically at 10 Hz is well illustrated in Figures 6.5 and 6.6. In the contour plots (Figures 6.5a and 6.5b), the lighter the shading the greater the FTIpP index. Note that the lowest burst frequency plotted was 10 Hz in Figure 6.5a and 5 Hz in Figure 6.5b so that the 'white' region from the abscissa to the start of the grey shading indicates an absence of data.

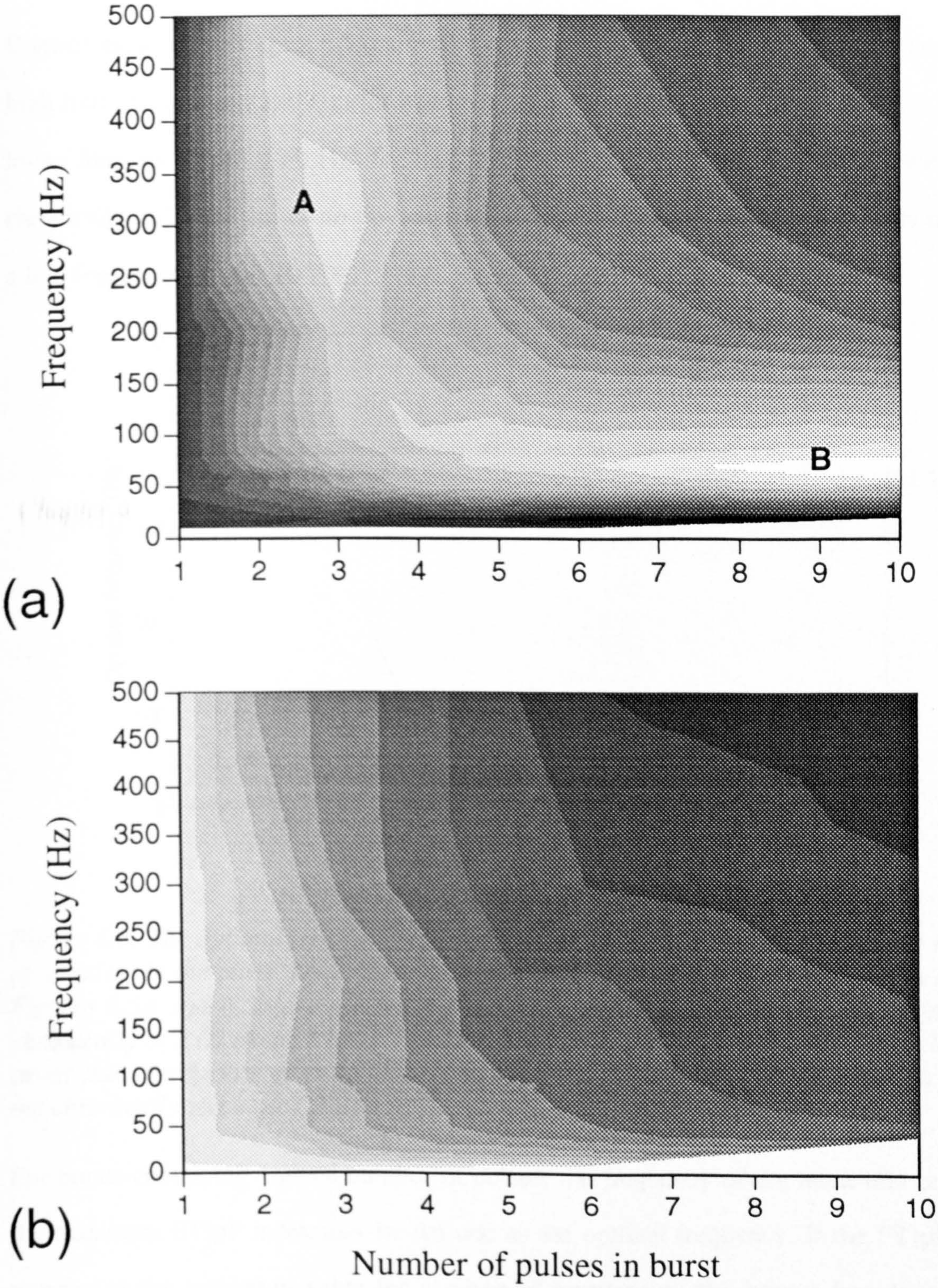

***Figure 6.5**. Contour plot of frequency, number of pulses in a burst and FTIpP index for (a) control muscle and (b) muscle chronically stimulated at 10 Hz. Lighter shading indicates a higher FTIpP index. The control muscle shows two peaks, A and B. A occurs at a high frequency (about 300 Hz) for bursts of 2-3 pulses while B is found at a much lower frequency for bursts of more than 4 pulses. Some combinations of frequency and number of pulses could not be accommodated within a burst duration of 600 ms; data is therefore lacking in the white region from the abscissa to the start of the grey shading.*

Control muscle (see Figure 6.5a) shows two peaks in its output: the first (A) occurs at a high frequency (about 300 Hz) for bursts of 2-3 pulses; the second (B) is found at a much lower frequency (about 60 Hz) for bursts of more than 4 pulses. The muscle stimulated chronically at 10 Hz shows no obvious peaks but the lightest areas for all bursts occur at a low frequency (about 10 Hz).

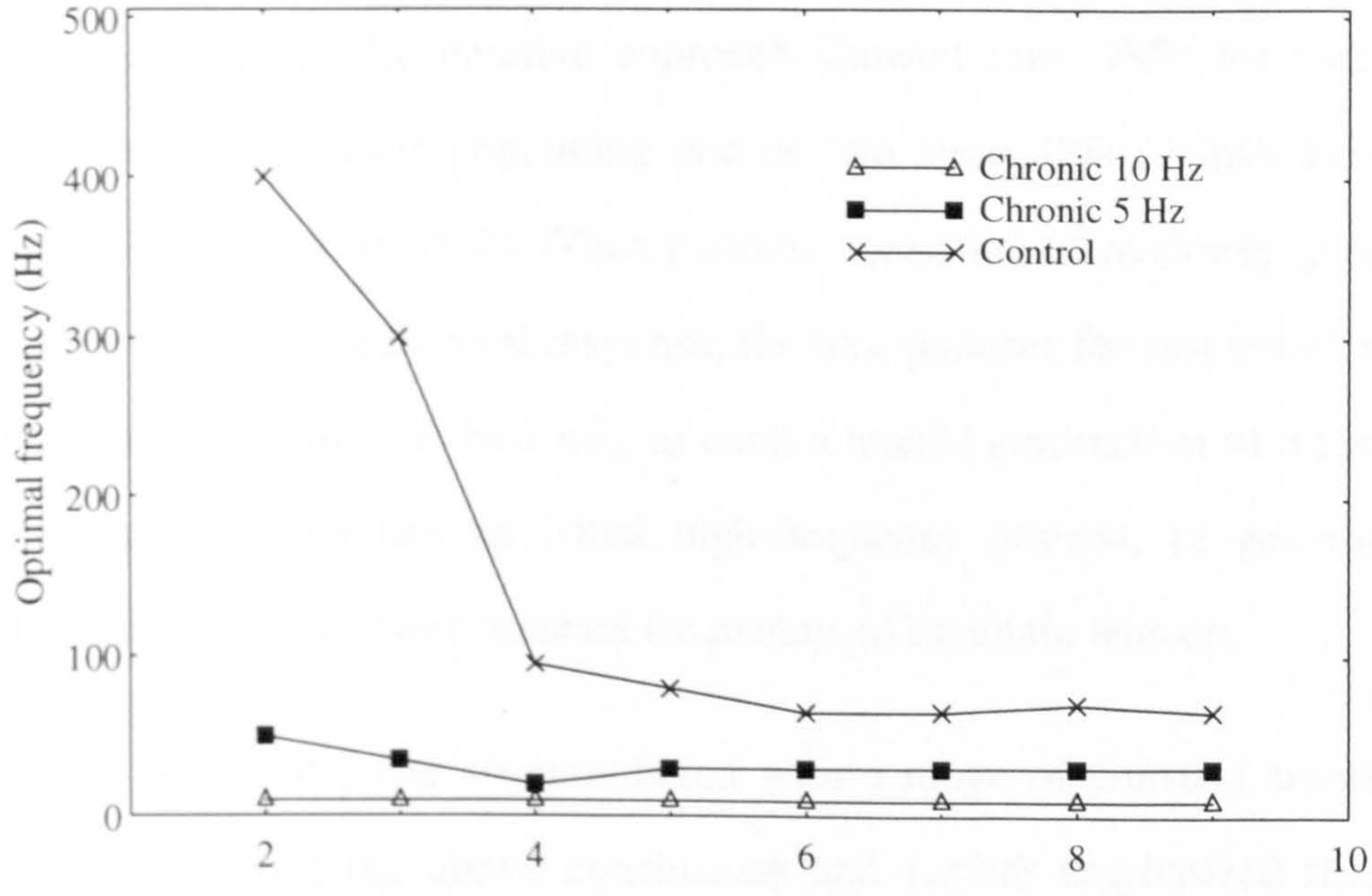

***Figure 6.6**. The optimal frequency (see text for definition) is plotted against the number of impulses in the burst. Loci of the optimal frequencies abstracted from graphs such as Figures 6.5a and 6.5b are plotted for control muscle (✖), and for muscles stimulated chronically at 5 Hz (■) and 10 Hz (Δ). The peaks A and B lie on the control muscle curve (✖) at the appropriate co-ordinates as in Figure 6.5a. Note the intermediate nature of the chronically stimulated 5 Hz muscle.*

For bursts containing a given number of pulses, the frequency of the burst that produces the maximum FTIpP index may be defined as the optimal frequency. If the FTIpP index remains at the maximum value for a range of frequencies, the lowest frequency in the range is taken as optimal. Figure 6.6 abstracts from contour plots such as Figures 6.5a and 6.5b the loci of the optimal frequencies for control muscle and muscles stimulated chronically at 5 Hz and 10 Hz. It shows that the optimal frequency does not change appreciably for stimulation bursts containing more than five pulses.

In control muscle (Figure 6.6), the rise in frequency at shorter train lengths (equivalent to peak A in Figure 6.5a) reflects the doublet effect. This effect is not seen in the muscles stimulated chronically at 10 Hz. Muscles stimulated at 5 Hz show an intermediate behaviour, with a slight doublet effect.

6.5. Conclusions

For control fast muscles the iterative approach showed that OSPs for force and FTI consisted of an initial portion containing one or two short IPIs (3 ms), followed by a series of pulses at longer intervals. When patterns consisting of randomly generated IPIs were ranked in order of mechanical response, the best patterns for fast muscles contained some short intervals. Thus, the best way to elicit a tetanic contraction of a fast muscle is to deliver a pattern that has an initial high-frequency portion, to generate tension, followed by impulses at a lower constant frequency, to maintain tension.

Contour plots of the response to stimulation with a range of constant frequencies and burst lengths confirmed the above conclusions and further emphasized the difference between bursts with a few impulses and bursts with many impulses. For bursts of less than four impulses, the highest FTIpP occurred at high frequencies (greater than 200 Hz, corresponding to IPIs less than 5 ms), another manifestation of the doublet effect. For bursts of more than 5 pulses, the highest FTIpP occurred at a much lower constant frequency (50 Hz, corresponding to an IPI of 20 ms), reflecting the dilution of the doublet effect over these longer trains.

6.6. Discussion

The purpose of the present study was to improve on current protocols for clinical applications of electrical stimulation by investigating the relationship between the neural input and the mechanical output of skeletal muscles. An understanding of this relationship would lead to general rules for designing ideal stimulation patterns that provided an

adequate tension profile over the active period with the minimum redundancy in the impulse train.

It is instructive to compare FTI outputs for bursts of increasing number of impulses, optimized by the iterative approach, to constant-frequency bursts optimized from the contour plots. Figure 6.7 shows that 2-pulse bursts from the two sources have a similar FTIpP index. However, bursts with 3 pulses have an FTIpP index more than double the index for the corresponding constant-frequency burst. This difference depends heavily on the long second IPI that was a feature of OSPs generated by the iterative approach. In constant-frequency stimulation, the price paid for a first IPI that is short enough to produce the doublet effect is a subsequent impulse that is almost redundant, and which therefore lowers the FTIpP. For fast muscles, at least, optimal stimulation cannot be achieved without the use of variable IPIs.

Because the doublet effect acts only during the short transitional period from the resting to the active state, its effect on FTIpP is averaged over the duration of a tetanic contraction. As a result, the benefit of the doublet effect declines as a burst increases in length. The FTIpP indices for bursts with variable IPIs therefore converge towards those with constant IPIs for bursts of more than 5 pulses (Figure 6.7). The IPI of constant-frequency bursts of more than 5 pulses that produce the best FTIpP index can therefore be used to estimate the constant low-frequency portion of an OSP.

Chronic stimulation at 5 Hz reduced, and chronic stimulation at 10 Hz abolished, the doublet effect. The OSPs of muscles with a history of chronic stimulation, determined by the iterative approach, showed no initial short intervals. On the contrary, as was shown by rank-ordering of patterns with random IPIs, short intervals led to a reduction in force per impulse and FTI per impulse when these patterns were delivered to chronically stimulated muscles. The reason for this reduction is the absence in these muscles of the

doublet effect, illustrated in Figure 6.4. Therefore an initial high-frequency portion has no benefit in these muscles and, as the contour plot of Figure 6.5b shows, no combination of pulses produced a higher FTIpP than a single impulse.

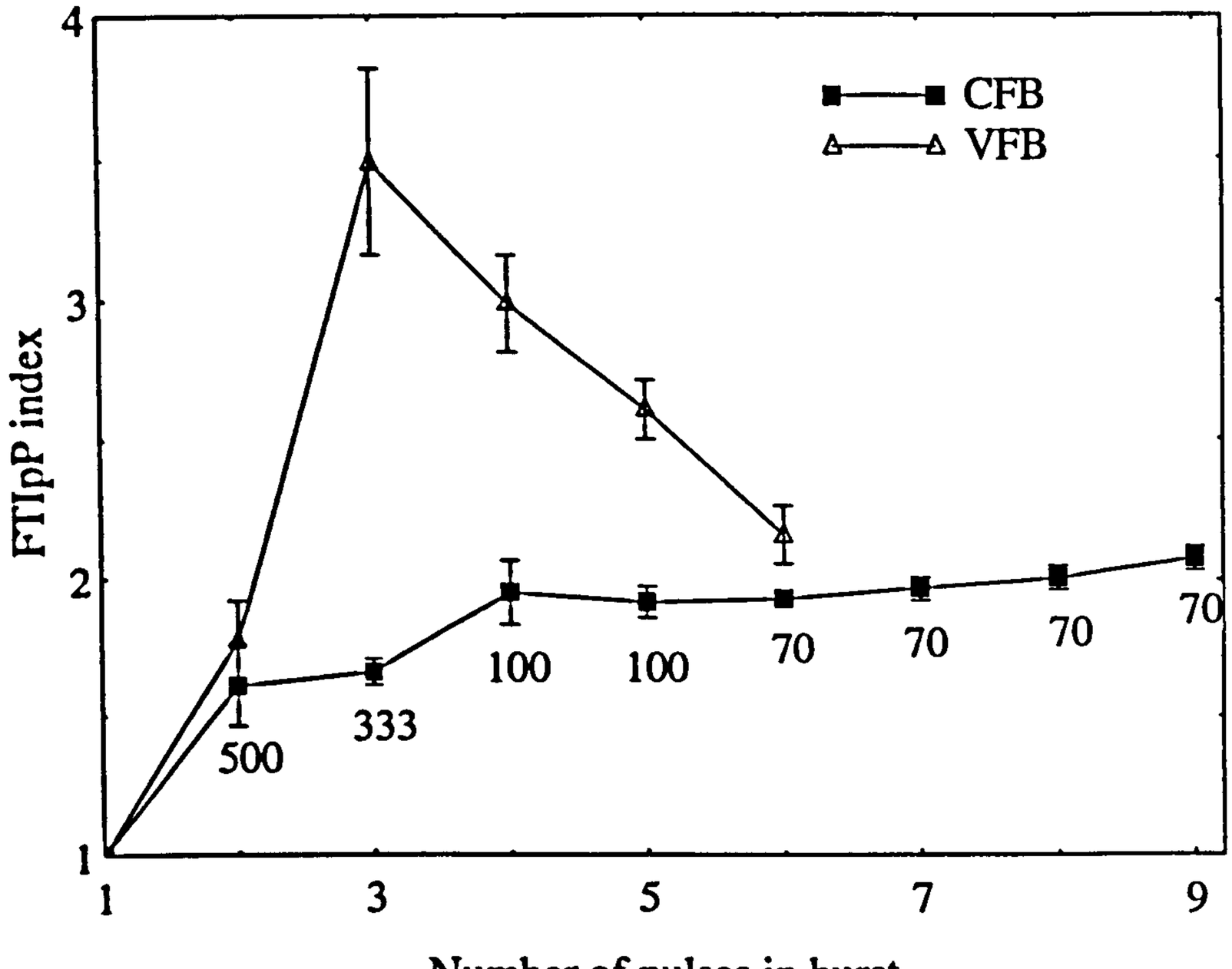

Figure 6.7. Comparison between the responses to the best constant-frequency bursts (CFBs, n = 3) and the responses to OSPs (◆, n = 3). The numbers below the CFB (■) curve indicate the best frequency for that number of pulses. The FTIpP indices are plotted as mean ± SEM.

The lack of a single clear explanation for the existence of the doublet effect in fast skeletal muscle reflects our incomplete understanding of the rate-limiting mechanisms for force generation in whole muscles. The fact that the doublet effect is lost with chronic stimulation suggests a link between the doublet effect and those intracellular changes brought about by chronic stimulation that affect muscle activation. One possibility is that activation of rested fast muscle by a single impulse is in some way incomplete, so that a second impulse is required to produce full activation. In this context, activation has to be visualized as a process that has more than one stage. The initial stage, the release of Ca^{2+}

in response to a single impulse, appears to be supramaximal, since 80-90% of crossbridges are activated (Kress *et al.* 1986) and a reduction in the magnitude of the Ca^{2+} transient does not result in a decline in force production. Subsequent stages, which lead to the appearance of force at the muscle tendon, are considerably delayed with respect to the Ca^{2+} transient, and the occupancy of Ca^{2+}-binding sites during a single twitch may be too short in fast muscles for all of the activated crossbridges to undergo attachment and force generation (Rüegg 1992). In terms of activation, the most striking features of chronically stimulated muscle are a marked reduction in the volume of the sarcoplasmic reticulum, changes in the Ca^{2+}-transport ATPase, which result in a decreased capacity for active sequestration of Ca^{2+} (Sréter *et al.* 1974; Salmons & Sréter 1976; Heilmann & Pette 1979; Eisenberg & Salmons 1981), and a decrease in the content of parvalbumin, a cytosolic Ca^{2+} buffer (Klug *et al.* 1983). All of these changes would be expected to extend the time course of the Ca^{2+} transient in chronically stimulated muscle, leading to the effective generation of force even in response to a single pulse and hence a reduced scope for enhancement of force by a double impulse.

The changes induced by chronic stimulation lead to a more extreme state of differentiation than that seen in slow motor units (Salmons & Sréter 1976). Thus the present observations do not necessarily conflict with those of Burke *et al.* (1976) and Zajac and Young (1980a), who observed the doublet effect in slow, as well as fast, motor units in the medial gastrocnemius muscle of the cat. Based on this finding they proposed a method of determining OSPs in which the CT of the muscle was used as a scaling factor. Their OSP would consist of an initial portion that contained one or two short IPIs followed by a train of impulses with a constant interval between 1 and 2×CT of the muscle. Figure 6.8 shows the effect of applying this method to the present data to find the constant-frequency portion. The FTIpP indices of 9-pulse constant-frequency bursts for control muscles and muscles stimulated chronically at 5 Hz and 10 Hz have been plotted

against the interpulse interval expressed as a fraction of the CT (contraction times for these muscles are given in Table 6.1). From Figure 6.8, the optimal IPIs for the 9-pulse bursts are as follows: 0.77×CT (64 Hz, since frequency is the reciprocal of IPI) for control muscle, 0.95×CT (38 Hz) for 5-Hz stimulated muscles, and more than 1.34×CT (less than 11 Hz) for 10-Hz stimulated muscles. These values are close to the range of 1 to 2×CT that Zajac and Young would recommend for the constant-frequency portion of the OSP. However, Zajac and Young's method can only apply to muscles in which the doublet effect is present. Since the chronically stimulated muscles retain little or no doublet effect (Figure 6.6 and Figure 6.4b), adding an initial portion of one or two short IPIs to the constant-frequency portion would lead to a false OSP.

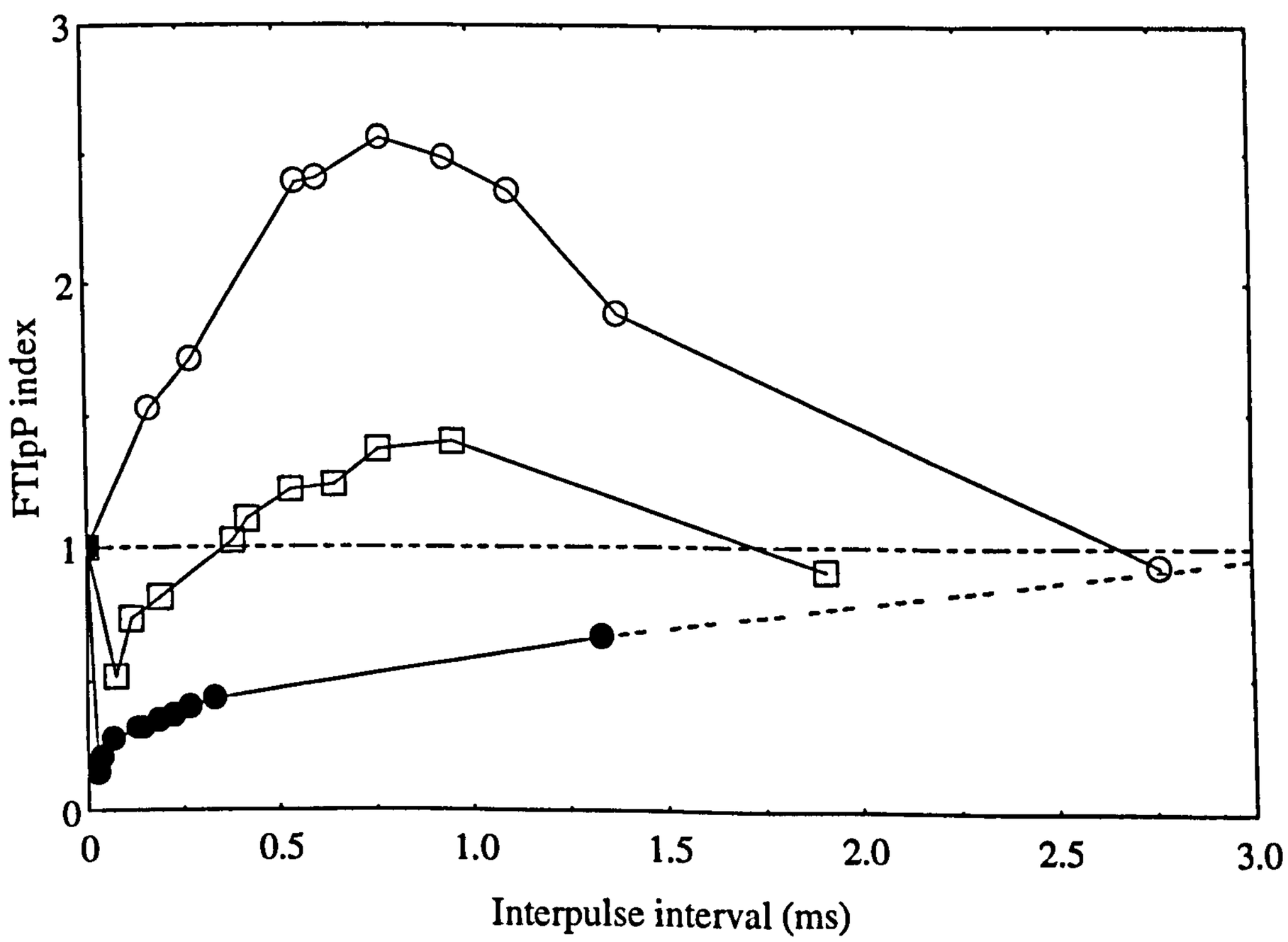

Figure 6.8. *FTIpP indices for 9-pulse bursts plotted against interpulse interval expressed as a fraction of muscle contraction time (CT) for control muscle (○), and muscles stimulated chronically at 5 Hz (□) and 10 Hz (●). The maximum FTIpP indices occur at 0.77×CT (64 Hz) and 0.95×CT (38 Hz) for control muscle and muscle stimulated chronically at 5 Hz, respectively. The muscle that had been chronically stimulated at 10 Hz had not reached its peak FTIpP, but its maximum value can be predicted to approach unity when two pulses no longer interact, as indicated by the broken line.*

Although it may reasonably be supposed that the contraction time of a muscle gives an indication of its activation characteristics, such information is not an adequate basis for determining the OSP of a muscle. This is illustrated by the muscles stimulated chronically at 5 Hz. These muscles have a twitch CT of 27.35 ± 3.37 ms (mean ± SEM), and should thus be classified as fast muscles, since their CT is less than 35 ms (Burke 1967, 1968). Nonetheless, they retained the doublet effect to a much smaller extent than the control muscles, and OSPs for these muscles would not contain short intervals. In this way, the long-term history of activation of a muscle can profoundly influence the nature of its OSP.

The doublet effect is an important phenomenon that could be exploited with advantage in clinical applications involving fewer than 6 pulses per burst. For example, a burst of five pulses delivered as an OSP can give the same mechanical output as a burst of six pulses at a constant frequency. Moreover, OSPs are useful for generating muscle force with a rapid rate of development. Thus the OSP provides an additional degree of freedom that helps the designer to achieve a stimulation pattern that is matched appropriately to the functional needs of the application.

Cardiac assistance from skeletal muscle (Salmons & Jarvis 1991a; Hooper and Salmons 1993) is an example of a clinical application of functional electrical stimulation that could benefit from the use of OSPs. It makes use of chronically stimulated muscle that must be both fatigue-resistant and capable of generating force rapidly with a highly controlled tension profile. However, current protocols of chronic stimulation abolish the doublet effect, leaving no scope for modulating muscle output in this way. It will therefore be important to develop strategies of chronic electrical stimulation that preserve the doublet effect. Chronically stimulated muscles that have OSPs with variable IPIs would require less stimulation to achieve the desired output. This would lead to reduced muscle fatigue, an increase in the lifetime of the internally implanted stimulation systems that deliver these

stimulation patterns, and potential for reducing the post-operative delay that is an undesirable aspect of current protocols.

7. Conclusions and Further Work

7.1. Introduction

This thesis is part of a programme working towards the development of a new surgical treatment for end-stage cardiac failure. In the procedure, an SMV will be fashioned from the patient's back muscle to provide heart assist. Because the use of SMVs is still in an empirical stage, some of the parameters that are important for maximum performance of SMVs were studied. These parameters included stimulation patterns for maximal muscle output and SMV configurations for peak work output. The aims of the work presented in this thesis were thus as follows:

I. To develop software to control a servomotor system for use in the measurement of the linear mechanical properties of skeletal muscle.

II. To use the mechanical properties of muscle in a mathematical model to predict its function when formed into a pumping chamber to provide circulatory assist.

III. To investigate the properties of hydraulic properties of acute SMVs formed in sheep, and then to test the validity of the numerical predictions.

IV. To study methods to design optimal stimulation patterns for muscle activation, and possibly muscle transformation.

The above objectives were completed successfully, and results from some of the work presented here have already been published (Jarvis *et al.* 1993b, c; Donaldson *et al.* 1995; Kwende *et al.* 1995 - see Appendix for details). The manuscript for the studies presented in Chapters 4 and 5 is almost ready for submission. Below are conclusions based solely on the work presented in this thesis.

7.2. Summary and Conclusions

Software was developed to control a servomotor system designed specifically for the measurement of muscle mechanical characteristics. The system is reliable and versatile, and additional software were written to provide other useful features such as cyclic control of the servomotor arm. The system is now routinely used in Professor Salmons' laboratory to characterize skeletal muscle.

A numerical model that incorporated the mechanical properties of rabbit and sheep muscles, and a part numerical-part physical model in which rabbit TA contracted linearly against complex loads, were successfully developed to predict the hydraulic performance of SMVs formed from the same muscles. Lamé's equation seemed adequate in quantifying the stress in the SMV wall. The model predicted useful indices of ventricular performance that have been reported in literature; the R/Th and V/M ratios were of particular interest.

Two sizes of acute SMVs were constructed from control and chronically stimulated sheep LD muscles. The large ventricles performed consistently better than the small ventricles. The function of the control ventricles was similar to that measured in ventricles formed from canine LD in another laboratory (Oda *et al.* 1993). However, the stimulated ventricles performed very poorly compared to the control SMVs. The numerical model predicted reasonably well the qualitative and quantitative relations of the acute SMVs, though the power output was overestimated by 3- to 6-fold; but this power level was similar to the actual linear power. The considerable power loss in the acute SMVs could be attributed to their surgical formation, and to the slowing of the muscles following long-term electrical stimulation. The study therefore points to the surgical technique and to chronic stimulation protocols as two areas that need particular attention in order to improve the performance of SMVs.

Three methods were used to determine the properties of OSPs that use fewer impulses to produce a desired output. The doublet effect, which is crucial in controlling a muscle's force profile especially at the start of contraction, is abolished following long-term constant low-frequency stimulation. Chronic stimulation paradigms that retain the doublet effect, an important component of OSPs, should therefore be developed. Because OSPs use fewer pulses to produce a desired output, they have the potential to reduce muscle fatigue, maintain muscle speed and mass, and increase the lifetime of pacemakers. OSPs could be important in FES applications, especially in cardiac assist in which the power requirements can be difficult to meet.

7.3. Further Work

7.3.1. Introduction

Although the work presented in this thesis has advanced current knowledge on the use of skeletal muscle for cardiac assist, it has presented more questions than answers. For example, the doublet effect, which has been shown to be an important component of OSPs, is abolished with chronic constant low-frequency stimulation. Could long-term stimulation paradigms that maintain the doublet effect be designed? Also, the surgical formation of ventricles has been identified as an area that needs further attention in maximizing the power output of SMVs. But will SMVs constructed with improved surgical techniques be able to provide sustained cardiac assist? These are some of the important questions that need to be answered. The apparatus developed and the investigations presented here provide a stepping stone for designing studies to fully characterize skeletal muscle as a contractile surgical biomaterial.

7.3.2. Chronic optimal stimulation patterns

In Chapter 6, the properties of OSPs were investigated. This study had two major drawbacks: first, the outputs were optimized only for isometric contractions and second,

optimization was in acute contractions only. But most of the situations in which a muscle would be required to provide an assist would involve repeated lengthening and shortening contractions, so that the optimal patterns presented here may not be adequate. Further work is therefore needed to establish the possible benefits of muscle transformation with optimal bursts. This would be dependent on whether these optimal bursts result in the retention of the doublet effect; preliminary studies in our laboratory indicate that this is the case. Investigation of the usefulness of OSPs for lengthening and shortening contractions could exploit the cyclic control feature of the servomotor system.

7.3.3. Work-loop measurements

Work-loop measurements are more representative of a muscle providing circulatory assist. Software was written to provide cyclical control of the load on a muscle (see Chapter 2); however, this facility was not exploited in the present work. The cyclical control routines could therefore be used to investigate the ability of the OSPs to allow the muscle to provide useful cardiac-type work, for example, by delaying the onset of muscle fatigue. An important relationship could be forged between the cycle frequency and the velocity for maximum muscle power output. The capacity of stimulated muscles to provide heart-like work could be adequately tested.

7.3.4. Post-tetanic potentiation and OSPs

The use of variable IPIs in modulating the force profile of skeletal muscle in FES applications is affected by post-tetanic potentiation and depression of the muscle outputs. It would therefore be useful to determine how the doublet effect is affected by potentiation. If such knowledge was available, clinicians would be able to control more accurately the force profile of a muscle in FES applications. Software was written to allow such a study to be performed.

Clearly, chronic stimulation of muscle stands out as the area that is crucial in the use of skeletal muscle as a surgical biomaterial. A detailed understanding of the input-output characteristics of skeletal muscle would therefore be invaluable in clinical applications.

References

Acker, M., Anderson, W.A., Hammomd, R.L., DiMeo Jr., B.S., McCullum, B.S., Staum, M., Velchik, M., Brown, W.E., Gale, D., Salmons, S., Stephenson, L.W. 1987a Oxygen consumption of chronically stimulated skeletal muscle. *J. Thorac. Cardiovasc. Surg.* **94**: 702-709.

Acker, M.A., Anderson, W.A., Hammond, R.L., Chin, A.V., Buchanan, J.W., Morse, C.C., Kelly, A.M.,Stephenson, L.W. 1987b Skeletal muscle ventricles in circulation: one to eleven weeks' experience. *J. Thorac. Cardiovasc. Surg.* **94**(2): 163-174.

Acker, M.A., Hammond, R.L., Mannion, J.D.,Salmons, S, Stephenson, L.W. 1986 An autologous biologic pump motor. *J. Thorac. Cardiovasc. Surg.* **92**: 733-746.

Acker, M.A., Hammond, R.L., Mannion, J.D., Salmons, S., Stephenson, L.W. 1987c Skeletal muscle as the potential power source for a cardiovascular pump: Assessment in vivo. *Science* **236**: 324-327.

Al-Amood, W.S., Buller, A.J., Pope, R. 1973 Long-term stimulation of cat fast-twitch skeletal muscle. *Nature* **244**: 225-227.

Alderman, E.L., Fisher, L.D., Litwin, P., Kaiser, G.C., Myers, W.O., Maynard, C., Levine, F., Schloss, M. 1983 Results of coronary artery surgery in patients with poor left ventricular function. *Circulation* **68**: 785-794.

Anderson, D.R., Pochettino, A., Hammond, R.L., Hohenhause, E., Spanta, A.D., Bridges Jr., C.R., Lavine, S., Colson, M., Stephenson, LW. 1991 Autogenously lined skeletal muscle ventricles in circulation. Up to nine months' experience. *J. Thorac. Cardiovasc. Surg.* **101**: 661-70.

Andersen, P. & Henriksson, J. 1977 Capillary supply of the quadriceps femoris muscle of man: adaptive response to exercise. *J. Physiol.* **270**: 677-690.

Anderson, W.A., Anderson, J.S., Bridges, C.R., Hammond, R.L., Dimeo, F., Frisch, E.E., Salmons, S., Stephenson. L.W. 1988 Skeletal muscle ventricles as a potential right heart assist or substitute. *ASAIO Transactrions* **34**: 241-246.

Antonatos, P.G., Moulopoulos, S.D. 1993 The use of a small intra-aortic balloon pump to increase coronary flow. *Life support systems* 1993, July-September; **1**(3): 151-64.

Armenti, F., Bitto, T., Macoviak, J., Kelly, A., Chase, N., Hoffman, B., Rubinstein, N., St. John Sutton, M., Edmunds, L.H., Stephenson, L.W. 1985 Transformation of canine diaphragm to fatigue-resistant muscle by phrenic nerve stimulation. *Surg. Forum* **35**: 258-60.

Arts, T., Bovendeerd, P.H.M., Prinzen, F.W., Reneman, R.S. 1991 Relation between left ventricular cavity pressure and volume and systolic fiber stress and strain in the wall. *Biophys. J.* **59**: 93-102.

Arts, T., Veenstra, P.C., Reneman, R.S. 1982 Epicardial deformation and left ventricular wall mechanics during ejection in the dog. *Am. J. Physiol.* **243** (Heart Circ. Physiol. 12): H379-H390.

Babbs, C.F., Weaver, J.C., Ralston, S.H., et al. 1994 Cardiac, thoracic, and abdominal pump mechanisms in cardiopulmonary resuscitation: Studies in an electrical model of the circulation. *Am. J. Emerg. Med.* **2**: 299-308.

Badylak, S.F., Hinds, M., Geddese, L.A. 1990 Comparison of three methods of electrical stimulation for converting skeletal muscle to a fatigue-resistant power source suitable for cardiac assistance. *Ann. Biomed. Eng.* **18**: 239-250.

Badylak, S.F. 1991 The potential power output for skeletal muscle to provide cardiac assistance. *Sem. Thorac. Cardiovasc. Surg.* **3**: 116-118.

Baeten, C., Spaans, F., Fluks, A. 1988 An implanted neuromuscular stimulator for faecal continence following previously implanted gracillis muscle. report of a case. *Dis. Colon Rectum* **31**: 134-137.

Bailey, L.L., Nehlsen-Cannarella, S.L., Concepcion, W., Jolley, W.D. 1985 Baboon-to-human cardiac xenotransplantation in a neonate. *JAMA 254*: 3321-29.

Bajd, T. & Jaeger, R. 1994 FES for movement restoration. *Basic and Applied Myology* **4**: 124-211.

Bar, A. & Pette, D. 1988 Three fast myosin heavy chains in adult rat muscle. *FEBS Lett.* **235**: 153-55.

Baratta, R.V., Solomonow, M., Best, R., D'Ambrosia, R. 1993 Isotonic length/force models of nine different skeletal muscles. *Med. & Biol. Eng. & Comput.* **31**: 449-458.

Barnard, E.A., Barnard, P.J., Jarvis, J.C. & Lai, J. 1986 Low frequency chronic electrical stimulation of normal and dystrophic chicken muscle. *J. Physiol.* **376**: 377-409.

Beck, C.S. 1935 A new blood supply to the heart by operation. *Surg. Gynec. & Obstet.* **61**: 407-410.

Beyar, R. & Sideman, S. 1984 A computer study of the left ventricular performance based on fiber structure, sarcomere dynamics, and transmural electrical propagation velocity. *Circ. Res.* **55**: 358-375.

Billian, C. & Gorman, P.H. 1992 Upper extremity applications of functional neuromuscular stimulation. *Assist. Technol.* **4** (1): 31-39.

Bounous, E.P., Mark, D.B., Pollock, B.G., Hlatky, M.A., Harrell, Jr, F.E., Lee, K.L., Rankin, J.S., Wechsler, A.S., Pryor, D.B., Califf, R.M. 1988 Surgical survival benefits for coronary disease patients with left ventricular dysfunction. *Circulation* **78** (Suppl. I): I-151-I-157.

Bovendeerd, P.H.M. 1990 The Mechanics of the Normal and ischemic left ventricle during the cardiac cycle. ISBN 90-5291-033-2.

Bowles, C.T., Shah, S.S., Nishimura, K., Clark, C., Cumming, D.V.E., Pattison, C.W., Pepper, J.R., Yacoub, M.H. 1991 Development of mock circulation models for the assessment of counterpulsative systems. *Cardiovasc. Res.* **25**: 901-908.

Bridges, C.R., Anderson, J.S., Anderson, W.A., Hammond, R.L., Acker, M.A., Stephenson, L.W. 1989a Skeletal muscle ventricles: preliminary results and theoretical design configurations. In *Recent Advances in Cardiovascular Surgery*, 1st ed., (Ed. B. Reichart). Munich, Verlag R.S. Schulz, pp182-202.

Bridges, C.R., Hammond, R.L., Dimeo, F., Anderson, W.A., Stephenson, L.W. 1989b Functional right heart replacement with a skeletal muscle ventricle. Circulation 80 (supll. III): III-1-III-9.

Bridges, C.R., Brown, W.E., Hammond, R.L., Anderson, D.R., Anderson, W.A., Dimeo, F., Stephenson, L.W. 1989c Skeletal muscle ventricles: improved performance at physiologic preloads. *Surgery* **106**: 275-82.

Brindley, G.S. 1977 An implant to empty the bladder or close the urethra. *J. Neurol.* **40**: 358-369.

Brown, J.M.C., Henriksson, J., Salmons, S. 1989 Restoration of fast muscle characteristics following cessation of chronic stimulation : physiological, histochemical and metabolic changes during slow-to-fast transformation. *Proc. R. Soc. Lond.* **B235**: 321-346.

Brown, M.D., Cotter, M.A., Hudlická, O., Vrbová, G. 1976 The effects of different patterns of muscle activity on capillary density, mechanical properties and structure of slow and fast rabbit muscles. *Pflügers Arch.* **361**: 241-250.

Brown, W.E., Salmons, S., Whalen, R.G. 1983 The sequential replacement of myosin subunit isoforms during muscle type transformation induced by long-term electrical stimulation. *J. Biol. Chem.* **258**: 14686-14692.

Brown, W.E., Salmons, S., Whalen, R.G. 1985 Mechanisms underlying the synchronous replacement of myosin light chain isoforms during stimulation-induced fibre-type transformation of skeletal muscle. *FEBS Lett.* **192**: 235-38.

Brownson, C., Isenberg, H., Brown, W., Salmons, S., Edwards, Y. 1988 Changes in skeletal muscle gene transcription induced by chronic stimulation. *Muscle & Nerve 11*: 1183-89.

Bullard, H.H. 1919 Histological as related to physiological and chemical differences in certain muscles of the cat. *Johns Hopkins Hospital Reports* **18**: 323.

Buller, A.J., Eccles, J.C., Eccles, R.M. 1960 Interaction between motor-neurones and muscles in respect of the characteristic speeds of their responses. *J. Physiol.* **150**: 417.

Buller, A.J., Eccles, J.C., Eccles, R.M. 1960 Differentiation of fast and slow muscles in the cat hind limb. *J. Physiol.* **150**: 399-416.

Burke, R.E., Rudomin, P. & Zajac, III, F.E. 1970 Catch property in single mammalian motor units. *Science* **168**: 122-124.

Burke, R.E., Rudomin, P. & Zajac, III, F.E. 1976 The effect of activation history on tension production by individual muscle units. *Brain Res.* **109**: 515-529.

Burke, R.E. 1967 Motor unit types of cat triceps surae muscle. *J. Physiol.* **193**: 141-160.

Burke, R.E. 1968 Firing patterns of gastrocnemius motor units in the decerebrate cat. *J. Physiol.* **196**: 631-654.

Butler, K.C., Maher, T.R., Borovetz, H.S., Kormos, R.L., Antaki, J.F., Kameneva, M., Griffith, B.P., Zerbe, T., Schaffer, F.D. 1992 Development of an axial flow blood pump LVAS. *ASAIO Journal* **38**: M296-M300.

Caplan, A.L. 1985 Ethical issues raised by research involving xenografts. *JAMA* **254**: 3339-43.

Carpentier, A.C. & Chachques, J.C. 1985 Myocardial substitution with a stimulated skeletal muscle: first successful clinical case. *The Lancet* **1**: 1267.

Carpentier, A. & Chachques, J.C. 1985 Myocardial substitution with a stimulated skeletal muscle: first successful clinical case. *The Lancet* **1**: 1267.

Carpentier, A. & Chachques, J.C. 1991 Clinical dynamic cardiomyoplasty: method and outcome. *Sem. Thorac. Cardiovasc. Surg.* **3**: 136-139.

Carraro, U. (ed) 1988 *Sarcomeric and Non-Sarcomeric Muscles: Basic and Applied Research. Prospects for the 90's.* Padova, Italy, Unipress, Padova.

Carraro, U. 1989 Gel elettroforesi bidimensionale sec. O'Farrell, in Carraro, U. e Dalla Libera, L. (eds): *Elettroforesi e HPLC di Biopolimeri e loro Frammenti.* Padova, Italia, Unipress, Padova, pp. 101-103.

Celio, M.R. & Heizmann, C.W. 1982 Calcium-binding parvalbumin is associated with fast contracting fibres. *Nature* (Lond.) **201**: 535-539.

Celio, M.R. & Heizmann, C.W. 1982 Calcium-binding protein parvalbumin is associated with fast contracting fibres. *Nature* (Lond.) **201**: 535-539.

Chachques, J.C., Carpentier, A. et al. 1990 Dynamic aortomyoplasty to assist left ventricular failure. *Ann. Thorac. Surg.* **49**: 225.

Chachques, J.C., Mitz, V., Hero, M., Arhan, P., Gallix, P., Fontaliran, F. & Vilain, R. 1986a Experimental cardiomyoplasty using the latissimus dorsi muscle flap. *J. Cardiovasc. Surg.* **26**: 457- 462.

Chachques, J.C., Grandjean, P.A. & Carpentier, A. 1986b Dynamic cardiomyoplasty: experimental cardiac wall replacement with a stimulated skeletal muscle. In R.C.-J.

Chiu (ed): *Biomechanical Cardiac Assist.* Mount Kisco, NY, Futura Publishing Co., pp. 59-84.

Chachques, J.C., Grandjean, P.A. & Carpentier, A. 1989 Latissimus dorsi cardiomyoplasty. *Ann. Thorac. Surg.* **47**: 600-604.

Chachques, J.C., Grandjean, P.A. & Carpentier, A. 1991 Patient management and clinical follow-up after cardiomyoplasty. *J. Cardiac. Surg.* **6**: 89-99.

Chagas, A.C.P., Moreira, L.F.P., da Luz, P.L., Camarano, G.P. Leirner, A., Stolf, N.A.G., Jatene, A.D. 1989 Stimulated preconditioned skeletal muscle cardiomyoplasty. An effective means of cardiac assist. *Circulation* **80** (suppl. III): III-202 - III-208.

Chi, M.M-Y., Hintz, C.S., Henriksson, J., Salmons, S., Hellendahl, R.P., Park, J.L., Nemeth, P.M., Lowry, O.H. 1986 Chronic stimulation of mammalian muscle: Enzyme changes in individual fibers. *Am. J. Physiol.* **251**: C633-C642.

Chiu, R.C.-J., Odim, J.N.K., Burgess, J. 1993 Responses to dynamic cardiomyplasty in idiopathic dialted cardiomyopathy. *Am. J. Cardiol.* **72**: 475-9.

Clark, B.J., Acker, M.A., McCully, K., Subramanian, H.V., Hammond, R.L., Salmons, S., Chance, B. & Stephenson, L.W. 1988 In vivo 13P-NMR spectroscopy of chronically stimulated canine skeletal muscle. *Am. J. Physiol.* **254**(*Cell Physiol* **23**): C258-C266.

Cody, R.J. 1988 Do positive inotropic agents adversely affect the survival of patients with chronic congestive heart failure? *J. Am. Coll. Cardiol.* **12**: 559-561.

Cohn, J.N., Archibald, D.G., Ziesche, S., **et al.** 1986 Effect of vasodilator therapy on mortality in chronic congestive heart failure. Results of VA Cooperative Study. *N. Eng. J. Med.* **314**: 547-1552.

Cohn, J.N. 1988 Current therapy of the failing heart. *Circulation* **78**: 1099-1107.

Cohn, P.F., Gorlin, R., Cohn, L.H., Collins, Jr, J.J. 1974 Left ventricular ejection fraction as a prognostic guide in surgical treatment of coronary and valvular heart disease. *Am. J. Cardiol.* **34**: 136-141.

Council on Scientific Affairs. 1985 Council Report - Xenografts: review of the literature and current status. *JAMA* **254**: 3353-57.

Crow, M.T. & Kushmerick, M.J. 1982 Chemical energetics of slow- and fast-twitch muscles of the mouse. *J. Gen. Physiol.* **79**: 147-166.

Cummings, D.V.E., Pattison, C.W., Yacoub, M.H. 1990 Autologous skeletal muscle and cardiac assistance. In: Yacoub M.H. (ed): *Annual of Cardiac Surgery.* London, UK, Current Science: **75**.

Curtin, N. A. & Woledge, R.C. 1988 Power and force-velocity relationship of live fibres from white myotomal muscle of the dogfish, *Scyliorhinus canicula*. *J. exp. Biol.* **140**: 187-197.

Cybulski, G., Penn, R., Jaegar, R. 1984 Lower extremity functional neuromuscular stimulation in cases of spianl cord injury. *Nuerosurgery* **15** (1): 132-146.

Davis, R., Kudzma, J., Gray. E., Engle, H., Ryan, T. 1984 Graded clinical effects in spastic cerebral palsy groups following cerebellar stimulation. In Davis, R., Bloedel, J.R. (eds.) *Cerebellar Stimulation for Spasticity and Seizures*, Boca Baton, Florida, CRC Press, Inc., pp. 233-239.

Davis, R. & Emmonds, S.E. 1992 Cerebellar stimulation for seizure control: 17-year study. *Stereotact. Funct. Neurosurg.* **58**: 200-208.

De Jesus, F.R. 1931 Breve consideraciones sobre un case de herida penetrnate del corazon. *Bol. Asoc. Med. Puerto Rico* **23**:380-382.

DeVries, W.C., Anderson, J.L., Joyce, L.D., Anderson, F.L., Hammond, E.H., Jarvik, R.K., Kolff, W.J. 1984 Clinical use of the total artificial heart. *N. Engl. J. Med.* **310**: 273-8.

Dewar, M.L., Drinkwater, D.C., Wittnich, C., Chiu, R.C. 1984 Synchronously stimulated skeletal muscle graft for myocardial repair. *J. Thorac. Cardiovasc. Surg.* **87**: 325-331.

Dubowitz, W. 1967 Cross-innervated mammalian skeletal muscle: Histochemical, physiological and biochemical observations. *J. Physiol.* **193**: 481-496.

Edman, K.A.P., Mulieri, L.A., Scubon-Mulieri, B. 1976 Non-hyperbolic force-velocity relationship in single muscle fibres. *Acta Physiol. Scand.* **98**: 143-156.

Eisenberg, B.R., Brown, J.M.C., Salmons, S. 1984 Restoration of fast muscle characteristics following cessation of chronic stimulation. *Cell Tissue Res.* **238**: 221-230.

Eisenberg, B.R. & Salmons, S. 1981 The reorganisation of subcellular structure in muscle undergoing fast-to-slow type transformation: a stereological study. *Cell Tiss. Res.* **220**: 449-471.

El Oakley, R.M. & Jarvis, J.C. 1994 Cardiomyoplasty: a critical review of experimental and clinical results. *Circulation* **90**: 2085-2090.

Engel, W.K. 1962 The essentiality of histo- and cytochemical studies of skeletal muscle in the investigation of neuromuscular disease. *Neurology* (Minneapolis) **12**: 778.

Evans, R.W., Manninen, D.L., Garrison, L.P., Maier, A.M. 1986 Donor availability as the primary determination of the future of heart transplantation. *JAMA* **255** (14): 1892-1896.

Fales, J.T., Lilienthal, J.R., Talbot, S.A., Zierler, K.L. 1958 A pneumatic isotonic lever system for dog skeletal muscle. *J. Appl. Physiol.* **13**: 307-308.

Faulker, J.A., Zerba, E., Brooks, S.V. 1990 Muscle temperature of mammals: cooling impairs most functional properties. *Am. J. Physiol.* **259** (Regulatory Integrative Comp. Physiol. 28): R259-R265.

Feigl, E.O & Fry, D.L. 1964 Myocardial thickness during the cardiac cycle. *Circ. Res.* **14**: 541-45.

Fenn, W.O. & Marsh, B.S. 1935 Muscular force at different speeds of shortening. *J. Physiol. Lond.* **85**: 277-297.

Ferguson, A.S., Stone, H.E., Roessmann, U., Burke, M., Tisdale, E., Mortimer, J.T. 1989 Muscle plasticity: comparison of a 30-Hz burst with 10-Hz continuous stimulation. *J. Appl. Physiol.* **66**: 1143-1151.

Ford, L.E. 1976 Heart size. *Circ. Res.* **39**: 297-303.

Fox, S.I. 1993 *Human Physiology*. 4th Edition, Wm. C. Brown Publishers, Dubuque, USA, pp 370-400.

Franciosca, J.A., Wilen, M., Ziesche, S., Cohn, J.N. 1983 Survival in men with severe chronic left ventricular failure due to either coronary heart disease or idiopathic dilated cardiomyopathy. *Am. J. Cardiol.* **51**: 831-836.

Frey, M., Thoma, H., Gruber, H., Stöhr, H., Havel, M. 1986 The chronically stimulated psoas muscle as an energy source for artificial organs: an experimental study in sheep. In Chiu RC-J., ed. *Biomechanical Cardiac Assist. Cardiomyoplasty and Muscle-powered Devices*. Mount Kisco, New York: Futura Publishing Company, pp. 179-91.

Fuchs, R.M., Brin, K.P., Brinker, J.A., Guzman, P.A., Heuser, R.R., Yin, F.C.P. 1983 Augmentation of regional coronary blood flow by intra-aortic balloon counterpulsation in patients with unstable angina. *Circulation* **68**: 117-123.

Furberg, C.D. & Yusuf, S. 1985 Effect of vasodilators on survival in congestive heart failure. *Am. J. Cardiol.* **55**: 1109-1115.

Gaasch, W.H. 1979 Left ventricular radius to wall thickness ratio. *Am. J. Cardiol.* **43**: 1189-94.

Gaasch, W.H. 1994 Diagnosis and treatment of heart failure based on left ventricular systolic or diastolic dysfunction. *JAMA* **271**: 1276-80.

Geddes, L.A., Badylak, S.F., Wessale, J.L., **et al.** 1990 The use of electrically stimulated muscle to pump blood. *Pace* **13**: 344-362.

Geddes, L.A., Badylak, S.F., Tacker, W.A., Janas, W. 1992 Output power and metabolic input power of skeletal muscle contracting linearly to compress a pouch in a mock circulatory system. *J. Thorac. Cardiovasc. Surg.* **104**: 1435-42.

Geddes, L.A. & Badylak, S.F. 1991 Power capability of skeletal muscle to pump blood. *Am. Soc. Artif. Org. Trans.* **37**: 19-23.

Gewirtz, H., Ohley, W., Williams, D.O., Sun, Y., Most, A.S. 1982 Effect of intraaortic balloon counterpulsation on regional myocardial blood flow and oxygen consumption in the presence of coronary artery stenosis: observations in an awake animal model. *Am. J. Cardiol.* **50**: 829-837.

Giometti, C.S. 1981 Muscle protein analysis by two-dimensional gel electrophoresis. *CRC Crit. Rev. Clin. Lab. Sci.* **18**: 79-109.

Glenn, W.W.L., Hogan, J.F. & Phelps, M.L. 1980 Ventilatory support of the quadriplegic patient with respiratory paralysis by diaphragm pacing. *Surgical Clinics N. America* **60**: 1055-1078.

Golldnick, P.D. & King, D.W. 1969 Effect of exercise and training on mitochondria of rat skeletal muscle. *Am. J. Physiol.* **216**: 1502-1509.

Gollnick, P.D., Timson, B.F., More, R.L., Riedy, M. 1981 Muscular enlargement and number of fibres in skeletal muscles of rats. *J. Appl. Physiol.* **50**: 936-43.

Grandjean, P.A., Austin, L., Chan, S. **et al.** 1991 Dynamic cardiomyoplasty: clinical follow-up results. *J. Cardiac Surg.* **6**: 80-88.

Grandjean, P.A., Leinders, R., Bourgeois, I.M. 1991 Implantable stimulation systems for systolic and diastolic biomechanical cardiac assist. *Sem. Thoracic Cardiovasc. Surg.* **3**: 119-123.

Green, H.J., Klug, G.A., Reichmann, H., Seedorf, U., Wiehrer, W., Pette, D. 1984 Exercise-induced fibre type transitions with regard to myosin, parvalbumin, and sarcoplasmic reticulum in muscles of the rat. *Pflügers Arch.* **400**: 432-438.

Griepp, R.B., Stinson, E.B., Bieber, C.P., Reitz, B.A., Copeland, J.G., Oyer, P.E., Shumway, N.E. 1977 Control of graft arteriosclerosis in human heart transplant recipients. *Surgery* **81**: 262-269.

Griffith, B.P., Hardesty, R.L., Trenti, A., Kormos, R.L., Bohnson, H.T. 1986 Cardiac transplantation: emerging from an experiment to a service. *Ann. Surg.* **204**: 308-314.

Griffith, B.P., Kormos, R.L., Hardesty, R.L., Armitage, J.M., Dummer, S.J. 1988 The artificial heart: infection related morbidity and its effect on transplantation. *Ann. Thorac. Surg.* **45**: 409-414.

Guldner, N.W., Tilmans, M.H.J., Dehaan, H., Ruck, K., Bressers, M., Messmer, B.J. 1991 Development and training of skeletal muscle ventricles with low preload. *J. Cardiac Surgery* **6**: 175-183.

Hagege, A.A., Desnos, M., Chachques, J.C., Carpentier, A., Fernandez, F., Fontaliran, F., Guerot, C. 1990 Preliminary report: follow-up after dyanmic cardiomyoplasty. *Lancet* **335**: 1122-4.

Hambrecht, F.T. & Reswick, J.B. (ed.) 1977 *Functional electrical stimulation: applications in neural prostheses*. New York: Marcel Dekker.

Hammond, R.L., Bridges, Jr., C.R., DiMeo, F., Stephenson, L.W. 1990 Performance of skeletal muscle ventricles: effects of ventricular chamber size. *J. Heart Transplant.* **9**: 252-57.

Handa, J. & Hoshiyama, N. 1988 FES for the control of upper extremities. *Medical Progress Technol.* **12**: 51-63.

Haselgrove, J.C & Reedy, M.K. Modeling rigor cross-bridge patterns in muscle. I. Initial studies of the rigor lattice of insect flight muscle. *Biophysics. J.* **24**: 713-28.

Hastillo, A. & Hess, M.L. 1993 Heart xenografting: a route not yet trod. *J. Heart Lung Transplant* **12**: 3-4.

Hearn, E.J. 1985 *Mechanics of Materials*, Vol. 1, 2nd edition, Oxford, Pergamon Press, Ltd.

Heilig, A., Seedorf, K., Seedorf, U., Pette, D. 1984 Transcriptional and translational control of myosin light chain expression in adult muscle. In: *Developmental Processes in Normal and Deceased Muscle*, Vol. 9. Basel: S. Karger, 1984, pp. 182-6.

Heilig, A. & Pette, D. 1983 Changes in transcriptional activity of chronically stimulated fast muscle. *FEBS Lett.* **151**: 211-214.

Heilmann, C., Müller, W., Pette, D. 1981 Correlation between ultrastructural and functional changes in sarcoplasmic reticulum during chronic stimulation of fast rabbit muscle. *J. Membrane Biol.* **59**: 143-149.

Heilmann, C. & Pette, D. 1979 Molecular transformations in sarcoplasmic reticulum of fast-twitch muscle by electrostimulation. *Eur. J. Biochem.* **93**: 437-446.

Hennig, R. & Lømo, T. 1985 Firing patterns of motor units in normal rats. *Nature* **314**: 164-166.

Henriksson, J., Nemeth, P.M., Borg, K., Salmons, S., Lowry, O.H. 1990 Fibre-type-specific enzyme activity profiles: A single fibre study of the effects of chronic stimulation on the rabbit fast-twitch tibialis anterior muscle. In: *The Dynamic State of Muscle Fibres*, Pette D. (ed.), Berlin: Walter de Gruyter, pp. 385-398.

Hester, Jr., T.R. & Bostwick, III, J. 1982 Poland's syndrome: correction with latissimus dorsi transposition. *Plastic Reconstructive Surg.* **69** (2): 226-233.

Hill, A.V. 1938 The heat of shortening and the dynamic constants of muscle. *Proc. Roy. Soc. B.* **126**: 136-195.

Hill, J.D. 1988 Bridge to cardiac transplantation. *Ann. Thorac. Surg.* **46**: 131-2.

Ho, K.L., Anderson, K.M., Kannel, W.B., Grossman, W., Levy, D. 1993 Survival after the onset of congestive heart failure in Framingham Heart Study subjects. *Circulation* **88**: 107-115.

Hooper, T.L. & Salmons, S. 1993 Skeletal muscle assistance in heart failure. *Cardiovasc. Res.* **27**, 1404-1406.

Hoppeler, H., Hudlická, O., Uhlmann, E. 1987 Relationship between mitochondria and oxygen consumption in isolated cat muscles. *J. Physiol.* **385**: 661-675.

Hudlická, O., Brown, M., Cotter, M., Smith, M., Vrbová, G. 1977 The effect of long-term stimulation of fast muscles on their blood flow, metabolism and ability to withstand fatigue. *Pflügers Arch.* **369**: 141-149.

Hudlická, O., Dodd, L., Renkin, E.M., Gray, S.D. 1982 Early changes in fiber profile and capillary density in long-term stimulated muscles. *Am. J. Physiol.* **243**: H528-H535.

Hudlická, O., Tyler, K.R., Srihari, T., Heilig, A., Pette, D. 1982 The effect of different patterns of long-term stimulation on contractile properties and myosin light chains in rabbit fast muscles. *Pflügers Arch.* **393**: 164-170.

Hudlická, O., Tyler, K.R., Wright, A.J.A, et al. 1984 Growth of capillaries in skeletal muscles. *Prog. Appl. Microcirc.* **5**: 44-61.

Hudlická, O. & Price, S. 1990 The role of blood flow and/or muscle hypoxia in capillary growth in chronically stimulated fast muscles. *Pflügers Arch.* **417**: 67-72.

Hudlická, O. & Tyler, K.R. 1984 The effect of long-term high-frequency stimulation on capillary density and fiber types in rabbit fast muscles. *J. Physiol.* **353**: 435-445.

Hulme, W.I. 1986 Construction of a functioning accessory myocardium. *Trans. South Surg. Assoc.* **79**: 200-202.

Hunter, W.C., Janicki, J.S., Weber, K.T., Noordergraaf, A. 1979 Flow-pulse response: a new method for the characterization of ventricular mechanics. *Am. J. Physiol.* **237**: H282-H292.

Huxley, A.F. & Niedergerke, R. 1954 Structural changes in muscle during contraction. *Nature* **173**: 971-973.

Huxley, A.F. & Simmons, R.M. 1971 Proposed mechanism of force generation in striated muscle. *Nature* **233**: 533-38.

Huxley, A.F. 1957 Muscle structure and theories of contraction. *Progress in Biophysics* **7**: 255-318.

Huxley, H.E. & Hanson, J. 1954 Changes in the cross-striations of muscle during contraction and stretch and their structural interpretation. *Nature* **173**: 973-976.

Huxley, H.E. 1960 Muscle cells. In *The Cell* (J.Brachet and A.E. Mirsky, eds.), **4**: 365-481. New York: Academic.

Imachi, K., Chinzei, T., Abe, Y., Mabuchi, K., Imanishi, K., Yonezawa, T., Kouno, A., Ono, T., Atsumi, K., Isoyama, T., Suzuki, A., Fujimasa, I. 1991 A new pulsatile total artificial heart using a single centrifugal pump. *ASAIO Trans.* **37**: M242-M243.

Imanishi, K., Imachi, K., Abe, Y., Chinzei, T., Mabuchi, K., Fujimasa, I., Atsumi, K., Sumo, K. 1989 Development of a new circulatory assist method with the combined effects of intra-aortic balloon pumping and counter pulsation. *ASAIO Trans.* **35**: 715-17.

Jaegar, R.J., Yarkony, G., Smith, R. 1989 Standing the spinal cord injured patient by electrical stimulation: refinement of a protocol for clinical use. *IEEE Trans. Biomed. Eng.* **36**(7).

Jaegar, R.J. 1992 Lower extremity applications of functional neuromuscular stimulation. Assist. Technol. 4 (1): 19-30.

Jansson, E., Sjödin, B., Tesch, P. 1978 Changes in muscle fibre type distribution in man after physical training: a sign of fibre type transformation? *Acta Physiol. Scand.* **104**: 235-237.

Jarvis, J.C., Brownson, C., Sutherland, H., Salmons, S. 1991b Comparison between the effects of continuous long-term stimulation of rabbit skeletal muscle at 2.5 Hz and 10 Hz. *BAM: Perspectives for the 90's.* (eds. U. Carraro & S. Salmons), pp. 109-113. Padova: Unipress.

Jarvis, J.C., Hitchings, D.J., Taylor, I., Sutherland, H., Kwende, M.M.N., Gilroy, S., Grainger, S.R.W., Salmons, S. 1993a Implantable stimulators that preserve skeletal muscle power for cardiac assistance. *Proc. Medical and Biological Implant Technology 93*, Coventry (UK).

Jarvis, J.C., Sutherland, H., Mayne, C.N, Gilroy, S.J. & Salmons, S. 1994 Contractile properties, fatigue resistance and myosin isoform composition of rabbit fast skeletal muscle transformed to a fast-oxidative state by long-term electrical stimulation at 2.5 Hz. *Am. J. Physiol.* (In press).

Jarvis, J.C., Mayne, C.N., Salmons, S. 1991c Basic studies on skeletal muscle for cardiac assist. *J. Cardiac Surg.* **6** (suppl.): 204-209.

Jarvis, J.C. 1992 Chronic electrical stimulation of skeletal muscles: power output and fatigue resistance. In: *Restoration of Walking for Paraplegics*, (eds. A. Pedotti & M. Ferrarin) pp. 45-50, Milan: Edizioni Pro Juventute. ISBN 88-85936-10-5.

Jarvis, J.C., Mokrusch, T., Mayne, C.N., Kwende, M.M.N., Gilroy, S.J., Sutherland, H., Salmons, S. 1993c Fast-to-slow fibre type conversion does occur in continuously stimulated rat hind-limb muscle. *J. Physiol.* **467**: 112P.

Jarvis, J.C., Sutherland, H., Kwende, M.M.N., Mayne, C.N. & Salmons, S. 1993b Relationship between working capacity and activation frequency of chronically stimulated skeletal muscle. In: *Proc. World Symposium on Cardiomyoplasty, Biomechanical Assist and Artificial Heart.* Paris: Futura (In press).

Jarvis, J.C., Sutherland, H., Mayne, C.N., Gilroy, S.J., Salmons, S. 1994 Contractile properties, fatigue resistance and myosin isoform composition of rabbit fast skeletal muscle transformed to a fast-oxidative state by long-term electrical stimulation at 2.5 Hz. Am. J. Physiol. (Accepted, subject to revision).

Jarvis, J.C. & Salmons, S. 1991a A family of neuromuscular stimulators with optical transcutaneous control. *J. Med. Eng. Technol.* **15**: 53-57.

Jarvis, J.C. & Salmons, S. 1991b An electrohydraulic apparatus for the measurement of static and dynamic properties of rabbit muscles. *J. Appl. Physiol.* **70**: 938-941.

Jarvis, J.C. 1991 The power-generating capacity of normal and conditioned skeletal muscle. In *Concerted Action HEART: Proc. Expert Meeting on Harnessing Skeletal Muscle Power for Cardiac Assistance* (ed. S. Salmons & J.C. Jarvis), pp 15-19. Liverpool, England.

Jarvis, J.C. 1993 Power production and working capacity of rabbit tibialis anterior muscles after chronic electrical stimulation at 10 Hz. *J. Physiol.* **470**: 157-169.

Jöbsis, F.F. & Duffield, J.C. 1967 Force, shortening and work in muscular contractions: relative contributions to overall energy utilization. *Science*, **156**: 1388-1392.

Johnston, I.A. 1991 Muscle action during locomotion: a comparative perspective. *J. exp. Biol.* **160**: 167-185.

Johnston, I.A. & Altringham, J. 1988 Muscle function in locomotion. *Nature* **335**: 767-8.

Jones, D.A & Round, J.M. 1990 *Skeletal Muscle in Health and Disease*. Manchester: Manchester University Press, ISBN 0-7190-3164-8.

Josephson, R.K. 1993 Contraction dynamics and power output of skeletal muscle. *Annu. Rev. Physiol.* **55**: 527-46.

Kantrowitz, A., Freed, P.S., Cardona, R.R., Gage, K., Marinescu, G.N., Westveld, A.H., Litch, B., Suzuki, A., Hayakawa, H., Takano, T., Rios, C.E., Rubenfire, M. 1992 Initial clinical trial of a closed loop, fully automatic intra-aortic balloon pump. *ASAIO Journal* **38**: M617-M621.

Kantrowitz, A. & Mckinnon, W. 1959 The experimental use of the diaphragm as an auxiliary myocardium. *Surg. Forum* **9**: 266-268.

Kantrowitz, A. 1960 Functioning autogenous muscle used as an auxiliary ventricle. *Trans. Am. Soc. Artif. Intern. Organs* **6**: 305-310.

Kao, R.L., Christlieb, I.Y., Magovern, G.J., Park, S.B., Magovern, Jr., G.J. 1990 The importance of skeletal muscle fiber orientation for dynamic cardiomyoplasty. *J. Thorac. Cardiovasc. Surg.* **99**: 134-40.

Kass, D.A., Baughman, K.L., Pak, P.H., Cho, P.W., Levin, H.R., Gardner, T.J., Halperin, H.R., Tsitlik, J.E., Acker, M.A. 1995 Reverse remodeling from

cardiomyoplasty in human heart failure: external constraint versus active assist. *Circulation* **91**: 2314-2318.

Keith, M.W., Peckham, P.H., Thrope. G.B., Bucket, J.R., Stroh, K.C., Menger, V. 1988 Functional neuromuscular stimulation neuroprosthesis for the tetraplegic hand. *Clin. Orth. Related Res.* **233**: 25-33.

Kernell, D., Eerbeek, O., Verhey, B.A., Donselaar, Y. 1987a Effects of physiological amounts of high- and low-rate chronic stimulation on fast-twitch muscle of the cat hindlimb. I. Speed- and force-related properties. *J. Nueophysiol.* **58**: 598-613.

Kernell, D., Eerbeek, O., Donselaar, Y. 1987b Effects of physiological amounts of high- and low-rate chronic stimulation on fast-twitch muscle of the cat hindlimb. II. Endurance-related properties. *J. Nueophysiol.* **58**: 614-627.

Kernell, D. & Eerbeek, O. 1991. Recovery after intense chronic stimulation: a physiological study of cat's fast muscle. *J. Appl. Physiol.* **70**: 1763-1769.

Klug, G., Wiehrer, W., Pette, D. 1983a Rapid reduction in parvalbumin concentration during chronic stimulation of rabbit fast twitch muscle. *FEBS Lett.* **152**: 180-2.

Klug, G., Wiehrer, W., Reichmann, H., Leberer, E., Pette, D. 1983b Relationships between early alterations in parvalbumins, sarcoplasmic reticulum and metabolic enzymes in chronically stimulated fast twitch muscle. *Pflügers Arch.* **399**: 280-284.

Kochamba, G., Desrosiers, C., Dewar, M., Chiu, R-C. 1988 The muscle-powered dual-chamber counterpulsator: rheologically superior implantable cardiac assist device. *Ann. Thorac. Surg.* **45**: 620-5.

Kralj, A.R. & Bajd, T. 1989 *Functional Electrical Stimulation: Standing and Walking After Spinal Cord Injury.* CRC Press.

Kress, M., Huxley, H.E., Faruqi, A.R., Hendrix, J. 1986 Structural changes during activation of frog muscle studied by time-resolved X-ray diffraction. *J. molec. Biol.* **188**: 325-342.

Kusaba, E., Schraut, W., Sawatani, S., Jaron, D., Freed, P. & Kantrowitz, A. 1973 A diaphragmatic graft for augmenting left ventricular function: a feasibility study. *Trans. Am. Soc. Artif. Intern. Organs* **19**: 251-257.

Kwende, M.M.N, Jarvis, J.C., Salmons, S. 1995 The input-output relationships of skeletal muscle. *Proc. Roy. Soc. B* (In press).

Laitung, J.K. & Peck, F. 1979 Shoulder function following the loss of latissimus dorsi muscle. *Br. J. Plast. Surg.* **32**: 275.

Lee, K.F., Dignan, R.J., Parnar, J.M., **et al.** 1991 Effects of dynamic cardiomyoplasty on left ventricular performance and myocardial mechanics in dilated cardiomyopathy. *J. Thorac. Cardiovasc. Surg.* **6**: 119-122.

Lericbe, R. & Fontaine, R. 1933 Essai experimental de traitement de certain infarctus du myocarde et de l'aneuvrisme du coeur par une greffe de muscle strie. *Bull. Soc. Nat. Chir.* **59**: 229-232.

Liao, Y., Cooper, R.S., Ghali, J.K., Szocka, A. 1992 Survival rates with coronary artery disease for black women compared with black men. *JAMA.* **268**: 1867-71.

Liberson, W. et al. 1961 Functional electrotherapy: stimulation of the peroneal nerve synchronized with the swing phase of gait of hemiplegic patients. *Arch. Phys. Med. Rehab.* **42**: 101-105.

Loisance, D.Y. (ed.) 1990 *Intraventricular Blood Pumps.* Commission of the European Communities, pp 5-9, ISBN 90-365-0410-4.

Lorenzini: in Dubowitz, V., Brooke, M.H., Neville, H.E. (eds.) 1973 *Muscle Biopsy: A Modern Approach.* Philadelphia, PA, Saunders, p 44.

Lu, H., Fietsam, R., Hammond, R.L., Nakajima, H., Mocek, F., Thomas, G.A., Ruggiero, R., Nakajima, H., Golson, M., Stephenson, L.W. 1993 Skeletal muscle ventricles: left ventricular apex to aorta configuartion. *Ann. Thorac. Surg.* **55**: 78-85.

Mabuchi, K., Szvetko, D., Pinter, K., Sréter, F.A. 1982 Type IIB to IIA fiber transformation in intermittently stimulated rabbit muscles. *Am. J. Physiol.* **242**: C373-C381.

MacDonald, R.G., Hill, J.A., Feldman, R.L. 1987 Failure of intraaortic balloon counterpulsation to augment distal coronary perfusion pressure during percutaneous transluminal coronary angioplasty. *Am. J. Cardiol.* **59**: 359-61.

Magovern, G.J. 1991 Introduction to the history and development of skeletal muscle plasticity and its clinical application to cardiomyoplasty and skeletal muscle ventricle. *Sem. Thorac. Cardiovasc. Surg.* **3**: 95-97.

Magovern, J.A., Magovern, G.J., Maher, T.D., Benckart, D.H., Park, S.B., Christlieb, I.Y., Magovern, Jr, G.J. 1993 Operation for congestive heart failure: transplantation, coronary artery bypass, and cardiomyoplasty. *Ann. Thorac. Surg.* **56**: 418-25.

Magovern, Jr., G.J. 1985 Case presentation at annual contractor's meeting (Round table discussion). National Institutes of Health, Bethesda, MD, December 15-18.

Mannion, J.D., Bitto, T., Hammond, R.L., Rubinstein, N.A., Stephenson, L.W. 1986 Histochemical and fatigue characteristics of conditioned canine latissimus dorsi muscle. *Circ. Res.* **58**: 298-304.

Mannion, J.D., Hammond, R.L., Stephenson, L.W. 1986 Hydraulic pouches of canine latissimus dorsi: potential for left ventricular assist. *J. Thorac. Cardiovasc. Surg.* **91**: 534-544.

Mannion, J.D., Velchik, M., Hammond, R.L., Alavi, A., Mackler, T., Daukett, S., Staum, M., Hurwitz, S., Brown, W. & Stephenson, L.W. 1989 Effects of collateral blood

vessel litigation and electrical conditioning on blood flow in dog latissimus dorsi muscle. *J. Surg. Res.* **47**: 332-340.

Marsden, C.D., Meadows, J.C & Merton, P.A. 1971 Isolated single motor units in human muscle and their rate of discharge during maximal voluntary effort. *J. Physiol.* **217**: 12-13P.

Marsden, C.D., Meadows, J.C & Merton, P.A. 1976 Fatigue in human muscle in relation to the number and frequency of motor impulses. *J. Physiol.* **258**: 94-95P.

Marsden, C.D., Meadows, J.C. & Merton, P.A. 1983 "Muscular wisdom" that minimises fatigue during prolonged effort in man: peak rates of motoneuron discharge and slowing of discharge during fatigue. In *Advances in neurology 39: motor control mechanisms in health and disease*. (ed. J.E. Desmedt), pp 169-211. New York: Raven Press.

Marsolais, E.B., Kobetic, R. 1988 Development of a practical electrical stimulation system for restoring gait in the paralysed patient. *Clin. Orth. Related Res.***233**: 64-74.

Mathes, S.J. & Nahai, F. 1982 *Clinical Applications for Muscle and Musculocutaneous Flaps*. St Loius, MO, Mosby.

Maxwell, D.J., Granat, M.H. & Baxendale, R.H. 1993 Novel stimulation strategies for the recruitment of paralysed muscle. In *Concerted Action RAFT: Proc. Muscular Components in Functional Electrical Stimulation* (ed. J. Edwards), pp. 37-43. Salford, UK: University College Salford.

Mayne, C.N., Sutherland, H., Jarvis, J.C., Gilroy, S.J., Craven, A.J. and Salmons, S. 1994 Patterns of histochemical and metabolic transformation in rabbit fast skeletal muscle transformed to a fast-oxidative state by long-term electrical stimulation at 2.5 Hz. *Am. J. Physiol.* (In press).

McCraw, J.B. & Arnold, P.J. 1986 *McCraw and Arnold's Atlas of Muscle and Musculocutaneous Flaps*. Norfolk, VA, Hampton.

McKay, R.G., Preffer, M.A., Pasternak, R.L. 1986 Left ventricular remodelling after myocardial infarct: a corollary to infarct expansion. *Circulation* **74**: 693-702.

McMahon, T.A. 1984 Muscles, Reflexes, and Locomotion.

McManus, R.P, Kinney, T., Komorowski, R., Hunter, J. 1991 Reversibility of cardiac xenograft rejection in primates. *J. Heart Lung Transplant.* **10**: 567-597.

McManus, R.P., Kinney, T., Komorowski, R., Hunter, J. 1991 Reversibility of cardiac xenograft rejection in primates. *J. Heart Lung Transplant* **10**: 567-597.

Merhige, M.E., Smalling, R.W., Cassidy, D., Barret, R., Wise, G., Short, J., Wampler, R.K. 1989 Effect of hemopump left ventricular assist device on regional myocardial perfusion and function: reduction of ischemia during coronary occlusion. *Circulation* **80** (suppl. III): III-159-III-166.

Miller, L.J., Peckham, P.H. & Keith, M.W. 1989 Elbow extension in the C5 quadriplegic using functional neuromuscular stimulation. *IEE Trans. Biomed. Eng.* **37** (7): 771-780.

Minsky, M. 1994 Will robots inherit the earth? *Scientific American* pp: 87-91, October-94.

Mohan, R., Walter, P.J., Vandermast, M., Amsel, B.J., Vanaken, D. 1992 Isolated coronary artery bypass grafting in patients 75 years of age and older: is age per se a contraindication? *Thorac. Cardiovasc. Surg.* **40**: 365-70.

Moriarty, T.F. 1980 The Law of Lapalce: its limitations as a relation for diastolic pressure, volume, or wall stress of the left ventricle. *Circ. Res.* **46**: 321-331.

Moreira, L.F.P., Stolf, N.A.G., Bocchi, E.A., **et al.** 1990 Latissimus dorsi cardiomyoplasty in the treatment of patients with dilated cardiomyopathy. Circulation **82**: IV257-63.

Myrhage, R. & Hudlická, O. 1978 Capillary growth in chronically stimulated adult skeletal muscle as studied by intravital microscopy and histological methods in rabbits and rats. *Microvasc. Res.* **16**: 73-90.

Nakamura, K. & Glenn, W.W.L. 1964 Graft of the diaphragm as a functioning substitute for the myocardium. *J. Surg. Res.* **4**: 435-439.

Nanas, J.N., Poyiadjis, A., Chatitos, C., Nana, S.N., Kontoyiannis, D., Anastasiou-Nana, M., Alevizakos, N., Voudris, V., Moulopoulos, S.D. 1990 Additional salutary hemodynamic effects of the combined use of the paraaortic counterpulsation device and the intraaortic balloon pump versus the paraaortic counterpulsation device alone. *ASAIO Trans.* **36**: M505-M509.

Nathan, R.H. 1989 An FNS-based system for generating upper limb function in the C4 quadriplegic. *Med. Biol. Eng. Comput.* **27**: 549-556.

Norris, R.M., Caughy, D.E., Mercer, C.J., Neeming, L.W., Scott, P.J. 1970 Coronary prognostic index for predicting survival after recovery from acute myocardial infarction. *Lancet* **2**: 485-488.

Oda, T., Miyamoto, A.T., Ban, T., Okamoto, Y. 1993 Skeletal muscle-powered ventricle: effect of size and configuration on ventricular function. *J. Thorac. Cardiovasc. Surg.* **105**: 68-77.

Olivari, N. 1976 The latissimus dorsi flap. *Br. J. Plastic Surg.* **29**: 126-128.

Ommen, van, G.V.A. 1990 Hemopump versus intra-aortic balloon pump (IABP). In Loisance, D.Y. (ed.), *Concerted Action HEART. Intravascular Blood Pumps,pp* 13-18, ISBN 90-365-0410-4.

Orie, J.E. 1991 Dynamic cardiomyoplasty - possible alternative treatment of congestive heart failure. *Seminars Thorac. Cardiovasc. Surg.* **3**: 98-100.

Orime, Y., Takatani, S., Tasia, K., Ohara, Y., Naito, K., Mizuguchi, K., Meier, D., Wernicke, J.T., Damm, G., Glueck, J., Noon, G.P., Nosé, Y. 1994 The Baylor total artificial heart: flow visualization studies. *ASAIO Journal* **40**: M499-M505.

Pattison, C.W., Cumming, D.V.E., Williamson, A., Clayton-Jones, D.G., Dunn, M.J., Goldspink, G., Yacoub, M. 1991 Aortic counterpulsation for up to 28 days with an autologous latissimus dorsi in sheep. *J. Thorac. Cardiovasc. Surg.* **102**: 766-73.

Peckham, P.H., Keith, M.W., Freehaffer, A.A. 1988 Restoration of functional control by electrical stimulation in the upper extremity of the quadriplegic patient. *J. Bone Joint Surg.* **70-A**: 144-148.

Peckham, P.H. & Keith, M.W. 1992 Motor prostheses for restoration of upper extremity function. In: *Nueral Prostheses: Replacing Motor Function After Disease or Disability* (eds. R.B. Stein, P.H. Peckham & D.P. Popovic), pp. 162-187. Oxford University Press.

Peckham, P.H. 1987 Functional electrical stimulation: current status and future prospects of applications to the neuromuscular system in SCI. *Paraplegia* **25**: 279-288.

Pennington, D.G., Codd, J.E., Merjavy, J.P., et al. 1983 The expanded use of ventricular bypass systems for severe cardiac failure and as a bridge to cardiac transplantation. *Heart Transplant* **3**: 38-46.

Petrofsky, J.S. & Phillips, C.A. 1981 The influence of temperature, initial length and electrical activity on the force-velocity relationship of the medial gastrocnemius muscle of the cat. J. Biomechanics **14**: 297-306.

Petrovsky, B.V. 1961 The use of the diaphragm grafts for plastic operations in thoracic surgery. *J. Thorac. Cardiovasc. Surg.* **41**: 348-355.

Pette, D. 1986 Adaptability of skeletal muscle to long-term use. In: *Sports Medicine for the Mature Athlete*. J.R. Sutton, R.M. Brock (eds), Benchmark Press, Indianapolis.

Pette, D. 1991 Effects of chronic electrostimulation on muscle gene expression. *Sem. Thorac. Cardiovasc. Surg.* **3**: 101-105.

Pette, D., Müller, W., Leisner, E., Vrbová, G. 1976 Time dependent effects on contractile properties, fibre population, myosin light chains and enzymes of energy metabolism in intermittently and continuously stimulated fast-twitch muscles of the rabbit. *Pflügers Arch.* **364**: 103-112.

Pette, D., Ramirez, B.U., Müller, W., Simon, R., Exner, G.U., Hildebrand, R. 1975 Influence of intermittent long-term stimulation on contractile, histochemical and metabolic properties of fibre population in fast and slow rabbit muscles. *Pflügers Arch.* **361**: 1-7.

Pette, D., Smith, M.E., Staudte, H.W., Vrbová, G. 1973 Effects of long-term stimulation on some contractile and metabolic characteristics of fast rabbit muscles. *Pflügers Arch* **338**: 257-272.

Pette, D. & Heilmann, C. 1977 Transformation of morphological, functional and metabolic properties of fast-twitch muscle as induced by long-term electrical stimulation. *Basic Res. Cardiol.* **72**: 247-253.

Pette, D. & Vrbová, G. 1985 Neural control of phenotypic expression in mammalian muscle fibers. *Musc. Nerve* **8**: 676-89.

Pette, D. 1984 Activity-induced fast to slow transitions in mammalian muscle. *Med. Sci. Sports Exerc.* **16**: 517-528.

Pfeffer, M.A., Pfeffer, J.M., Lamas, G.A. 1993 Development and prevention of congestive heart failure following myocardial infarction. *Circulation* **87** (suppl. IV): IV-120-IV-125.

Pfeffer, M.A. & Pfeffer, J.M. 1987 Ventricular enlargement and reduced survival after myocardial infarct. *Circulation* **75**: 93-97.

Pierson, R.N., 3rd, Tew, D.N., Konig, W.K., Dunning, J.J., White, D.J., Walwork, J. 1994 Pig lungs are susceptible to hyperacute rejection by human blood in a working ex vivo heart-lung model. *Transplant Proc.* **26**: 1318.

Pinto, J.G. & Fung, Y.C. 1973 Mechanical properties of the heart muscle in the passive state. *J. Biomech.* **6**: 597-616.

Pluskal, M.G. & Sréter, F.A. 1983 Correlation between protein phenotype and gene expression in adult rabbit fast twitch muscles undergoing a fast to slow fiber transformation in response to electrical stimulation in vivo. *Biochem Biophys. Res. Commun.* **113**: 325-331.

Pochettino, A., Anderson, D.R., Hammond, R.L., Salmons, S., Stephenson, L.W. 1991 Skeletal muscle ventricles. *Seminars Thorac. Cardiovasc. Surg.* **3**: 154-9.

Pryor, D.B., Harrell, Jr, F.E., Rankin, J.S., Lee, K.E., Muhlbaier, L.H., Oldham, H.N., Hlatky, M.A., Mark, D.B., Reves, J.G., Califf, R.M. 1987 The changing survival benefits of coronary revascularization over time. *Circulation* **76** (suppl. V): V-13-V-21.

Ramirez, B.U & Pette, D. 1974 Effects of long-term electrical stimulation on sarcoplasmic reticulum of fast rabbit muscle. *FEBS Lett.* **49**: 188-190.

Ranatunga, K.W. 1982 Temperature-dependence of shortening velocity and rate of isometric tension development in rat skeletal muscle. *J. Physiol.* **329**: 465-483.

Ranvier, L. 1873 Proprieties et structures different des muscle rouge et des muscles blancs. *Compt. Rend.* **77**: 1030.

Reichmann, H., Hoppeler, E., Mathieu-Costello, D. et al. 1985 Biochemical and ultrastructural changes of skeletal muscle mitochondria after chronic electrical stimulation in rabbits. *Pflügers Arch.* **404**: 1-9.

Reul, H. 1990 Hydromechanical principles of axial pumps. In Loisance, D.Y. (ed.), *Concerted Action HEART. Intravascular Blood Pumps.* pp 19-27, ISBN 90-365-0410-4.

Rubinstein, N., Mabuchi, K., Pepe, F., Salmons, S., Gergely, J., Sréter, F.A. 1978 Use of type-specific antimyosins to demonstrate the transformation of individual fibers in chronically stimulated rabbit fast muscles. *J. Cell Biol.* **79**: 252-261.

Ruëgg, J.C. 1987 Excitation-contraction coupling in fast- and slow-twitch muscle fibers. (Review), *Int. J. Sports Med.* **8**: 360-364.

Ruëgg, J.C. 1992 *Calcium in Muscle Contraction*, 2nd ed., Springer-Verlag, Berlin Heidelberg, Germany. pp 5. ISBN 0-387-55544-7.

Salmons, S. 1990 *Harnessing Skeletal Muscle Power for Cardiac Assist.* (ed. S. Salmons & J.C. Jarvis). Concerted Action, HEART, ISBN 90-365-0412-0.

Salmons, S., Gale, D.R., Sréter, F.A. 1978 Ultrastructural aspects of the transformation of muscle fibre type by long term stimulation: changes in Z discs and mitochondria. *J. Anat.* **127**: 17-31.

Salmons, S. & Henriksson, J. 1981 The adaptive response of skeletal muscle to increased use. *Muscle & Nerve* **4**: 94-105.

Salmons, S. & Jarvis, J.C. 1990a Cardiomyoplasty: the basic issues. *Cardiac Chron.* **4**: 1-7.

Salmons, S. & Jarvis, J.C. 1990b The working capacity of skeletal muscle transformed for use in cardiac assist role. In: Chiu, R.C-J., Bourgeois, I.M. (eds.) *Transformed Muscle for Cardiac Assist and Repair,* pp 89-104. Futura Publishing Company, Mount Kisco, NY.

Salmons, S. & Jarvis, J.C. 1991a Cardiomyoplasty: a look at the fundamentals. In *Cardiomyoplasty*, Carpentier, A., Chachques, J-C., Grandjean, P. (eds.) pp. 3-17, Futura Publishing Company, Mount Kisco, NY.

Salmons, S. & Jarvis, J.C. (eds.) 1991b *Harnessing Skeletal Muscle Power for Cardiac Assistance.* Commission of the European Communities, 123pp, ISBN 90-365-0412-0.

Salmons, S. & Jarvis, J.C. 1992 Cardiac assistance from skeletal muscle: a critical appraisal of the various approaches. *Br Heart J.* **68**: 333-8.

Salmons, S. & Jarvis, J.C. 1995 Educating skeletal muscle to do cardiac work. In: *Mechanical Circulatory Support* (eds. T. Lewis & T.R. Graham) pp. 259-262. Edward Arnold: London.

Salmons, P.H & Salmons, S. 1992 Psychological costs of high-tech heart surgery. *Br. J. Hospital Med.* **48**: 707-709.

Salmons, S. & Sréter, F.A. 1976 Significance of impulse activity in the transformation of skeletal muscle type. *Nature* **263**: 30-34.

Salmons, S. & Stephenson, L.W. 1989 Adaptive capacity of skeletal muscle and its therapeutic applications. In: *Neuromuscular Stimulation. Basic Concepts and Clinical Implications*, Rose, F.C., Jones, R., Vrbová, G. (eds.), New York: Demos, pp. 203-215.

Salmons, S. & Vrbová, G. 1967 Changes in the speed of mammalian fast muscle following long-term stimulation. *J. Physiol.* **192**: 39-40P.

Salmons, S. & Vrbová, G. 1969 The influence of activity on some contractile characteristics of mammalian fast and slow muscles. *J. Physiol.* **201**: 535-549.

Salmons, S. 1971 Skeletal Muscle - an adptive machine? *British Science News* (Spectrum) **83**: 2-4.

Salmons, S. 1980a Functional adaptation in skeletal muscle. *Trends in Neurosciences* 3: 134-137.

Salmons, S. 1980b The response of skeletal muscle to different patterns of use - some new developments and concepts. In: *Plasticity of Muscle*, Pette, D. (ed.), Berlin: Walter de Gruyter, pp 387-399.

Salmons, S. 1987 The importance of the adaptive properties of skeletal muscle in long-term electrophrenic stimulation of the diaphragm. *Acta Univers Tamperensis*, Ser B 30: 61-74. ISSN 0355-5232.

Salmons, S. 1990 On the reversibility of stimulation-induced muscle transformation. In *Proceedings of the International Symposium*, October 1-6, 1989, Konstanz, Germany. (ed. D. Pette). Berlin: Walter de Gruyter.

Schiaffano, S., Hanzlikova, V. Pierobaon, S. 1976 Relations between structure and function in rat skeletal fibers. *J. Cell Biol.* **47**: 107-119.

Schreuder, J.J., van der Veen, F.H., van der Velde, E.T., Delahaye, F., Alfieri, O., Jegaden, O., Lorusso, R., Jansen, J.R.C., Van Ommen, V., Finet, G., Wellens, H.J.J. 1995 Beat-to-beat analysis of left ventricular pressure-volume and stroke volume by conductance catheter and aortic modelflow in cardiomyoplasty patients. *Circulation* **91**: 2010-2017.

Schroeder, J.J. & Hunt, S. 1987 Cardiac transplantation, update 1987. *JAMA* **258**: 3142-3145.

Seedorf, K., Seerdorf, U., Pette, D. 1983 Coordinate expression of of alkali and DTNB myosin light chains during transformation of rabbit fast muscle by chronic stimulation. *FEBS Lett.* **158**: 321-324.

Shaver, J.A. (ed.) 1988 *Cardiomyopathies, Clinical Presentation, Differential Diagnosis and Management*. Philadelphia, PA, Davis.

Shiono, M., Takatani, S., Sasaki, T., Orime, Y., Swenson, C.A., Minato, N., Ohara, Y., Noon, G.P., Nosé, Y., DeBakey, M.E. 1992 Baylor multipurpose circulatory support system for short- and long-term use. *ASAIO Journal* **38**: M301-M305.

Shroff, S.G., Janicki, J.S., Weber, T. 1985 Evidence and quantitation of left ventricular resistance. *Am. J. Physiol.* **249** (Heart Circ. Physiol. 18): H358-H370.

Smith, W.M. 1985 Epidemiology of congestive heart failure. *Am. J. Cardiol.* **55**: 3A-8A.

Snyder, A., Rosenberg, G., Weiss, W., Pierce, W., Pae Jr., W., Marlotte, J., Nazarian, R., Ford, S. 1991 A completely implantable total artificial heart system. *ASAIO Trans.* **37**: M237-M238.

Sola, O.N., Kakulas, B.A., Haines, L.C., Thomas, R., Shoji, Y., Fujimura, Y., Hayashida, N., Sauvage, L.R. 1991 Morphology and histology of the latissimus dorsi muscle. *Sem. Thorac. Cardiovasc. Surg.* **3**: 124-127.

Spencer, F.C., Green, G.E., Tice, D.A., Wallsh, E., Mills, N.L., Glassman, E. 1971 Coronary artery bypass grafts for congestive heart failure: a report of experiences with 40 patients. *J. Thoracic Cardiovasc.* Surg. **76**: 529-542.

Spotnitz, H.M., Edmund, B.A., Sonnenblick, E.H., Spiro, D. 1966 Relation of ultrastructure to function in the intact heart: sarcomere structure relative to pressure volume curves of intact left ventricles of dog and cat. *Cardiovasc. Res.* **18**: 49-66.

Spotnitz, H.M., Merker, G., Malm, J.R. 1974 Applied physiology of the canine rectus abdominis. Force-length curves correlated with functional characteristics of a rectus-powered "ventricle". Potential for cardiac assistance. *Trans. Amer. Soc. Artif. Int. Organs* **20**: 747-756.

Spotnitz, W.D., Spotnitz, H.M., Truccone, N.J., Cottrell, T.S., Gersony, W., Malm, J.R., Sonnenblick, E.H. 1979 Relation of ultrastructure and function: sarcomere dimensions, pressure-volume curves, and geometry of the intact left ventricle of the immature canine heart. *Circ. Res.* **44**: 679-691.

Sréter, F.A., Gergely, J., Salmons, S., Romanul, F. 1973 Synthesis by fast muscles of light chains characteristic of slow muscle in response to long term stimulation. *Nature* **241**: 17-19.

Sréter, F.A., Luff, A.R., Gergeley, J. 1975 Effect of cross-reinnervation on physiological parameters and on properties of myosin and sarcoplasmic reticulum of fast and slow muscles of the rabbit. *J. Gen. Physiol.* **66**: 811-821.

Sréter, F.A., Pinter, K., Jolez, F., Mabuchi, K. 1982 Fast to slow transformation in response to long-term phasic stimulation. *Experimental Neurology* **75**: 95-102.

Sréter, F.A., Romanul, F.C.A., Salmons, S. & Gergely, J. 1974 The effect of a changed pattern of activity on some biochemical characteristics of muscle. In *Exploratory Concepts in Muscular Dystrophy II.* (ed. A.T. Milhorat), pp. 338-343. Amsterdam: Excerpta Medica.

Sréter, F.A., Elzinga, M., Mabuchi, K, Salmons, S., Luff, A.R. 1975 The N^{τ}-methylhistidine content of myosin in stimulated and cross-reinnervated skeletal muscles of the rabbit. *FEBS Letters* **57**: 107-111.

Stanaway, S.E.R.S. 1990 Gross and microscopic quantitative investigations of the human latissimus dorsi muscle. B.Sc. Thesis, Liverpool University.

Staron, R.S. & Pette, D. 1987 Non-uniform myosin expression along single fibres of chronically stimulated and contralateral rabbit tibialis anterior muscles. *Pflügers Arch.* **409**: 67-73.

Suga, H. & Sagawa, K. 1974 Instantaneous pressure-volume relationships and their ratio in the excised, supported canine left ventricle. *Circ. Res.* **35**: 117-126.

Sugiura, S., Harada, K., Yokoyama, I., Momomura, S., Naruse, Y., Maku-uchi, H., Serizawa, T., Matsunaga, H., Iiizuka, M., Furuse, A., Sugimoto, T. 1993 Analysis of cardiac assistance by latissimus dorsi cardiomyoplasty with a time varying elastance model. *Cardiovasc. Res.* **27**: 997-1003.

Tan, L.B. 1986 Cardiac pumping capability and prognosis in heart failure. *The Lancet* pp 1360-1363.

Tan, L.B. 1987 Clinical and research implications of new concepts in the assessment of cardiac pumping performance in heart failure. *Cardiovas. Res.* **21**: 615-622.

Termet, H., Chalencon, J.L., Estour, E., Gaillard, P. & Favre, J.P. 1966 Transplantation sur le myocarde d'un muscle strie excite par pacemaker. *Ann. Chir. Thor. Cardiol.* **5**: 260-263.

The Registry of the International Society for heart and Lung Transplantation. 1993 Tenth Official Report - 1993. *J. Heart Lung Transplant* **12**: 541-548.

Thomas, G.A. & Stephenson, L.W. 1994 In: *Heart Surgery Classics*, (eds. Stephenson, L.W. & Ruggiero, R.), p 370-73. Adams Publishing Group, Ltd.: Boston, MA. ISBN 0-944903-09-6.

Tommaso, C.L. 1986 Non-glycoside non-catecholamine inotropic agents in the treatment of congestive heart failure. *Am. J. Med.* **80** (suppl 2B): 36-39.

Ugolini, F. 1986 Skeletal muscle for artificial heart drive: theory and in vivo experiments. In Chiu RC-J., (ed.), *Biomechanical Cardiac Assist. Cardiomyoplasty and Muscle-powered Devices*. Mount Kisco, New York: Futura Publishing Company, pp 193-210.

Uretsky, B.F., Murali, S., Reddy, P.S., Rabin, B., Lee, A., Griffith, B.P., Hardesty, R.L., Trento, A., Bahnson, H.T. 1987 Development of coronary artery disease in cardiac transplant patients receiving immunosuppressive therapy with cyclosporine and prednisone. *Circulation* **76**: 827-834.

Van Leeuwen, J.L. & Spoor, C.W. 1992 Modelling mechanically stable muscle architectures. *Phil. Trans. R. Soc. Lond.* B **336**: 275-292.

Voytik, S.L., Babbs, C.F., Badylak, S.F. 1990 A simple electrical model of the circulation to explore design parameters for a skeletal muscle ventricle. *J. Heart Trans.* **9**: 160-174.

Waaler, B.A., Walløe, L., Wesche, J. 1987 Cardiac output as related to muscle blood flow during and following rhythmic exercise in humans. *J. Physiol.* **390**: 121P.

Walker, J.S. 1982 BSc thesis. University of Birmingham.

Waters, R., McNeal, D. & Perry, J. 1975 Experimental correction of footdrop by electrical stimulation of the peroneal nerve. *J. Bone Joint Surg.* **57A**: 1047-1054.

White, D. & Wallwork, J. 1993 Xenografting: probability, possibility, or pipe dream? *The Lancet* **342**: 879-80.

Wiehrer, W. & Pette, D. 1983 The ratio between intrinsic 115 kDa and 30 kDa peptides as a marker of fibre type-specific sarcoplasmic reticulum in mammalian muscles. *FEBS Lett.* **158**: 317-320.

Wilkie, D.R. 1976 *Muscle*. Edward Arnold, London.

Wilkie, D.R. 1985 Muscle function: a personal view. *J. exp. Biol.* **115**: 1-13.

Williams, D.O., Korr, K.S., Gewirtz, H., Most, A. 1982 Effect of intraaortic balloon counterpulsation on regional myocardial blood flow and oxygen consumption in the presence of coronary artery stenosis in patients with unsatble angina. *Circulation* **66**: 593-97.

Williams, N.S., Hallan, R.I., Koeze, D.H. & Watkins, E.S. 1989 Construction of a neorectum and a neonatal sphincter following previous proctolectomy. *Br. J. Surg.* **76**: 1191-1194.

Williams, R.S., Salmons, S., Newsholme, E.A., Kaufman, R.E., Mellor, J. 1986 Regulation of nuclear gene expression by contractile activity in skeletal muscle. *J. Biol. Chem.* **261**: 376-80.

Williams, R.S., Garcia-Moll, M., Mellor, J., Salmons, S., Harlan, W. 1987 Adaptation of skeletal muscle to increased contractile activity: expression of nuclear genes encoding mitochondrial proteins. *J. Biol. Chem.* **262**: 2764-67.

Wilson, D. & Larimer, J.L. 1968 The catch property of ordinary muscle. *Proc. Nat. Acad. Sci.* USA **61**: 909-916.

Wittenberg, B.A. & Wittenberg, J.B. 1989 Transport of oxygen in muscle. *Annu. Rev. Physiol.* **51**: 857-78.

Zajac, F.E. & Young, J.L. 1980a Properties of stimulus trains producing maximum tension-time area per pulse from single motor units in medial gastrocnemius muscle of the cat. *J. Neurophysiol.* **43**: 1206-1220.

Zajac, F.E. & Young, J.L. 1980b Discharge properties of hindlimb motoneurons in decerebrate cats during locomotion induced by mesencephalic stimulation. *J. Neurophysiol.* **43**: 1221-1235.

Zancolli, E. & Mitre, H. 1973 Latissimus dorsi transfer to restore elbow flexion. *J. Bone Joint Surg.* **55-A** (6): 1265-75.

Appendix

Publications

Appendix A **Kwende, M.M.N**, Jarvis, J.C. & Salmons, S. 1995 The input-output relations of skeletal muscle. *Proc. R. Soc. Lond.* B **261**: 193-201.

The input–output relations of skeletal muscle

MARTIN M. N. KWENDE, JONATHAN C. JARVIS AND STANLEY SALMONS

British Heart Foundation Skeletal Muscle Assist Research Group, Department of Human Anatomy and Cell Biology, University of Liverpool, Liverpool L69 3BX, U.K.

SUMMARY

We used three approaches to determine the stimulation patterns that maximize the isometric force–time integral per impulse (FTIpP) available from tibialis anterior muscles of the rabbit. Initially the interval between two pulses was fixed at the value that gave the maximum force-time integral, and successive pulses were added at intervals that maximized the FTIpP. We checked this iterative approach by a second method, in which a computer-generated protocol was used to deliver randomized bursts to the muscles. These experiments confirmed that optimal stimulation patterns for fast muscles consisted of an initial high-frequency portion followed by a train of impulses at a lower frequency. However, for muscles that had been stimulated chronically at a constant low frequency, an initial high-frequency portion conferred no advantage. In a third set of experiments we used constant-frequency bursts to generate contour surfaces that represented the dependence of FTIpP on the frequency and number of impulses. The results agreed with those from the earlier methods. We conclude that optimized patterns have potential for clinical use, but their value will depend strongly on the activation characteristics of the stimulated muscle.

1. INTRODUCTION

Skeletal muscles may be stimulated electrically to utilize their force-generating capacity in clinical applications. Stimulation can be applied to a muscle *in situ* to restore function to the diaphragm (Glenn *et al.* 1980) or to limb muscles (Hambrecht & Reswick 1977; Bajd & Jaeger 1994) that have been paralysed by spinal cord injury. Alternatively a muscle may be grafted, with the motor nerve intact, to replace the external anal sphincter (Baeten *et al.* 1988; Williams *et al.* 1989) or to provide cardiac assistance to a failing heart (Acker *et al.* 1987; Salmons & Jarvis 1992; Hooper & Salmons 1993).

It is conventional to use constant-frequency bursts in clinical applications, for no better reason than that they are convenient to generate. However, such patterns deliver more impulses to the muscles than are needed to maintain contraction: the associated high aggregate rate of impulse delivery results in premature muscle fatigue in the short term and loss of muscle power in the long term (Jarvis 1993). Constant-frequency bursts actually bear no resemblance to physiological patterns of motoneurone firing, which consist of trains of action potentials with changing interpulse intervals (Marsden *et al.* 1971; Zajac & Young 1980*b*; Hennig & Lomo 1985). Would it be advantageous to adopt impulse trains that are closer to these physiological firing patterns for clinical applications of electrical stimulation?

The mechanical response of a muscle fibre is not a simple function of the frequency of action potentials delivered to it by its motor axon. Wilson & Larimer (1968) showed that the force exerted by a crayfish claw-opener muscle could be maintained by less frequent stimulation than that required to generate it: a property known as 'catch'. A phenomenon somewhat analogous to 'catch' exists in mammalian skeletal muscle. Marsden *et al.* (1976) were able to simulate a maximal voluntary contraction in human muscle by an electrical tetanus whose frequency was progressively decreased. Such a strategy minimized the fatigue that resulted from prolonged contraction of the muscle, a phenomenon that they referred to as 'muscular wisdom' (Marsden *et al.* 1983). Burke and his colleagues found that, when slow-twitch (type S) muscle units were stimulated repetitively within a narrow frequency range (6–20 Hz), tension output could be increased significantly by adding a single pulse at a short interpulse interval (IPI) in an otherwise constant low-frequency train (Burke *et al.* 1970, 1976). This enhancement of force output could be elicited from both slow and fast motor units, the optimum timing depending only on the speed of the isometric twitch. Zajac & Young (1980*a*) determined the properties of stimulus trains that produced maximum force–time integral per impulse (FTIpP) from single motor units in the gastrocnemius muscle of the cat. They concluded that an iterative technique could be used to obtain the optimum stimulation pattern for a muscle, and they went on to establish that the optimal initial IPI was 5–10 ms (Burke *et al.* 1976; Zajac & Young 1980*a*).

Chronic stimulation of rabbit skeletal muscle at 10 Hz for several weeks renders it fatigue-resistant, a property that is crucial to clinical applications that call for sustained levels of activity. However, muscles stimulated in this way also undergo a reduction in bulk

(Pette *et al.* 1976; Salmons & Henriksson 1981) and contractile speed (Salmons & Vrbová 1969; Al-Amood *et al.* 1973; Pette *et al.* 1973; Salmons & Sréter 1976; Kernell *et al.* 1987), and this results in a substantial loss of power (Jarvis 1993). We have shown that chronic stimulation at 2.5 Hz produces muscles that are significantly faster and more powerful than those stimulated at 10 Hz, yet just as resistant to fatigue in tests conducted at a fixed working rate of 10 W kg^{-1} (Jarvis *et al.* 1995). Because an optimal stimulation pattern should enable the same mechanical response to be elicited by fewer impulses, it would deliver a lower aggregate number of impulses over time, and would therefore hold out the prospect of preserving muscle power more effectively in the long term. This would be a substantial benefit in applications such as cardiac assistance, in which the power requirements can be difficult to meet (Salmons & Jarvis 1992).

Here we have used three different approaches to determine patterns of stimulation that optimize the response of both control and chronically stimulated rabbit tibialis anterior muscle. A preliminary account of one of these approaches has appeared elsewhere (Jarvis 1991).

2. MATERIALS AND METHODS

(a) *Apparatus*

The apparatus consisted of a force and length transducer controlled by a personal computer (PC). The transducer was a Dual Mode Servo System (Cambridge Technology, Inc., Watertown, Massachusetts, U.S.A.; Model 310B), a force and length controller designed specifically for muscle measurements. It is capable of generating controlled forces of up to 50 N and length excursions of 20 mm to either side of its central position. An IBM-compatible PC (Viglen 386/486) was used to provide synchronized control of the servo motor, muscle stimulation, and data acquisition, the latter via a commercial I/O board (PC-30D, Amplicon Liveline, Brighton, U.K.). Code was written in Borland Turbo C++. Stimulus pulses were generated by an isolated stimulator (Mk. IV, Devices, Hertfordshire, U.K.), which was triggered by pulses from the PC.

(b) *Chronic stimulation*

Miniature electronic stimulators were designed and constructed as described previously (Jarvis & Salmons 1991; Salmons & Jarvis 1991). After encapsulation in silicone rubber (Dow Corning 3140RTV, Midland, Michigan), the devices were 35 mm in diameter and no more than 8 mm thick. A Dacron mesh extending from the encapsulant facilitated suturing. The output from the device was taken via multistrand PVC-insulated stainless steel wires (Cooner Sales Company, Chatsworth, California, U.S.A.) to loop electrodes formed from the bared wire and a velour pad. The implanted pulse generator incorporated a photosensitive switch so that it could be turned on and off remotely by flashes of light directed through the skin and subjacent tissues. The output pulses were of 0.2 ms duration and 3.2 V amplitude, and were delivered at a frequency of either 5 or 10 Hz. Under these conditions, all the motor units innervated by the common peroneal nerve are stimulated. The devices were sterilized by immersion in benzalkonium chloride (10 g l^{-1}) for 24 h and implanted into adult New Zealand White rabbits under fentanyl/fluanisone anaesthesia (Hypnorm: fentanyl citrate, 0.315 ml kg^{-1} and fluanisone, 10 mg ml^{-1}, Janssen Pharmaceutica, Grove, Wantage, Oxon; 0.3 mg kg^{-1}, I.M.) after premedication with atropine sulphate (Sigma Chemical Co. Ltd., U.K.; 3 mg kg^{-1}) and diazepam (Roche Products Ltd., U.K.; 5 mg kg^{-1}) given subcutaneously. Full aseptic precautions were taken. In each case the stimulator was placed subcutaneously and sutured lightly to the abdominal wall; leads were taken subcutaneously to the lower hind limb. One electrode was placed in a slip of the gastrocnemius muscle immediately beneath the common peroneal nerve. The other electrode was placed 20–30 mm distally on the surface of the lateral head of the gastrocnemius muscle. The wounds were closed with Prolene sutures (Ethicon Ltd., Edinburgh, U.K.) and the rabbit was left to recover for one week before the stimulator was switched on. Stimulation of the common peroneal nerve was then continued without interruption until the terminal experiment. At terminal experiments, data was collected from muscles stimulated for more than four weeks at either 5 Hz ($n = 3$) or 10 Hz ($n = 6$), and from the contralateral muscles, which served as controls ($n = 9$).

(c) *Terminal procedure*

The rabbits were anaesthetized with urethane (Sigma Chemical Co. Ltd.; 250 g l^{-1}; 500 mg kg^{-1} body mass) and pentobarbitone sodium (Sagatal, May & Baker Ltd., Manchester, U.K.; 30 mg kg^{-1}), administered via a 25 g butterfly catheter in the marginal ear vein. Supplementary doses of pentobarbitone sodium were given throughout the procedure as needed, to maintain deep anaesthesia. Although the trachea was routinely cannulated, it was seldom necessary to provide mechanical respiratory assistance. In animals that had been subjected to chronic stimulation, the implanted leads were cut at this stage. Flap electrodes (Barnard *et al.* 1986) were placed around both common peroneal nerves without disturbing the chronic stimulation electrodes on the left side. The nerve was then cut centrally, proximal to the electrodes. The tibialis anterior tendon was transected in the foot, threaded back through the extensor retinaculum and held in a miniature titanium alloy clamp, leaving a minimum of unclamped tendon. The alloy clamp was connected by a lightweight, non-compliant carbon fibre-epoxy link to the servo motor arm. The muscles were kept moist with liquid paraffin and warmed with electric heating lamps to maintain their temperature at 37 ± 1 °C.

The length at which the muscle developed the greatest isometric twitch force was determined and the muscle was maintained at this length for all subsequent measurements.

(d) *Optimization of stimulation pattern*

In the context of these experiments, an optimal stimulation pattern (OSP) is defined as the sequence of nerve impulses that elicits from the muscle the maximum mechanical output per impulse. An appropriate measure of mechanical output is the isometric force–time integral (FTI), which has been shown to be highly correlated with energy utilization and with work output measured in terms of resynthesis of reduced nicotinamide-adenine dinucleotide during oxidative recovery after activity (Jöbsis & Duffield 1967).

i) *Iterative method*

Isometric force was measured and converted to FTI by a Gould analogue integrator (Gould Electronics, Cleveland, Ohio, Model 13-4615-70). The FTI obtained in response to two stimulating pulses was plotted against the interval between the pulses. The interval was then fixed at the value

that gave the highest FTI and an additional pulse was added to the train, optimizing the interval in the same way. The procedure was repeated for successive pulses, up to a total of six. The same procedure was used to produce a stimulus train that maximized force rather than FTI. Measurements were carried out on three muscles chronically stimulated at 10 Hz and on the contralateral controls. An approach of this type has been used previously (Zajac & Young 1980*a*; Maxwell *et al.* 1993), but those experiments did not extend to chronically stimulated muscle.

ii *Random pattern method*

One hundred patterns were generated in which the IPIs were of quasi-random length. For control muscles, the response to an isolated single impulse was a twitch contraction with a time to peak (CT) of about 20 ms and a total time above resting force of about 80 ms. The maximum IPI used in the random patterns was therefore 70 ms (between three and four times the CT), as the mechanical responses to individual pulses would not interact if the intervals were any longer than this (Burke *et al.* 1970). IPIs were rounded to an integral number of milliseconds. The random pattern trains were generated by setting the first pulse and adding subsequent pulses at random intervals until the maximum burst length of 300 ms had been reached. Each random burst was then saved to disk as a stream of digital values representing the presence (1) or absence (0) of a supramaximal nerve stimulus (0.05 ms, 20 V) in 1 ms time slots. The computer-controlled measurement system delivered these digital values as triggers to the isolated stimulator, sampled and analysed the data on-line to obtain the FTIpP, and saved the results to disk. A 1 min rest period was interposed between stimulation bursts. Patterns were then placed in rank order according to the magnitude of the FTIpP that they elicited. A standard train of twelve pulses at 40 Hz was included at the beginning of the experiment ('rested' standard pulse train) and after every ten random burst trains, as a means of checking for possible deterioration or fatigue of the muscle preparation or, conversely, for signs of potentiation of muscle output. The preparations were in fact extremely stable (see below). Data was collected from three muscles that had undergone chronic stimulation at 10 Hz and from their contralateral controls.

iii *The FTIpP index*

The effectiveness of the patterned impulse train may be assessed as the amount by which the FTIpP exceeds that for a single pulse (i.e. a twitch contraction):

FTIpP = Burst FTIpP/Twitch FTI

However, this measure alone would not take account of systematic variation occurring during the 2.5 h duration of the experiment. The standard pulse trains were used to compensate for this variation. In figure 1 the ratio of the FTI of the standard trains to that of the 'rested' train is shown as a function of time for nine different muscles. The graph shows that the muscle preparations were in fact rather stable: the maximum coefficient of variation in the mean was 3.8%. This ratio was then used as a correction factor for the raw FTIpP index defined above:

FTIpP index = (Burst FTIpP/Twitch FTI)*(FTI of 'rested' standard train/FTI of preceding standard train)

If the mechanical response of a muscle increased in direct proportion to the number of pulses, the FTIpP index would always be unity. An index greater than unity for any pulse pattern represents a 'more-than-linear' summation of the mechanical response elicited by the impulses in that train.

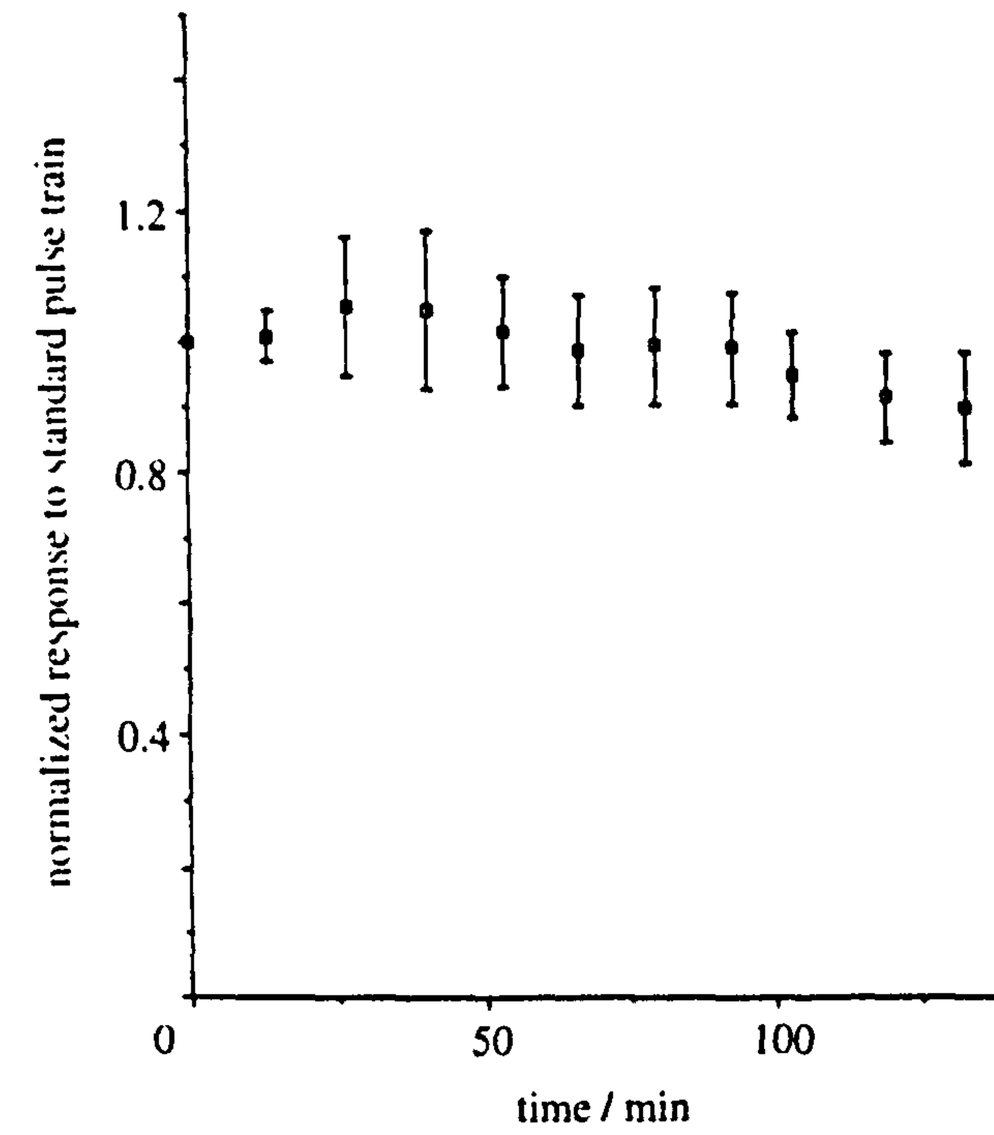

Figure 1. The mechanical response to a standard pulse train plotted as a function of time in nine experiments. The ordinate is normalized in terms of the response to the 'rested' standard train, and is plotted as the mean ± s.e.m.

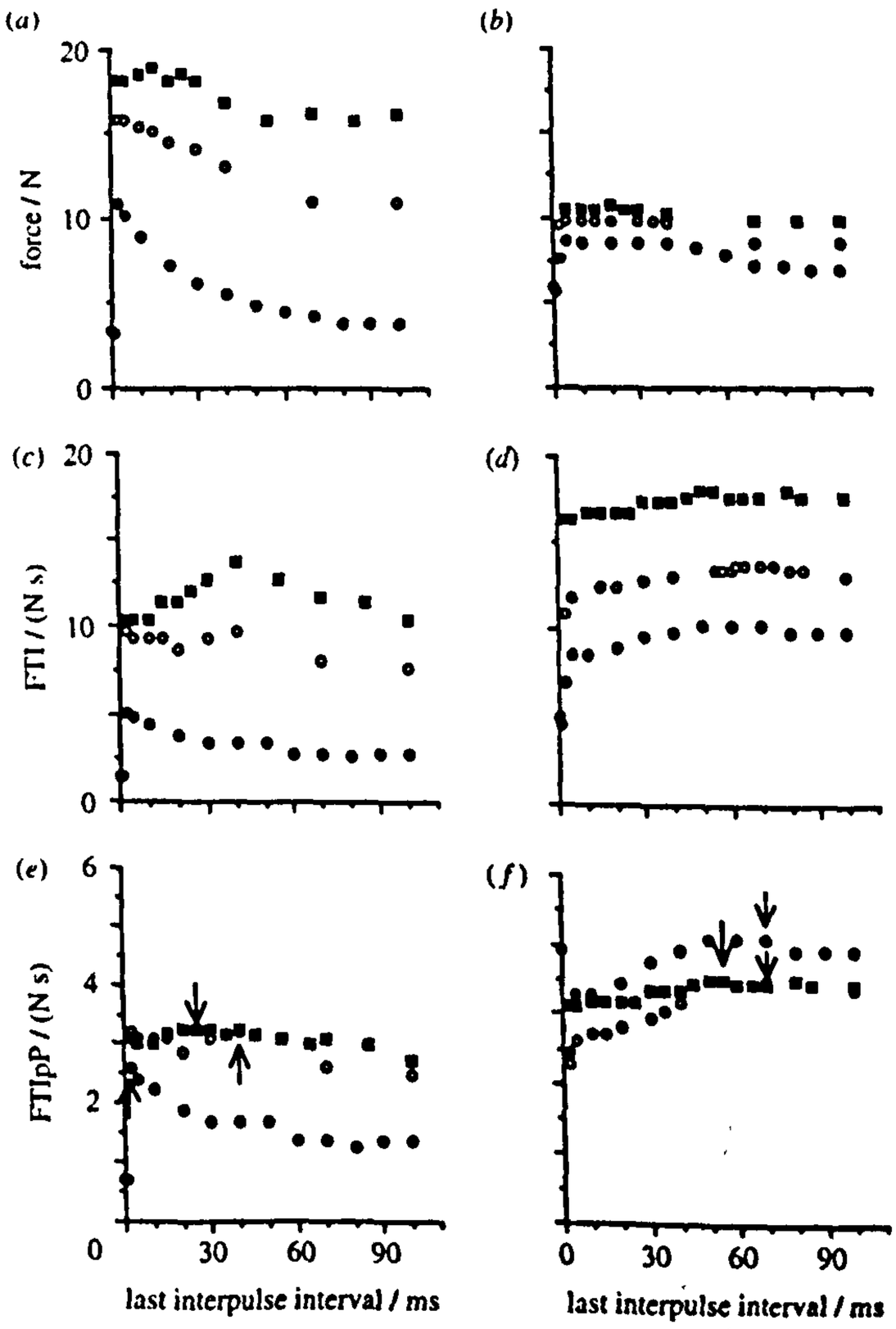

Figure 2. Graphs of force (N), FTI (Ns), and FTIpP (Ns) plotted as a function of the last IPI for 2 (filled circles), 3 (empty circles) and 4 (filled squares) pulses. The responses shown are typical of control muscles (*a*,*c*,*e*), and muscles stimulated chronically at 10 Hz for four weeks (*b*,*d*,*f*). The arrows in (*e*) and (*f*) show how optimal burst IPIs are determined by choosing the longest interval that gives the maximum FTIpP. Each curve is for a single muscle.

We refer to this as the 'doublet effect' because it occurs when at least two of the pulses are separated by a short IPI. A value less than unity reflects a reduced responsiveness of the chronically stimulated muscle to the second muscle action potential: this phenomenon has not previously been observed in either control fast or slow muscle (Burke *et al.* 1976; Zajac & Young 1980*a*).

(iv) *Constant frequency train method*

To develop a more general basis for determining OSPs for any type of muscle, constant frequency bursts of 1–10 pulses were generated over a frequency range of 1–500 Hz and delivered to control rabbit tibialis anterior muscles and muscles that had been stimulated chronically at 5 Hz ($n = 3$) and 10 Hz ($n = 3$). The protocol of burst delivery to the muscles was the same as for the random pattern method.

3. RESULTS

(*a*) *Iterative method*

Figure 2 illustrates the results obtained with the iterative method for determining OSPs; for clarity this is shown only for the first three IPIs. In this figure a control muscle (*a*,*c*,*e*) is compared with a muscle that had been stimulated chronically for four weeks at 10 Hz (*b*,*d*,*f*). In control muscles, peak force and FTI were produced when the intervals between the pulses were short (see figure 2*a*,*c*). The patterns that produced the optimal mechanical responses were made up of the following IPIs: 3, 3, 20, 10, 10, 10 ms for force, and 3, 40, 35, 20, 30 ms for FTI. Stimulated muscles contracted more slowly (see table 1) and peak FTI occurred at intervals greater than 50 ms (see figure 2*d*). For these muscles, optimal force and FTI were generated for pulse trains of 30, 30, 20 ms and 70, 70, 50 ms, respectively. For the chronically stimulated muscle, FTIpP was highest for the twitch response (see figure 2*f*, filled circle on the ordinate) and was depressed by up to 20% by the addition of further pulses at very short IPIs. The maximum FTIpP index for this muscle was therefore close to unity. In contrast, the maximum FTIpP index for the control muscle (see figure 2*e*) was about 2.0, representing a doubling of the twitch output, for two- and three-pulse bursts.

Table 1. *Twitch contraction times (time from a single stimulus to the peak of the force response to that stimulus) for rabbit tibialis anterior muscles stimulated chronically at 5 Hz or 10 Hz, and for contralateral control muscles (mean ± s.e.m.).*

force of stimulation	twitch contraction time
Hz	ms
control ($n = 6$)	20.24 ± 0.92
5 ($n = 3$)	27.35 ± 3.37
10 ($n = 6$)	65.22 ± 4.70

(*b*) *Random pattern method*

The random patterns that produced the highest FTIpP indices for the fast control muscles (see figure 3*a*) were characterized by one or more pairs of closely spaced pulses; thus short IPIs enhanced the response of the fast muscles. The average frequency of these bursts (see figure 3*a*) was about 45 Hz. On the other hand, the best patterns for the muscles stimulated chronically at 10 Hz for 6 weeks (see figure 3*b*) were characterized by long intervals between pulses, which reduced the average frequency to about 20 Hz. Figure 3*d*, which shows the worst patterns for this muscle, suggests that

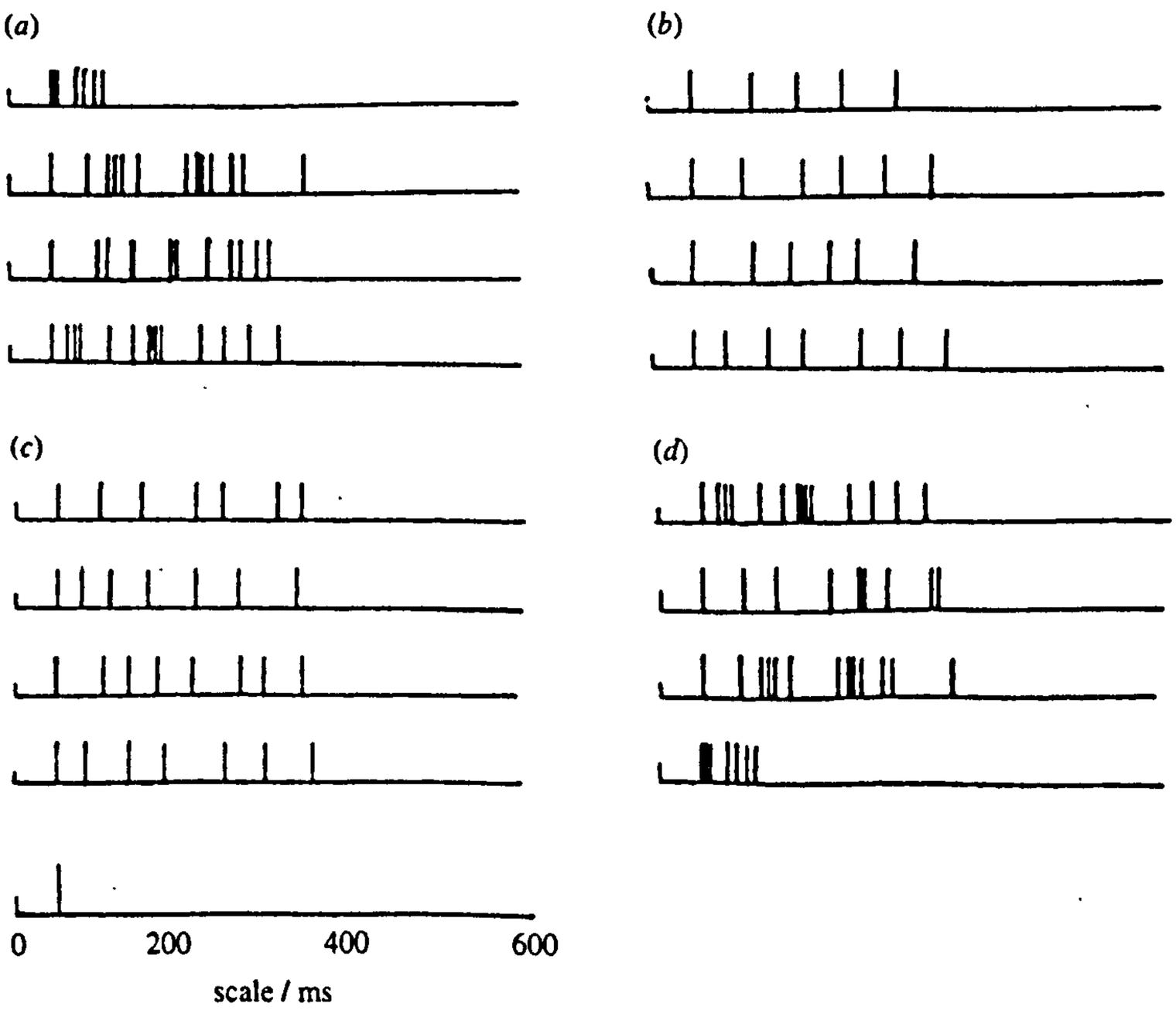

Figure 3. The results of rank-ordering the FTIpP indices for the responses to 100 random patterns. (*a*) 'Best' patterns for a control fast muscle. (*b*) 'Best' patterns for a chronically stimulated muscle (six weeks of stimulation at 10 Hz). (*c*) 'Worst' patterns for a control fast muscle. (*d*) 'Worst' patterns for the same chronically stimulated muscle.

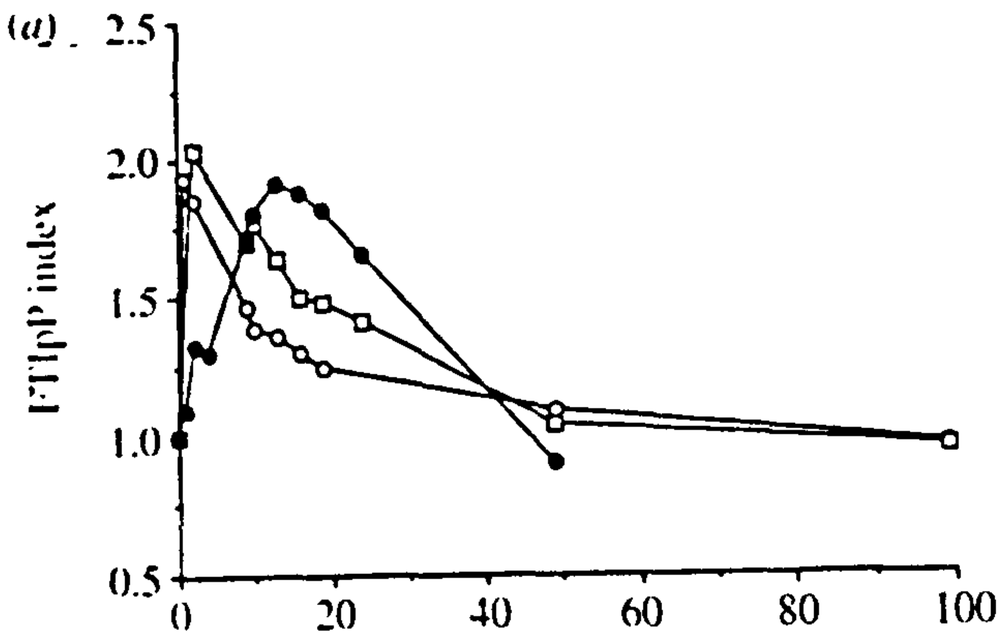

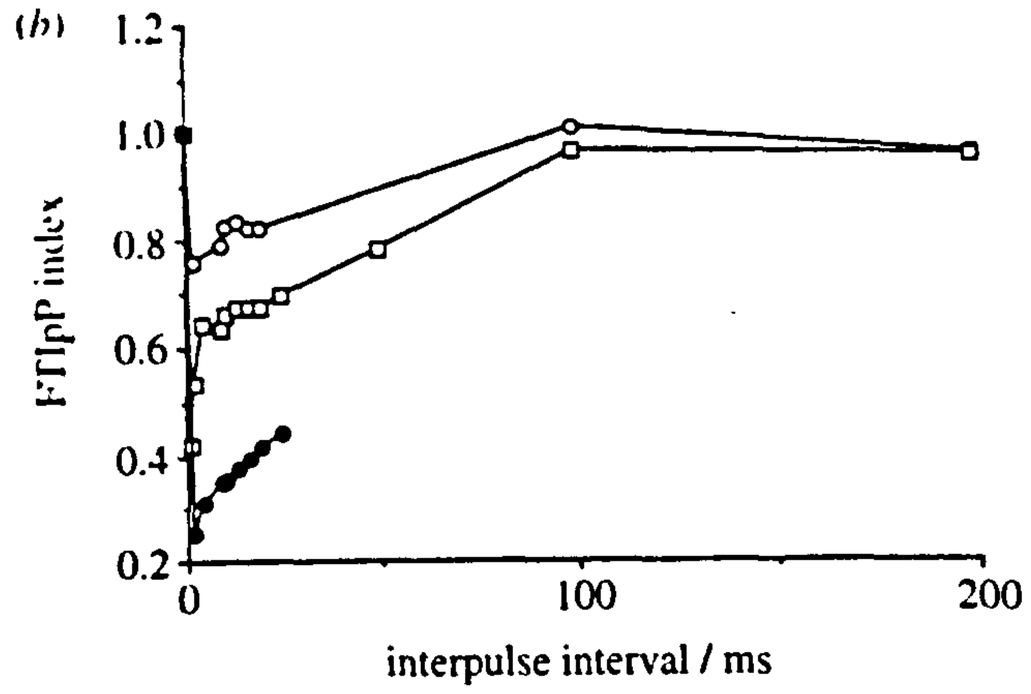

Figure 4. Graph of FTIpP index (ordinate) versus interpulse interval (abscissa) for two- (empty circle), three- (empty square) and eight-pulse (filled circle) constant-frequency bursts. (*a*) Control fast muscle. (*b*) Chronically stimulated muscle (six weeks of stimulation at 10 Hz).

the incidence of short IPIs within the burst was actually detrimental. The worst patterns for the control muscle (see figure 3*c*) were similar to the best patterns for the chronically stimulated muscles.

(*c*) *Constant-frequency train method*

When short, constant-frequency trains were delivered to control fast muscles, the two- and three-pulse bursts produced a peak in the FTIpP index for IPIs less than 5 ms (see figure 4*a*). Muscles that were chronically stimulated (see figure 4*b*) showed a trough for all bursts that contained very short IPIs. Nevertheless, these muscles showed a peak at a much longer IPI of 100 ms (10 Hz), a result that agrees with previous observations on slow muscle (Burke *et al.* 1970). Even at this peak value, the FTIpP index only approached unity, so the mechanical output per pulse never exceeded that for a single twitch.

The difference between control muscles and muscles stimulated chronically at 10 Hz is well illustrated in figure 5. In the contour plots (see figures 5*a*,*b*), the lighter the shading the greater the FTIpP index. Note that the white region from the abscissa to the start of the grey shading indicates a zone in which data was not collected because of the restriction of burst duration. Control muscle (see figure 5*a*) shows two peaks in its

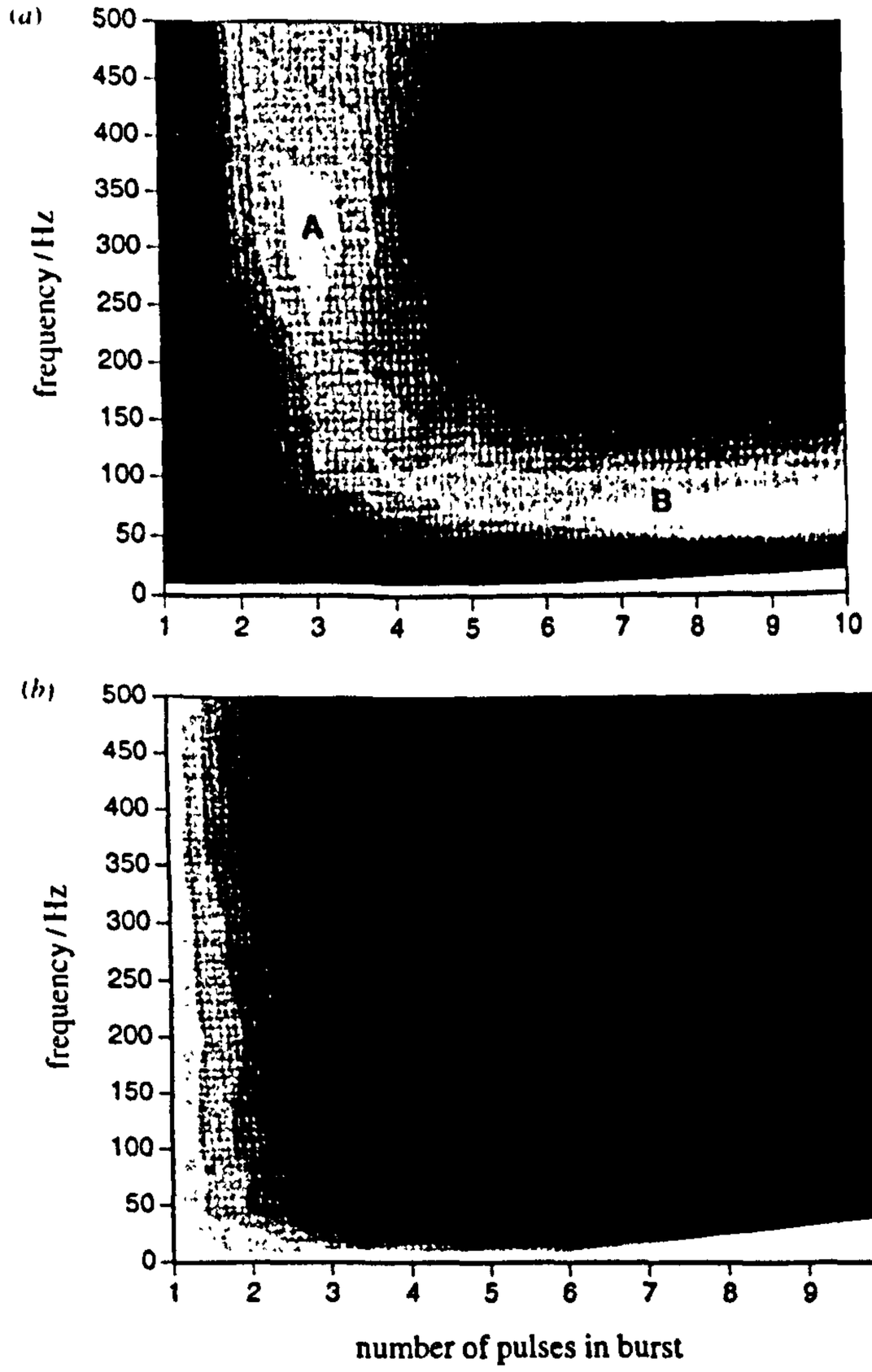

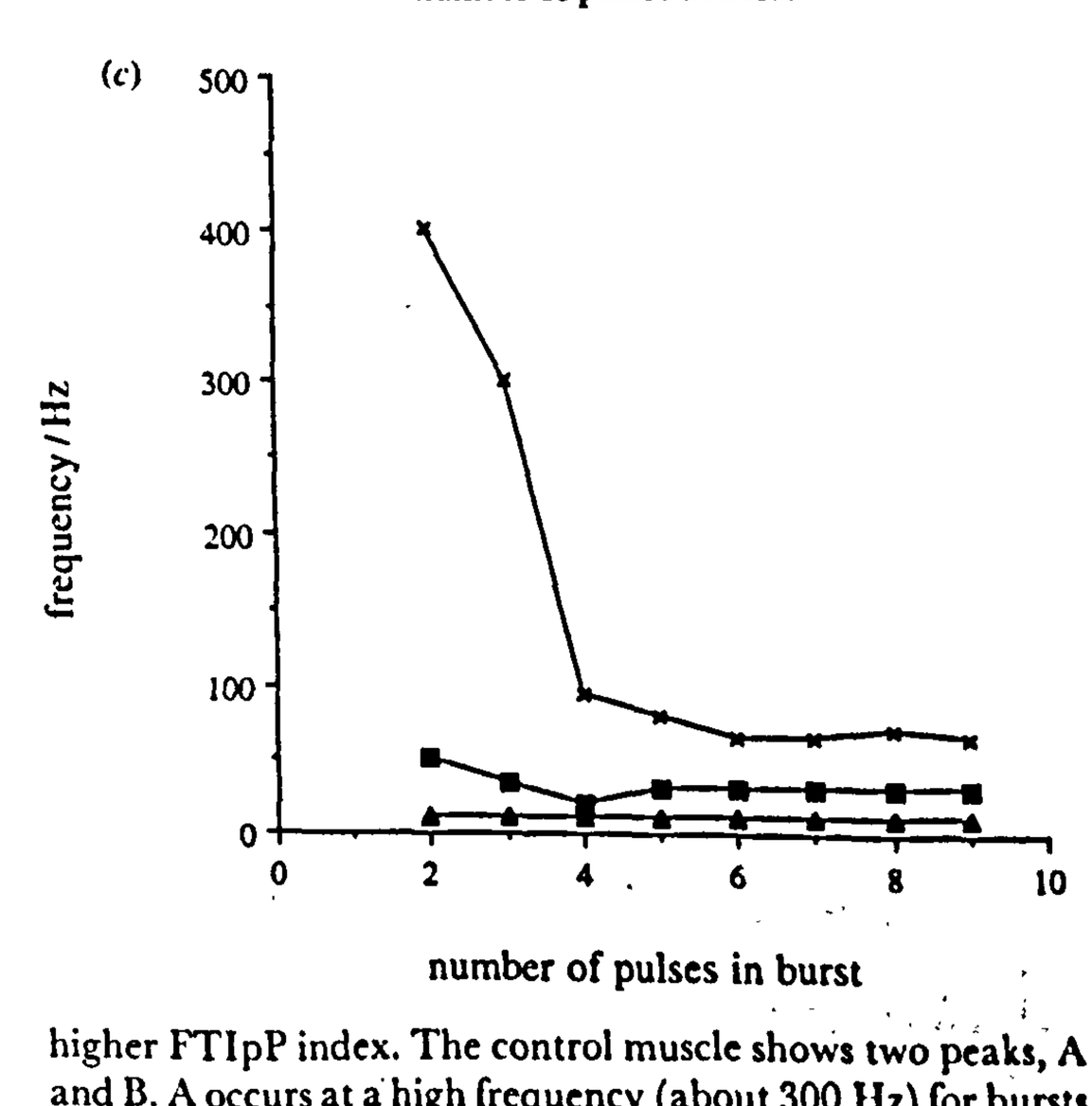

Figure 5. Contour plot of frequency, number of pulses in a burst and FTIpP index for (*a*) control muscle and (*b*) muscle chronically stimulated at 10 Hz. Lighter shading indicates a higher FTIpP index. The control muscle shows two peaks, A and B. A occurs at a high frequency (about 300 Hz) for bursts of 2–3 pulses while B is found at a much lower frequency for bursts of more than 4 pulses. Some combinations of frequency and number of pulses could not be accomodated within a burst duration of 600 ms; data is therefore lacking in the white region from the abscissa to the start of the grey shading. (*c*) The optimal frequency (see text for definition) is plotted against the number of impulses in the burst. Loci of the optimal frequencies abstracted from graphs such as 5*a*,*b* are plotted for control muscle (crosses), and for muscles stimulated chronically at 5 Hz (filled squares) and 10 Hz (filled triangles). Note the intermediate nature of the chronically stimulated 5 Hz muscle.

output: the first (A) occurs at a high frequency (about 300 Hz) for bursts of 2–3 pulses; the second (B) is found at a much lower frequency (about 60 Hz) for bursts of more than 4 pulses. The muscle stimulated chronically at 10 Hz shows no obvious peaks but the lightest areas for all bursts occur at a low frequency (about 10 Hz).

For bursts containing a given number of pulses, the frequency of the burst that produces the maximum FTIpP index may be defined as the optimal frequency. If the FTIpP index remains at the maximum value for a range of frequencies, the lowest frequency in the range is taken as optimal. Figure 5*c* abstracts from contour plots such as figures 5*a*,*b* the loci of the optimal frequencies for control muscle and muscles stimulated chronically at 5 Hz and 10 Hz. It shows that the optimal frequency does not change appreciably for stimulation bursts containing more than five pulses.

In control muscle (see figure 5*c*), the rise in frequency at shorter train lengths (equivalent to peak A in figure 5*a*) reflects the doublet effect. This effect is not seen in the muscles stimulated chronically at 10 Hz. Muscles stimulated at 5 Hz show an intermediate behaviour, with a slight doublet effect.

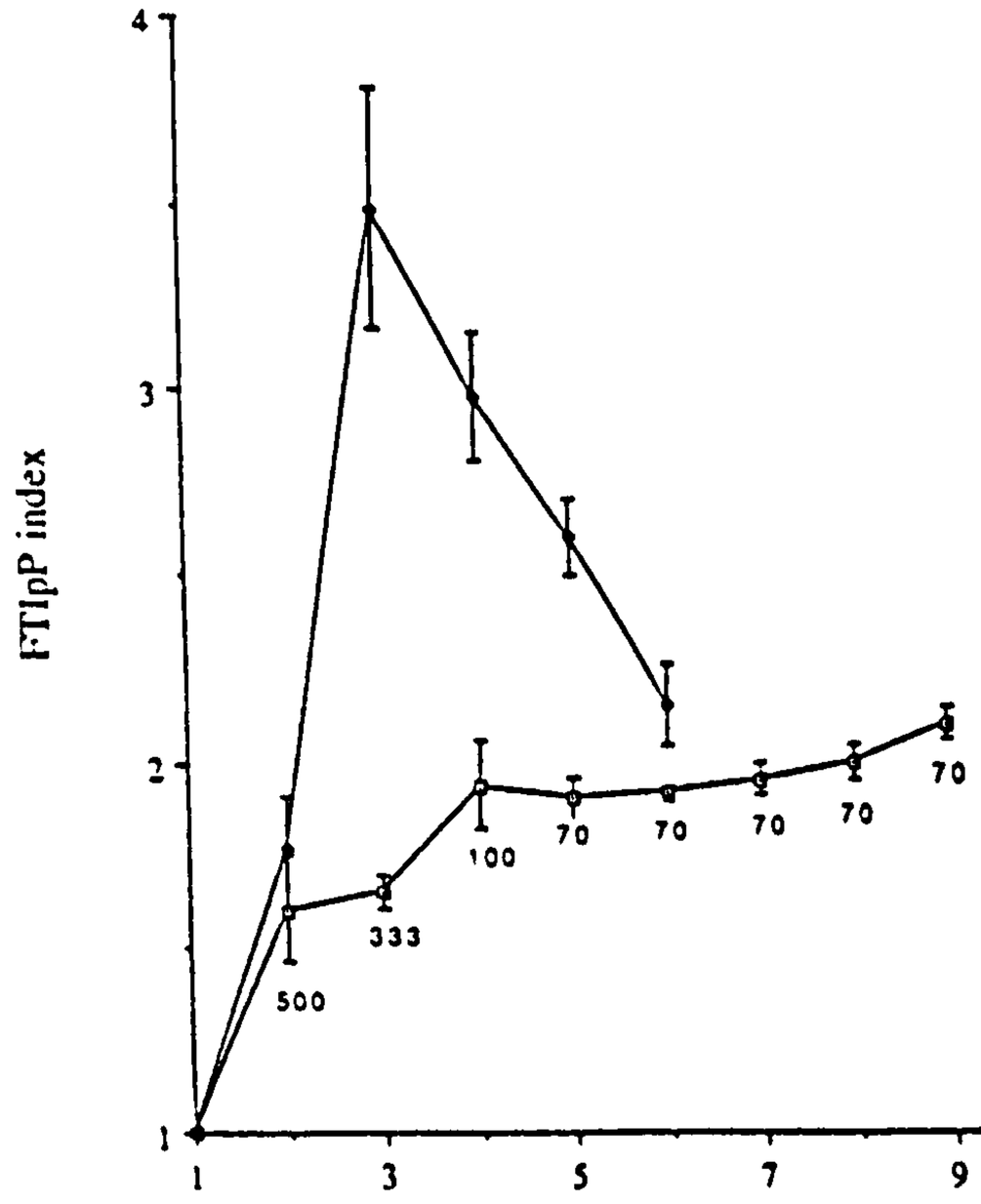

Figure 6. Comparison between the responses to the best constant-frequency bursts (CFBs) and the responses to OSPs (filled diamonds, $n = 3$). The numbers below the CFB curve (hollow squares, $n = 3$) indicate the best frequency for that number of pulses. The FTIpP indices are plotted as mean ± s.e.m.

4. DISCUSSION

The purpose of this study was to improve on current protocols for clinical applications of electrical stimulation by investigating the relation between the neural input and the mechanical output of skeletal muscles. An understanding of this relation would lead to general rules for designing ideal stimulation patterns that provided an adequate tension profile over the active period with the minimum redundancy in the impulse train.

For control fast muscles we showed by an iterative approach that OSPs for force and FTI consist of an initial portion containing one or two short IPIs (3 ms), followed by a series of pulses at longer intervals. When patterns consisting of randomly generated IPIs were ranked in order of mechanical response, the best patterns for fast muscles contained some short intervals. Thus the best way to elicit a tetanic contraction of a fast muscle is to deliver a pattern that has an initial high-frequency portion, to generate tension, followed by impulses at a lower constant frequency, to maintain tension.

Contour plots of the response to stimulation with a range of constant frequencies and burst lengths confirmed the above conclusions and further emphasized the difference between bursts with a few impulses and bursts with many impulses. For bursts of less than four impulses, the highest FTIpP occurred at high frequencies (greater than 200 Hz, corresponding to IPIs less than 5 ms), another manifestation of the doublet effect. For bursts of more than 5 pulses, the highest FTIpP occurred at a much lower constant frequency (50 Hz, corresponding to an IPI of 20 ms), reflecting the dilution of the doublet effect over these longer trains.

It is instructive to compare FTI outputs for bursts of increasing number of impulses, optimized by the iterative approach, to constant-frequency bursts optimized from the contour plots. Figure 6 shows that two-pulse bursts from the two sources have a similar FTIpP index. However, bursts with three pulses have an FTIpP index more than double the index for the corresponding constant-frequency burst. This difference depends heavily on the long second IPI that was a feature of OSPs generated by the iterative approach. In constant-frequency stimulation, the price paid for a first IPI that is short enough to produce the doublet effect is a subsequent impulse that is almost redundant, and which therefore lowers the FTIpP. For fast muscles, at least, optimal stimulation cannot be achieved without the use of variable IPIs.

Because the doublet effect acts only over a short initial period, its effect on FTIpP is averaged over the duration of a tetanic contraction. As a result, the benefit of the doublet effect declines as a burst increases in length. The FTIpP indices for bursts with variable IPIs therefore converge towards those with constant IPIs for bursts of more than five pulses (see figure 6). The IPI of constant-frequency bursts of more than five pulses that produce the best FTIpP index can therefore be used to estimate the constant low-frequency portion of an OSP.

Chronic stimulation at 5 Hz reduced, and chronic stimulation at 10 Hz abolished, the doublet effect. The OSPs of muscles with a history of chronic stimulation, determined by the iterative approach, showed no initial short intervals. On the contrary, as was shown by rank-ordering of patterns with random ISPs, short intervals led to a reduction in force per impulse and

FTI per impulse when these patterns were delivered to chronically stimulated muscles. The reason for this reduction is the absence in these muscles of the doublet effect, illustrated in figure 4. Therefore an initial high-frequency portion has no benefit in these muscles and, as the contour plot of figure 5*b* shows, no combination of pulses produced a higher FTIpP than a single impulse.

The lack of a single clear explanation for the existence of the doublet effect in fast skeletal muscle reflects our incomplete understanding of the rate-limiting mechanisms for force generation in whole muscles. The fact that the doublet effect is lost with chronic stimulation suggests a link between the doublet effect and those intracellular changes brought about by chronic stimulation that affect muscle activation. One possibility is that activation of rested fast muscle by a single impulse is in some way incomplete, so that a second impulse is required to produce full activation. In this context, activation has to be visualized as a process that has more than one stage. The initial stage, the release of Ca^{2+} in response to a single impulse, appears to be supramaximal, since 80–90 % of cross-bridges are activated (Kress *et al.* 1986) and a reduction in the magnitude of the Ca^{2+} transient does not result in a decline in force production. Subsequent stages, which lead to the appearance of force at the muscle tendon, are considerably delayed with respect to the Ca^{2+} transient, and the occupancy of Ca^{2+}-binding sites during a single twitch may be too short in fast muscles for all of the activated crossbridges to undergo attachment and force generation (Rüegg 1992). In terms of activation, the most striking features of chronically stimulated muscle are a marked reduction in the volume of the sarcoplasmic reticulum and changes in the Ca^{2+}-transport ATPase, which result in a decreased capacity for active sequestration of Ca^{2+} (Sréter *et al.* 1974; Salmons & Sréter 1976; Heilmann & Pette 1979; Eisenberg & Salmons 1981), and a decrease in the content of parvalbumin, a cytosolic Ca^{2+} buffer (Klug *et al.* 1983). All of these changes would be expected to extend the time course of the Ca^{2+} transient in chronically stimulated muscle, leading to the effective generation of force even in response to a single pulse and hence a reduced scope for enhancement of force by a double impulse.

The changes induced by chronic stimulation lead to a more extreme state of differentiation than that seen in slow motor units (Salmons & Sréter 1976). Thus our observations do not necessarily conflict with those of Burke *et al.* (1976) and Zajac & Young (1980*a*), who observed the doublet effect in slow, as well as fast, motor units in the medial gastrocnemius muscle of the cat. Based on this finding they proposed a method of determining OSPs in which the CT of the muscle was used as a scaling factor. Their OSP would consist of an initial portion that contained one or two short IPIs followed by a train of impulses with a constant interval between 1 and 2 × CT of the muscle. Figure 7 shows the effect of applying this method to the present data to find the constant-frequency portion. The FTIpP indices of nine pulse constant-frequency bursts for control muscles and muscles stimulated chronically at 5 Hz and 10 Hz have been plotted against the interpulse interval expressed as a fraction of the CT (contraction times for these muscles are given in table 1). From figure 7, the optimal IPIs for the nine-pulse bursts are as follows: 0.77 × CT (64 Hz, since frequency is the reciprocal of IPI) for control muscle, 0.95 × CT (38 Hz) for 5 Hz-stimulated muscles, and more than 1.34 × CT (less than 11 Hz) for 10 Hz-stimulated muscles. These values are close to the range of 1 to 2 × CT that Zajac & Young would recommend for the constant-frequency portion of the OSP. However, Zajac & Young's method can only apply to muscles in which the doublet effect is present. As the chronically stimulated muscles retain little or no doublet effect (see figure 5*c* and figure 4*b*), adding an initial portion of one or two short IPIs to the constant-frequency portion would lead to a false OSP.

Although it may reasonably be supposed that the contraction time of a muscle gives an indication of its activation characteristics, such information is not an adequate basis for determining the OSP of a muscle. This is illustrated by the muscles stimulated chronically at 5 Hz. These muscles have a twitch CT of 27.35 ± 3.37 ms (mean ± s.e.m.), and should thus be classified as fast muscles as their CT is less than 35 ms (Burke 1967, 1968). Nonetheless, they retained the doublet effect to a much smaller extent than the control muscles, and OSPs for these muscles would not

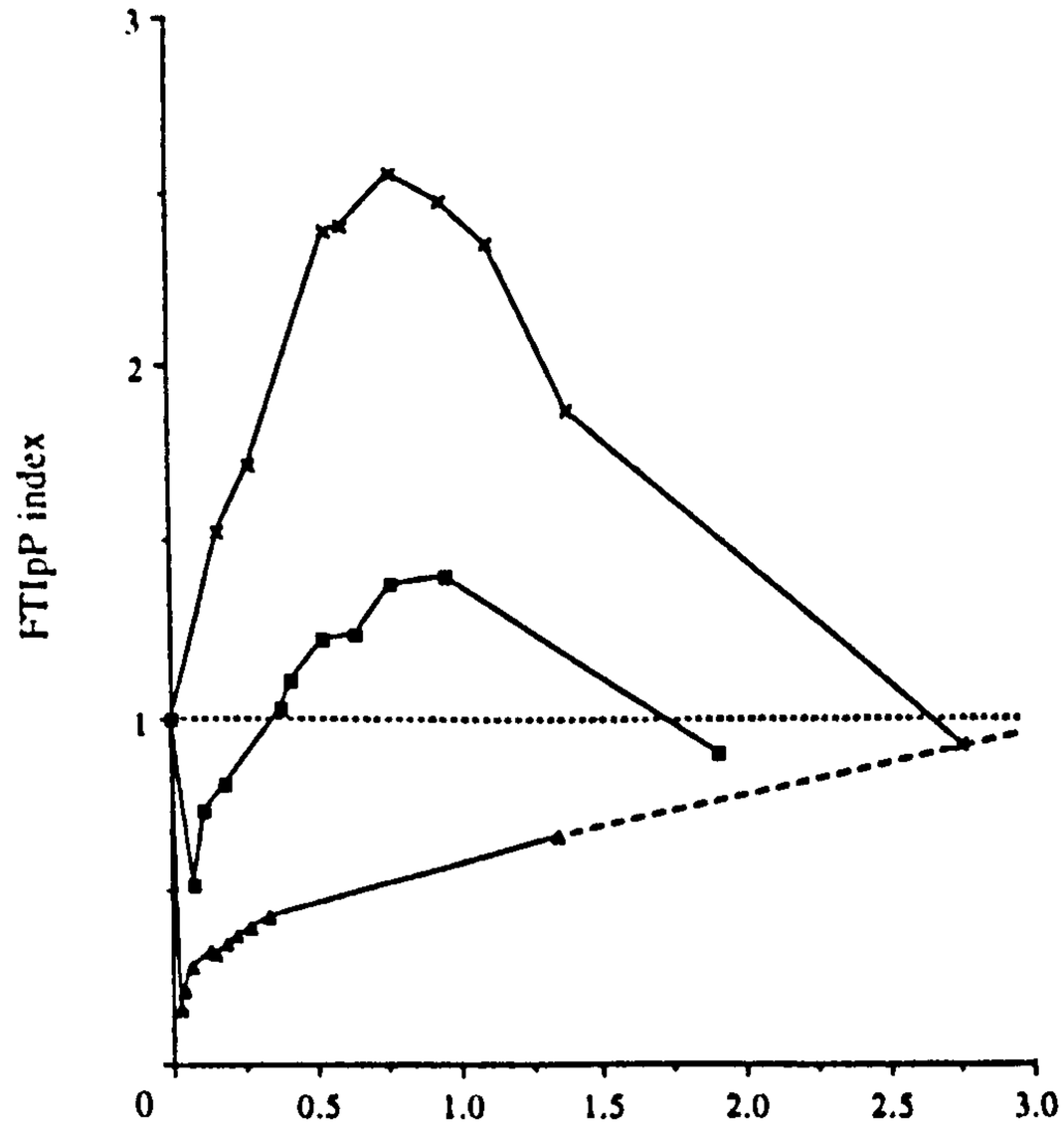

Figure 7. FTIpP indices for 9-pulse bursts plotted against interpulse interval expressed as a fraction of muscle contraction time (CT) for control muscle (crosses), and muscles stimulated chronically at 5 Hz (filled squares) and 10 Hz (filled triangles). The maximum FTIpP indices occur at 0.77 × CT (64 Hz) and 0.95 × CT (38 Hz) for control muscle and muscle stimulated chronically at 5 Hz, respectively. The muscle that had been chronically stimulated at 10 Hz had not reached its peak FTIpP, but would tend to unity as the pulses in a burst become so widely spaced in time that they cease to interact (dashed line).

contain short intervals. In this way, the long-term history of activation of a muscle can profoundly influence the nature of its OSP.

The doublet effect is an important phenomenon which could be exploited with advantage in clinical applications involving fewer than six pulses per burst. For example, a burst of five pulses delivered as an OSP can give the same mechanical output as a burst of six pulses at a constant frequency. Moreover, OSPs are useful for generating muscle force with a rapid rate of development. Thus the OSP provides an additional degree of freedom that helps the designer to achieve a stimulation pattern that is matched appropriately to the functional needs of the application.

Cardiac assistance from skeletal muscle Salmons & Jarvis 1992: Hooper & Salmons 1993 is an example of a clinical application of functional electrical stimulation that could benefit from the use of OSPs. It makes use of chronically stimulated muscle that must be both fatigue-resistant and capable of generating force rapidly with a highly controlled tension profile. However, current protocols of chronic stimulation abolish the doublet effect, leaving no scope for modulating muscle output in this way. It will therefore be important to develop strategies of chronic electrical stimulation that preserve the doublet effect. Chronically stimulated muscles that have OSPs with variable IPIs would require less stimulation to achieve the desired output. This would lead to reduced muscle fatigue, an increase in the lifetime of the internally implanted stimulation systems that deliver these stimulation patterns, and potential for reducing the post-operative delay that is an undesirable aspect of current protocols.

This work was supported by grants from the Wellcome Trust and the British Heart Foundation. M.K. is a Wellcome Prize Student. The authors acknowledge the assistance of Miss Hazel Sutherland in some of the operations, and of Emma Rhead in preliminary experiments.

REFERENCES

Acker, M. A., Hammond, R. L., Mannion, J. D., Salmons, S. & Stephenson L. W. 1987 Skeletal muscle as a potential source for a cardiovascular pump: assessment *in vivo*. *Science, Wash.* **3**, 324–327.

Al-Amood, W. S., Buller, A. J. & Pope, R. 1973 Long-term stimulation of cat fast-twitch skeletal muscle. *Nature, Lond.* **244**, 225–227.

Baeten, C., Spaans, F. & Fluks, A. 1988 An implanted neuromuscular stimulator for faecal continence following previously implanted gracilis muscle: report of a case. *Dis. Colon Rectum* **31**, 134–137.

Bajd, T. & Jaeger, R. 1994 FES for movement restoration. *Basic Appl. Myol.* **4**, 124–211.

Barnard, E. A., Barnard, P. J., Jarvis, J. C. & Lai, J. 1986 Low frequency chronic electrical stimulation of normal and dystrophic chicken muscle. *J. Physiol.* **376**, 377–409.

Burke, R. E. 1967 Motor unit types of cat triceps surae muscle. *J. Physiol.* **193**, 141–160.

Burke, R. E. 1968 Firing patterns of gastrocnemius motor units in the decerebrate cat. *J. Physiol.* **196**, 631–654.

Burke, R. E., Rudomin, P. & Zajac, III, F. E. 1970 Catch property in single mammalian motor units. *Science, Wash.* **168**, 122–124.

Burke, R. E., Rudomin, P. & Zajac, III, F. E. 1976 The effect of activation history on tension production by individual muscle units. *Brain Res.* **109**, 515–529.

Eisenberg, B. R. & Salmons, S. 1981 The reorganisation of subcellular structure in muscle undergoing fast-to-slow type transformation: a stereological study. *Cell Tiss. Res.* **220**, 449–471.

Glenn, W. W. L., Hogan, J. F. & Phelps, M. L. 1980 Ventilatory support of the quadriplegic patient with respiratory paralysis by diaphragm pacing. *Surg. Clin. N. America* **60**, 1055–1078.

Hambrecht, F. T. & Reswick, J. B. eds 1977 *Functional electrical stimulation: applications in neural prostheses*. New York: Marcel Dekker.

Heilmann, C. & Pette, D. 1979 Molecular transformations in sarcoplasmic reticulum of fast-twitch muscle by electrostimulation. *Eur. J. Biochem.* **93**, 437–446.

Hennig, R. & Lomo, T. 1985 Firing patterns of motor units in normal rats. *Nature, Lond.* **314**, 164–166.

Hooper, T. L. & Salmons, S. 1993 Skeletal muscle assistance in heart failure. *Cardiovasc. Res.* **27**, 1404–1406.

Jarvis, J. C. 1991 The power-generating capacity of normal and conditioned skeletal muscle. In *Concerted Action HEART: proceedings of expert meeting on harnessing skeletal muscle power for cardiac assistance* ed. S. Salmons & J. C. Jarvis , pp. 15–19. Commission of the European Communities.

Jarvis, J. C. 1993 Power production and working capacity of rabbit tibialis anterior muscles after chronic electrical stimulation at 10 Hz. *J. Physiol.* **470**, 157–169.

Jarvis, J. C., Brownson, C., Sutherland, H. & Salmons, S. 1991 Comparison between the effects of continuous long-term stimulation of rabbit skeletal muscle at 2.5 Hz and 10 Hz. In *Basic and applied myology: perspectives for the 90's* ed. C. Carraro & S. Salmons), pp. 109–113. Padova: Unipress.

Jarvis, J. C. & Salmons, S. 1991 A family of neuromuscular stimulators with optical transcutaneous control. *J. med. Engng Technol.* **15**, 53–57.

Jarvis, J. C., Sutherland, H., Mayne, C. N. Gilroy, S. J. & Salmons, S. 1995 Contractile properties, fatigue resistance and myosin isoform composition of rabbit fast skeletal muscle transformed to a fast-oxidative state by long-term electrical stimulation at 2.5 Hz. *Am. J. Physiol.* In the press.

Jobsis, F. F. & Duffield, J. C. 1967 Force, shortening and work in muscular contractions: relative contributions to overall energy utilization. *Science, Wash.* **156**, 1388–1392.

Kernell, D., Eerbeek, O., Verhey, B. A. & Donselaar, Y. 1987 Effects of physiological amounts of high- and low-rate chronic stimulation on fast-twitch muscle of the cat hindlimb. I. Speed- and force-related properties. *J. Neurophysiol.* **58**, 598–613.

Kress, M., Huxley, H. E., Faruqi, A. R. & Hendrix, J. 1986 Structural changes during activation of frog muscle studied by time-resolved X-ray diffraction. *J. molec. Biol.* **188**, 325–342.

Klug, G., Wiehrer, W. & Pette, D. 1983 Rapid reduction in parvalbumin concentration during chronic stimulation of rabbit fast twitch muscle. *FEBS Lett.* **152**, 180–2.

Klug, G., Wiehrer, W., Reichmann, H., Leberer, E. & Pette, D. 1983 Relationships between early alterations in parvalbumins, sarcoplasmic reticulum and metabolic enzymes in chronically stimulated fast twitch muscle. *Pflügers Arch. ges. Physiol.* **399**, 280–284.

Marsden, C. D., Meadows, J. C. & Merton, P. A. 1971 Isolated single motor units in human muscle and their rate of discharge during maximal voluntary effort. *J. Physiol.* **217**, 12–13.

Marsden, C. D., Meadows, J. C. & Merton, P. A. 1976 Fatigue in human muscle in relation to the number and frequency of motor impulses. *J. Physiol.* **258**, 94–95.

Marsden, C. D., Meadows, J. C. & Merton, P. A. 1983 'Muscular wisdom' that minimizes fatigue during prolonged effort in man: peak rates of motoneuron discharge and slowing of discharge during fatigue. In *Advances in neurology* 39: *motor control mechanisms in health and disease* ed. J. E. Desmedt , pp 169–211. New York: Raven Press.

Maxwell, D. J., Granat, M. H. & Baxendale, R. H. 1993 Novel stimulation strategies for the recruitment of paralysed muscle. In *Concerted Action RAFT*: *proceedings of expert meeting on muscular components in functional electrical stimulation* ed. J. Edwards , pp. 37–43. Commission of the European Communities.

Pette, D., Muller, W., Leisner, E. & Vrbová, G. 1976 Time dependent effects on contractile properties, fibre population, myosin light chains and enzymes of energy metabolism in intermittently and continuously stimulated fast-twitch muscles of the rabbit. *Pflügers Arch. ges. Physiol.* **364**, 103–112.

Pette, D., Smith, M. E., Staudte, H. W. & Vrbová, G. 1973 Effects of long-term electrical stimulation on some contractile and mechanical characteristics of fast rabbit muscles. *Pflügers Arch. ges. Physiol.* **338**, 257–272.

Rüegg, J. C. 1992 *Calcium in muscle contraction*, pp. 74–80. Heidelberg: Springer-Verlag.

Salmons, S. & Henriksson, J. 1981 The adaptive response of skeletal muscle to increased use. *Muscle Nerve* **4**, 94–105.

Salmons, S. & Jarvis, J. C. 1990 The working capacity of skeletal muscle transformed for use in a cardiac assist role. In *Transformed muscle for cardiac assist and repair* (ed. R. C.-J. Chiu & I. Bourgeois), pp. 89–104. Mount Kisco: Futura Publishing Company, Inc.

Salmons, S. & Jarvis, J. C. 1991*a* Cardiomyoplasty: a look at the fundamentals. In *Cardiomyoplasty* (ed. A. Carpentier, J.-C. Chachques & P. Grandjean), pp. 3–17. Mount Kisco: Futura Publishing Inc.

Salmons, S. & Jarvis, J. C. 1991*b* Simple optical switch for implantable devices. *Med. Biol. Engng Comput.* **29**, 554–556.

Salmons, S. & Jarvis, J. C. 1992 Cardiac assistance from skeletal muscle: a critical appraisal of the various approaches. *Br. Heart J.* **68**, 333–338.

Salmons, S. & Sréter, F. A. 1976 Significance of impulse activity in the transformation of skeletal muscle type. *Nature, Lond.* **263**, 30–34.

Salmons, S. & Vrbová, G. 1969 The influence of activity on some contractile characteristics of mammalian fast and slow muscles. *J. Physiol.* **201**, 535–549.

Sréter, F. A., Romanul, F. C. A., Salmons, S. & Gergely, J. 1974 The effect of a changed pattern of activity on some biochemical characteristics of muscle. In *Exploratory concepts in muscular dystrophy II* (ed. A. T. Milhorat), pp. 338–343. Amsterdam: Excerpta Medica.

Williams, N. S., Hallan, R. I., Koeze, D. H. & Watkins, E. S. 1989 Construction of a neorectum and a neonatal sphincter following previous proctolectomy. *Br. J. Surg.* **76**, 1191–1194.

Wilson, D. & Larimer, J. L. 1968 The catch property of ordinary muscle. *Proc. natn Acad. Sci.* U.S.A. **61**, 909–916.

Zajac, F. E. & Young, J. L. 1980*a* Properties of stimulus trains producing maximum tension-time area per pulse from single motor units in medial gastrocnemius muscle of the cat. *J. Neurophysiol.* **43**, 1206–1220.

Zajac, F. E. & Young, J. L. 1980*b* Discharge properties of hindlimb motoneurons in decerebrate cats during locomotion induced by mesencephalic stimulation. *J. Neurophysiol.* **43**, 1221–1235.

Received 28 March 1995; accepted 20 April 1995

Appendix B Donaldson, N. de N., Gollee, H., Hunt, K.J., Jarvis, J.C. & **Kwende, M.M.N.** 1995 A radial basis function model of muscle stimulated with irregular inter-pulse intervals. *Med. Eng. Phys.* **17**: 431-441..

BUTTERWORTH HEINEMANN

1350-4533(94)00013-1

Med. Eng. Phys. Vol. 17, No. 6, pp. 431–441, 1995
Elsevier Science Ltd for IPEM
Printed in Great Britain
1350-4533/95 $10.00 + 0.00

A radial basis function model of muscle stimulated with irregular inter-pulse intervals

N. de N. Donaldson*, H. Gollee†, K.J. Hunt‡, J.C. Jarvis§ and M.K.N. Kwende§

*Department of Medical Physics and Bioengineering, University College London, 11–20 Capper Street, London WC1E 6JA, UK; †Department of Electrical Engineering, Technical University of Berlin, Berlin, Germany; ‡Daimler-Benz AG, Systems Technology Research, Berlin, Germany; §Department of Human Anatomy and Cell Biology, University of Liverpoool, Liverpool, UK

Received 1 March 1994, accepted 13 September 1994

ABSTRACT

Paralysed muscle, or skeletal muscle which is to be used for cardiac assistance, may be given an artificial function if it is electrically stimulated to contract and the response can be adequately controlled. To design a controller, a model of the muscle or system is usually required. The most commonly used models are analogues, originating from A.V. Hill's model. However muscles exhibit many nonlinear and time-varying phenomena which, if they are to be modelled, make the analogue complex and cumbrous to work with. The system may further be complicated by pathological changes and secondary effects of stimulation. We propose that such a system can be modelled by nonlinear networks ('neural networks'). The radial basis function network (RBF) has two advantages over the better-known multi-layer perceptron (MLP). We describe the use of an RBF network to model rabbit muscle that is supramaximally stimulated at irregular inter-pulse intervals.

Keywords: FES, cardiomyoplasty, radial basis functions, neural networks, muscle modelling, dynamic systems.

Med. Eng. Phys., 1995, Vol. 17, 431–441, September

INTRODUCTION

We are interested in obtaining models of electrically activated muscles, together with the load on which they act[1]. Such models could be used in stimulator controllers for cardiac assistance from skeletal muscles or for functional electrical stimulation (FES) of limb muscles in paralysed patients. The models could also be used for simulation.

Artificially-stimulated muscle displays many nonlinear phenomena in space and time. While stimulating at constant frequency, the force and stiffness depend on the length[2,3]; the force being greatest at the mid-range. Joyce *et al.*[4] showed that if cat soleus muscle is subjected to constant-velocity changes in length, the force varies with velocity in a nonlinear manner which has a discontinuity in slope at zero velocity at some stimulus frequencies. The elasticity of muscle is a function of the force even if the stimulation suppresses modulation of the stiffness by reflex action[5]. If the muscle has reached a steady tension while isometric, subsequent isotonic stretching may cause the muscle to yield, increasing substantially in length before sufficient force is developed to balance the load[6]. When the inter-pulse intervals (IPI) are not constant, nonlinearity in the time domain is exhibited. Pairs of pulses with a small IPI, called doublets, can give a contraction with more than twice the force-time integral of two well-spaced pulses[7,8]. When stimulation is continued for a longer time, muscles may potentiate and eventually fatigue; these phenomena cause the force response to a repetitive stimulus pattern to increase and decrease respectively. Fatigue also renders the muscle slower. Post-tetanic potentiation increases the muscle stiffness through a subsequent increase in the load may then cause a muscle to yield[9]. Obviously a comprehensive model of muscle will be nonlinear and time-varying.

Different types of muscle model are used for different purposes. The range extends from biophysical models, which are based on the structure and the activation and contractile mechanisms of actual muscles, through analogue models, to purely mathematical descriptions. The purpose of a biophysical model is to help understand how the muscle works; mathematical models are

Correspondence to: N. de N. Donaldson, Department of Medical Physics and Bioengineering, University College London, 11–20 Capper Street, London WC1E 6JA, UK.

merely descriptions of observed behaviour. The earliest models were analogue (Hill-type)[10], and despite the success of more recent biophysical models (Huxley-type), analogue models remain most popular in biomechanics because they are, on the whole, mathematically more tractable and their behaviour is predictable by inspection. The Hill model of muscle comprises a contractile element, which for shortening muscle at supramaximal stimulation is a hyperbolic force–velocity relationship, in series with a spring, representing the elasticity of the muscle (and the tendon if included), all of which is in parallel with a second spring representing the passive tissue. Both these springs are nonlinear. Hill's original model[11] only describes supramaximal stimulation and the contractile element is assumed to be at the peak of its force–length curve, and length changes small, so that the force developed by the contractile element is independent of length. Since then, the model has been refined, but Winters recently[12] listed three phenomena which are still difficult to describe in a Hill-type model: these include yielding and 'force enhancement after stretch'. He also comments that too little is known about muscle behaviour at submaximal activation.

Muscle models used in studies of controllers for FES have been simpler than the Hill model. Often the muscle is, or is assumed to be, isometric, so that the effects of changing muscle length can be ignored[13], and the muscle is represented by a force generator, with some activation dynamics. If the nerve is not supramaximally stimulated, the nonlinear recruitment may be modelled by preceding the transfer function of the dynamics with a fixed nonlinear function. This is the Hammerstein model[14,15]. A model which does take account of the muscle stiffness and the variation force with length and velocity, has been described by Crago *et al.*[16]. Their model is used in finger controllers for tetraplegics and has inputs for stimulation, length and velocity. Nonlinearity is introduced into the model by making the velocity term depend on whether the muscle is getting longer or shorter. Flaherty *et al.* have tested a model of the paraplegic ankle which is a variant of the arrangement of the Hill model. They looked at the experimental fit with linear elements, at first[17], and improved the model, for high velocity displacements by making the dashpot speed-dependent (the viscosity diminishing at high velocity[18]). Allin and Inbar[19] used a version of the Hill-type model for describing the upper limb, but in their model, the elements were all linear except for the recruitment curve. None of these models is as complex as Hill's. Nevertheless, reasonably satisfactory performance may be obtained from muscle controllers based upon these models, if the range of operating conditions is narrow.

If we wish to use the muscle over a wider range of conditions, for example: (1) over a large range of length or joint angle; or (2) with irregular interpulse intervals; or (3) with high velocities; or (4) while the muscle tires; or some combination of these, then we need a model which describes these conditions. One approach would be to utilise more features of the modern Hill-type models; indeed to enhance them so as to describe the phenomena of, for example, recruitment and fatigue. However, this presents several disadvantages:

1. A Hill model which included all known features would be extremely complex with many parameters which would have to be estimated by experiment. In practice, one is bound to start with those features which one expects to need, in order to obtain a good fit to the observed behaviour. In effect, one is obliged to guess what model structure will be adequate.
2. The methods for measuring the model parameters sometimes makes the muscle move in ways which will not occur in functional use (e.g. step changes in position[17]). This may make the model inaccurate if, in fact, the muscle is more complex than the model.
3. To perform these experiments, particularly in humans, powerful apparatus is required to obtain sufficient acceleration of the masses involved[20].

An advantage of simple analogue models is that the estimated values of the parameters are meaningful. For example, from knowing the spring constant of the series elastic element of muscle, a resonant frequency with any massive load is implied, and this limits the speed of response when the muscle moves the mass. However, as the model becomes more complex, the effect of the parameter values on the behaviour of the muscle-and-load will become increasingly difficult to predict, except by simulation, and so this advantage of analogue models is lost.

There are further disadvantages in using analogue models in FES. The muscles and joints may exhibit pathological changes, and the model should be able to include these abnormalities. The normal range of movement may not be obtained due to contracture of the antagonist muscle, for example contracture of the gastrocnemius or soleus may restrict dorsiflexion of the ankle and prevent the tibialis anterior from raising the foot. In some cases, the joint may even become partially calcified, which will reduce the range of movement. As the stimulus intensity is increased, the spread of current from the stimulating electrode may cause contraction of adjacent muscles. Coactivation of an antagonist, for example, will reduce the external moment of the joint and make it stiffer. Or the spreading current may cause a muscle to contract which either acts at another joint or is biarticular. Furthermore, the inadvertent stimulation of sensory nerve fibres may induce reflex activity, such as the flexion withdrawal reflex provoked while stimulating the dorsiflexors. Finally, the recruitment within the target muscle may depend on the position of the muscle if the stimulating electrode is not fixed relative to the motor nerve. All these effects may influence the observed behaviour of the system.

We would like our model to represent that behaviour.

Considering all these difficulties, we are taking an alternative approach which is to seek an entirely mathematical model, which is tractable, and will fit the input–output data, but has no representation either of the biophysics of the mechanisms involved, or of an analogue. The great advantage of this is that the model is 'data-driven' or in Kosko's term 'model-free[21], in the sense that no prior knowledge of the behaviour of the system is assumed, except that the response depends systematically on the inputs.

In this paper we give an initial report on the use of radial basis function (RBF) networks in muscle models. We have investigated one nonlinear phenomenon: the dependence of isometric force on an irregular supramaximal pulse train for which the force integral with time depends in some manner on the sequence of pulse intervals. The known non-linearity of this effect[22] may be exploited to obtain a required average force from fewer pulses than would be needed with constant inter-pulse intervals. From the model of the muscle itself—the forward model—an inverse model may be obtained[23]. Several types of nonlinear controller can then be constructed. The simplest, which utilises no feedback, concatenates the inverse model with the muscle (see Discussion). We report here on the formulation and testing of an RBF forward model of a muscle.

MODEL DESCRIPTION

We consider both linear and nonlinear models. The most general form used is the nonlinear relation

$$y(t) = f(y(t-1), \ldots, y(t-n_y); u(t-1), \ldots, u(t-n_u)) + e(t) . \quad (1)$$

Here, $y \in \mathcal{R}$ and $u \in \mathcal{R}$ are the output and input of the system, respectively, and e is an unknown disturbance. [More generally, lagged noise terms may also affect the output and could be included in $f(\cdot)$. The model is then known as the NARMAX model[24].] The integers n_y and n_u represent the numbers of lagged outputs and inputs affecting the current system output, with n_y the order of the system, while t represents discrete instants of time. The vector defining the argument to the nonlinear function f is denoted as $\mathbf{x} \in \mathcal{R}^{n_y+n_u}$ and is defined by

$$\mathbf{x}'(t) = (y(t-1) \ldots y(t-n_y); u(t-1) \ldots u(t-n_u)) \quad (2)$$

where bold type denotes a vector and $'$ denotes matrix transpose.

The unknown nonlinear model (1) is clearly very general. It is convenient for parameter estimation to proceed by considering a specific finite-dimensional parameterisation of (1) known as a linear regression,

$$y(t) = \boldsymbol{\theta}'\boldsymbol{\phi}(t) + e(t) . \quad (3)$$

This model is linear in the parameter vector $\boldsymbol{\theta} \in \mathcal{R}^{n_\theta}$ but the regression vector $\boldsymbol{\phi} \in \mathcal{R}^{n_\theta}$ consists of arbitrary nonlinear functions of the vector $\mathbf{x}$, i.e., $\phi_i = \phi_i(\mathbf{x}(t))$.

Assuming the disturbance e is unknown the best prediction of the system output is the linear-in-the-parameters model

$$\hat{y}(t) = \boldsymbol{\theta}'\boldsymbol{\phi}(t) \quad (4)$$

which expands to

$$\hat{y}(t) = \theta_1\phi_1(\mathbf{x}(t)) + \ldots + \theta_{n_\theta}\phi_{n_\theta}(\mathbf{x}(t)) = \sum_{i=1}^{n_\theta} \theta_i\phi_i(\mathbf{x}(t)) . \quad (5)$$

It is important to note that equations (4)–(5) define the one-step-ahead prediction of the model. This is the form used in model estimation of training. When testing a model, however, it is better to evaluate performance using the model predicted output which is defined by replacing the measured system output in (2) by the model predicted output, i.e., we define

$$\mathbf{x}'(t) = (\hat{y}(t-1) \ldots \hat{y}(t-n_y); u(t-1) \ldots u(t-n_u)) \quad (6)$$

as the model input vector to be used during testing.

The results presented in the sequel consider both linear and nonlinear forms of the regression vector $\boldsymbol{\phi}$ as defined in the following two sub-sections. A detailed account of methods for estimating the parameter vector $\boldsymbol{\theta}$ can be found in the books by Ljung and Söderström[25,26].

Linear model

In the standard linear time-invariant model the regression vector consists simply of elements of the vector $\mathbf{x}$ and is defined as

$$\boldsymbol{\phi}'(t) = (-y(t-1) \ldots -y(t-n_y); u(t-1) \ldots u(t-n_u)) . \quad (7)$$

Defining the parameter vector as

$$\boldsymbol{\theta}' = (a_1 \ldots a_{n_y}; b_0 \ldots b_{n_u-1}) \quad (8)$$

the linear model becomes

$$\hat{y}(t) = -a_1y(t-1) - \ldots - a_{n_y}y(t-n_y) + b_0u(t-1) + \ldots + b_{n_u-1}u(t-n_u) . \quad (9)$$

This model can be written in the compact transfer-function, or ARMA (auto-regressive moving average), form

$$\hat{y}(t) = \frac{q^{-1}B(q^{-1})}{A(q^{-1})}u(t) \quad (10)$$

where q^{-1} is the unit delay operator [i.e., $q^{-1}y(t) = y(t-1)$] and the polynomials A and B are defined as

$$A(q^{-1}) = 1 + a_1q^{-1} + \ldots + a_{n_y}q^{-n_y} , \quad (11)$$

$$B(q^{-1}) = b_0 + b_1q^{-1} + \ldots + b_{n_u-1}q^{-n_u+1} . \quad (12)$$

The system transfer-function, which we denote as $G(q^{-1}) = q^{-1}[B(q^{-1})/A(q^{-1})]$, may also be written as the infinite series impulse response

$$G(q^{-1}) = \sum_{k=1}^{\infty} q^{-k} g_k \tag{13}$$

where the g_k terms are the impulse response coefficients.

Nonlinear model: RBF network

A radial basis function (RBF) network consists of a network of local 'processing units'; each unit acts on only a localised part of the input space as defined by the parameters which define the unit. The RBF network can be thought of as an approximation to the general nonlinear system (1) and has exactly the form of the linear regression (5)

$$\hat{y}(t) = \hat{f}(\mathbf{x}(t)) = \sum_{i=1}^{n_\theta} \theta_i \phi_i(\mathbf{x}(t)) \; . \tag{14}$$

Many forms of nonlinearity ϕ can be employed[27]. In this work we use the standard Gaussian nonlinearity (basis function) as defined by

$$\phi_i(\mathbf{x}) = \exp\left(\frac{-\|\mathbf{x} - \mathbf{c}_i\|^2}{2\sigma_i^2}\right) . \tag{15}$$

Each function ϕ_i has two parameters: a centre $\mathbf{c}_i \in \mathcal{R}^{n_y + n_u}$, and a variance $\sigma_i \in \mathcal{R}$. The output of each function ϕ_i thus depends on the radial distance of the input vector $\mathbf{x}$ from the centre $\mathbf{c}_i$ and on the variance of the function, σ_i.

The flow of computation in equation (14) can be represented graphically as the network in *Figure 1* [where $\mathbf{x} = (x_1, x_2, x_3)'$]. Such graphical representations of the flow of a computation in parameterised interconnections of simple nonlinear functions are popularly referred to as 'artificial neural networks' or simply 'neural networks' [This comes about due to the loose analogy with biological neural networks.]. The processing units ϕ_i in (14) are known as basis functions and following tradition we refer to nonlinear parameterisations of the form (14) as basis function networks (BFNs) or, when radial basis functions such as (15) are utilised, as RBF networks.

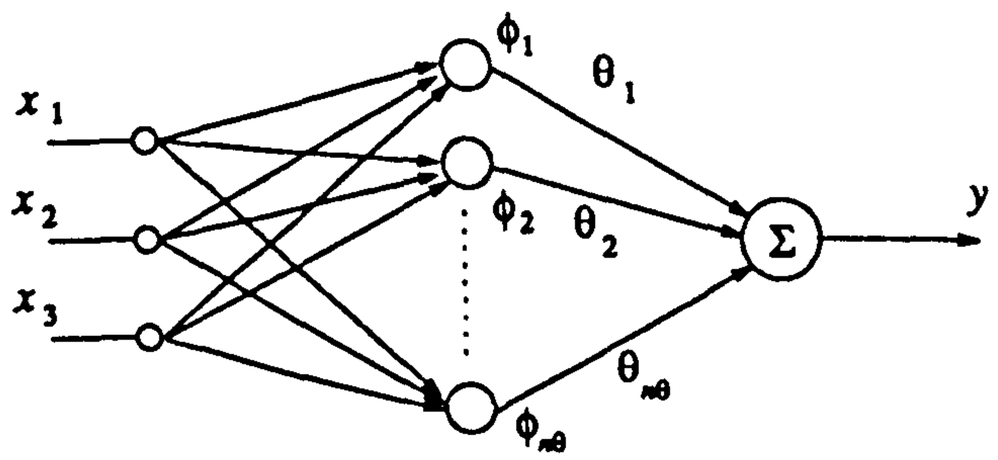

Figure 1 Basis function network

PARAMETER ESTIMATION AND TRAINING

Cost function

Given a record of measured input-output data pairs $(u(t), y(t))$ we aim to estimate the parameters θ_i in the linear regression (5). With a data record of length N a useful criterion to evaluate θ is

$$J_N(\boldsymbol{\theta}) = \frac{1}{N} \sum_{t=1}^{N} (y(t) - \hat{y}(t))^2$$

$$= \frac{1}{N} \sum_{t=1}^{N} (y(t) - \boldsymbol{\theta}' \boldsymbol{\phi}(t))^2 \; , \tag{16}$$

which is a standard least-squares criterion. We apply this criterion to both the linear case (defined by equations (7)–(8)) and the nonlinear case (defined by (14)–(15)) to find the estimate $\boldsymbol{\theta}$, i.e.,

$$\hat{\boldsymbol{\theta}}_N = \arg\min J_N(\boldsymbol{\theta}) \; . \tag{17}$$

Although we estimate the parameter $\boldsymbol{\theta}$ in both cases in the same manner, an additional requirement in the nonlinear RBF case is to select the basis function centres $\mathbf{c}_i$ and widths σ_i. The algorithm for estimation of $\boldsymbol{\theta}$ is described in the next section while the selection of RBF parameters $\mathbf{c}_i$ and σ_i is discussed in the section after that.

Estimation of linear coefficients

A key feature of the linear regression structure is that it leads to a cost function (16) which is quadratic in the parameter $\boldsymbol{\theta}$. It is very straightforward to analytically minimise the criterion. This leads to the expression[25,26]

$$\left[\frac{1}{N} \sum_{t=1}^{N} \boldsymbol{\phi}(t) \boldsymbol{\phi}'(t)\right] \hat{\boldsymbol{\theta}}_N = \frac{1}{N} \sum_{t=1}^{N} \boldsymbol{\phi}(t) y(t) \; . \tag{18}$$

All $\hat{\boldsymbol{\theta}}_N$ satisfying this expression yield the global minimum of $J_N(\boldsymbol{\theta})$. When the left side of this expression in invertible we obtain the least-squares estimates of $\boldsymbol{\theta}$,

$$\hat{\boldsymbol{\theta}}_N = \left[\frac{1}{N} \sum_{t=1}^{N} \boldsymbol{\phi}(t) \boldsymbol{\phi}'(t)\right]^{-1} \frac{1}{N} \sum_{t=1}^{N} \boldsymbol{\phi}(t) y(t) \; . \tag{19}$$

This is the expression used in the experiments reported in the sequel. Calculation of the solution to (19), which is an overdetermined set of linear equations, was performed using the Moore–Penrose pseudoinverse technique[28].

RBF internal parameter selection

To match the structure of the RBF network with the modelling problem the selection of the internal parameters of the basis functions ϕ_i is very important.

Centres. The first step of the training procedure for RBF networks is to determine the location of the units in the input space. The most straightfor-

ward method is to spread the centres uniformly over the entire input space. For multidimensional problems this results in an unnecessarily high number of units. It is more appropriate to locate the centres according to the demands of the system to be modelled. A number of clustering techniques have been proposed for selection of RBF centres[29]. Our approach was developed by Neumerkel *et al.*[30] and is outlined here. This is similar to the ART (adaptive resonance theory) approach of Carpenter and Grossberg[31]. Because it is a good idea to pay more attention to regions where large changes in the output occur we build a sample vector, $\mathbf{X} \in \mathcal{R}^{n_x + n_u + 1}$, consisting of the network input $\mathbf{x}$ and the actual output of the process $y(t)$, weighted with some factor γ,

$$\mathbf{X}^T(t) = (\mathbf{x}^T(t), \gamma y(t)) . \quad (20)$$

The sample $\mathbf{X}$ becomes a cluster (i.e., defines the position of an RBF unit) if the minimal distance to existing clusters $\mathbf{C}_i$ exceeds some threshold ϵ,

$$\min\|\mathbf{X} - \mathbf{C}_i\| > \epsilon, \; i = 1 \ldots n_\theta . \quad (21)$$

When this relation holds a new cluster is created at $\mathbf{X}$ and n_θ is increased by 1. Otherwise, $\mathbf{X}$ is considered to belong to the nearest existing cluster and no new cluster is created. The factor γ controls the significance of changes in the output.

This procedure is started with initially no clusters existing (which means of course that the first data sample forms a cluster) and continues until all data points have been considered. From the clusters $\mathbf{C}_i \in \mathcal{R}^{n_x + n_u + 1}$ the centres $\mathbf{c}_i \in \mathcal{R}^{n_x + n_u}$ are built by removing the last element $\gamma y(t)$ from the cluster vectors.

Variances. Determination of the variances σ_i once the centres have been found is also very important. We used the two-nearest neighbour heuristic, i.e., the geometric mean

$$\sigma_i = s\sqrt{d_{1_i} d_{2_i}}, \; i = 1 \ldots n_\theta . \quad (22)$$

where d_{1_i} and d_{2_i} are the distances from the current centre to the two nearest neighbours and s is a constant scaling factor whose value must be tuned experimentally.

EXPERIMENT

Physiological Measurements

The nerve–muscle preparation was made as described previously[32]. Briefly, the distal tendons of the tibialis anterior muscles of rabbits, under pentobarbitone anaesthesia, were cut and threaded through a titanium alloy clamp, placed to allow the minimum of free tendon between the myotendinous junction and the clamp. The clamp served as a hook which was attached via a carbon fibre/epoxy composite link to a servomotor (Cambridge Technology, Watertown, Massachusetts, USA). The rabbit was positioned supine on a steel myograph table with stout C-clamps fixing the distal femur and the malleoli of the ankle. Electrodes were implanted underneath the common peroneal nerve so that the muscle could be activated from an external stimulator. The nerve was cut proximal to the electrodes.

The force produced by the muscles was measured from the coil current in the servomotor used in length-control mode. A series of twitch contractions was used to establish l_0, the length at which maximal twitch tension was produced. The muscle was maintained at this length throughout the experiment.

Stimulation Protocol

A program was written to produce a series of random pulse patterns within the following constraints—(a) each pulse had an amplitude three times the threshold for muscle stimulation; (b) each pulse had a duration of 200 microseconds; (c) each pattern had a duration from first to last pulse not exceeding 300 ms. Random numbers were used to generate successive inter-pulse intervals of integer values from 1 to 70 ms (the force response of a single twitch lasts about 80 ms in this muscle).

A set of 100 random patterns were stored on disc, and were delivered to the muscle under computer control with 30 s rest between contractions. A constant-frequency burst of impulses (40 Hz, 300 ms) was delivered every 5 minutes to check that the preparation did not show progressive deterioration during the experiment. The force response from the muscle was recorded at 1 kHz sampling frequency but as explained below, this rate was unnecessarily high for dynamic modelling. In the estimation experiments, the data was decimated and only every sixth force sample used. If, in each six samples, a stimulus pulse occured, the decimated stimulus data was set to 1, otherwise it was set to 0. A typical input–output record is shown in *Figure 2*.

RESULTS

Linear model estimation

Our first step was to describe the system as a linear model of the form described in equation (7) *et*

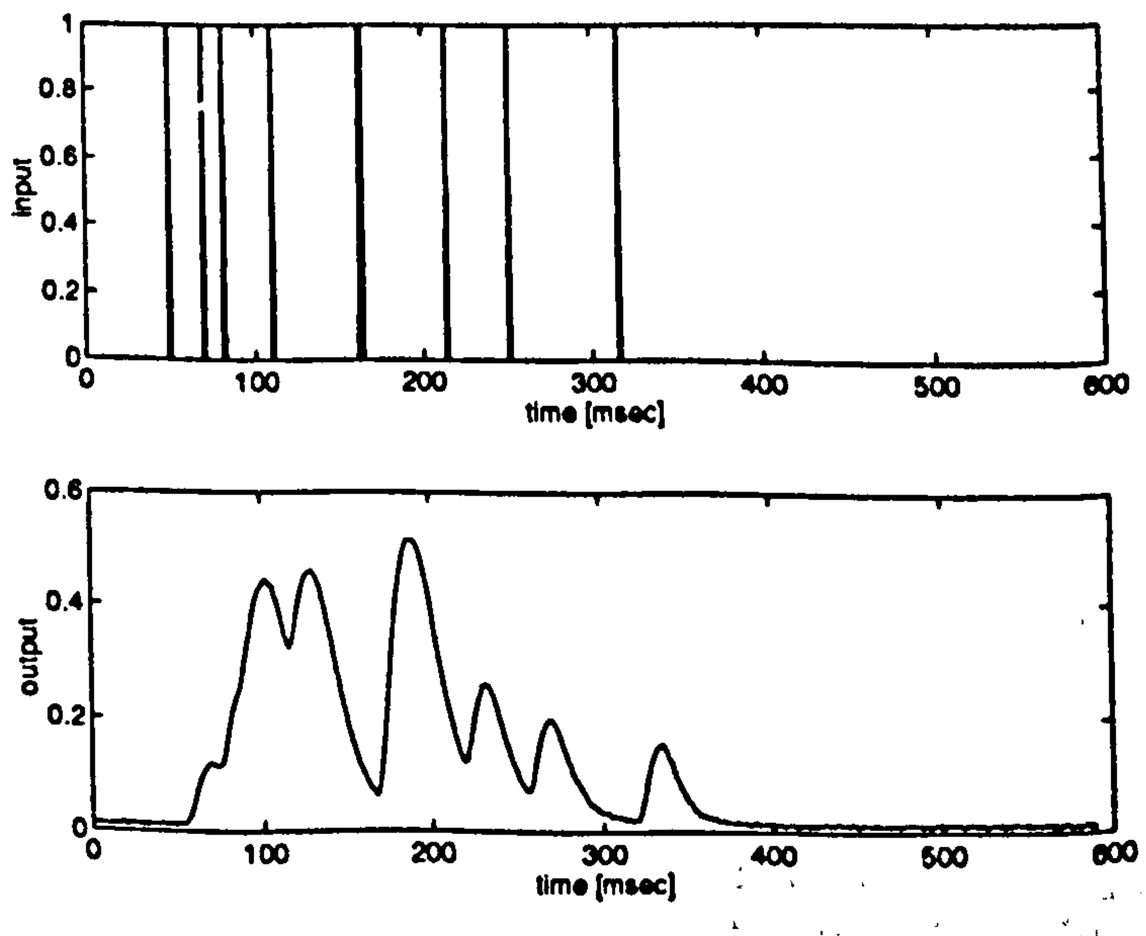

Figure 2 Typical experiment input–output record

seq. The input variable $u(t)$ corresponds to stimulation and the output $y(t)$ to measured tension. Since the input to the system is a sequence of pulses the most direct approach is to estimate the impulse response coefficients as in equation (13). The impulse response coefficients g_k are read directly from the output sequence following the pulse input at $t = 316$ ms of the data set in *Figure 2* (the non-zero offset was first removed and the sequence suitably truncated). The response of this model to an actual input sequence is compared with the measured response in *Figure 3* for an alternative data set. It is quite clear from the figure that the system is strongly nonlinear—the model appears reasonable for low values of tension (since the impulse response coefficients were obtained from a similar state) but a large discrepancy is evident at higher tensions. The result shown typifies the responses obtained on a number of experimental data sets.

Although the linear model appears poor we may still use it to determine approximately the order of the system (this is required for the nonlinear RBF network model). To do this we fed the impulse response model with a random input sequence and attempted to fit a range of linear transfer-function models of the form (10) of differing orders to the resulting input–output sequence. The responses of the linear impulse response model and the third order transfer-function approximation are compared in *Figure 4* (the responses of both models are indistinguishable). The response of the third order transfer-function model to the actual input of *Figure 3* is shown in *Figure 5*. The fidelity of a second order transfer-function model deteriorated slightly with respect to the impulse response model. We conclude that a reasonable choice of model order is three and proceed on that basis for the nonlinear modelling.

Nonlinear RBF network model

The input vector **x** for the nonlinear RBF network model is chosen as

$$\mathbf{x}'(t) = (y(t-1), y(t-2), y(t-3);$$

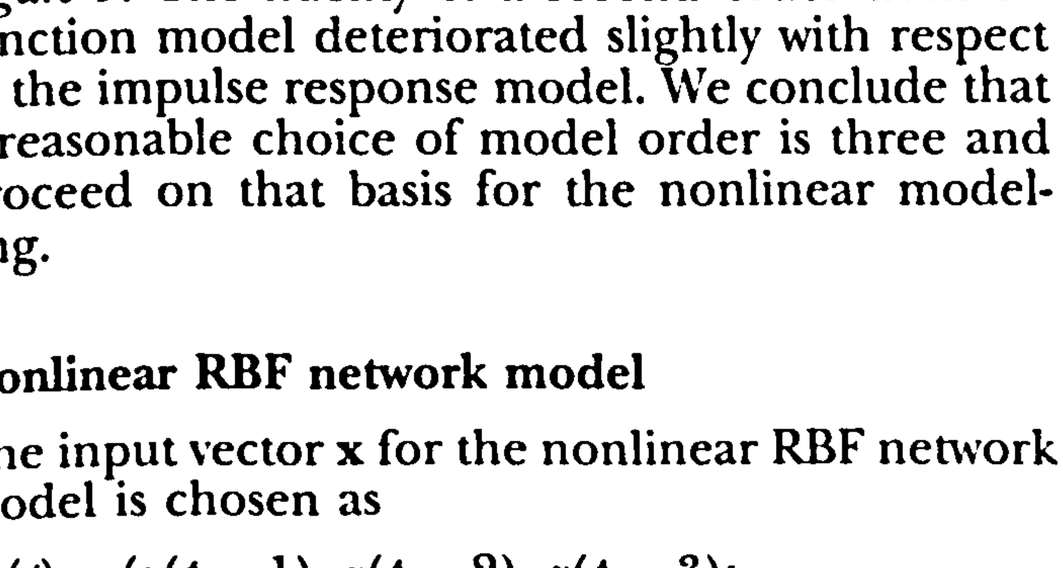

Figure 3 Response of linear impulse response model

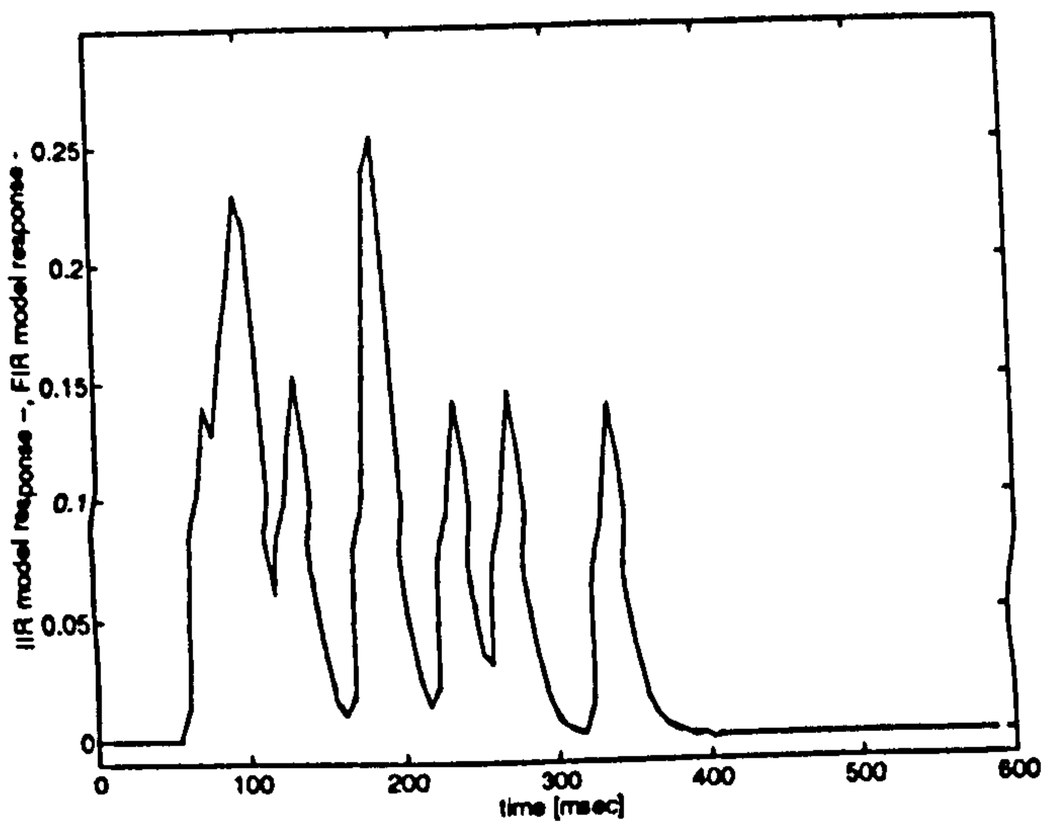

Figure 4 Linear impulse response and transfer-function models

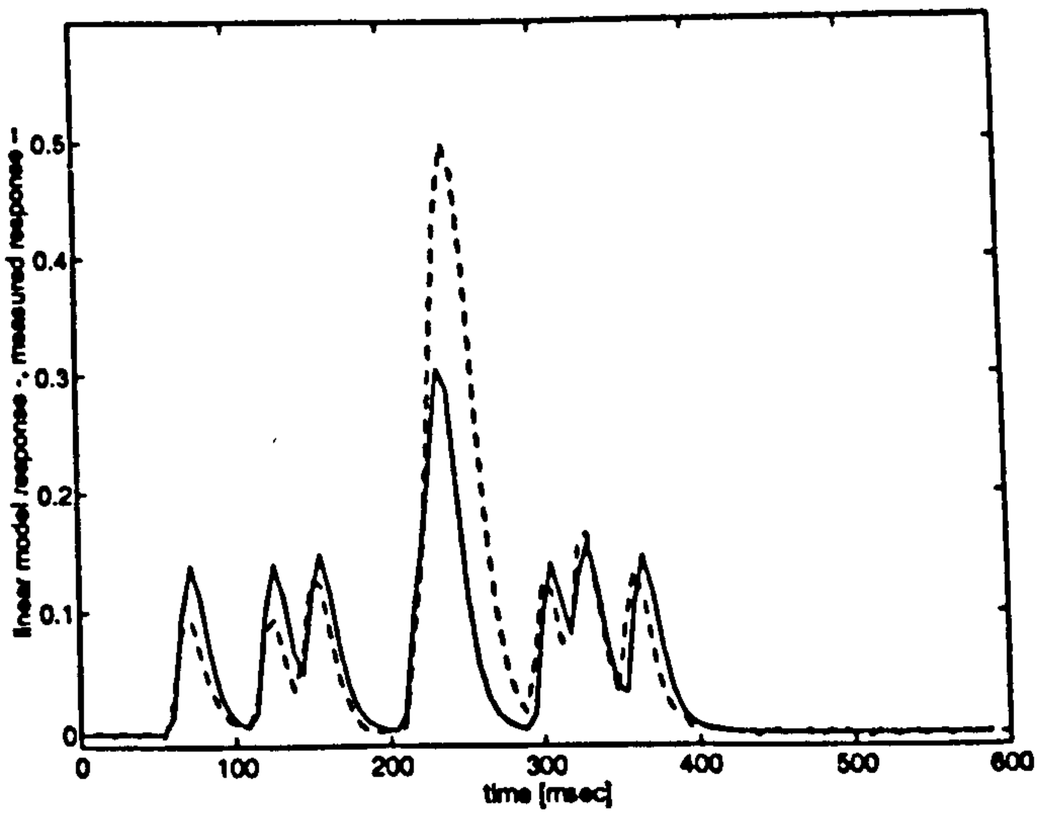

Figure 5 Kesponse of linear transfer-function model

$$u(t-1), u(t-2), u(t-3)), \qquad (23)$$

i.e., the model is third order.

To train the network we used a stream of 2000 measured input–output data points. The clustering algorithm, equations (20)–(21), generated 68 units, and the parameters in these equations were chosen as $\gamma = 4$ and $\epsilon = 0.1$. For variance selection the value $s = 2$ was used in equation (22). The performance of the trained network was tested on a number of new data sets which were not used in the training procedure. The response of the model to an actual input sequence is compared with the measured output for three data sets in *Figures 6–8*. These reponses are typical of results obtained when testing with further data sets. Note that these responses are the model predicted outputs obtained when the network input is defined as in equation (6).

The response of the model to a tetanic input sequence is shown in *Figure 9*.

DISCUSSION

Figure 10 shows the RBF muscle model, represented as a network. For the modelling described above, this network was simulated in a

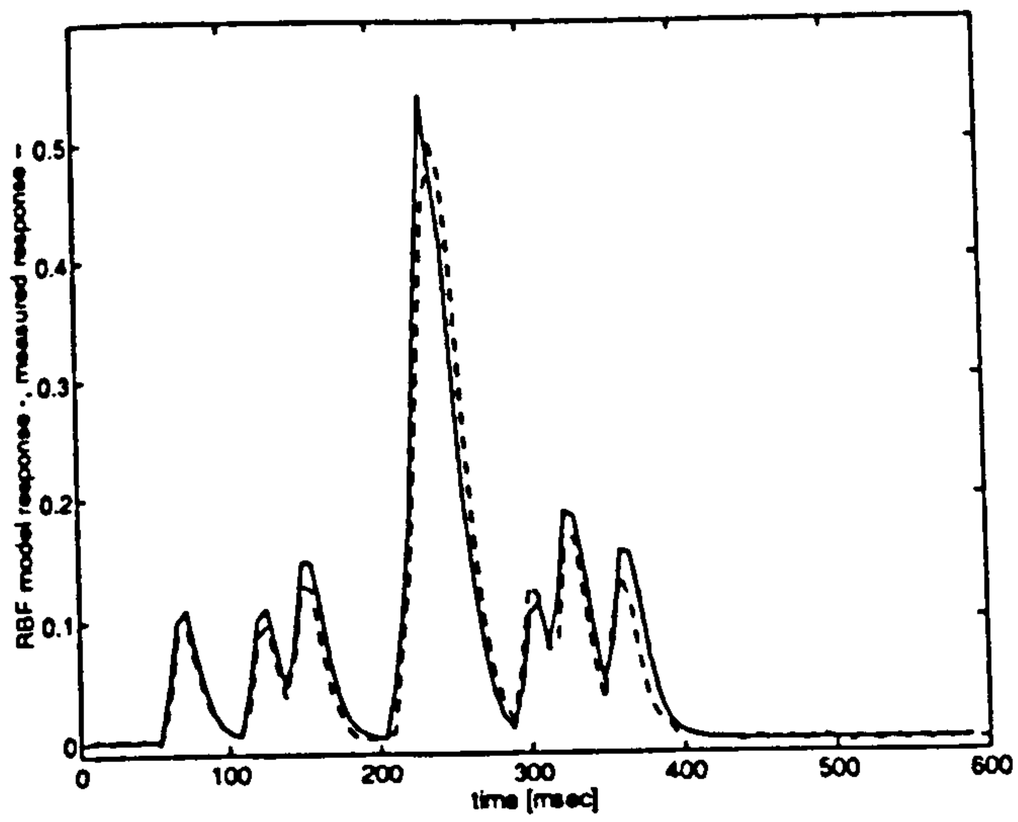

Figure 6 Response of nonlinear RBF model

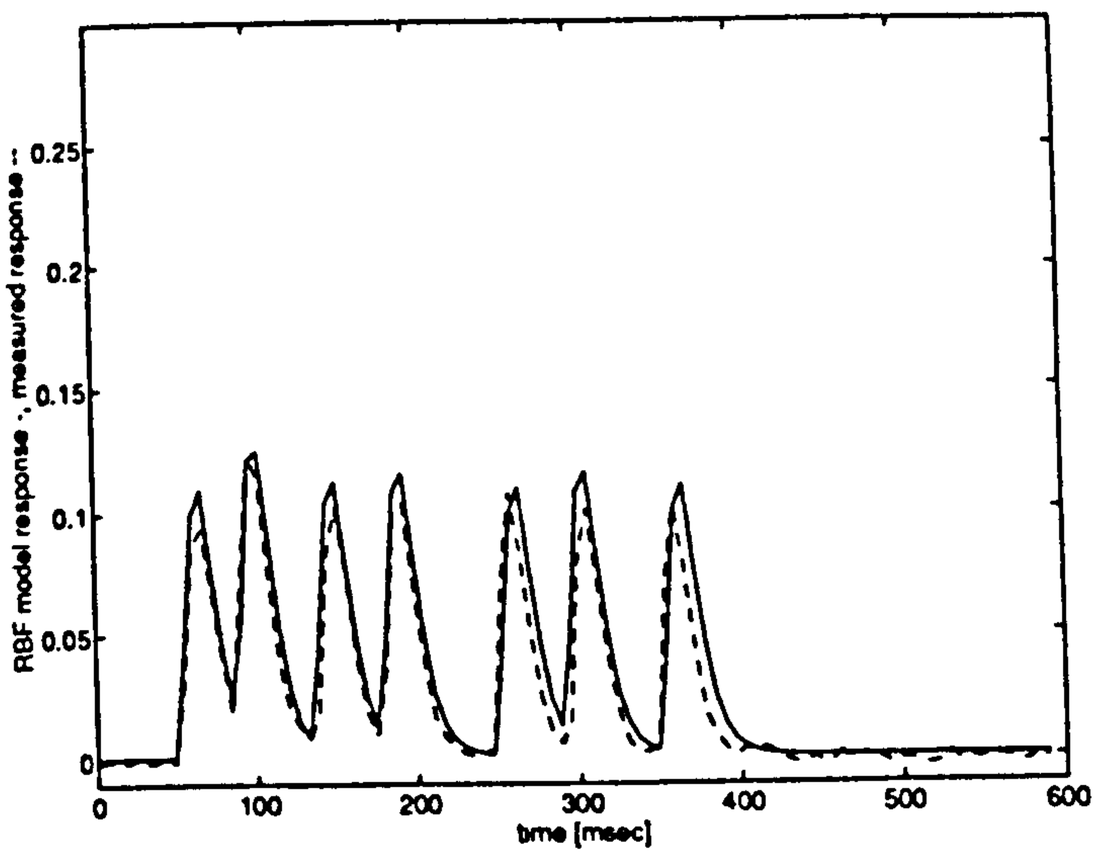

Figure 7 Response of nonlinear RBF model (contd)

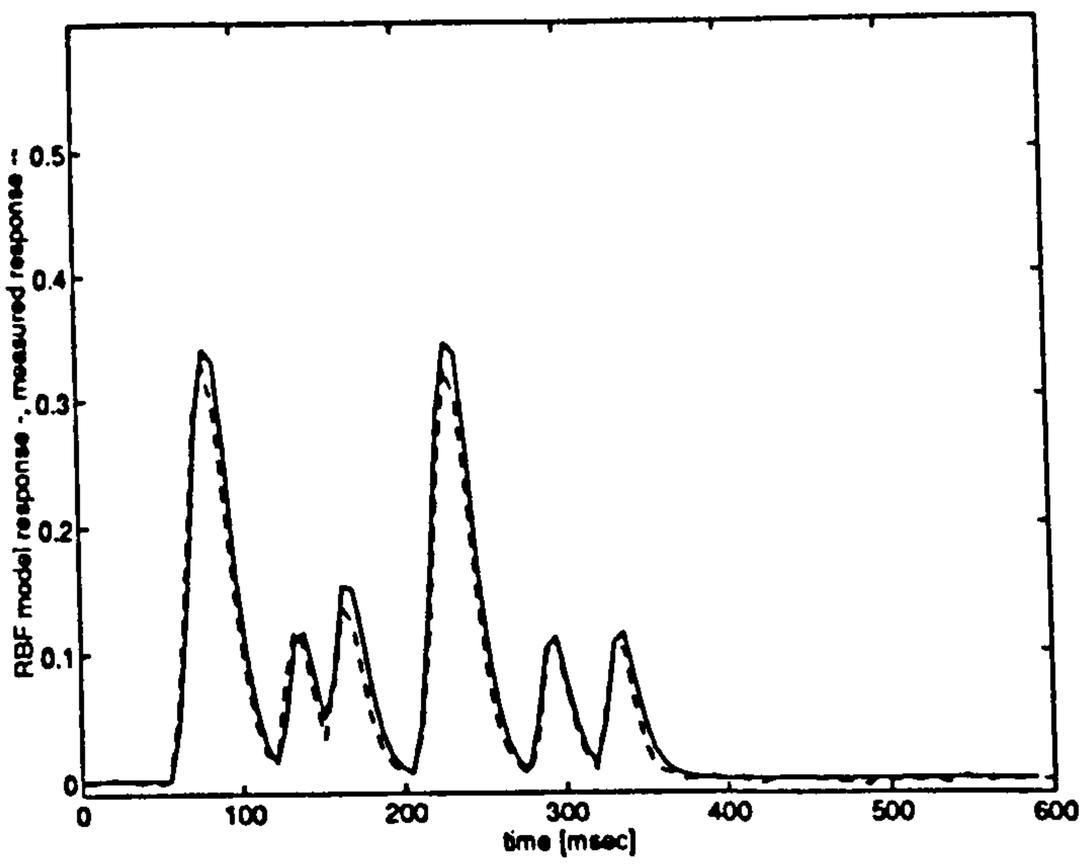

Figure 8 Response of nonlinear RBF model (contd)

conventional computer, but similar results could be obtained by using parallel processors for the RBFs, either digital or analogue. The network is connected in this way only after training; during training the force signal comes from the muscle

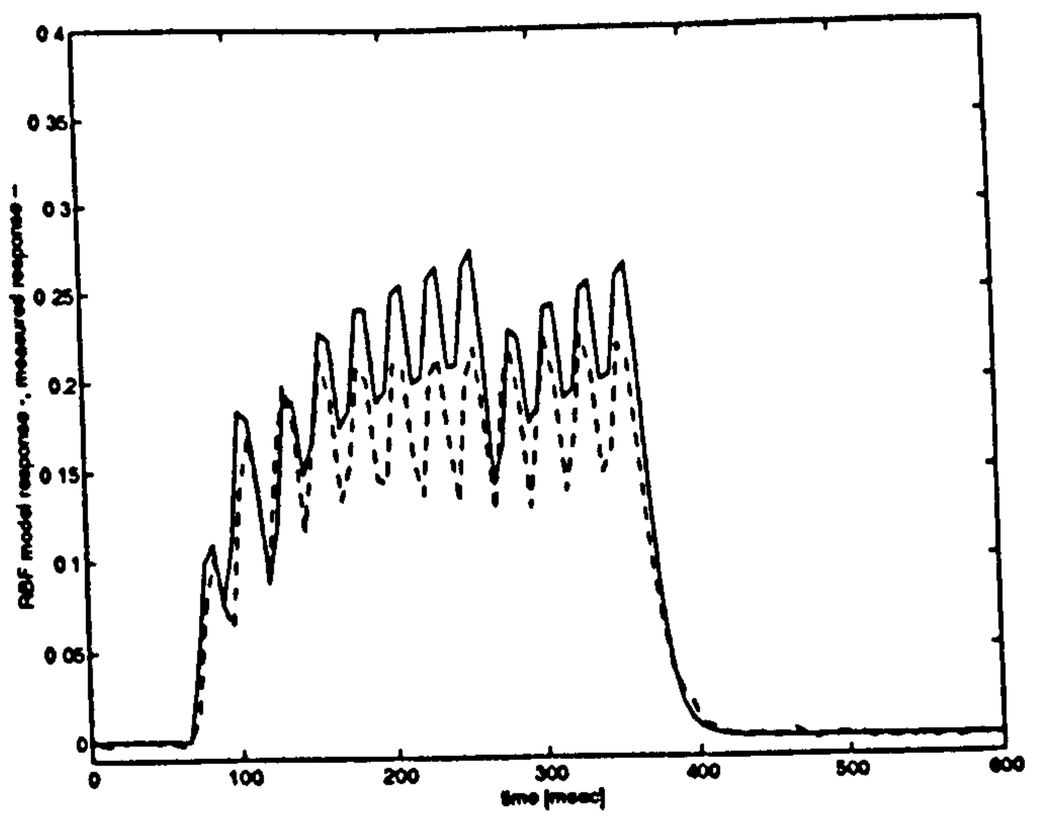

Figure 9 Response for tetanic contraction

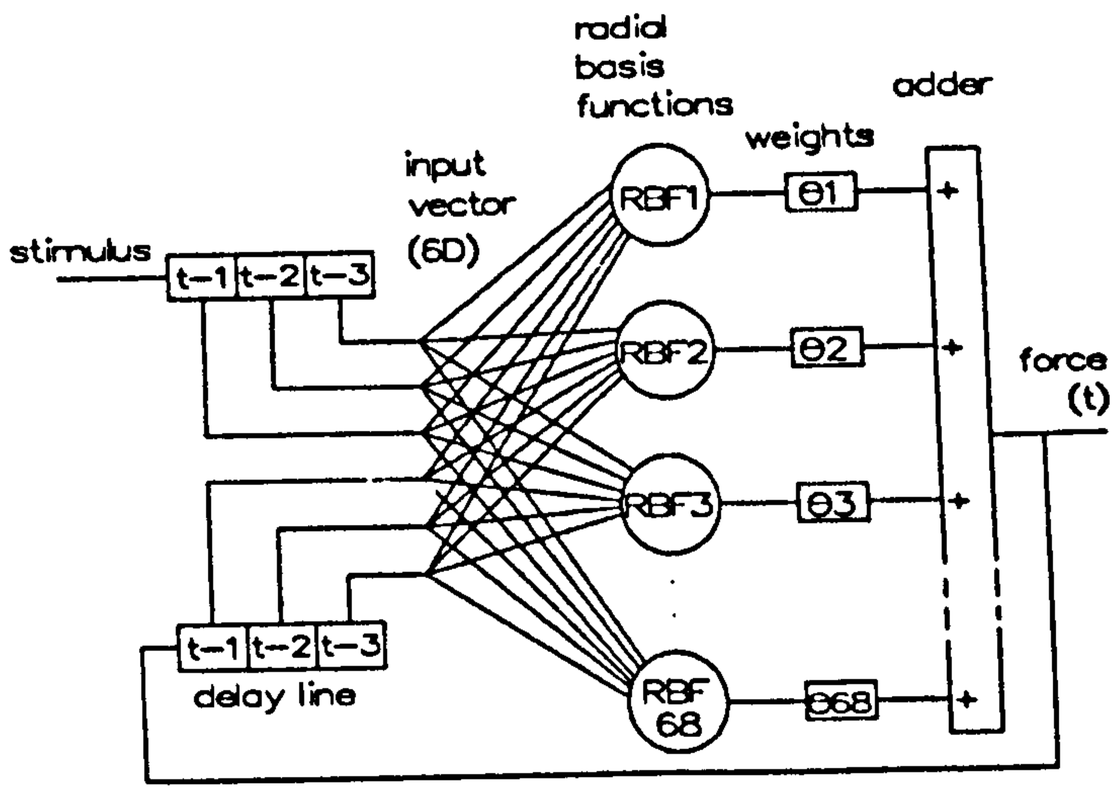

Figure 10 RBF muscle model

rather than from the network itself. The two delay lines are each three stages long because the model is third order, and together, they provide the six signals which are fed to the network. The output of the network (force(t)) is updated every sample period. At every sample time, the values of the six signals are thought of as a vector in 6-dimensional Cartesian space. The 68 radial basis functions each have a centre in that space. At every sample time, the radial distance from all these centres must be computed. This is done using the Euclidean norm, which means that the square of the radial distance equals the sum of the squares of the distances along all six axes (c.f. Pythagoras's theorem).

In this network, the basis functions are Gaussian (equation 15), so each is evaluated by dividing the square of the radial distance by the appropriate value of $(-2\sigma^2)$ (or multiplying by its reciprocal), and raising e to this power. This gives 68 numbers between 0 and 1. These are multiplied by their corresponding weights θ, and added, to give the output. Thus when running the model: for each RBF, at each sample time, the following arithmetic operations are required: 6 subtractions, 6 squarings, 5 additions, 2 multiplications and 1 exponentiation. To train the RBF network, having decided on the order and the clustering para-

hyperspace, may increase more slowly than the total volume of that space, as the number of dimensions rises. Consequently, the performance of the network may be maintained while increasing the number of basis functions less than exponentially. In practice, if an unacceptable number of clusters are produced, the clustering parameters are altered and clustering repeated until a reasonable number results and these are made the basis function centres. Another way to takle this dimensionality problem, which is a topic of current research, is to use a generalised form of basis function network having 'local models' (e.g. linear transfer functions) in place of the usual constant output weights. The framework for this approach has been established[36,37] and we plan to investigate this further in the context of muscle modelling. Initial work has shown the richness of this representation leads to a very significant reduction in the number of basis functions required to reach a given fidelity. Clearly, as more comprehensive models are sought, which represent more of the nonlinear phenomena cited in the Introduction, it is of great practical interest to known how many basis functions are actually required to give an acceptable fit.

As mentioned in the Introduction, one use of the forward model of the muscle is to find the inverse. Appropriate techniques have been described by Hunt and Sbarbaro[23]. *Figure 11* shows how the inverse model might be used when the muscle force is to be controlled over a range of muscle lengths. We suppose that the actual muscle length is measured and provided to the inverse RBF network. Given the length and the required force, the inverse network must deliver the appropriate stimulus pattern. Cascading an inverse model with the muscle in this way provides no feedback pathway to improve performance. There are, however, nonlinear controller structures which can incorporate nonlinear models and use feedback. One type is internal model control[38,39].

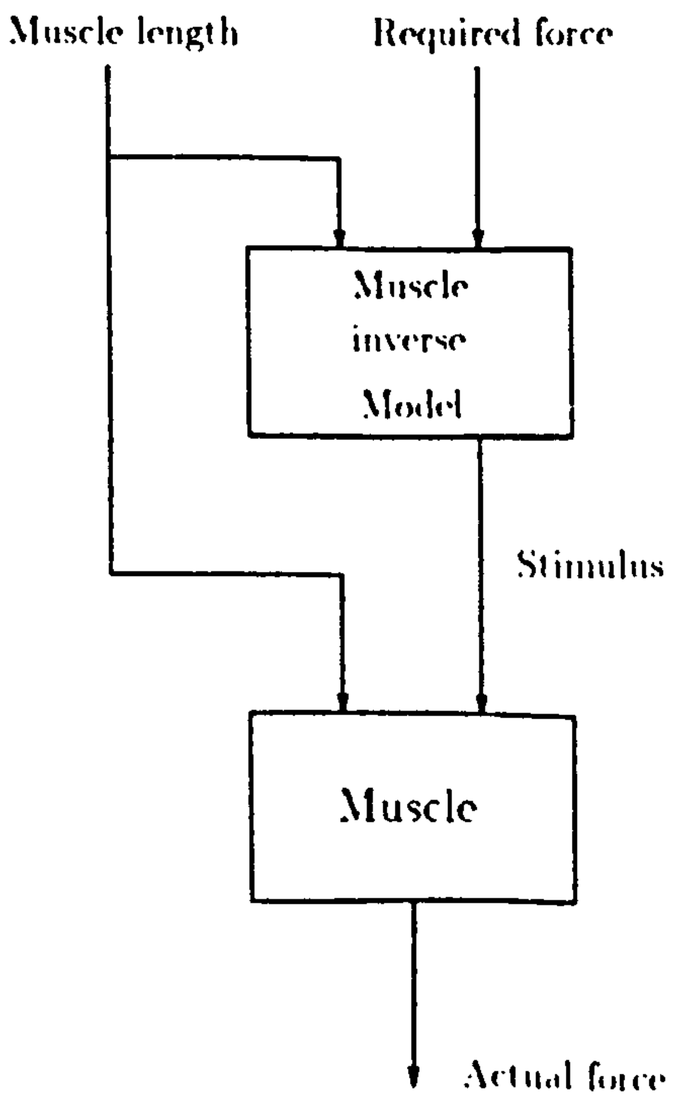

Figure 11 Use of muscle inverse model

Other possible structures have been surveyed by Hunt *et al.*[23].

For muscle, and therefore for the forward model of muscle, there will generally be a many-to-one relationship between the input and output: the same output force will be produced by more than one combination of inputs (length, stimulus). Thus it is possible that the inverse will be one-to-many, so that for every combination of required force and length (*Figure 11*), more than one stimulus pattern will be possible. Obviously it is desirable that the best of these possibilities is actually used, so the working version of the inverse model should be modified to be one-to-one. This may be achieved by extending the cost function (equation 16) used for training the network, by applying an additional criterion, such as: if there are more than one possible pulse patterns, select that with fewest pulses. The inverse model will thus optimise the output/input ratio.

In this study, the muscle is isometric and does no work. For nonlinear models to be useful for cardiomyoplasty and FES, the model must account for the changing length of a working muscle. We hope to use methods similar to those described here to optimise the ratio of work output to number of stimulating pulses, instead of force–time integral at constant length to the number of pulses (Jarvis[32]).

In the Introduction, we included among the nonlinear phenomena, seen in muscle, the slow changes called potentiation and fatigue which affect the muscle 'gain' and the dynamic behaviour. If these changes are reproducible, it should be possible to include them within a RBF network model, of the muscle or its inverse, which have some of their inputs connected to the actual muscle output. Such a model would be adaptive, in the sense that the models would continue to behave like the muscle during these slow changes. However, the network weights would remain fixed throughout, rather than 'tracking' the muscle parameters, as in, for example, a self-tuning PID controller. Such an adaptive RBF model would need to be larger than a non-adaptive model but the computation flow (*Figure 1*) would be no more complicated.

The conventional approach to linear modelling in systems identification[26] is to consider the input–output data either in the time domain, or, after spectral analysis, in the frequency domain. As Bode plots, for example, in the frequency domain, the curves are a nonparametric model of the system. Although a valid description of the system, this is not a compact form as the gain and phase curves represent many numbers. Often, it is desirable to find a transfer function which fits the data reasonably well. This is done by making the transfer function coefficients the parameters of the model. When these values of the parametric model have been found, the model may be regarded as an analogue of the system, since the transfer function could also represent a collection of lumped-parameter elements (springs, dashpots, etc). There are two benefits from obtaining a parametric model: its behaviour, in response to

new inputs, may be predicted qualitatively and in simulation.

For nonlinear systems, radial basis functions provide a parametric model and thus can be used for simulation studies, such as pseudo-experiments on muscle or trials of nonlinear controllers. However, they have the disadvantage that they are not readily comprehensible. Information about the muscle is contained in many numbers which do not themselves suggest how the model will behave in response to particular inputs; the response must be found by running the model. Furthermore the function which the RBF network represents cannot generally be shown graphically because the number of dimensions is greater than three. It would be helpful, for example to show abnormal behaviour in a particular pathological muscle, if the function represented by the network could be converted to a linguistic form. One possibility is to exploit the fact that each RBF model has an equivalent Tagaki–Sugeno fuzzy system[40,41] in which the behaviour is described as a set of fuzzy if–then rules. Unfortunately, each rule is equivalent to one basis function so rather a large number of rules must be understood before the behaviour can be grasped. We are working on a method which will allow the premises of the rules to be simplified (Hunt *et al.*[37]).

CONCLUSIONS

Radial basis function networks are a type of artificial neural network which have three advantages for muscle modelling compared to the multilayer perceptron. (1) the global minimum will always be found; (2) 'learning' is relatively quick; and (3), the RBF model may be converted to a fuzzy rule linguistic description. We have shown that the nonlinear RBF model is superior to a linear model in describing the effect of irregular supramaximal stimulating pulses on a rabbit tibialis anterior muscle.

RBF networks should be able to describe other nonlinear phenomena seen in stimulated muscle, either singly or in combination. In particular, we wish to model the effect of changing muscle length, which includes the effect of velocity because of the delay lines in the model; and of slow changes, potentiation and fatigue. If forward and inverse models can be realised, they can be used in muscle controllers which work over a wide range of muscle conditions.

In cardiomyoplasty, such controllers would help to reduce the energy cost to the muscle of delivering work to assist the heart. The stimulus inter-pulse intervals will not generally be constant.

REFERENCES

1. Durfee WK. Model identification in neural prosthesis systems, in *Neural Prostheses* (RB Stein, PH Peckham, and DP Popović, eds.) Oxford University Press, 1992.
2. Gordon AM, Huxley AF, Julian FJ. The variation in isometric tension with sarcomere length in vertebrate muscle fibres. *J Physiol* 1966; **184:** 170–192.
3. Rack PMH, Westbury DR. The effects of length and stimulus rate on tension in the isometric cat soleus muscle, *J Physiol.* 1969; **204:** 443–60.
4. Joyce GC, Rack PMH, Westbury DR. The mechanical properties of the cat soleus muscle during controlled lengthening and shortening movements. *J Physiol* 1969; **204:** 461–74.
5. Toft E, Sinkjaer T, Andreassen S, Larsen K. Mechanical and electromyographic responses to stretch of the human ankle extensors. *J NeuroPhysiol* 1991; **65:** 1402–10.
6. Joyce GC, Rack PMH. Isotonic lengthening and shortening movements of cat soleus muscle. *J Physiol* 1969; **204:** 475–91.
7. Cooper S, Eccles JC. The isometric responses of mammalian muscles. *J Physiol* 1930; **69:** 377–85.
8. Parmiggiani F, Stein RB. Nonlinear summation of contractions in cat muscles. II Later facilitation and stiffness changes. *J Gen Physiol* 1981; **78:** 295–311.
9. Sinkjaer T, Gantchev N, Arendt-Nielsen L. Mechanical properties of human ankle extensors after muscle potentiation. *EEG Clin Neurophysiol* 1992; **85:** 412–8.
10. Zahalak GI. An overview of muscle modelling, in *Neural Prostheses* (RB Stein, PH Peckham and DP Popović, eds.), Oxford University Press, 1992.
11. Hill AV. The heat of shortening and the dynamic constants of muscle. *Proc Roy Soc* 1938; **B126:** 136–95.
12. Winters JM. Hill-based muscle models: a systems engineering perspective, in *Multiple Muscle Systems* (JM Winters and SL-Y Woo, eds.), Springer Verlag, 1990.
13. Jaeger RJ. Design and simulation of closed-loop electrical stimulation orthoses for restoration of quiet standing in paraplegia. *J. Biomech* 1986; **19:** 825–35.
14. Durfee WK, Maclean KE. Methods for estimating the isometric recruitment curve of electrically stimulated muscle. *IEEE Trans Biomed Eng* 1989; **36:** 654–67.
15. Bernotas LA, Crago PE, Chizeck HJ. A discrete-time model of electrically stimulated muscle. *IEEE Trans Biomed Eng* 1986; **33:** 829–38.
16. Crago PE, Lemay MA, Liu L. External control of limb movements involving environmental interactions, in *Multiple Muscle Systems* (JM Winter and SL-Y Woo, eds.), Springer Verlag, 1990.
17. Flaherty B, Robinson C, Agarwal G. Determining appropriate models for joint control using surface electrical stimulation of soleus in spinal cord injury. *Med Biol Engng Computing* 1994; **32(3):** 273–82.
18. Flaherty B, Robinson C, Agarwal G. Identification of nonlinear model of ankle dynamics during electrical stimulation of the soleus. *Med Biol Eng Computing.* (in press).
19. Allin J, Inbar GF. FNS parameter selection and upper limb characterisation. *IEEE Trans Biomed Eng* 1986; **33:** 809–17.
20. Robinson CJ, Flaherty B, Fehr L, Agarwal GC, Harris GF, Gottlieb GL. Biomechanical and reflex responses to joint perturbations during electrical stimulation of muscle: instrumentation and measurement techniques. *Med Biol Engng Computing* 1994; **32(3):** 261–72.
21. Kosko B. *Neural Nets and Fuzzy Systems.* Prentice-Hall, 1992.
22. Kwende MMN, Jarvis JC, Salmons S. The input-output relationships of skeletal muscle. (submitted *Proc R Soc Series B*).
23. Hunt KJ, Sbarbaro D. Studies in neural network based control, in *Neural Networks for Control and Systems: principles and applications.* (K Warwick, GR Irwin and KJ Hunt, eds.), IEE Control Engineering Series, Peter Peregrinus, 1992.
24. Billings SA, Leontaratis IJ. Identification of non-linear systems using parameter estimation techniques, in *Proc IEE Conf Control and its Applications, Warwick, UK,* 1981.
25. Ljung L, Söderström T. *Theory and Practice of Recursive Identification.* London: MIT Press, 1983.

26. Ljung L. *System Identification—Theory for the User.* Englewood Cliffs, New Jersey, USA: Prentice Hall, 1987.
27. Broomhead DS, Lowe D. Multivariable functional interpolation and adaptive networks. *Complex Systems* 1988; **2:** 321–55.
28. Albert AE. *Regression and the Moore–Penrose Pseudoinverse.* New York: Academic Press, 1972.
29. Moody J, Darken C. Fast learning in networks of locally-tuned processing units. *Neural Computation* 1989; **1:** 281–94.
30. Neumerkel D, Murray-Smith R, Gollee H. Modelling dynamic processes with clustered time-delay neurons, in *Proc International Joint Conference, Neural Networks, Nagoya, Japan,* 1993.
31. Carpenter GA, Grossberg S. ART 2: Self-organization of stable category recognition codes for analog input patterns. *Applied Optics* 1987; **26:** 4919–30.
32. Jarvis JC. Power production and working capacity of rabbit tibialis anterior muscles after chronic electrical stimulation. *J Physiol* 1993; **470**: 157–69.
33. Werbos P. *Beyond Regression: New Tools for Prediction and Analysis in the Behavior Sciences.* [PhD Thesis]. Harvard University, Committee on Applied Mathematics, 1974.
34. Rumelhart DE, Hinton GE, Williams RJ. Learning representations by backpropagation errors. *Nature* 1986; **323:** 533–6.
35. Sepulveda F, Wells DM, Vaughan CL. A neural network representation of electromyography and joint dynamics in human gait. *J Biomech* 1993; **26:** 101–9.
36. Johansen TA, Foss BA. A NARMAX model representation for adaptive control based on local models. *Modelling, Identification and Control* 1992; **13(1):** 25–39.
37. Hunt KJ, Haas R, Murray-Smith R. Dimensionality reduction in basis-function networks: exploiting the link with fuzzy systems, in *Proc IEEE Workshop on Computer-intensive methods in control and signal processing, Prague, Czech Republic,* 1994.
38. Economou CG, Morari M, Palsson BO. Internal model control. 5. Extension to nonlinear systems. *Ind Eng Chem Process Des Dev* 1986; **25:** 403–11.
39. Hunt KJ, Sbarbar D. Neural networks for non-linear internal model control. *Proc IEE Pt D,* September 1991; 138: 431–8.
40. Jang JSR, Sun CT. Functional equivalence between radial basis function networks and fuzzy inference systems. *IEEE Trans Neural Networks* 1993; **4:** 156–9.
41. Hunt KJ, Haas R, Murray-Smith R. Extending the functional equivalence of radial basis function networks and fuzzy inference systems, *IEEE Trans Neural Network* 1994 (in press).

Appendix C Jarvis, J.C., Mokrusch, T., Mayne, C.N., **Kwende, M.M.N.**, Gilroy, S., Sutherland, S. & Salmons, S. 1993 Fast-to-slow fibre type conversion does occur in continuously stimulated rat hindlimb muscle. *J. Physiol.* **467**: 112P.

Journal of Physiology (1993), 467, 112P

Fast-to-slow fibre type conversion does occur in continuously stimulated rat hindlimb muscle

J.C. Jarvis, T. Mokrusch, C.N. Mayne, M.M.N. Kwende, S. Gilroy, H. Sutherland and S. Salmons

Department of Human Anatomy & Cell Biology, University of Liverpool, Liverpool L69 3BX

In response to chronic stimulation, fast-twitch muscles in the rabbit acquire all the characteristics of slow-twitch muscles (Salmons & Henriksson, 1981). Previous attempts to demonstrate a conversion of this extent in the rat have been unsuccessful. On this basis it is widely believed that fast muscles in the normal rat have a restricted adaptive range (Frischknecht & Vrbová, 1991; Kirschbaum *et al.* 1990).

In seven adult male Wistar rats, we tested the hypothesis that fast-to-slow conversion would occur with stimulation patterns that delivered higher aggregate amounts of activity than those used before. Under Hypnorm anaesthesia miniature stimulators were implanted into the peritoneal cavity. The left common peroneal nerve was stimulated for 55–61 days continuously at 10 or 20 Hz. In preliminary experiments, less than 1 % of fibres showed damage after 9 days of stimulation.

Mechanical measurements were made from the extensor digitorum longus (EDL) muscles *in situ* under urethane anaesthesia. The chronically stimulated EDL muscle and its contralateral control were removed for further analysis. The following results are expressed as means ± S.E.M.

	Control	Stimulated
Wet weight (mg)	222 ± 6	115 ± 16
Maximum tetanic tension (N)	4.6 ± 0.4	2.0 ± 0.4
Time to peak twitch contraction (ms)	16.3 ± 0.6	29.8 ± 3.4
Time to half-relaxation (ms)	13.7 ± 0.6	31.1 ± 3.8
Twitch : tetanus ratio	0.18 ± 0.02	0.29 ± 0.02
Maximum velocity of shortening (mm s^{-1})	151 ± 5	75 ± 12
Shortening velocity for maximum power (mm s^{-1})	50 ± 2	27 ± 4
Peak power (mW)	74 ± 4	19 ± 6
Percentage type 1 fibres	5.0 ± 2.0	6.1–89.4

Stimulated muscles contained slow myosin light and heavy chains, although fast isoforms were still present in all cases. The extent of transformation was similar for the two stimulation frequencies.

Thus, contrary to previous reports, fast-to-slow transformation does take place in hindlimb muscles of normal rats that are subjected to continuous activity by chronic stimulation. The time course of the response to stimulation is more extended than that seen in the rabbit.

REFERENCES

Frischknecht, R. & Vrbová, G. (1991). *Pflügers Arch.* **419**, 319–326.

Kirschbaum, B.J., Kucher, H.-B., Termin, A., Kelly, A. & Pette, D. (1990). *J. Biol. Chem.* **265**, 13974–13980.

Salmons, S. & Henriksson, J. (1981). *Muscle and Nerve* **4**, 94–105.

Appendix D Jarvis, J.C., Sutherland, H., **Kwende, M.M.N.,** Mayne, C.N. & Salmons, S. 1993 Relationship between working capacity and activation frequency of chronically stimulated skeletal muscle. Chapter In: *Proceedings of World Symposium on Cardiomyoplasty, Biomechanical assist and Artificial Heart*, Paris, May 24-26. Futura (in press).